AFWL-TR-
74-255

SSN 204

SPHERICAL CAVITY RESONANT DAMPING THROUGH THE USE OF AN IMPEDANCE LOADED SHELL INSIDE THE CHAMBER

Terry L. Brown
The Dikewood Corporation
1009 Bradbury Drive, SE
Albuquerque, NM 87106

June 1975

Final Report for Period 28 September 1973 - 31 March 1974

AIR FORCE WEAPONS LABORATORY
Air Force Systems Command
Kirtland Air Force Base, NM 87117

Sensor and Simulation Notes

Note 204

1 July 1974

Spherical Cavity Resonant Damping Through the Use of an Impedance Loaded Shell Inside the Chamber

Terry L. Brown
The Dikewood Corporation

Abstract

This note presents a complete parameter study of the resonant frequencies of a perfectly conducting spherical chamber with an inner spherically shaped impedance loaded damping structure. Frequency shifts are given for a wide range of damper location and loading. The resulting cavity damping is given for several lower order E and H modes.

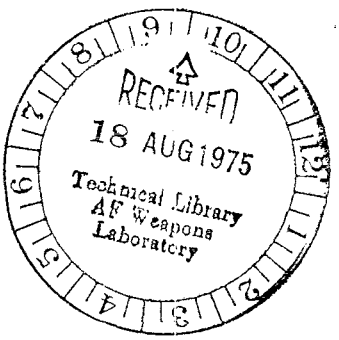

CONTENTS

ACKNOWLEDGEMENT

The many interesting and helpful suggestions of Dr. Carl E. Baum of AFWL are gratefully acknowledged. A note of thanks also goes to Mr. Joe P. Martinez of Dikewood for many helpful discussions concerning this work.

I. INTRODUCTION

This report addresses itself to one aspect of a simulator concept described by Baum[1] for simulating EMP in exoatmospheric regions by the incorporation of a spherical vacuum test chamber. Many important features affect the electromagnetic interactions of a space system with this type of spherical cavity. One of these is the problem of resonance. This report considers only the technique of an impedance loaded concentric shell inside but not in contact with the wall of a spherical cavity to damp the interior resonances of the cavity.

Ideally, in a system of this kind, the objective is to obtain the most damping possible through the proper selection of parameters involved. However, there exist many cavity resonant frequencies for many modes (n in the spherical vector wave index) and concentrating on damping only one of these does not produce an optimum simulator design. A reasonable selection of parameters is also desirable. Therefore, only the first few resonances of the first few modes are considered here for a fairly wide range of parameters.

Within this framework then, this report is an attempt to supplement previous work with a comprehensive numerical study of the shifts of various spherical cavity resonant frequencies for an arbitrarily positioned sheet liner. In addition it is intended that calculations and graphs presented will give some general insight to pole patterns as well as aid in establishing design optimization criteria.

II. MODEL FOR NUMERICAL STUDY

Natural frequencies for an object are values s_α (complex frequency) for which the object has a response without an incident excitation. That is the s_α are those frequencies that produce a nontrivial solution to the response vector of some homogeneous vector wave equation by making the system impedance vector vanish. Damping the complex resonant frequencies s_α then corresponds to moving these poles off the imaginary axis in the complex frequency plane. By maximizing $|\Omega_\alpha|/|\omega_\alpha|$ where $s_\alpha = \Omega_\alpha + i\omega_\alpha$ the optimum damping can be achieved.

Figure 2.1 illustrates the geometry of the object considered here. The perfect conducting spherical shell of radius a has a concentric spherical sheet with impedance Z_s at radius b. The electrical parameters in the cavity as well as between the spheres are those of free space.

The solutions for the interior modes of this geometry are based on the spherical wave functions and are solved for by Baum[1] in terms of E and H modes. The resonant frequencies for the E modes are solutions of

$$[\gamma a i_n(\gamma a)]' \left\{ 1 - \frac{Z_o}{Z_s} [\gamma b k_n(\gamma b)]' [\gamma b i_n(\gamma b)]' \right\}$$

$$+ [\gamma a k_n(\gamma a)]' \frac{Z_o}{Z_s} \left\{ [\gamma b i_n(\gamma b)]' \right\}^2 = 0 \qquad (2.1)$$

The H mode resonant frequencies arise from

$$i_n(\gamma a)\left\{1 + \frac{Z_o}{Z_s}\gamma b k_n(\gamma b)\gamma b i_n(\gamma b)\right\} - k_n(\gamma a)\frac{Z_o}{Z_s}\left\{\gamma b i_n(\gamma b)\right\}^2 = 0 \qquad (2.2)$$

where

$$\gamma a = \frac{sa}{c} = sa\sqrt{\mu_o \epsilon_o}$$

$$Z_o = \sqrt{\frac{\mu_o}{\epsilon_o}} \qquad (2.3)$$

The k_n and i_n functions can be expressed in terms of the spherical Bessel and spherical Hankel functions, respectively, as

$$i_n(\zeta) = i^n j_n(\xi)$$

$$k_n(\zeta) = i^{-n-2} h_n^{(2)}(\xi) \qquad (2.4)$$

with $\zeta = i\xi$.

All derivatives are taken with respect to the argument of the function. For convenience let $z_s \equiv Z_s/Z_o$ and equations 2.1 and 2.2 can be rewritten as

$$[\gamma a i_n(\gamma a)]'\left\{z_s - [\gamma b k_n(\gamma b)]'[\gamma b i_n(\gamma b)]'\right\} + [\gamma a k_n(\gamma a)]'\left\{[\gamma b i_n(\gamma b)]'\right\}^2 = 0 \quad (2.5)$$

and

$$\gamma a i_n(\gamma a)\{z_s + \gamma b k_n(\gamma b)\gamma b i_n(\gamma b)\} - \gamma a k_n(\gamma a)\{\gamma b i_n(\gamma b)\}^2 = 0 \qquad (2.6)$$

As $Z_s \to \infty$ and/or $b \to a$ (equivalent to removing the damper) the E mode resonant frequencies (equation 2.1) reduce to

$$[\gamma a i_n(\gamma a)]' = 0 \qquad (2.7)$$

and the H mode resonant frequencies (equation 2.2) reduce to

$$i_n(\gamma a) = 0 \quad \text{or} \quad \gamma a i_n(\gamma a) = 0 \qquad (2.8)$$

For $Z_s = 0$ the cavity resonances of equation 2.1 can be written

$$[\gamma b i_n(\gamma b)]' = 0 \qquad (2.9)$$

and

$$[\gamma a i_n(\gamma a)]'[\gamma b k_n(\gamma b)]' - [\gamma a k_n(\gamma a)]'[\gamma b i_n(\gamma b)]' = 0 \qquad (2.10)$$

Equation 2.2 for $Z_s = 0$ reduces to

$$i_n(\gamma b) = 0 \quad \text{or} \quad \gamma b i_n(\gamma b) = 0 \qquad (2.11)$$

and

$$i_n(\gamma a)k_n(\gamma b) - k_n(\gamma a)i_n(\gamma b) = 0 \qquad (2.12a)$$

or

$$\gamma a i_n(\gamma a)\gamma b k_n(\gamma b) - \gamma a k_n(\gamma a)\gamma b i_n(\gamma b) = 0 \qquad (2.12b)$$

Equations 2.7 and 2.8 give the resonant frequencies for a sphere of radius b while equations 2.10 and 2.12 give the resonances between two perfectly conducting spherical shells. These equations are used to identify the region from which a pole might arise and subsequently help define a given pole trajectory. Thinking in terms of increasing loading from zero to infinity for a fixed d/a, equations 2.7 and 2.8 determine where trajectories originate. Of course all trajectories must terminate (infinite loading) as equations 2.5 and 2.6.

A definition made in reference 1 concerning the solutions to equations 2.7 and 2.8 should be reiterated here. Let $\gamma a = u_{n,n'_o}$ be a solution to equation 2.7 and $\gamma a = v_{n,n'_o}$ be a solution to equation 2.8. These subscripts give a "handle" to any γa of concern. The n designates the order of the spherical Bessel and Hankel functions and n'_o denotes the ordinal number of the resonance frequency encountered moving positively along the $i\omega$ axis for the unloaded ($z_s \to \infty$) cavity. Obviously the terminal position (in terms of increasing z_s) of any pole trajectory is some u_{n,n'_o} or v_{n,n'_o}. It is necessary to extend this definition to better describe the various poles and their loci for changing parameters as encountered in this report. With the addition of a superscript define

$$u^{(0)}_{n,n'} \equiv u_{n,n'_o}$$

$$v^{(0)}_{n,n'} \equiv v_{n,n'_o} \qquad (2.13)$$

The empirical considerations of this definition become apparent with the definition below. A fairly comprehensive listing of $u^{(0)}_{n,n'}$ and $v^{(0)}_{n,n'}$ is given in table 2.1.

While the values of $u^{(0)}_{n,n'}$ and $v^{(0)}_{n,n'}$ are under consideration it might be noted (as was pointed out in reference 1) the significance of the ratios

$$\frac{b}{a} = \frac{u^{(0)}_{n,n'}}{u^{(0)}_{n,n''}} \quad \text{or} \quad \frac{b}{a} = \frac{v^{(0)}_{n,n'}}{v^{(0)}_{n,n''}} \qquad (2.14)$$

where $n'' > n' \geq 1$. If the resistive sheet is located at one of these values (a null of the tangential electric field) no damping will occur for some resonant frequency of that mode. Table 2.2 gives a somewhat expanded listing of these unwanted values to augment those found in reference 1. An obvious lack of damping for d/a values close to these undesirable ratios can be seen from the trajectories in section III. Care should be taken in using this table, if some other frequency bound is chosen, that is, if a lower bound will delete values of d/a and a higher bound would add them.

Since this report is a parameter study of all the resonant frequency poles, that arise in a spherical cavity with an impedance loaded sheet

	$n' = 1$	2.7437i		$n' = 1$	4.4934i
	2	6.1168i		2	7.7253i
$u^{(0)}_{1,n'}$	3	9.3166i	$v^{(0)}_{1,n'}$	3	10.9041i
	4	12.4859i		4	14.0662i
	5	15.6439i		5	17.2208i
	6	18.7963i		6	20.3713i
	$n' = 1$	3.8702i		$n' = 1$	5.7635i
	2	7.4431i		2	9.0950i
$u^{(0)}_{2,n'}$	3	10.7130i	$v^{(0)}_{2,n'}$	3	12.3229i
	4	13.9205i		4	15.5146i
	5	17.1027i		5	18.6890i
	6	20.2720i		6	21.8539i
	$n' = 1$	4.9734i		$n' = 1$	6.9879i
	2	8.7218i		2	10.4171i
$u^{(0)}_{3,n'}$	3	12.0636i	$v^{(0)}_{3,n'}$	3	13.6980i
	4	15.3136i		4	16.9236i
	5	18.5242i		5	20.1218i
	6	21.7139i		6	23.3042i
	$n' = 1$	6.0619i		$n' = 1$	8.1826i
	2	9.9675i		2	11.7049i
$u^{(0)}_{4,n'}$	3	13.3801i	$v^{(0)}_{4,n'}$	3	15.0397i
	4	16.6742i		4	18.3013i
	5	19.9154i		5	21.5254i
	6	23.1278i		6	24.7276i
	$n' = 1$	7.1402i		$n' = 1$	9.3558i
	2	11.1890i		2	12.9665i
$u^{(0)}_{5,n'}$	3	14.6701i	$v^{(0)}_{5,n'}$	3	16.3547i
	4	18.0085i		4	19.6532i
	5	21.2815i		5	22.9046i
	6	24.5178i		6	26.1278i
	$n' = 1$	8.2108i		$n' = 1$	10.5128i
	2	12.3915i		2	14.2074i
$u^{(0)}_{6,n'}$	3	15.9387i	$v^{(0)}_{6,n'}$	3	17.6480i
	4	19.3212i		4	20.9835i
	5	22.6263i		5	24.2628i
	6	25.8873i		6	27.5079i
	$n' = 1$	9.2755i		$n' = 1$	11.6570i
	2	13.5787i		2	15.4313i
$u^{(0)}_{7,n'}$	3	17.1896i	$v^{(0)}_{7,n'}$	3	18.9230i
	4	20.6154i		4	22.2953i
	5	23.9528i		5	25.6029i
	6	27.2390i		6	28.8704i

Table 2.1. The First Six Resonant Frequencies for the Unloaded Spherical Cavity for the First Seven E and H Modes

	b/a	d/a
$u^{(0)}_{1,1}/u^{(0)}_{1,2}$	.4486	.5514
$u^{(0)}_{1,1}/u^{(0)}_{1,3}$	.2945	.7055
$u^{(0)}_{1,2}/u^{(0)}_{1,3}$	.6565	.3435
$u^{(0)}_{2,1}/u^{(0)}_{2,2}$	.5200	.4800
$u^{(0)}_{2,1}/u^{(0)}_{2,3}$	.3613	.6387
$u^{(0)}_{2,2}/u^{(0)}_{2,3}$	.6948	.3052
$u^{(0)}_{3,1}/u^{(0)}_{3,2}$	.5702	.4298
$u^{(0)}_{4,1}/u^{(0)}_{4,2}$	.6082	.3918
$v^{(0)}_{1,1}/v^{(0)}_{1,2}$	.5817	.4183
$v^{(0)}_{2,1}/v^{(0)}_{2,1}$	.6337	.3663
$v^{(0)}_{3,1}/v^{(0)}_{3,2}$	.6708	.3292

Ordered Unwanted d/a Values
.3052
.3292
.3435
.3663
.3918
.4183
.4298
.4800
.5514
.6387
.7055

Table 2.2. Unwanted Values of d/a for the Lower Order E and H Modes with an Upper Normalized Frequency Bound of 10.5ia/c

liner without restriction to d/a or z_s, some designation of the various poles is desirable. Two distinct kinds of poles are immediately apparent: first, those arising from the innermost resonances, and, secondly, those originating between the liner and the shell itself. The predominance of the first or second kind of resonant poles is of course dependent upon the parameter values (d/a and z_s) under consideration. Naturally for lower frequency considerations the innermost resonances tend to dominate for smaller d/a values, whereas for larger d/a values the resonances from between the sheet and wall are more significant. The following definition is made in order to aid in identifying the multiple pole activity as $0 \leq d/a \leq 1$. Let $u^{(k)}_{n,n'}$ and $v^{(k)}_{n,n'}$ be a solution to equations 2.5 and 2.6, respectively, for $z_s = 0$ (or simply equations 2.8 and 2.10) where

n is the order of the spherical Bessel and Hankel functions (same as above and reference 1)

n' is the ordinal number of the resonant frequency along the $i\omega$ axis for a given n and d/a (same as above and reference 1)

and

k is an identifier that denotes interior resonances (k = 1), resonances between the sheet and shell (k = 2), or the unloaded cavity mode (k = 0)

This definition provides a convenient label for identifying from where trajectories arise, especially for cases where d/a is fixed and the resistively loaded sheet varies as $0 \leq z_s \leq \infty$. It should be noted that

$$u^{(0)}_{n,n'} \equiv u^{(1)}_{n,n'}\Big|_{\frac{d}{a}=0} \qquad \left(v^{(0)}_{n,n'} \equiv v^{(1)}_{n,n'}\Big|_{\frac{d}{a}=0}\right)$$

and

$$u^{(0)}_{n,n'} \equiv n^{(2)}_{n,n'}\Big|_{\frac{d}{a}=1} \qquad \left(v^{(0)}_{n,n'} \equiv v^{(2)}_{n,n'}\Big|_{\frac{d}{a}=1}\right)$$

An entire trajectory, for fixed d/a and changing z_s, can be identified by its initial position ($z_s = 0$ where $k = 1,2$) or its terminal position ($z_s = \infty$ where $k = 0$) since both are unique for a given d/a. The approach taken in this report will be to reference trajectories from their initial positions ($z_s = 0$ with $k = 1,2$).

The position on the $i\omega$ axis of any given resonant pole for $z_s = 0$ (equations 2.8 and 2.10) is a function of the parameter d/a. The complete solution for this special case (unloaded concentric spheres) with $0 \leq d/a \leq 1$ is plotted in figures 2.2 and 2.3 for the E mode ($u^{(2)}_{n,n'}$) resonances. Figures 2.4 and 2.5 give the H mode ($v^{(2)}_{n,n'}$) resonant solution. Since there exists an unlimited number of poles (n') for an unlimited number of modes (n) these figures represent a frequency bounded solution. As can be seen from the graphs

$$u^{(2)}_{n,1}\Big|_{\frac{d}{a}=0}$$

tends toward $i(n(n+1))^{1/2}$ and

$$u^{(2)}_{n,n'}\Big|_{\frac{d}{a}=0,\, n'>1}$$

increases without bound as does

$$v^{(2)}_{n,n'}\Big|_{\frac{d}{a}=0}$$

As $d/a \rightarrow 1$ $u^{(2)}_{n,n'} \rightarrow u^{(0)}_{n,n'}$ as does $v^{(2)}_{n,n'} \rightarrow v^{(0)}_{n,n'}$.

The unwanted values of d/a mentioned above are also graphically illustrated in the figures for two concentric perfectly conducting spheres. These objectionable damper positions occur at the intersections of $u^{(2)}_{n,n'}$ and constant $u^{(0)}_{n,n'}$ (dotted line). Also observable in these same figures is the difficulty in damping the higher order modes (n) as d/a approaches 1.

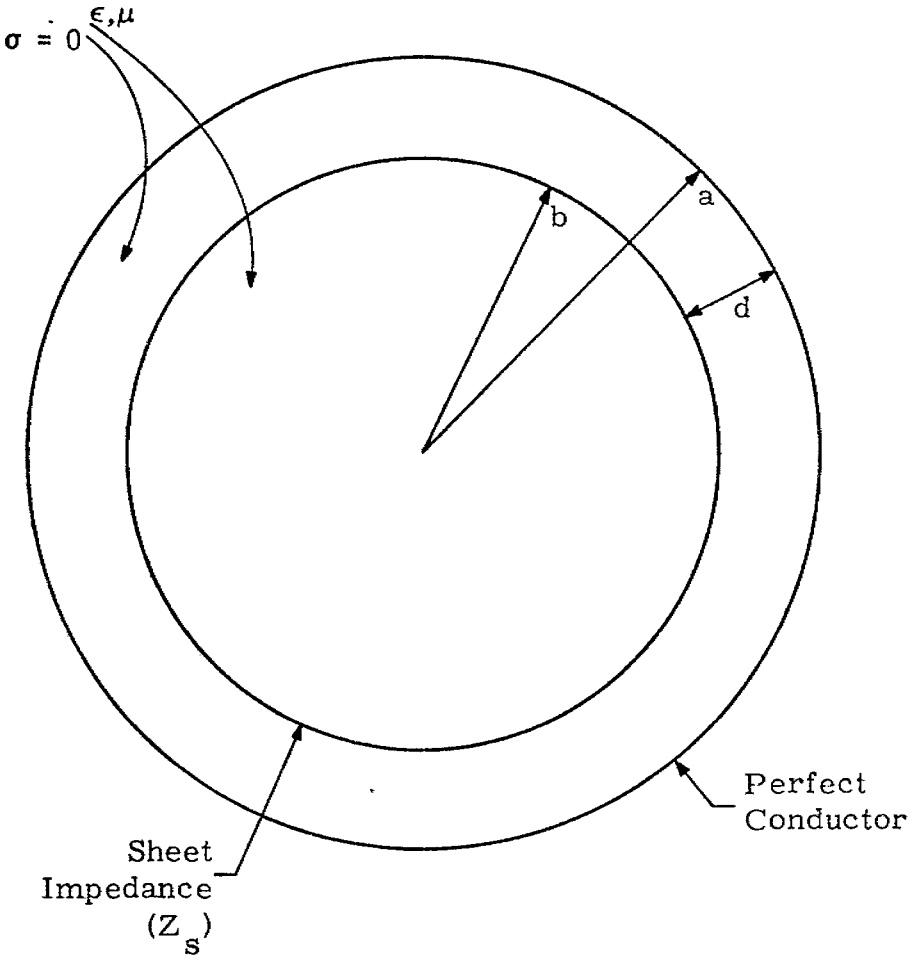

Figure 2.1. Impedance Loaded Shell for Damping Cavity Resonances

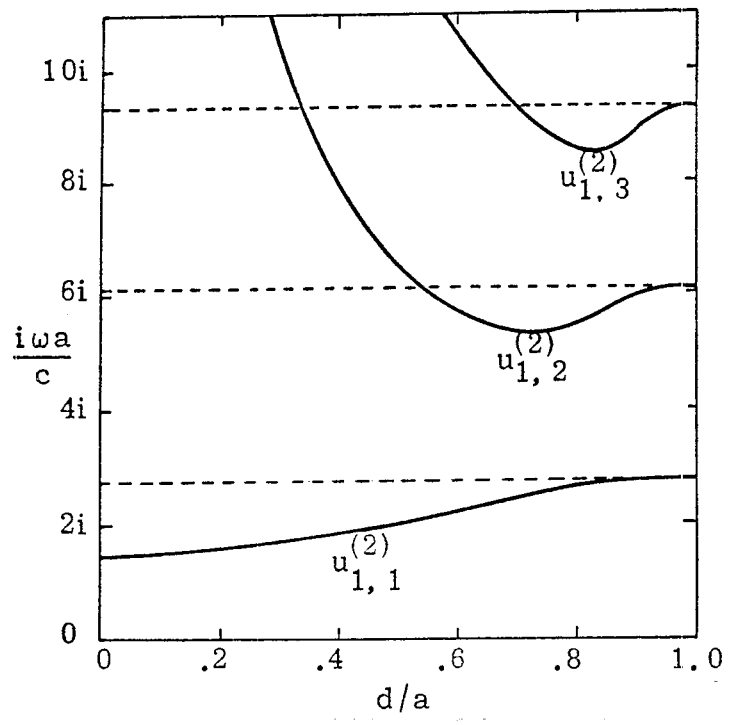

A. $u^{(2)}_{1,n'}$

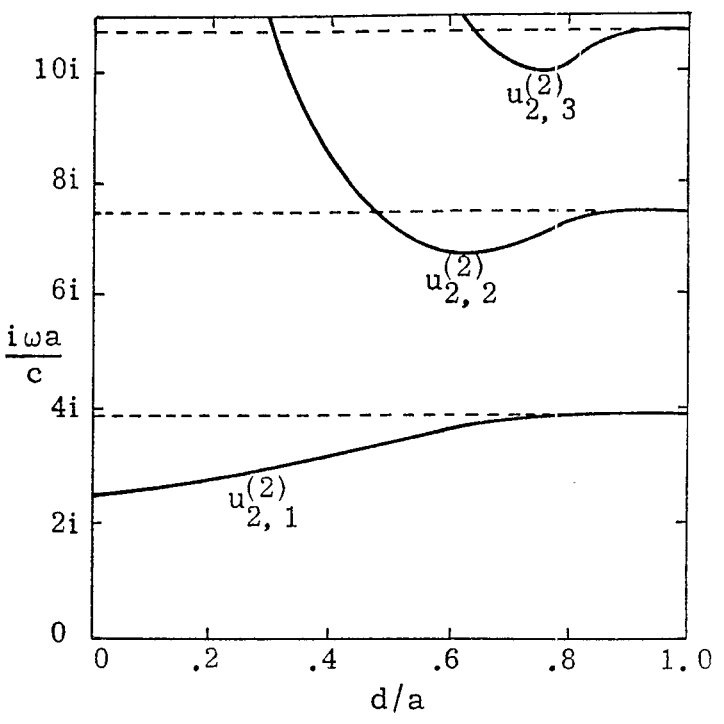

B. $u^{(2)}_{2,n'}$

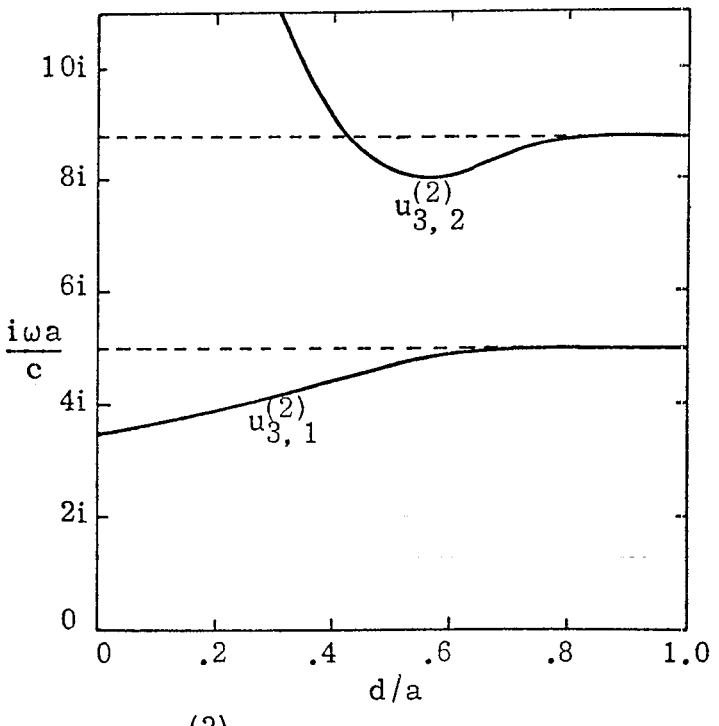

C. $u^{(2)}_{3,n'}$

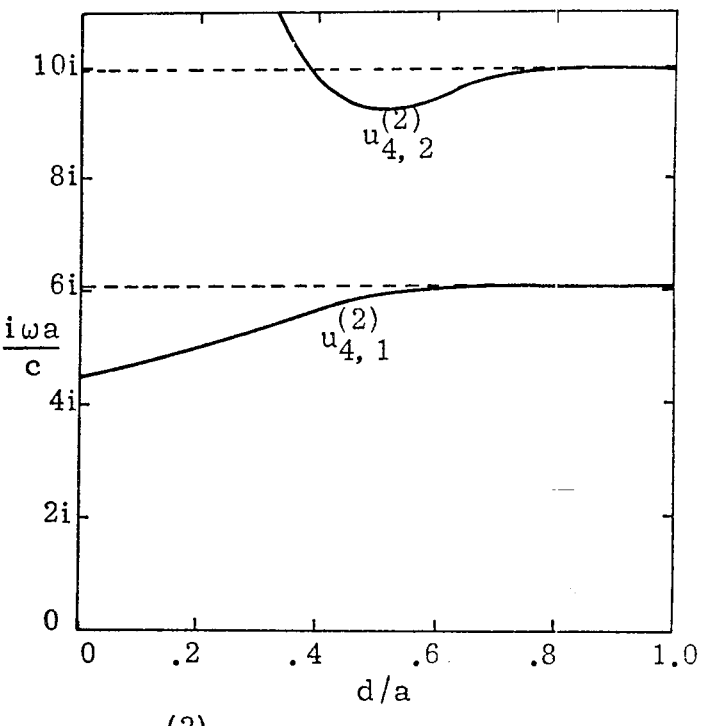

D. $u^{(2)}_{4,n'}$

Figure 2.2. Location of Natural E-Mode Resonances for Two Concentric Perfectly Conducting Spheres (Dotted Line Represents Constant $u^{(0)}_{n,n'}$)

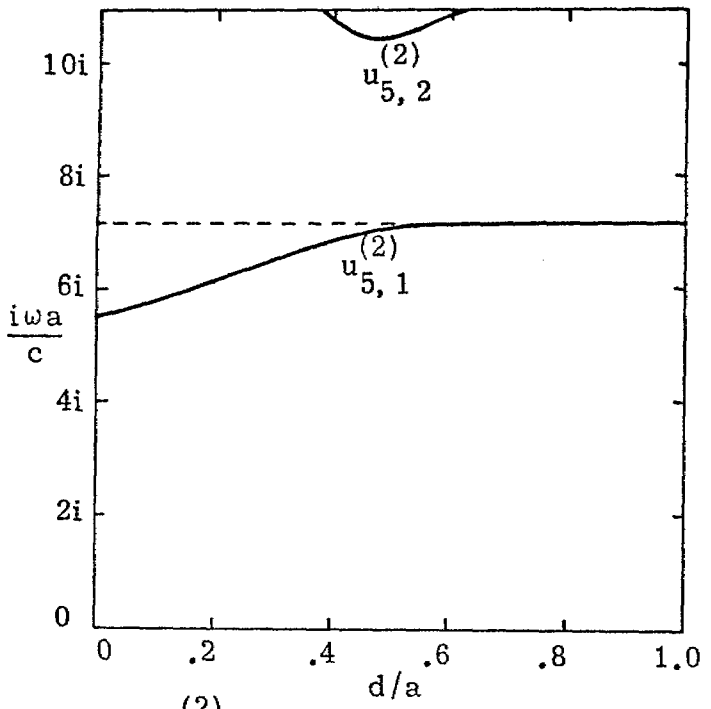

A. $u^{(2)}_{5,n'}$

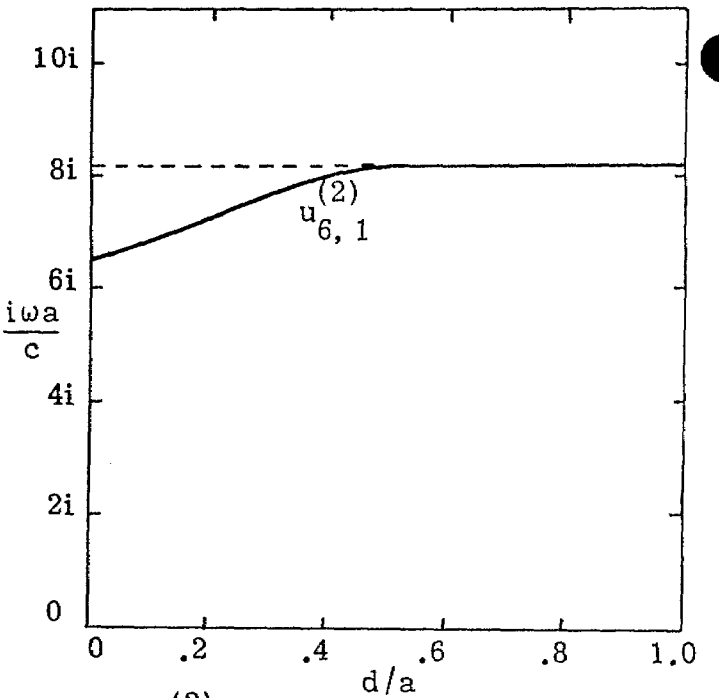

B. $u^{(2)}_{6,1}$

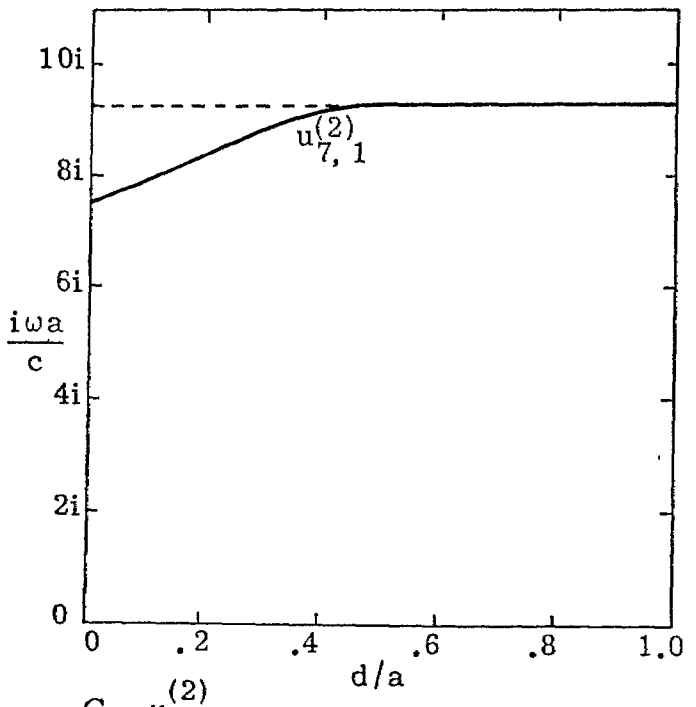

C. $u^{(2)}_{7,1}$

Figure 2.3. Location of Natural E-Mode Resonances for Two Concentric Perfectly Conducting Spheres (Dotted Line Represents Constant $u^{(0)}_{n,n'}$)

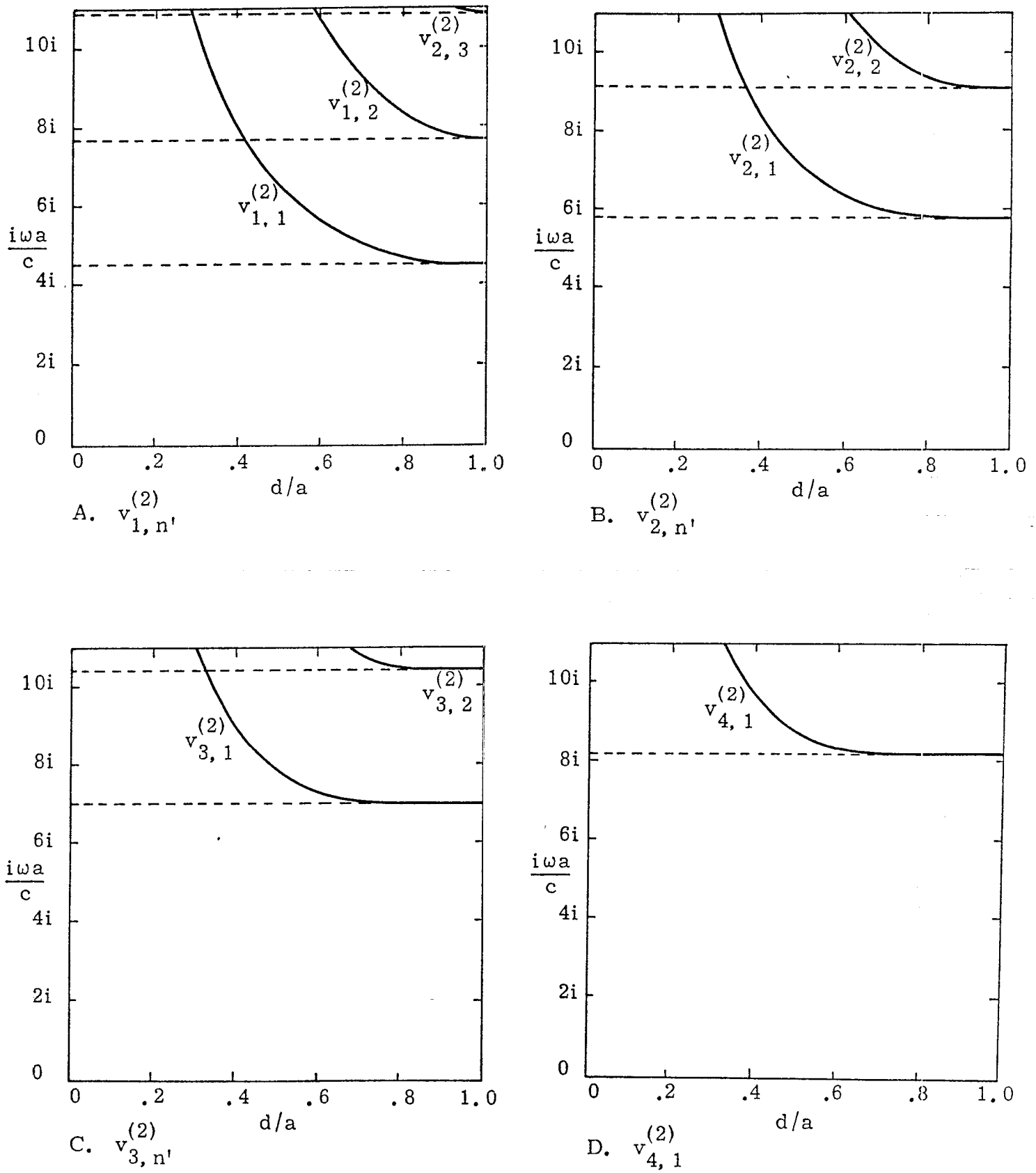

Figure 2.4. Location of Natural H-Mode Resonances for Two Concentric Perfectly Conducting Spheres (Dotted Line Represents Constant $v^{(0)}_{n,n'}$)

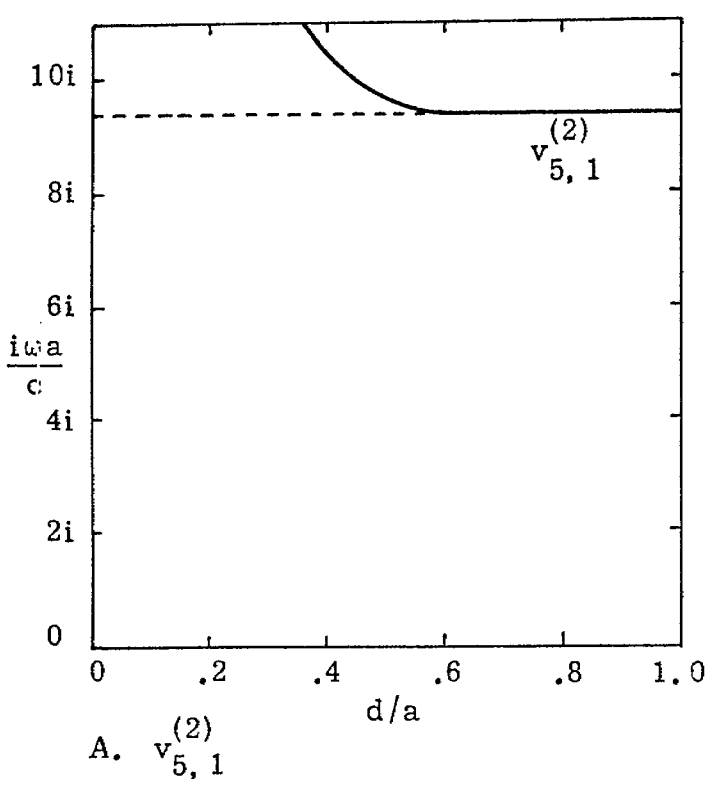

A. $v^{(2)}_{5,1}$

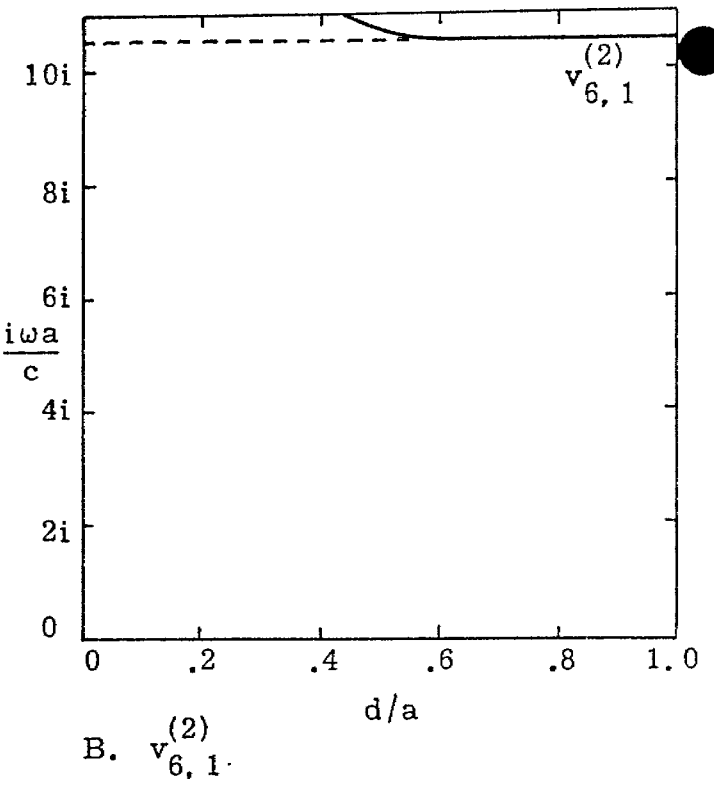

B. $v^{(2)}_{6,1}$

Figure 2.5. Location of Natural II-Mode Resonances for Two Concentric Perfectly Conducting Spheres (Dotted Line Represents Constant $v^{(0)}_{n,n'}$)

III. IMPACT OF VARYING RESISTIVE LOADING AND LINER LOCATION ON RESONANT FREQUENCIES

It was determined in reference 1 that the trajectories or pole shifts ($\Delta u_{n,n'}$ and $\Delta v_{n,n'}$) of the resonant poles are circles in the normalized complex frequency plane for a changing resistive loading (z_s) for small d/a. Typical trajectories for small d/a along with the asymptotic form as presented in reference 1 are illustrated at the end of this section. The object here is to explore the exact pole patterns for a fairly wide spectrum of d/a values ($0 \leq d/a \leq 1$) and resistive loading quantities ($0 \leq z_s \leq \infty$).

In order to calculate the trajectories of poles in the complex frequency plane a standard Newton-Raphson iteration technique was employed with the derivative of the E mode function (equation 2.5) taken as

$$\frac{d}{dS}\left\{[Si_n(S)]'\left\{z_s - \left[S\frac{b}{a}k_n\left(S\frac{b}{a}\right)\right]'\left[S\frac{b}{a}i_n\left(S\frac{b}{a}\right)\right]\right\} + [Sk_n(S)]'\left\{\left[S\frac{b}{a}i_n\left(S\frac{b}{a}\right)\right]'\right\}^2\right\} =$$

$$[Si_n(S)]'\left(-1\left\{\left[S\frac{b}{a}k_n\left(S\frac{b}{a}\right)\right]'\frac{b}{a}\left[S\frac{b}{a}i_n\left(S\frac{b}{a}\right)\right]''\right.\right.$$

$$\left.\left. + \left[S\frac{b}{a}i_n\left(S\frac{b}{a}\right)\right]'\frac{b}{a}\left[S\frac{b}{a}k_n\left(S\frac{b}{a}\right)\right]''\right\}\right)$$

$$+ \left\{z_s - \left[S\frac{b}{a}k_n\left(S\frac{b}{a}\right)\right]'\left[S\frac{b}{a}i_n\left(S\frac{b}{a}\right)\right]'\right\}[Si_n(S)]''$$

$$+ 2[Sk_n(S)]'\left[S\frac{b}{a}i_n\left(S\frac{b}{a}\right)\right]'\frac{b}{a}\left[S\frac{b}{a}i_n\left(S\frac{b}{a}\right)\right]''$$

$$+ \left\{\left[S\frac{b}{a}i_n\left(S\frac{b}{a}\right)\right]'\right\}^2 \cdot [Sk_n(S)]'' \qquad (3.1)$$

where

$$S \equiv \gamma a = \frac{sa}{c}, \qquad S\frac{b}{a} \equiv \gamma b \tag{3.2}$$

and all derivatives are taken with respect to argument of the modified spherical Bessel and Hankel functions.

To evaluate equation 3.1 the derivatives of modified spherical Bessel and Hankel functions are taken from

$$\varsigma i_n(\varsigma) = i^{n+1} \xi j_n(\xi) \tag{3.3}$$

so that

$$[\varsigma i_n(\varsigma)]' \equiv \frac{d[\varsigma i_n(\varsigma)]}{d\varsigma} = i^n [\xi j_n'(\xi) + j_n(\xi)] \tag{3.4}$$

where $\varsigma = i\xi$. Similarly,

$$[\varsigma k_n(\varsigma)]' \equiv \frac{d[\varsigma i_n(\varsigma)]}{d\varsigma} = i^{-n-2} \left[\xi h_n^{2'}(\xi) + h_n^2(\xi)\right] \tag{3.5}$$

The second derivatives are taken, using the Riccati-Bessel function relation,[2] as

$$[\varsigma i_n(\varsigma)]'' = \frac{\varsigma^2 + n(n+1)}{\varsigma^2} [\varsigma i_n(\varsigma)] \tag{3.6}$$

Similarly,

$$[\xi k_n(\xi)]'' = \frac{\xi^2 + n(n+1)}{\xi^2}[\xi k_n(\xi)] \tag{3.7}$$

The derivative of the H mode function (equation 2.6) is taken as

$$\frac{d}{dS}\left\{Si_n(S)\left\{z_s + S\frac{b}{a}k_n\left(S\frac{b}{a}\right)S\frac{b}{a}i_n\left(S\frac{b}{a}\right)\right\} - Sk_n(S)\left[S\frac{b}{a}i_n\left(S\frac{b}{a}\right)\right]^2\right\} =$$

$$Si_n(S)\left\{S\frac{b}{a}k_n\left(S\frac{b}{a}\right)\frac{b}{a}\left[S\frac{b}{a}i_n\left(S\frac{b}{a}\right)\right]' + S\frac{b}{a}i_n\left(S\frac{b}{a}\right)\frac{b}{a}\left[S\frac{b}{a}k_n\left(S\frac{b}{a}\right)\right]'\right\}$$

$$+ \left[z_s + S\frac{b}{a}k_n\left(S\frac{b}{a}\right)S\frac{b}{a}i_n\left(S\frac{b}{a}\right)\right][Si_n(S)]'$$

$$- 2Sk_n(S)S\frac{b}{a}i_n\left(S\frac{b}{a}\right)\frac{b}{a}\left[S\frac{b}{a}i_n\left(S\frac{b}{a}\right)\right]' - \left[Sbi_n\left(S\frac{b}{a}\right)\right]^2[Sk_n(S)]' \tag{3.8}$$

Again $S \equiv \gamma a = sa/c$, $S(b/a) \equiv \gamma b$ and the i_n and k_n function being taken as given in equation 2.4.

The trajectories of the resonant frequency poles can thus be determined by numerically[3,4] evaluating the spherical Bessel and Hankel functions ($j_n(\xi)$, $j_n'(\xi)$, $h_n^2(\xi)$ and $h_n^{2'}(\xi)$) for arbitrary values of the parameters.

Two conclusions can immediately be drawn concerning the location of the natural frequency poles. As both Baum[5] and Tesche[6] point out the natural resonances occur in conjugate pairs in the left half plane of the

complex frequency (or Laplace) domain. For this reason, only the upper left half plane ($\Omega \leq 0$ and $i\omega \geq 0$) of the normalized complex frequency plane will be represented in this report.

The circle approximation of the resonant frequency trajectory naturally begins to deteriorate as d/a is increased. As can be seen in figure 3.1 for the trajectories originating from $u^{(1)}_{n,n'}$ the asymptotic form is very good for d/a = .05, but the difference becomes significant, as the locus begins to bulge for larger d/a. A similar result is shown in figure 3.2 for the H mode resonant shifts. The higher one goes in frequency (n') or mode (n) the faster the deviation from a circle for a fixed d/a. As pointed out in reference 1, for the asymptotic approximation to be correct, the higher the order of the resonant mode the smaller d/a must become so that d is still small compared to the complex radian wavelength.

An interesting and somewhat predictable phenomenon occurs in the trajectories as d/a continues to increase. The path of a given pole from $u^{(1)}_{n,n'}$ ($v^{(1)}_{n,n'}$), that has a terminal position ($z_s = \infty$) of $u^{(0)}_{n,n'}$ ($v^{(0)}_{n,n'}$) for small d/a, diverts to a terminal position on the imaginary axis in a direction toward $u^{(0)}_{n,n'+'}$ ($v^{(0)}_{n,n'+'}$). Larger resonant frequencies (smaller wavelengths) would be expected in the innermost cavity as its radius decreases. This upper shift in frequency is illustrated in figure 3.3 for the lowest order E mode resonance with arrows indicating the movement of the pole for increasing z_s. Equivalently the resonant frequencies arising from between the linear and the outer shell decrease

(longer wavelengths) and the trajectory shift is downward for increasing d/a. The trajectories from $u^{(1)}_{n,1}$ are of special interest in that coalescence occurs on the negative Ω axis for some d/a values. This pole will be dealt with in more detail below. Again, all poles whether arising from the innermost sphere (k = 1) or from between the liner and the shell (k = 2) must terminate at some $u^{(0)}_{n,n'}$ or $v^{(0)}_{n,n'}$ (including $u^{(0)}_{n,0}$ and possibly $u^{(0)}_{n,\infty}$) for all d/a.

Obviously some bounds must be imposed on the number of resonant frequencies presented and/or the region in which these resonant frequencies occur. For the purpose of this report the normalized complex frequency bounds will be taken as $0 \leq |i\omega a/c| \leq 10.5$ and $-8.0 \leq \Omega a/c \leq 0$. This upper $i\omega a/c$ limit is taken to be approximately $u^{(0)}_{7,1}$ for the E modes which includes up to $v^{(0)}_{5,1}$ for the H modes. The number of resonant frequencies for each of these modes is $n' \leq 3$. Occasionally these limits will be exceeded for the purpose of illustrating complete trajectories.

Tables 3.1 through 3.12 summarize and somewhat extend the numerous initial and terminal positions of trajectories found in this section. Given in these tables for d/a at .05 intervals is the position of the various poles ($u^{(k)}_{n,n'}$ and $v^{(k)}_{n,n'}$) at $z_s = 0$ and their terminal positions $u^{(0)}_{n,n'}$ ($v^{(0)}_{n,n'}$) as $z_s \longrightarrow \infty$. The uniqueness of n' in $u^{(0)}_{n,n'}$ ($v^{(0)}_{n,n'}$) for a given d/a is apparent when both k = 1 and k = 2 are considered. The bold line in the tables separates trajectories found in this report from those not included.

The individual lower order loci that originate ($z_s = 0$) at $u^{(1)}_{n,n'}$ and $v^{(1)}_{n,n'}$ are represented in figures 3.5 through 3.15. These plots

d/a	$u^{(1)}_{1,1}$	$u^{(0)}_{1,n'}$	$u^{(1)}_{1,2}$	$u^{(0)}_{1,n'}$	$u^{(1)}_{1,3}$	$u^{(0)}_{1,n'}$	$u^{(1)}_{1,4}$	$u^{(0)}_{1,n'}$	$u^{(2)}_{1,1}$	$u^{(0)}_{1,n'}$	$u^{(2)}_{1,2}$	$u^{(0)}_{1,n'}$	$u^{(2)}_{1,3}$	$u^{(0)}_{1,n'}$	$u^{(2)}_{1,4}$	$u^{(0)}_{1,n'}$	$u^{(2)}_{1,5}$	$u^{(0)}_{1,n'}$
.05	2.89i	$u^{(0)}_{1,1}$	6.44i	$u^{(0)}_{1,2}$	9.81i	$u^{(0)}_{1,3}$	13.14i	$u^{(0)}_{1,4}$	1.45i	$u^{(0)}_{1,10}$								
.10	3.05i	$u^{(0)}_{1,1}$	6.80i	$u^{(0)}_{1,2}$	10.35i	$u^{(0)}_{1,3}$	13.87i	$u^{(0)}_{1,4}$	1.49i	$u^{(0)}_{1,5}$								
.15	3.23i	$u^{(0)}_{1,1}$	7.20i	$u^{(0)}_{1,2}$	10.96i	$u^{(0)}_{1,4}$	14.69i	$u^{(0)}_{1,5}$	1.53i	$u^{(0)}_{1,3}$								
.20	3.43i	$u^{(0)}_{1,1}$	7.65i	$u^{(0)}_{1,2}$	11.65i	$u^{(0)}_{1,4}$	15.60i	$u^{(0)}_{1,5}$	1.58i	$u^{(0)}_{1,3}$	15.79i							
.25	3.66i	$u^{(0)}_{1,1}$	8.16i	$u^{(0)}_{1,3}$	12.42i	$u^{(0)}_{1,4}$	16.60i		1.63i	$u^{(0)}_{1,2}$	12.67i	$u^{(0)}_{1,6}$						
.30	3.90i	$u^{(0)}_{1,2}$	8.70i	$u^{(0)}_{1,3}$	13.31i	$u^{(0)}_{1,4}$			1.69i	$u^{(0)}_{1,1}$	10.61i	$u^{(0)}_{1,5}$						
.35	4.20i	$u^{(0)}_{1,2}$	9.40i	$u^{(0)}_{1,3}$	14.33i	$u^{(0)}_{1,5}$			1.75i	$u^{(0)}_{1,1}$	9.15i	$u^{(0)}_{1,4}$						
.40	4.57i	$u^{(0)}_{1,2}$	10.19i	$u^{(0)}_{1,3}$	15.50i	$u^{(0)}_{1,5}$			1.82i	$u^{(0)}_{1,1}$	8.07i	$u^{(0)}_{1,4}$	15.81i					
.45	4.99i	$u^{(0)}_{1,2}$	11.12i	$u^{(0)}_{1,4}$	16.90i				1.90i	$u^{(0)}_{1,1}$	7.25i	$u^{(0)}_{1,3}$	14.09i	$u^{(0)}_{1,6}$				
.50	5.49i	$u^{(0)}_{1,3}$	12.23i	$u^{(0)}_{1,5}$					1.98i	$u^{(0)}_{1,1}$	6.62i	$u^{(0)}_{1,2}$	12.73i	$u^{(0)}_{1,4}$				
.55	6.10i	$u^{(0)}_{1,3}$	13.50i	$u^{(0)}_{1,5}$					2.08i	$u^{(0)}_{1,1}$	6.13i	$u^{(0)}_{1,2}$	11.62i	$u^{(0)}_{1,4}$				
.60	6.86i	$u^{(0)}_{1,4}$	15.29i	$u^{(0)}_{1,6}$					2.18i	$u^{(0)}_{1,1}$	5.76i	$u^{(0)}_{1,2}$	10.72i	$u^{(0)}_{1,3}$	15.88			
.65	7.80i	$u^{(0)}_{1,4}$	17.48i						2.30i	$u^{(0)}_{1,1}$	5.50i	$u^{(0)}_{1,2}$	9.98i	$u^{(0)}_{1,3}$	14.70i	$u^{(0)}_{1,5}$		
.70	9.15i	$u^{(0)}_{1,5}$							2.41i	$u^{(0)}_{1,1}$	5.35i	$u^{(0)}_{1,2}$	9.37i	$u^{(0)}_{1,3}$	13.72i	$u^{(0)}_{1,4}$		
.75	10.98i	$u^{(0)}_{1,5}$							2.52i	$u^{(0)}_{1,1}$	5.33i	$u^{(0)}_{1,2}$	8.91i	$u^{(0)}_{1,3}$	12.90i	$u^{(0)}_{1,4}$		
.80	13.70i	$u^{(0)}_{1,6}$							2.62i	$u^{(0)}_{1,1}$	5.44i	$u^{(0)}_{1,2}$	8.61i	$u^{(0)}_{1,3}$	12.25i	$u^{(0)}_{1,4}$	16.04i	
.85	18.30i	$u^{(0)}_{1,7}$							2.69i	$u^{(0)}_{1,1}$	5.69i	$u^{(0)}_{1,2}$	8.55i	$u^{(0)}_{1,3}$	11.80i	$u^{(0)}_{1,4}$	15.29i	$u^{(0)}_{1,5}$
.90									2.73i	$u^{(0)}_{1,1}$	5.96i	$u^{(0)}_{1,2}$	8.86i	$u^{(0)}_{1,3}$	11.77i	$u^{(0)}_{1,4}$	14.87i	$u^{(0)}_{1,5}$
.95									2.74i	$u^{(0)}_{1,1}$	6.10i	$u^{(0)}_{1,2}$	9.25i	$u^{(0)}_{1,3}$	12.32i	$u^{(0)}_{1,4}$	15.33i	$u^{(0)}_{1,5}$

Table 3.1. Initial ($u^{(k)}_{1,n'}$) and Terminal Positions ($u^{(0)}_{1,n'}$) of E-Mode Trajectories for Increasing z_s from 0 to ∞

d/a	$u^{(1)}_{2,1}$	$u^{(0)}_{2,n'}$	$u^{(1)}_{2,2}$	$u^{(0)}_{2,n'}$	$u^{(1)}_{2,3}$	$u^{(0)}_{2,n'}$	$u^{(1)}_{2,4}$	$u^{(0)}_{2,n'}$	$u^{(2)}_{2,1}$	$u^{(0)}_{2,n'}$	$u^{(2)}_{2,2}$	$u^{(0)}_{2,n'}$	$u^{(2)}_{2,3}$	$u^{(0)}_{2,n'}$	$u^{(2)}_{2,4}$	$u^{(0)}_{2,n'}$	$u^{(2)}_{2,5}$
.05	4.07i	$u^{(0)}_{2,1}$	7.83i	$u^{(0)}_{2,2}$	11.28i	$u^{(0)}_{2,3}$	14.65i	$u^{(0)}_{2,4}$	2.51i	$u^{(0)}_{2,10}$							
.10	4.30i	$u^{(0)}_{2,1}$	8.27i	$u^{(0)}_{2,2}$	11.90i	$u^{(0)}_{2,3}$	15.47i	$u^{(0)}_{2,4}$	2.58i	$u^{(0)}_{2,5}$							
.15	4.55i	$u^{(0)}_{2,1}$	8.76i	$u^{(0)}_{2,2}$	12.60i	$u^{(0)}_{2,4}$	16.38i		2.66i	$u^{(0)}_{2,3}$							
.20	4.84i	$u^{(0)}_{2,1}$	9.30i	$u^{(0)}_{2,3}$	13.39i	$u^{(0)}_{2,4}$			2.74i	$u^{(0)}_{2,2}$	15.95i						
.25	5.16i	$u^{(0)}_{2,2}$	9.92i	$u^{(0)}_{2,3}$	14.28i	$u^{(0)}_{2,4}$			2.83i	$u^{(0)}_{2,1}$	12.88i	$u^{(0)}_{2,6}$					
.30	5.53i	$u^{(0)}_{2,2}$	10.63i	$u^{(0)}_{2,3}$	15.30i	$u^{(0)}_{2,4}$			2.92i	$u^{(0)}_{2,1}$	10.88i	$u^{(0)}_{2,5}$					
.35	5.95i	$u^{(0)}_{2,2}$	11.45i	$u^{(0)}_{2,3}$	16.48i				3.03i	$u^{(0)}_{2,1}$	9.49i	$u^{(0)}_{2,4}$					
.40	6.45i	$u^{(0)}_{2,2}$	12.40i	$u^{(0)}_{2,4}$					3.14i	$u^{(0)}_{2,1}$	8.50i	$u^{(0)}_{2,3}$	16.03i				
.45	7.04i	$u^{(0)}_{2,3}$	13.55i	$u^{(0)}_{2,4}$					3.26i	$u^{(0)}_{2,1}$	7.77i	$u^{(0)}_{2,2}$	14.35i	$u^{(0)}_{2.5}$			
.50	7.74i	$u^{(0)}_{2,3}$	14.89i	$u^{(0)}_{2,5}$					3.39i	$u^{(0)}_{2,1}$	7.26i	$u^{(0)}_{2,2}$	13.05i	$u^{(0)}_{2,4}$			
.55	8.60i	$u^{(0)}_{2,4}$	16.54i	$u^{(0)}_{2,6}$					3.51i	$u^{(0)}_{2,1}$	6.92i	$u^{(0)}_{2,2}$	12.02i	$u^{(0)}_{2,3}$			
.60	9.68i	$u^{(0)}_{2,4}$							3.63i	$u^{(0)}_{2,1}$	6.74i	$u^{(0)}_{2,2}$	11.21i	$u^{(0)}_{2,3}$	16.19i		
.65	10.06i	$u^{(0)}_{2,5}$							3.72i	$u^{(0)}_{2,1}$	6.71i	$u^{(0)}_{2,2}$	10.59i	$u^{(0)}_{2,3}$	15.10i	$u^{(0)}_{2,4}$	
.70	12.90i	$u^{(0)}_{2,6}$							3.79i	$u^{(0)}_{2,1}$	6.82i	$u^{(0)}_{2,2}$	10.18i	$u^{(0)}_{2,3}$	14.23i	$u^{(0)}_{2,4}$	
.75	15.48i	$u^{(0)}_{2,6}$							3.84i	$u^{(0)}_{2,1}$	7.04i	$u^{(0)}_{2,2}$	10.00i	$u^{(0)}_{2,3}$	13.59i	$u^{(0)}_{2,4}$	
.80	19.35i								3.86i	$u^{(0)}_{2,1}$	7.26i	$u^{(0)}_{2,2}$	10.13i	$u^{(0)}_{2,3}$	13.24i	$u^{(0)}_{2,4}$	
.85									3.88i	$u^{(0)}_{2,1}$	7.39i	$u^{(0)}_{2,2}$	10.46i	$u^{(0)}_{2,3}$	13.36i	$u^{(0)}_{2,4}$	
.90									3.87i	$u^{(0)}_{2,1}$	7.44i	$u^{(0)}_{2,2}$	10.67i	$u^{(0)}_{2,3}$	13.78i	$u^{(0)}_{2,4}$	16.78i
.95									3.87i	$u^{(0)}_{2,1}$	7.44i	$u^{(0)}_{2,2}$	10.71i	$u^{(0)}_{2,3}$	13.92i	$u^{(0)}_{2,4}$	17.09i

Table 3.2. Initial ($u^{(k)}_{2,n'}$) and Terminal Positions ($u^{(0)}_{2,n'}$) of E-Mode Trajectories for Increasing z_s from 0 to ∞

d/a	$u^{(1)}_{3,1}$	$u^{(0)}_{3,n'}$	$u^{(1)}_{3,2}$	$u^{(0)}_{3,n'}$	$u^{(1)}_{3,3}$	$u^{(0)}_{3,n'}$	$u^{(2)}_{3,1}$	$u^{(0)}_{3,n'}$	$u^{(2)}_{3,2}$	$u^{(0)}_{3,n'}$	$u^{(2)}_{3,3}$	$u^{(0)}_{3,n'}$
.05	5.24i	$u^{(0)}_{3,1}$	9.18i	$u^{(0)}_{3,2}$	12.70i	$u^{(0)}_{3,3}$	3.55i					
.10	5.53i	$u^{(0)}_{3,1}$	9.69i	$u^{(0)}_{3,2}$	13.40i	$u^{(0)}_{3,3}$	3.65i	$u^{(0)}_{3,4}$				
.15	5.85i	$u^{(0)}_{3,1}$	10.26i	$u^{(0)}_{3,2}$	14.19i	$u^{(0)}_{3,4}$	3.76i	$u^{(0)}_{3,3}$				
.20	6.22i	$u^{(0)}_{3,2}$	10.90i	$u^{(0)}_{3,3}$	15.08i	$u^{(0)}_{3,4}$	3.87i	$u^{(0)}_{3,1}$				
.25	6.63i	$u^{(0)}_{3,2}$	11.63i	$u^{(0)}_{3,3}$			3.99i	$u^{(0)}_{3,1}$	13.20i			
.30	7.10i	$u^{(0)}_{3,2}$	12.46i	$u^{(0)}_{3,3}$			4.13i	$u^{(0)}_{3,1}$	11.28i			
.35	7.65i	$u^{(0)}_{3,2}$	13.42i	$u^{(0)}_{3,3}$			4.27i	$u^{(0)}_{3,1}$	9.99i	$u^{(0)}_{3,4}$		
.40	8.29i	$u^{(0)}_{3,3}$					4.41i	$u^{(0)}_{3,1}$	9.10i	$u^{(0)}_{3,2}$		
.45	9.04i	$u^{(0)}_{3,3}$					4.55i	$u^{(0)}_{3,1}$	8.51i	$u^{(0)}_{3,2}$		
.50	9.95i	$u^{(0)}_{3,3}$					4.69i	$u^{(0)}_{3,1}$	8.16i	$u^{(0)}_{3,2}$	13.52i	
.55	11.05i	$u^{(0)}_{3,4}$					4.80i	$u^{(0)}_{3,1}$	8.01i	$u^{(0)}_{3,2}$	12.59i	
.60	12.43i	$u^{(0)}_{3,5}$					4.88i	$u^{(0)}_{3,1}$	8.03i	$u^{(0)}_{3,2}$	11.92i	
.65	14.21i	$u^{(0)}_{3,5}$					4.93i	$u^{(0)}_{3,1}$	8.20i	$u^{(0)}_{3,2}$	11.51i	
.70							4.96i	$u^{(0)}_{3,1}$	8.42i	$u^{(0)}_{3,2}$	11.38i	
.75							4.97i	$u^{(0)}_{3,1}$	8.60i	$u^{(0)}_{3,2}$	11.55i	
.80							4.97i	$u^{(0)}_{3,1}$	8.69i	$u^{(0)}_{3,2}$	11.86i	
.85							4.97i	$u^{(0)}_{3,1}$	8.72i	$u^{(0)}_{3,2}$	12.02i	$u^{(0)}_{3,3}$
.90							4.97i	$u^{(0)}_{3,1}$	8.72i	$u^{(0)}_{3,2}$	12.06i	$u^{(0)}_{3,3}$
.95							4.97i	$u^{(0)}_{3,1}$	8.72i	$u^{(0)}_{3,2}$	12.06i	$u^{(0)}_{3,3}$

Table 3.3. Initial ($u^{(k)}_{3,n'}$) and Terminal Positions ($u^{(0)}_{3,n'}$) of E-Mode Trajectories for Increasing z_s

d/a	$u^{(1)}_{4,1}$	$u^{(0)}_{4,n'}$	$u^{(1)}_{4,2}$	$u^{(0)}_{4,n'}$	$u^{(2)}_{4,1}$	$u^{(0)}_{4,n'}$	$u^{(2)}_{4,2}$	$u^{(0)}_{4,n'}$	$u^{(2)}_{4,3}$	$u^{(0)}_{4,n'}$
.05	6.38i	$u^{(0)}_{4,1}$	10.49i	$u^{(0)}_{4,2}$	4.59i	$u^{(0)}_{4,7}$				
.10	6.74i	$u^{(0)}_{4,1}$	11.08i	$u^{(0)}_{4,2}$	4.71i	$u^{(0)}_{4,4}$				
.15	7.13i	$u^{(0)}_{4,1}$	11.73i	$u^{(0)}_{4,3}$	4.85i	$u^{(0)}_{4,2}$				
.20	7.58i	$u^{(0)}_{4,2}$	12.46i		5.00i	$u^{(0)}_{4,1}$				
.25	8.08i	$u^{(0)}_{4,2}$	13.29i		5.15i	$u^{(0)}_{4,1}$	13.60i			
.30	8.66i	$u^{(0)}_{4,2}$	14.24i		5.32i	$u^{(0)}_{4,1}$	11.79i			
.35	9.33i	$u^{(0)}_{4,2}$			5.48i	$u^{(0)}_{4,1}$	10.62i	$u^{(0)}_{4,3}$		
.40	10.10i	$u^{(0)}_{4,3}$			5.65i	$u^{(0)}_{4,1}$	9.87i	$u^{(0)}_{4,2}$		
.45	11.02i				5.79i	$u^{(0)}_{4,1}$	9.44	$u^{(0)}_{4,2}$		
.50	12.12i				5.91i	$u^{(0)}_{4,1}$	9.26	$u^{(0)}_{4,2}$		
.55	13.47i				5.98i	$u^{(0)}_{4,1}$	9.29i	$u^{(0)}_{4,2}$	13.34i	
.60					6.03i	$u^{(0)}_{4,1}$	9.46i	$u^{(0)}_{4,2}$	12.86i	
.65					6.05i	$u^{(0)}_{4,1}$	9.69i	$u^{(0)}_{4,2}$	12.71i	
.70					6.06i	$u^{(0)}_{4,1}$	9.86i	$u^{(0)}_{4,2}$	12.87i	
.75					6.06i	$u^{(0)}_{4,1}$	9.94i	$u^{(0)}_{4,2}$	13.16i	
.80					6.06i	$u^{(0)}_{4,1}$	9.96i	$u^{(0)}_{4,2}$	13.33i	$u^{(0)}_{4,3}$
.85					6.06i	$u^{(0)}_{4,1}$	9.97i	$u^{(0)}_{4,2}$	13.38i	$u^{(0)}_{4,3}$
.90					6.06i	$u^{(0)}_{4,1}$	9.97i	$u^{(0)}_{4,2}$	13.38i	$u^{(0)}_{4,3}$
.95					6.06i	$u^{(0)}_{4,1}$	9.97i	$u^{(0)}_{4,2}$	13.38i	$u^{(0)}_{4,3}$

Table 3.4. Initial ($u^{(k)}_{4,n'}$) and Terminal Positions ($u^{(0)}_{4,n'}$) of E-Mode Trajectories for Increasing z_s

d/a	$u^{(1)}_{5,1}$	$u^{(0)}_{5,n'}$	$u^{(1)}_{5,2}$	$u^{(0)}_{5,n'}$	$u^{(2)}_{5,1}$	$u^{(0)}_{5,n'}$	$u^{(2)}_{5,2}$	$u^{(0)}_{5,n'}$
.05	7.52i	$u^{(0)}_{5,1}$	11.78i	$u^{(0)}_{5,2}$	5.62i			
.10	7.93i	$u^{(0)}_{5,1}$			5.77i	$u^{(0)}_{5,4}$		
.15	8.40i	$u^{(0)}_{5,2}$			5.94i	$u^{(0)}_{5,1}$		
.20	8.93i	$u^{(0)}_{5,2}$			6.12i	$u^{(0)}_{5,1}$		
.25	9.52i	$u^{(0)}_{5,2}$			6.30i	$u^{(0)}_{5,1}$	14.09i	
.30	10.20i	$u^{(0)}_{5,2}$			6.49i	$u^{(0)}_{5,1}$	12.40i	
.35	10.98i				6.68i	$u^{(0)}_{5,1}$	11.37i	
.40					6.85i	$u^{(0)}_{5,1}$	10.77i	
.45					6.98i	$u^{(0)}_{5,1}$	10.50i	
.50					7.06i	$u^{(0)}_{5,1}$	10.49i	$u^{(0)}_{5,2}$
.55					7.11i	$u^{(0)}_{5,1}$	10.65i	
.60					7.13i	$u^{(0)}_{5,1}$	10.89i	
.65					7.14i	$u^{(0)}_{5,1}$	11.07i	
.70					7.14i	$u^{(0)}_{5,1}$	11.16i	$u^{(0)}_{5,2}$
.75					7.14i	$u^{(0)}_{5,1}$	11.18i	$u^{(0)}_{5,2}$
.80					7.14i	$u^{(0)}_{5,1}$	11.19i	$u^{(0)}_{5,2}$
.85					7.14i	$u^{(0)}_{5,1}$	11.19i	$u^{(0)}_{5,2}$
.90					7.14i	$u^{(0)}_{5,1}$	11.19i	$u^{(0)}_{5,2}$
.95					7.14i	$u^{(0)}_{5,1}$	11.19i	$u^{(0)}_{5,2}$

Table 3.5. Initial ($u^{(k)}_{5,n'}$) and Terminal Positions ($u^{(0)}_{5,n'}$) of E-Mode Trajectories for Increasing z_s

d/a	$u^{(1)}_{6,1}$	$u^{(0)}_{6,n'}$	$u^{(2)}_{6,1}$	$u^{(0)}_{6,n'}$
.05	8.64i	$u^{(0)}_{6,1}$	6.65i	
.10	9.12i	$u^{(0)}_{6,1}$	6.83i	$u^{(0)}_{6,3}$
.15	9.66i	$u^{(0)}_{6,2}$	7.03i	$u^{(0)}_{6,1}$
.20	10.26i	$u^{(0)}_{6,2}$	7.23i	$u^{(0)}_{6,1}$
.25	10.95i		7.45i	$u^{(0)}_{6,1}$
.30			7.66i	$u^{(0)}_{6,1}$
.35			7.85i	$u^{(0)}_{6,1}$
.40			8.01i	$u^{(0)}_{6,1}$
.45			8.115i	$u^{(0)}_{6,1}$
.50			8.173i	$u^{(0)}_{6,1}$
.55			8.198i	$u^{(0)}_{6,1}$
.60			8.207i	$u^{(0)}_{6,1}$
.65			8.210i	$u^{(0)}_{6,1}$
.70			8.211i	$u^{(0)}_{6,1}$
.75			8.211i	$u^{(0)}_{6,1}$
.80			8.211i	$u^{(0)}_{6,1}$
.85			8.211i	$u^{(0)}_{6,1}$
.90			8.211i	$u^{(0)}_{6,1}$
.95			8.211i	$u^{(0)}_{6,1}$

Table 3.6. Initial ($u^{(k)}_{6,n'}$) and Terminal Positions ($u^{(0)}_{6,n'}$) of E-Mode Trajectories for Increasing z_s

d/a	$u^{(1)}_{7,1}$	$u^{(0)}_{7,n'}$	$u^{(2)}_{7,1}$	$u^{(0)}_{7,n'}$
.05	9.76i	$u^{(0)}_{7,1}$	7.68i	
.10	10.31i	$u^{(0)}_{7,1}$	7.89i	$u^{(0)}_{7,3}$
.15	10.91i		8.11i	$u^{(0)}_{7,1}$
.20			8.35i	$u^{(0)}_{7,1}$
.25			8.59i	$u^{(0)}_{7,1}$
.30			8.81i	$u^{(0)}_{7,1}$
.35			9.01i	$u^{(0)}_{7,1}$
.40			9.14i	$u^{(0)}_{7,1}$
.45			9.222i	$u^{(0)}_{7,1}$
.50			9.258i	$u^{(0)}_{7,1}$
.55			9.271i	$u^{(0)}_{7,1}$
.60			9.274i	$u^{(0)}_{7,1}$
.65			9.275i	$u^{(0)}_{7,1}$
.70			9.275i	$u^{(0)}_{7,1}$
.75			9.275i	$u^{(0)}_{7,1}$
.80			9.275i	$u^{(0)}_{7,1}$
.85			9.275i	$u^{(0)}_{7,1}$
.90			9.275i	$u^{(0)}_{7,1}$
.95			9.275i	$u^{(0)}_{7,1}$

Table 3.7. Initial ($u^{(k)}_{7,n'}$) and Terminal Positions ($u^{(0)}_{7,n'}$) of E-Mode Trajectories for Increasing z_s

d/a	$v^{(1)}_{1,1}$	$v^{(0)}_{1,n'}$	$v^{(1)}_{1,2}$	$v^{(0)}_{1,n'}$	$v^{(1)}_{1,3}$	$v^{(0)}_{1,n'}$	$v^{(2)}_{1,1}$	$v^{(0)}_{1,n'}$	$v^{(2)}_{1,2}$	$v^{(0)}_{1,n'}$	$v^{(2)}_{1,3}$	$v^{(0)}_{1,n'}$
.05	4.730i	$v^{(0)}_{1,1}$	8.132i	$v^{(0)}_{1,2}$	11.478i	$v^{(0)}_{1,3}$						
.10	4.993i	$v^{(0)}_{1,1}$	8.584i	$v^{(0)}_{1,2}$	12.116i	$v^{(0)}_{1,3}$						
.15	5.286i	$v^{(0)}_{1,1}$	9.089i	$v^{(0)}_{1,2}$	12.828i							
.20	5.617i	$v^{(0)}_{1,1}$	9.657i	$v^{(0)}_{1,3}$	13.630i		15.787i	$v^{(0)}_{1,3}$				
.25	5.991i	$v^{(0)}_{1,1}$	10.300i	$v^{(0)}_{1,3}$			12.671i	$v^{(0)}_{1,2}$				
.30	6.419i	$v^{(0)}_{1,2}$	11.036i	$v^{(0)}_{1,3}$			10.604i	$v^{(0)}_{1,1}$				
.35	6.913i	$v^{(0)}_{1,2}$	11.885i	$v^{(0)}_{1,3}$			9.141i	$v^{(0)}_{1,1}$				
.40	7.489i	$v^{(0)}_{1,2}$	12.875i	$v^{(0)}_{1,4}$			8.055i	$v^{(0)}_{1,1}$				
.45	8.170i	$v^{(0)}_{1,2}$	14.046i	$v^{(0)}_{1,4}$			7.224i	$v^{(0)}_{1,1}$				
.50	8.987i	$v^{(0)}_{1,i}$					6.572i	$v^{(0)}_{1,2}$				
.55	9.985i	$v^{(0)}_{1,2}$					6.054i	$v^{(0)}_{1,1}$				
.60	11.233i	$v^{(0)}_{1,2}$					5.639i	$v^{(0)}_{1,1}$	10.699i	$v^{(0)}_{1,3}$		
.65	12.838i	$v^{(0)}_{1,2}$					5.307i	$v^{(0)}_{1,1}$	9.943i	$v^{(0)}_{1,3}$		
.70	14.978i	$v^{(0)}_{1,3}$					5.043i	$v^{(0)}_{1,1}$	9.314i	$v^{(0)}_{1,2}$		
.75							4.838i	$v^{(0)}_{1,1}$	8.796i	$v^{(0)}_{1,2}$		
.80							4.686i	$v^{(0)}_{1,1}$	8.378i	$v^{(0)}_{1,2}$		
.85							4.583i	$v^{(0)}_{1,1}$	8.060i	$v^{(0)}_{1,2}$		
.90							4.522i	$v^{(0)}_{1,1}$	7.847i	$v^{(0)}_{1,2}$		
.95							4.497i	$v^{(0)}_{1,1}$	7.743i	$v^{(0)}_{1,2}$	10.951i	$v^{(0)}_{1,3}$

Table 3.8. Initial ($v^{(k)}_{1,n'}$) and Terminal Positions ($v^{(0)}_{1,n'}$) of H-Mode Trajectories for Increasing z_s

d/a	$v_{2,1}^{(1)}$	$v_{2,n'}^{(0)}$	$v_{2,2}^{(1)}$	$v_{2,n'}^{(0)}$	$v_{2,3}^{(1)}$	$v_{2,n'}^{(0)}$	$v_{2,1}^{(2)}$	$v_{2,n'}^{(0)}$	$v_{2,2}^{(2)}$	$v_{2,n'}^{(0)}$	$v_{2,3}^{(2)}$	$v_{2,n'}^{(0)}$
.05	6.067i	$v_{2,1}^{(0)}$	9.574i	$v_{2,2}^{(0)}$	12.971i	$v_{2,3}^{(0)}$						
.10	6.404i	$v_{2,1}^{(0)}$	10.106i	$v_{2,2}^{(0)}$	13.692i	$v_{2,3}^{(0)}$						
.15	6.781i	$v_{2,1}^{(0)}$	10.700i	$v_{2,2}^{(0)}$								
.20	7.204i	$v_{2,1}^{(0)}$	11.369i	$v_{2,3}^{(0)}$			15.943i	$v_{2,2}^{(0)}$				
.25	7.685i	$v_{2,2}^{(0)}$	12.127i	$v_{2,3}^{(0)}$			12.877i	$v_{2,1}^{(0)}$				
.30	8.234i	$v_{2,2}^{(0)}$	12.993i	$v_{2,3}^{(0)}$			10.866i	$v_{2,1}^{(0)}$				
.35	8.867i	$v_{2,2}^{(0)}$	13.992i	$v_{2,4}^{(0)}$			9.462i	$v_{2,1}^{(0)}$				
.40	9.606i	$v_{2,2}^{(0)}$	15.158i	$v_{2,4}^{(0)}$			8.443i	$v_{2,1}^{(0)}$				
.45	10.479i	$v_{2,2}^{(0)}$					7.684i	$v_{2,1}^{(0)}$				
.50	11.527i	$v_{2,2}^{(0)}$					7.112i	$v_{2,1}^{(0)}$	13.026i	$v_{2,3}^{(0)}$		
.55	12.808i	$v_{2,2}^{(0)}$					6.680i	$v_{2,1}^{(0)}$	11.979i	$v_{2,3}^{(0)}$		
.60	14.409i	$v_{2,2}^{(0)}$					6.357i	$v_{2,1}^{(0)}$	11.141i	$v_{2,3}^{(0)}$		
.65							6.123i	$v_{2,1}^{(0)}$	10.474i	$v_{2,2}^{(0)}$		
.70							5.961i	$v_{2,1}^{(0)}$	9.955i	$v_{2,2}^{(0)}$		
.75							5.858i	$v_{2,1}^{(0)}$	9.570i	$v_{2,2}^{(0)}$		
.80							5.800i	$v_{2,1}^{(0)}$	9.310i	$v_{2,2}^{(0)}$		
.85							5.773i	$v_{2,1}^{(0)}$	9.164i	$v_{2,2}^{(0)}$		
.90							5.765i	$v_{2,1}^{(0)}$	9.107i	$v_{2,2}^{(0)}$		
.95							5.764i	$v_{2,1}^{(0)}$	9.095i	$v_{2,2}^{(0)}$	12.325i	$v_{2,3}^{(0)}$

Table 3.9. Initial ($v_{2,n'}^{(k)}$) and Terminal Positions ($v_{2,n'}^{(0)}$) of H-Mode Trajectories for Increasing z_s

d/a	$v_{3,1}^{(1)}$	$v_{3,n'}^{(0)}$	$v_{3,2}^{(1)}$	$v_{3,n'}^{(0)}$	$v_{3,1}^{(2)}$	$v_{3,n'}^{(0)}$	$v_{3,2}^{(2)}$	$v_{3,n'}^{(0)}$
.05	7.355i	$v_{3,1}^{(0)}$	10.965i	$v_{3,2}^{(0)}$				
.10	7.764i	$v_{3,1}^{(0)}$	11.575i	$v_{3,2}^{(0)}$				
.15	8.221i	$v_{3,1}^{(0)}$	12.255i					
.20	8.735i	$v_{3,1}^{(0)}$	13.021i					
.25	9.317i	$v_{3,2}^{(0)}$			13.180i	$v_{3,1}^{(0)}$		
.30	9.983i	$v_{3,2}^{(0)}$			11.246i	$v_{3,1}^{(0)}$		
.35	10.751i	$v_{3,2}^{(0)}$			9.924i	$v_{3,1}^{(0)}$		
.40					8.991i	$v_{3,1}^{(0)}$		
.45					8.323i	$v_{3,1}^{(0)}$		
.50					7.845i	$v_{3,1}^{(0)}$		
.55					7.509i	$v_{3,1}^{(0)}$		
.60					7.280i	$v_{3,1}^{(0)}$		
.65					7.135i	$v_{3,1}^{(0)}$		
.70					7.051i	$v_{3,1}^{(0)}$	10.839i	$v_{3,2}^{(0)}$
.75					7.010i	$v_{3,1}^{(0)}$	10.597i	$v_{3,2}^{(0)}$
.80					6.993i	$v_{3,1}^{(0)}$	10.473i	$v_{3,2}^{(0)}$
.85					6.989i	$v_{3,1}^{(0)}$	10.427i	$v_{3,2}^{(0)}$
.90					6.988i	$v_{3,1}^{(0)}$	10.418i	$v_{3,2}^{(0)}$
.95					6.988i	$v_{3,1}^{(0)}$	10.417i	$v_{3,2}^{(0)}$

Table 3.10. Initial ($v_{3,n'}^{(k)}$) and Terminal Positions ($v_{3,n'}^{(0)}$) of H-Mode Trajectories for Increasing z_s

d/a	$v^{(1)}_{4,1}$	$v^{(0)}_{4,n'}$	$v^{(1)}_{4,2}$	$v^{(0)}_{4,n'}$	$v^{(2)}_{4,1}$	$v^{(0)}_{4,n'}$
.05	8.613i	$v^{(0)}_{4,1}$	12.321i	$v^{(0)}_{4,2}$		
.10	9.092i	$v^{(0)}_{4,1}$	13.005			
.15	9.626i	$v^{(0)}_{4,1}$				
.20	10.223i	$v^{(0)}_{4,2}$			16.479i	$v^{(0)}_{4,1}$
.25	10.910i	$v^{(0)}_{4,2}$			13.573i	$v^{(0)}_{4,1}$
.30	11.689i	$v^{(0)}_{4,2}$			11.732i	$v^{(0)}_{4,1}$
.35	12.288i	$v^{(0)}_{4,2}$			10.507i	$v^{(0)}_{4,1}$
.40	13.637i	$v^{(0)}_{4,2}$			9.672i	$v^{(0)}_{4,1}$
.45	14.877i	$v^{(0)}_{4,2}$			9.101i	$v^{(0)}_{4,1}$
.50					8.717i	$v^{(0)}_{4,1}$
.55					8.469i	$v^{(0)}_{4,1}$
.60					8.319i	$v^{(0)}_{4,1}$
.65					8.238i	$v^{(0)}_{4,1}$
.70					8.201i	$v^{(0)}_{4,1}$
.75					8.187i	$v^{(0)}_{4,1}$
.80					8.183i	$v^{(0)}_{4,1}$
.85					8.183i	$v^{(0)}_{4,1}$
.90					8.183i	$v^{(0)}_{4,1}$
.95					8.183i	$v^{(0)}_{4,1}$

Table 3.11. Initial ($v^{(k)}_{v,n'}$) and Terminal Positions ($v^{(0)}_{4,n'}$) of H-Mode Trajectories for Increasing z_s

d/a	$v^{(1)}_{5,1}$	$v^{(0)}_{5,n'}$	$v^{(1)}_{5,2}$	$v^{(0)}_{5,n'}$	$v^{(2)}_{5,1}$	$v^{(0)}_{5,n'}$
.05	9.848i	$v^{(0)}_{5,1}$	13.649i	$v^{(0)}_{5,2}$		
.10	10.395i	$v^{(0)}_{5,1}$				
.15	11.007i	$v^{(0)}_{5,1}$				
.20	11.695i	$v^{(0)}_{5,2}$			16.851i	$v^{(0)}_{5,1}$
.25	12.474i	$v^{(0)}_{5,2}$			14.049i	$v^{(0)}_{5,1}$
.30	13.365i	$v^{(0)}_{5,2}$			12.313i	$v^{(0)}_{5,1}$
.35	14.394i	$v^{(0)}_{5,2}$			11.191i	$v^{(0)}_{5,1}$
.40					10.456i	$v^{(0)}_{5,1}$
.45					9.980i	$v^{(0)}_{5,1}$
.50					9.682i	$v^{(0)}_{5,1}$
.55					9.508i	$v^{(0)}_{5,1}$
.60					9.417i	$v^{(0)}_{5,1}$
.65					9.376i	$v^{(0)}_{5,1}$
.70					9.361i	$v^{(0)}_{5,1}$
.75					9.357i	$v^{(0)}_{5,1}$
.80					9.356i	$v^{(0)}_{5,1}$
.85					9.356i	$v^{(0)}_{5,1}$
.90					9.356i	$v^{(0)}_{5,1}$
.95					9.356i	$v^{(0)}_{5,1}$

Table 3.12. Initial ($v^{(k)}_{5,n'}$) and Terminal Positions ($v^{(0)}_{5,n'}$) of H-Mode Trajectories for Increasing z_s

demonstrate the trajectory of a given pole through the entire z_s spectrum for a fixed d/a. Note that in these graphs only the pole designated has been plotted with no attempt to illustrate various other poles that might come into play in that region of the complex frequency plane of concern. Additional graphs will hopefully clarify the trajectory interaction of the poles originating from the innermost sphere (k = 1) with those from between the liner and the outer shell (k = 2). This approach is simply an effort to organize the data presented and avoid the confusion from the multiplicity of pole patterns that arise for a given area. Because of the extreme variation in pole paths and wide d/a range more than one graph is sometimes employed to avoid undue loss of detail.

As a rough guide to the relation between the pole shift and the change in the resistive load, some trajectories are tagged to indicate the loading at that point. The parameter value at these points is $z_s = .2, .4, .6$. The arrow indicates the direction of movement as z_s increases.

The trajectories of the E and H mode resonant poles arising from the region between the resistive liner and the shell wall are represented individually in figures 3.21 through 3.44. Again several graphs are employed to avoid loss of detail in widely varying loci.

The pole originating at $u^{(2)}_{n,1}$ is of special interest in that it coalesces on the negative Ω axis for certain ranges of the d/a parameter as the loading varies $0 \leq z_s \leq \infty$. In terms of increasing z_s, the pole which coalesces with its image from the lower half plane (complex conjugate)

splits and proceeds positively and negatively along the Ω axis. The pole moving negatively along the Ω axis coalesces again with yet another pole with a positive movement on the Ω axis. After this second collision the trajectory returns to some $u^{(0)}_{n,n'}$ along the $i\omega a/c$ axis as $z_s \longrightarrow \infty$. The "second" positively moving pole is possibly from infinity ($u^{(0)}_{n,\infty}$) or some higher n' pole of the same order. Figure 3.15 depicts the movement involved in the double coalescence. It is obvious that this entire pattern could be repeating any number of times outside the limits under investigation. The interaction of this returning pole with other poles in the region for $n = 1$ (before other $u^{(2)}_{1,n'}$ come into play) is given in figure 3.16.

The point of coalescence and the corresponding resistive value is taken as the definition of critical damping for a given mode (n). Figure 3.17 gives the resistive sheet loading plotted against d/a for critical damping of the lower E modes.

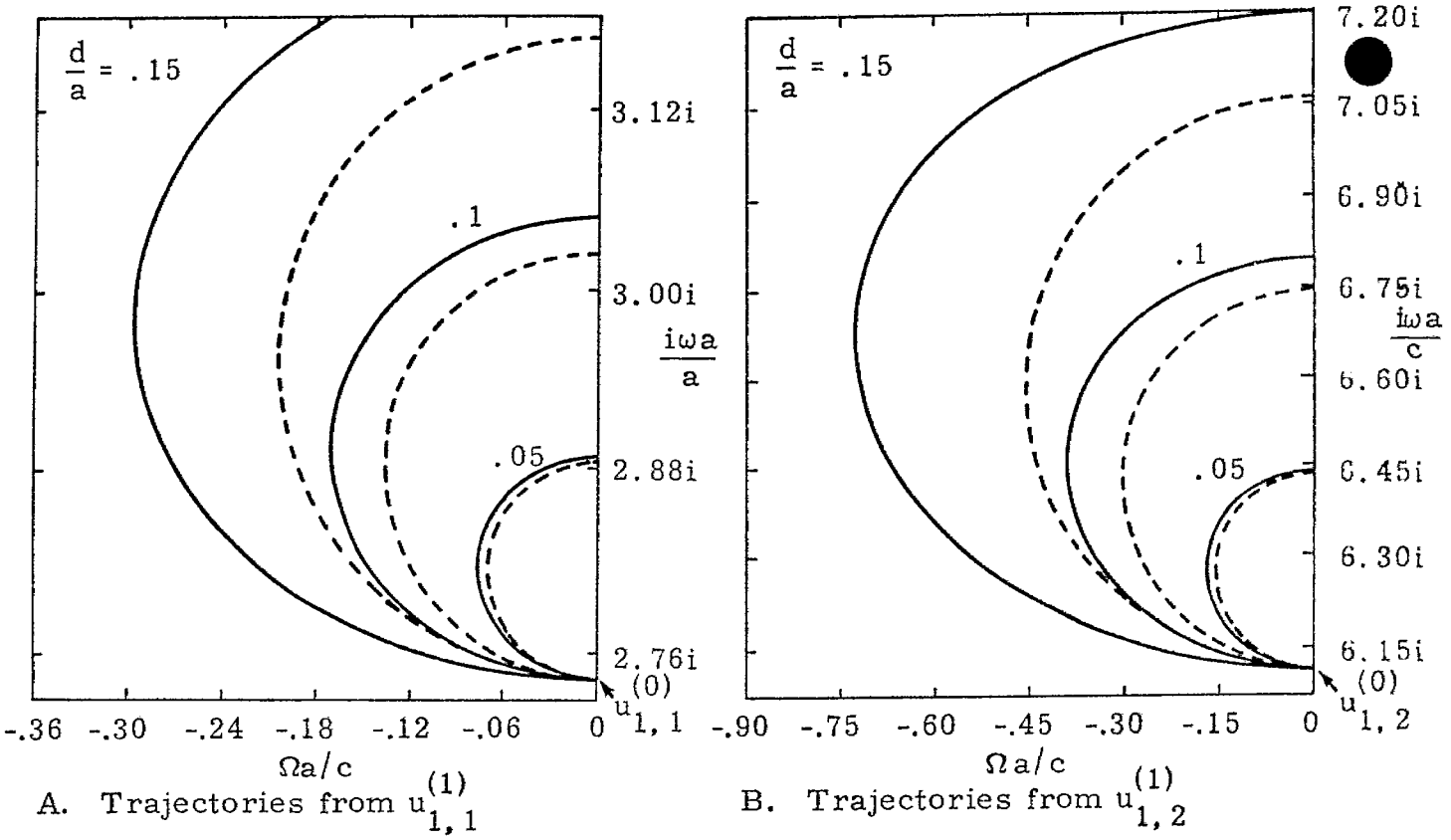

A. Trajectories from $u^{(1)}_{1,1}$

B. Trajectories from $u^{(1)}_{1,2}$

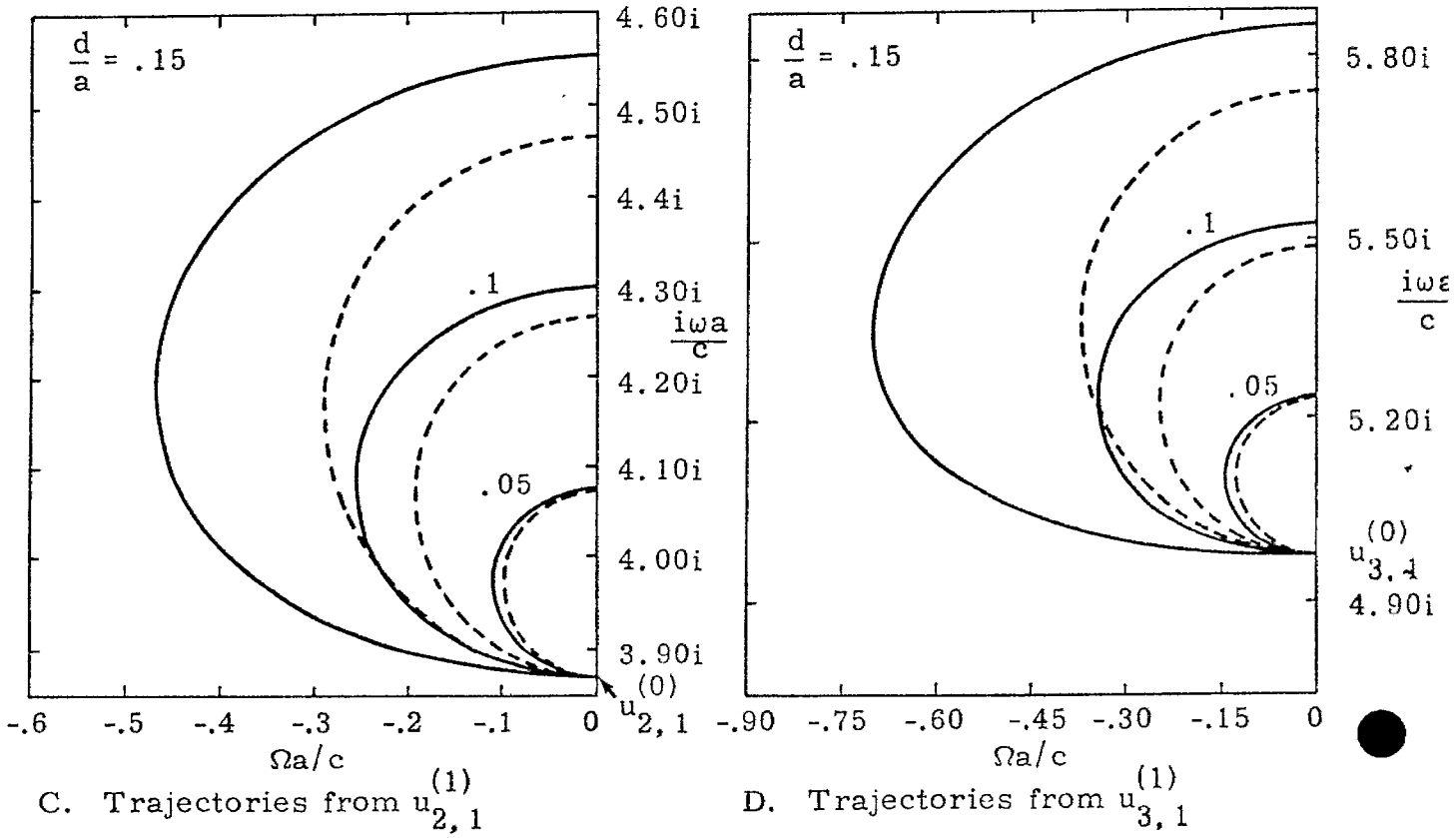

C. Trajectories from $u^{(1)}_{2,1}$

D. Trajectories from $u^{(1)}_{3,1}$

Figure 3.1. Asymptotic Approximation (Dotted Line) Compared to Trajectory for $0 \leq z_s \leq \infty$ of E-Mode Resonances, d/a a Parameter

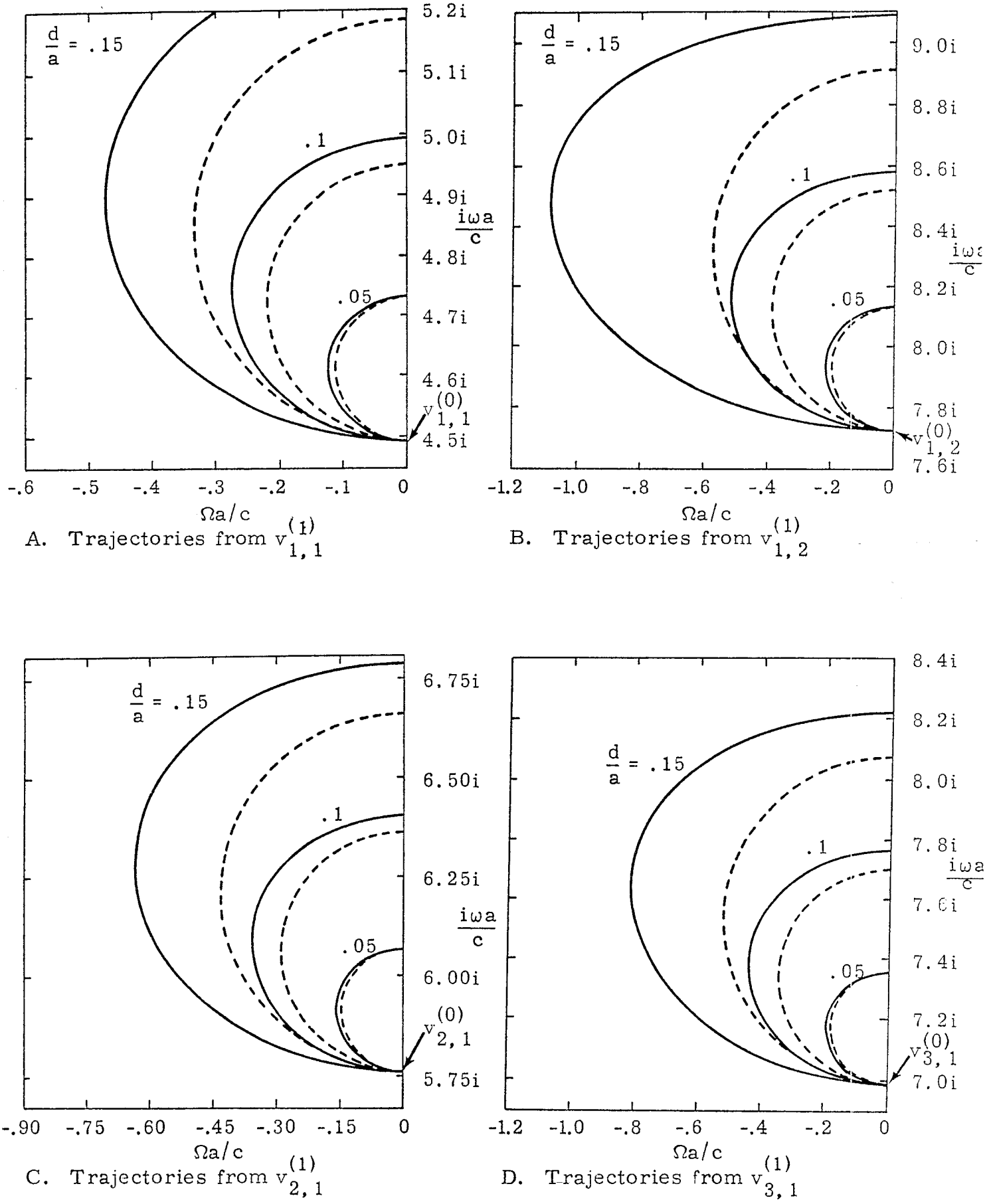

Figure 3.2. Asymptotic Approximation (Dotted Line) Compared to Trajectory for $0 \leq z_s \leq \infty$ of H-Mode Resonances, d/a a Parameter

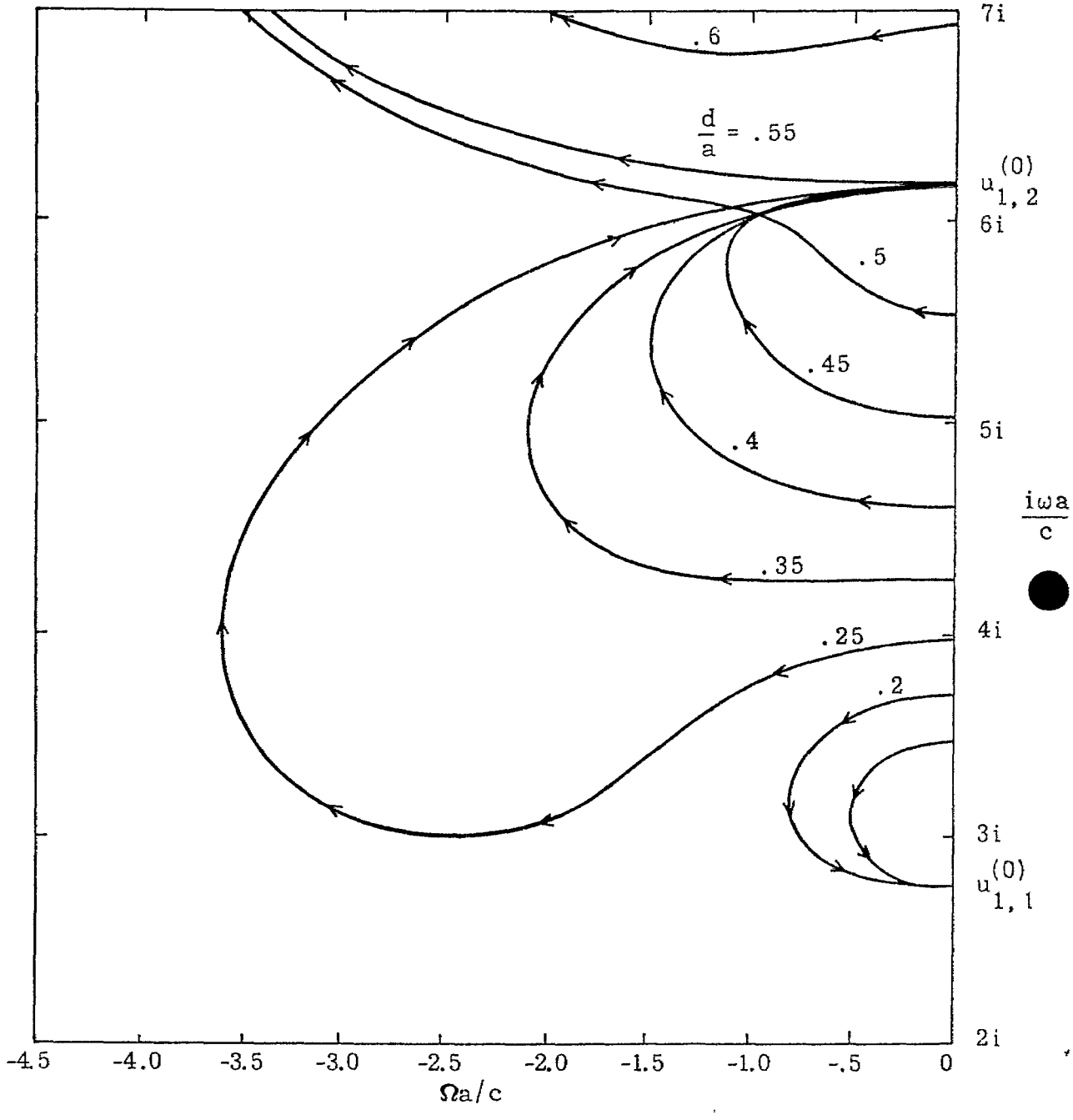

Figure 3.3. Upper Shifting of Trajectories from $u_{1,1}^{(1)}$ as d/a Increases, $0 \leq z_s \leq \infty$; Arrow Indicates Increasing z_s

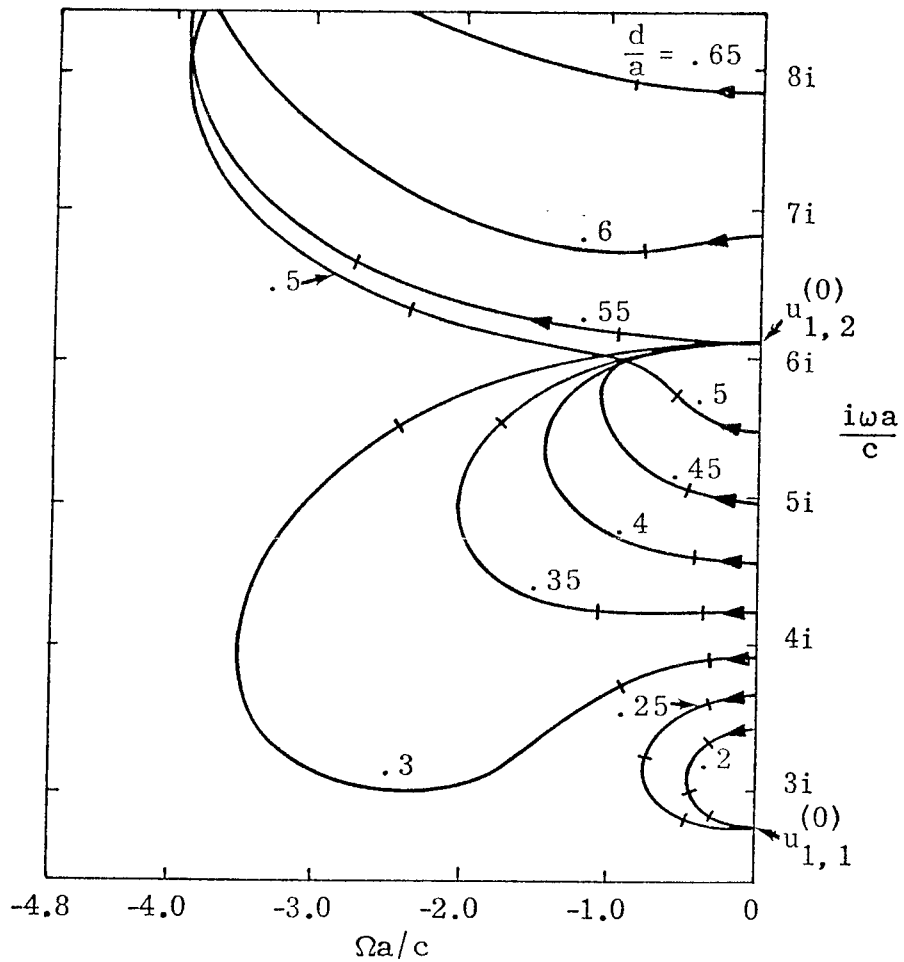

A. Values $.2 \leq d/a \leq .65$ from $u^{(1)}_{1,1}$

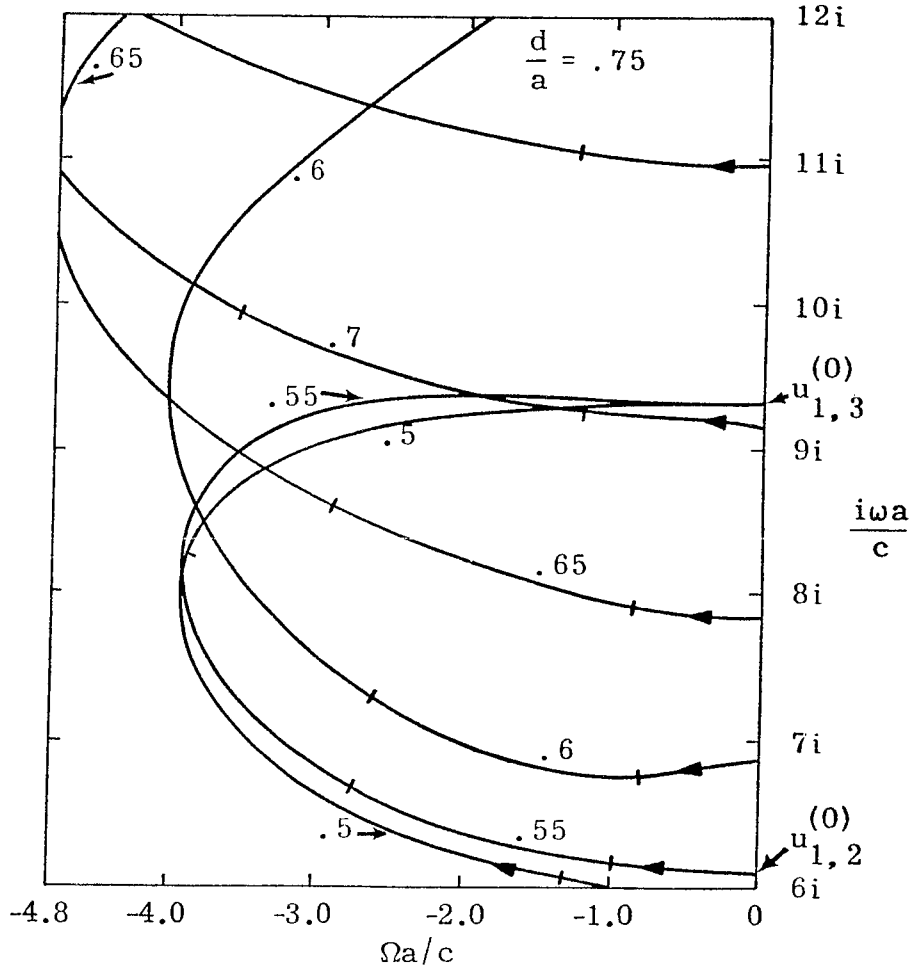

B. Values $.5 \leq d/a \leq .75$ from $u^{(1)}_{1,1}$

Figure 3.4. Trajectories from $u^{(1)}_{1,1}$ for Increasing z_s, $0 \leq z_s \leq \infty$, with d/a a Parameter

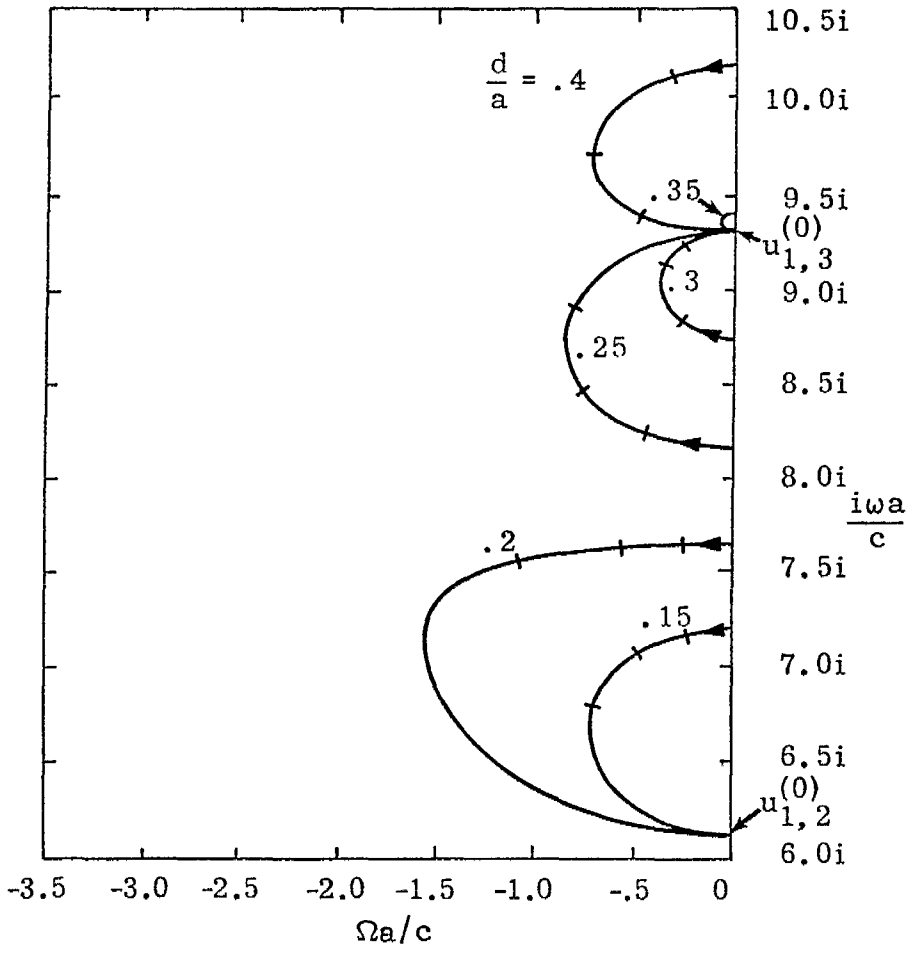

A. $u^{(1)}_{1,2}$

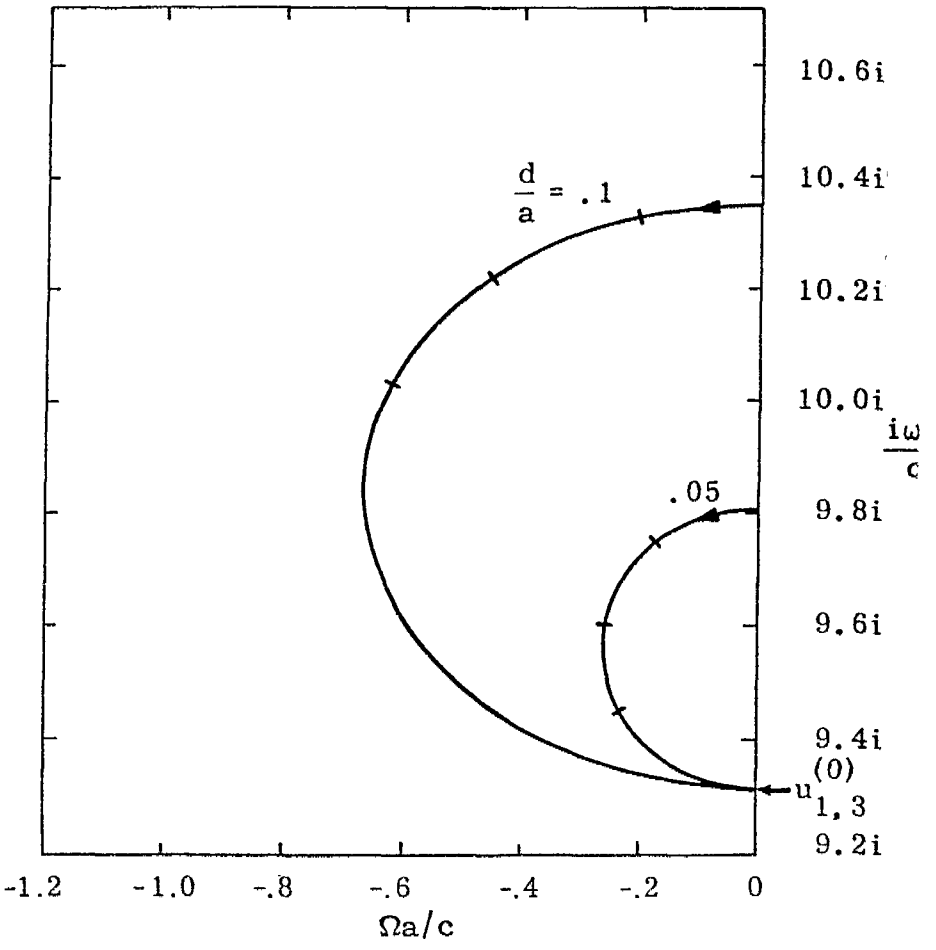

B. $u^{(1)}_{1,3}$

Figure 3.5. Trajectories from $u^{(1)}_{1,n}$, for Increasing z_s, $0 \leq z_s \leq \infty$, with d/a a Parameter

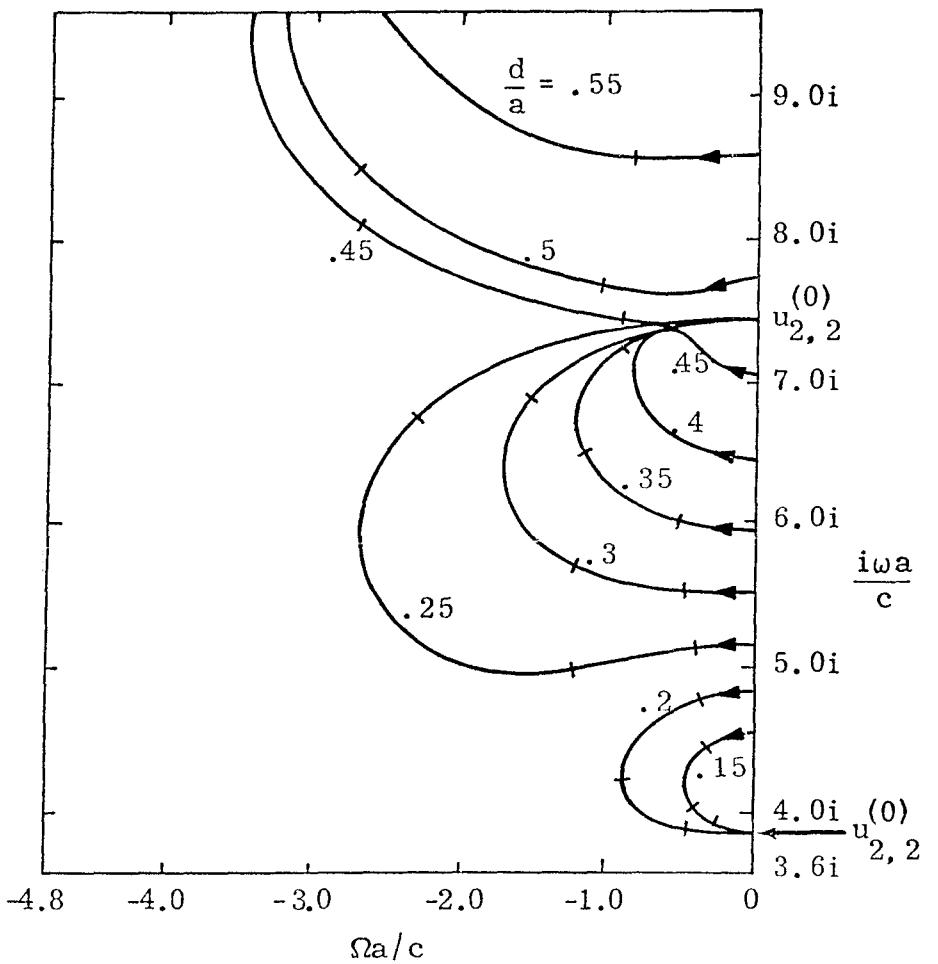

A. Values $.15 \leq d/a \leq .55$ from $u^{(1)}_{2,1}$

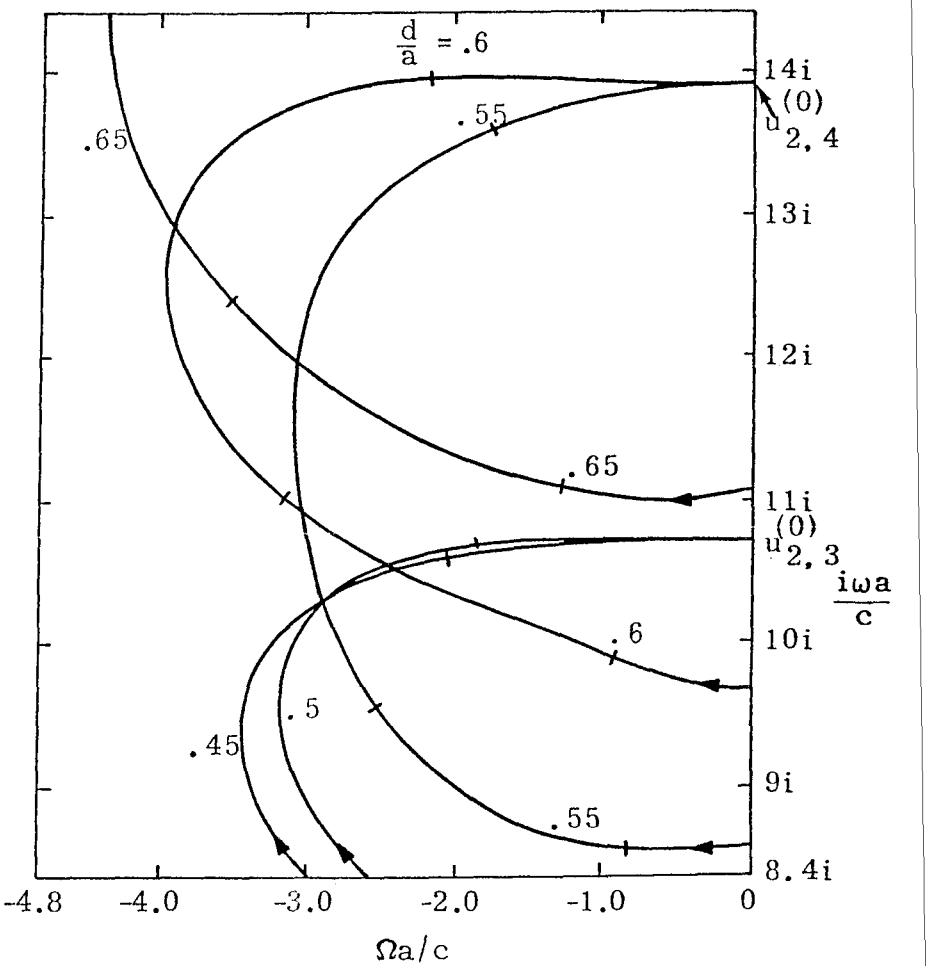

B. Values $.45 \leq d/a \leq .65$ from $u^{(1)}_{2,1}$

Figure 3.6. Trajectories from $u^{(1)}_{2,1}$ for Increasing z_s, $0 \leq z_s \leq \infty$, with d/a a Parameter

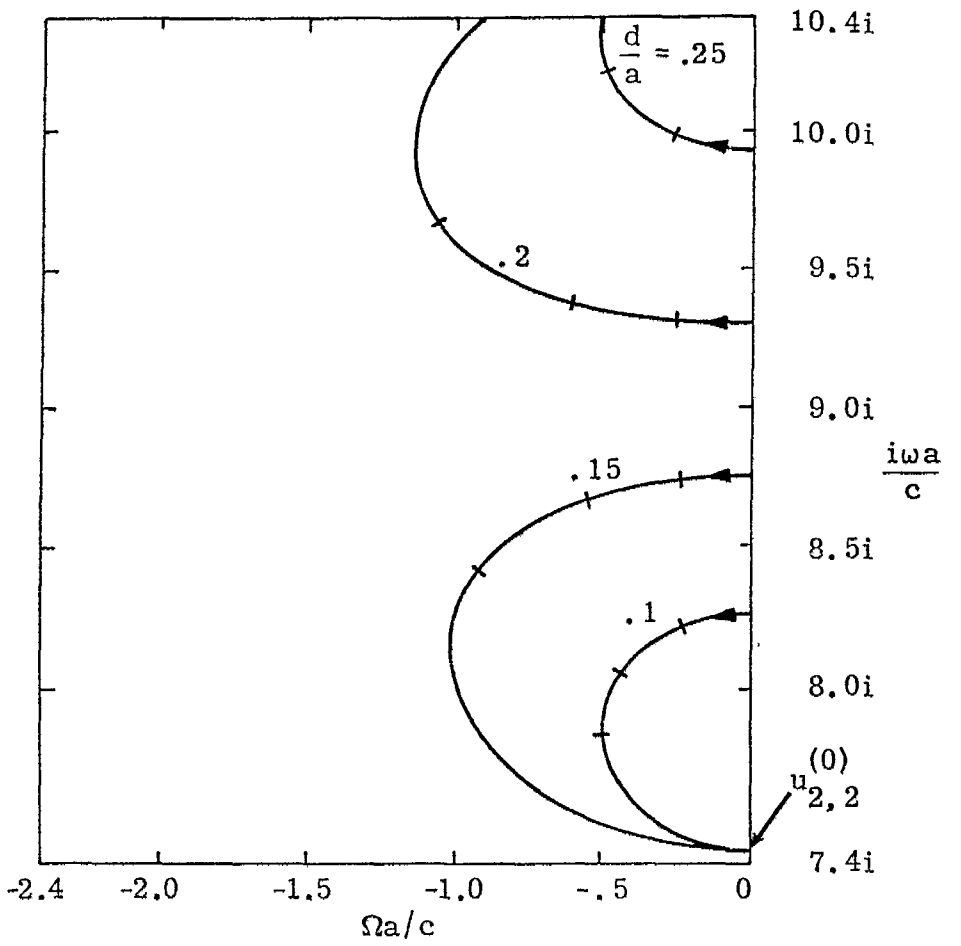

Figure 3.7. Trajectories from $u_{2,2}^{(1)}$ for Increasing z_s, $0 \leq z_s \leq \infty$, with d/a a Parameter

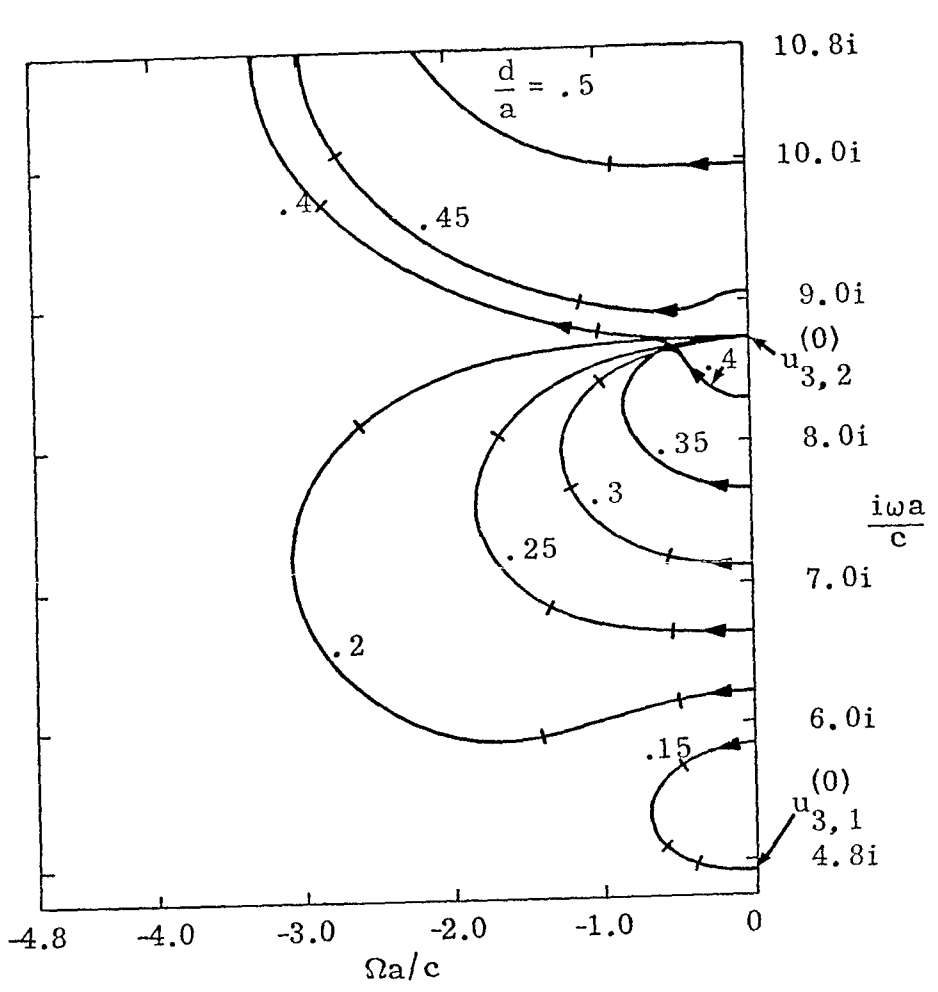

A. $u^{(1)}_{3,1}$

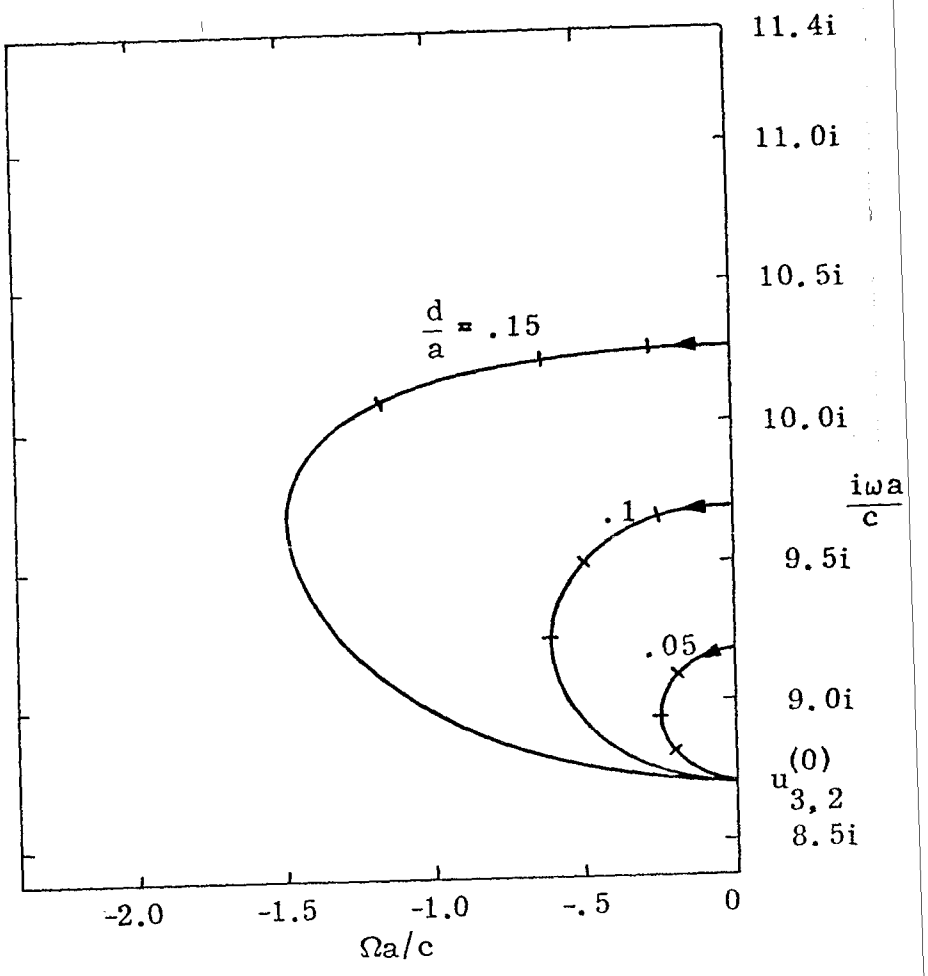

B. $u^{(1)}_{3,2}$

Figure 3.8. Trajectories from $u^{(1)}_{3,n}$, for Increasing z_s, $0 \leq z_s \leq \infty$, with d/a a Parameter

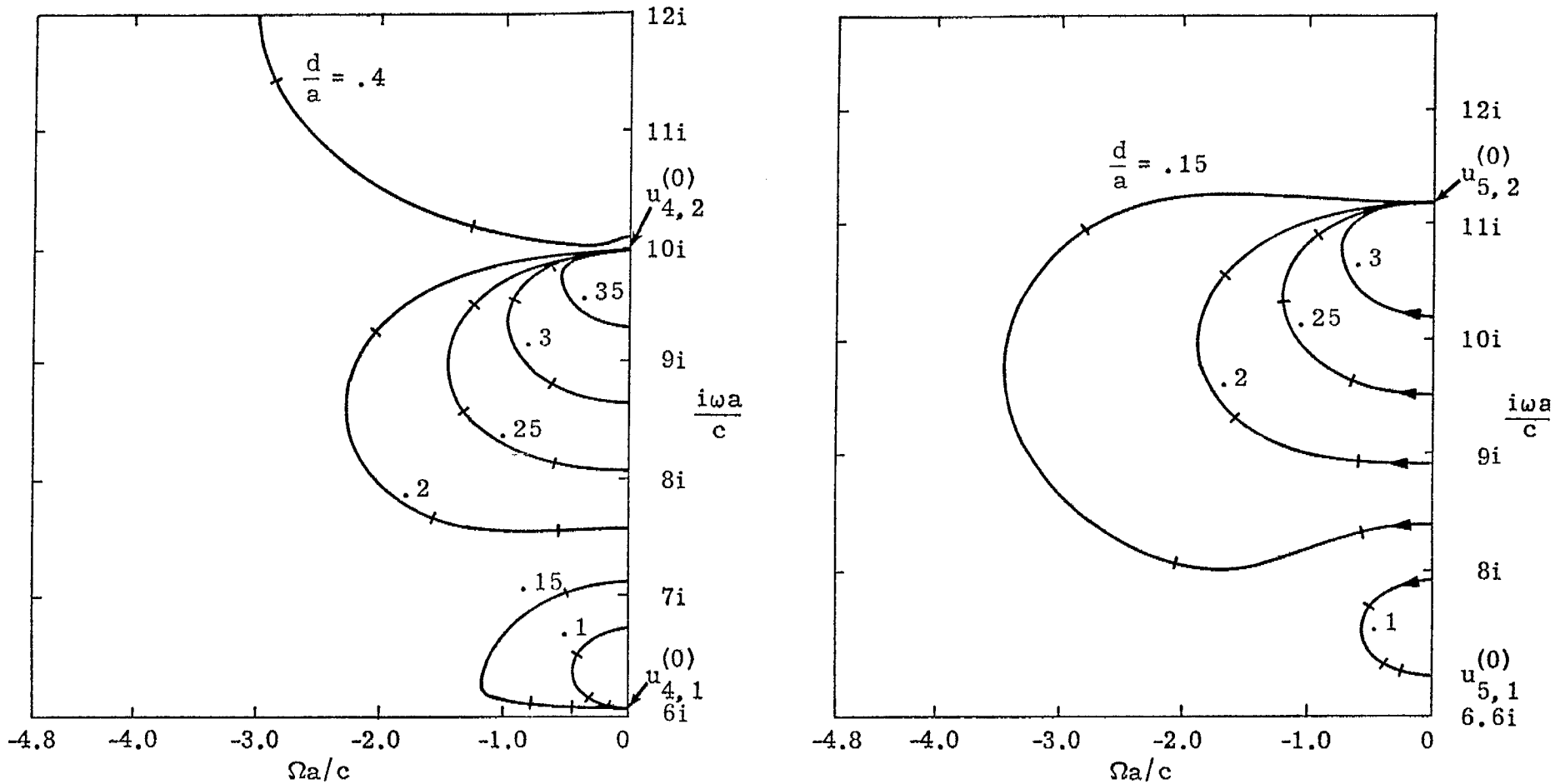

Figure 3.9. Trajectories from $u^{(1)}_{n,1}$ for Increasing z_s, $0 \leq z_s \leq \infty$, with d/a a Parameter

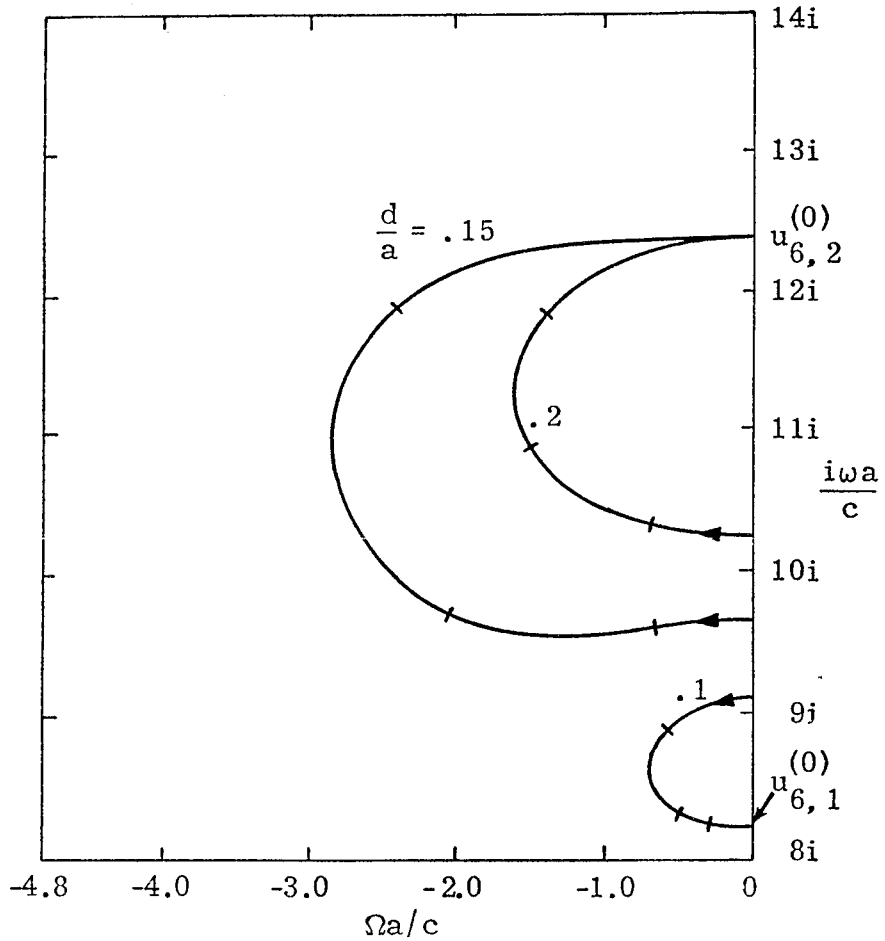

A. $u^{(1)}_{6,1}$

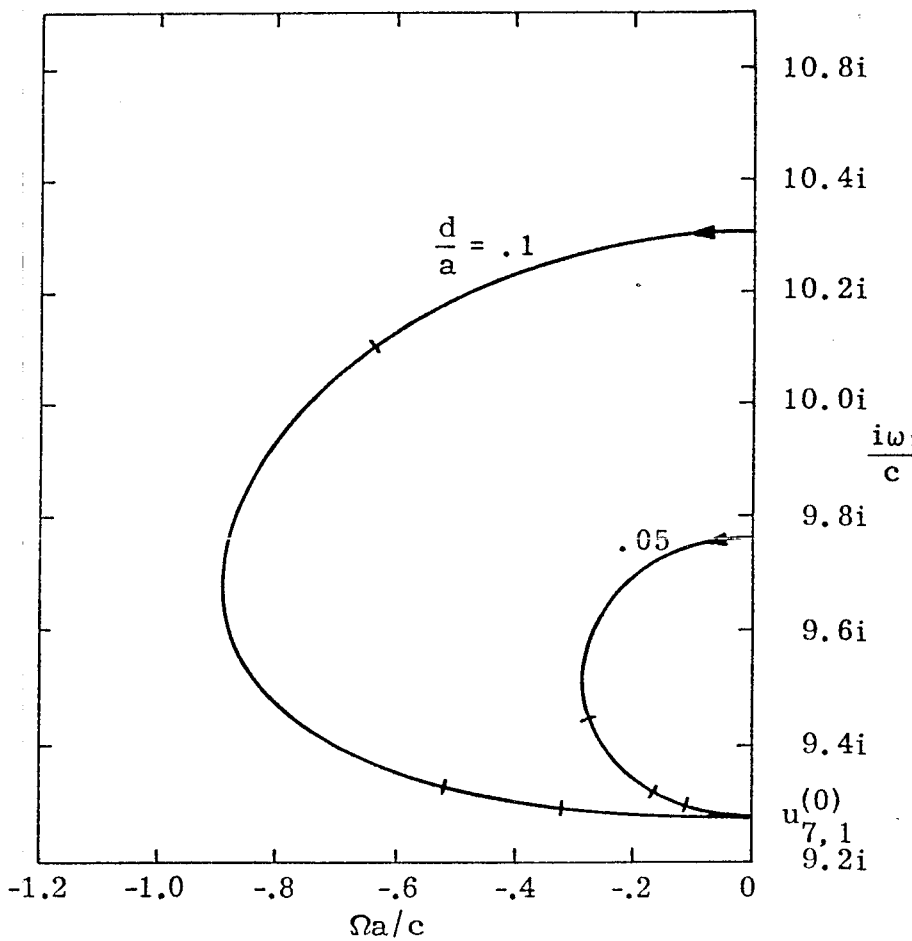

B. $u^{(1)}_{7,1}$

Figure 3.10. Trajectories from $u^{(1)}_{n,1}$ for Increasing z_s, $0 \leq z_s \leq \infty$, with d/a a Parameter

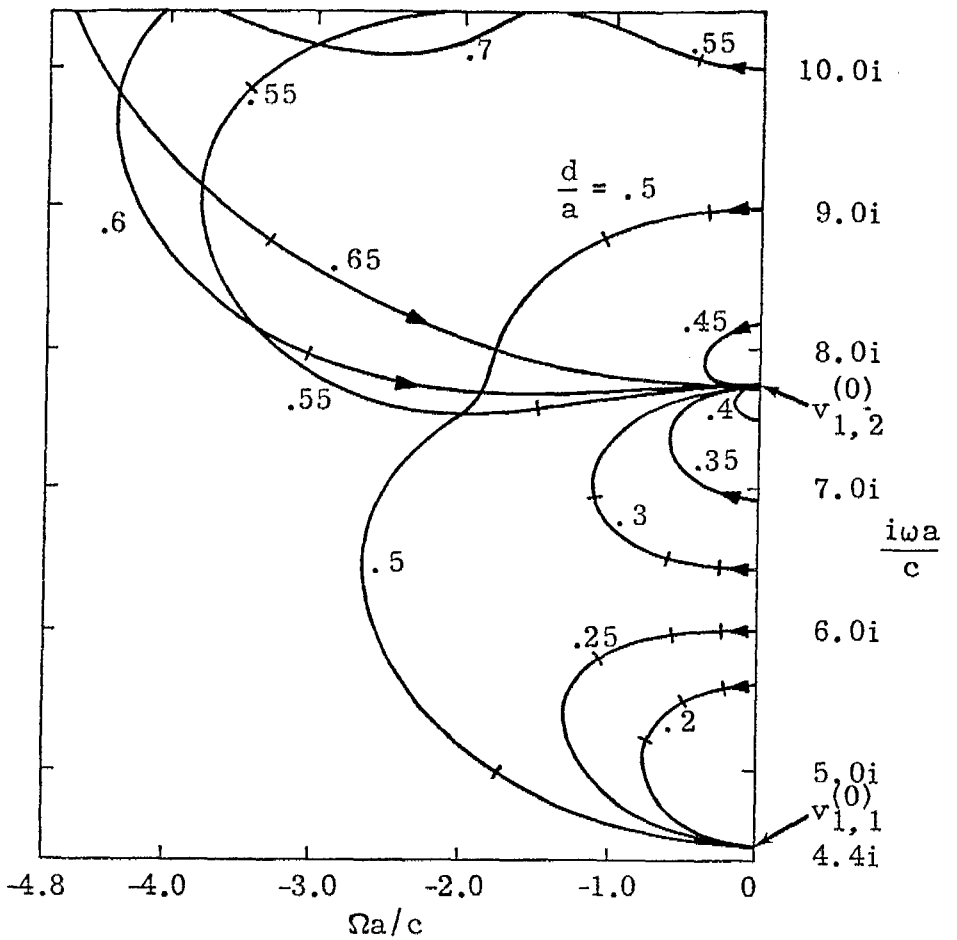

A. $v^{(1)}_{1,1}$

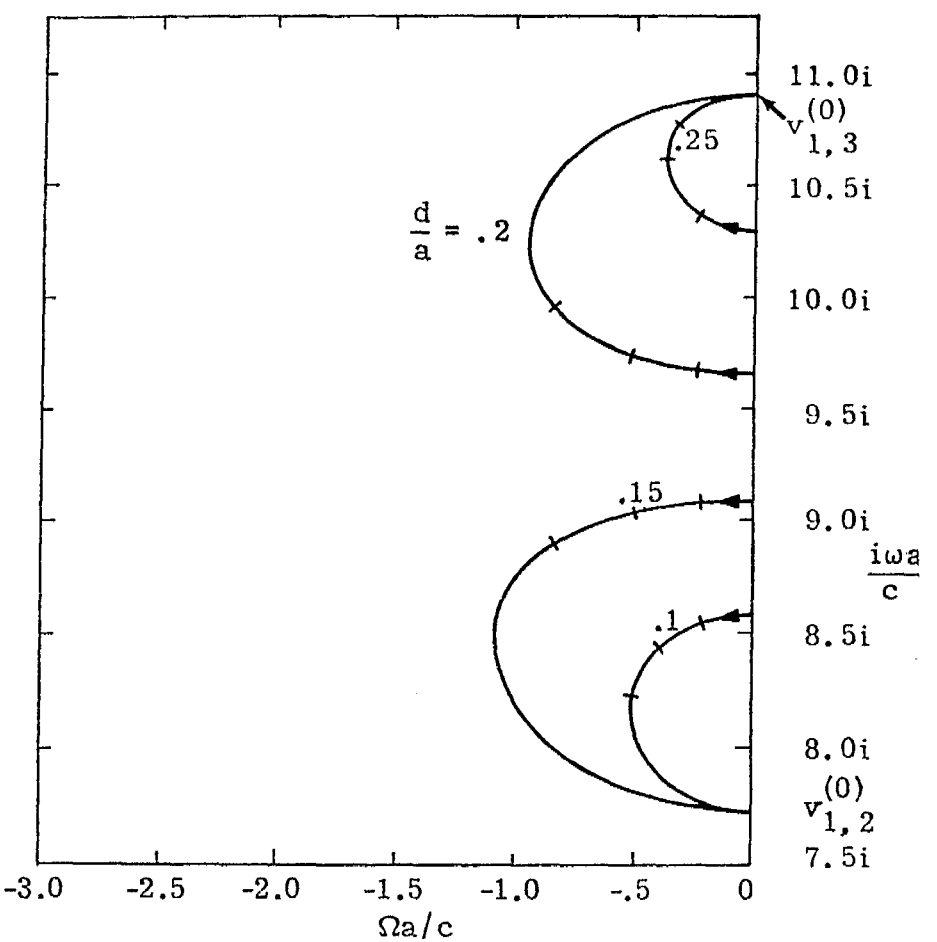

B. $v^{(1)}_{1,2}$

Figure 3.11. Trajectories from $v^{(1)}_{1,n}$, for Increasing z_s, $0 \leq z_s \leq \infty$, with d/a a Parameter

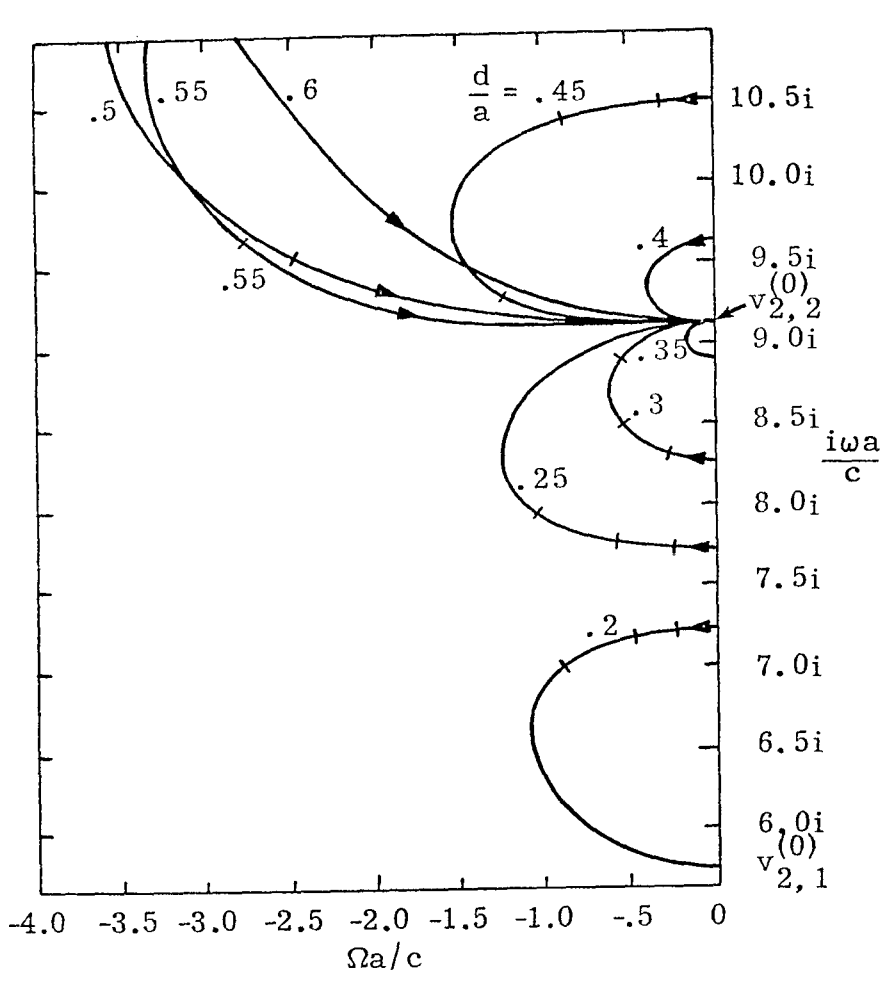

A. $v^{(1)}_{2,1}$

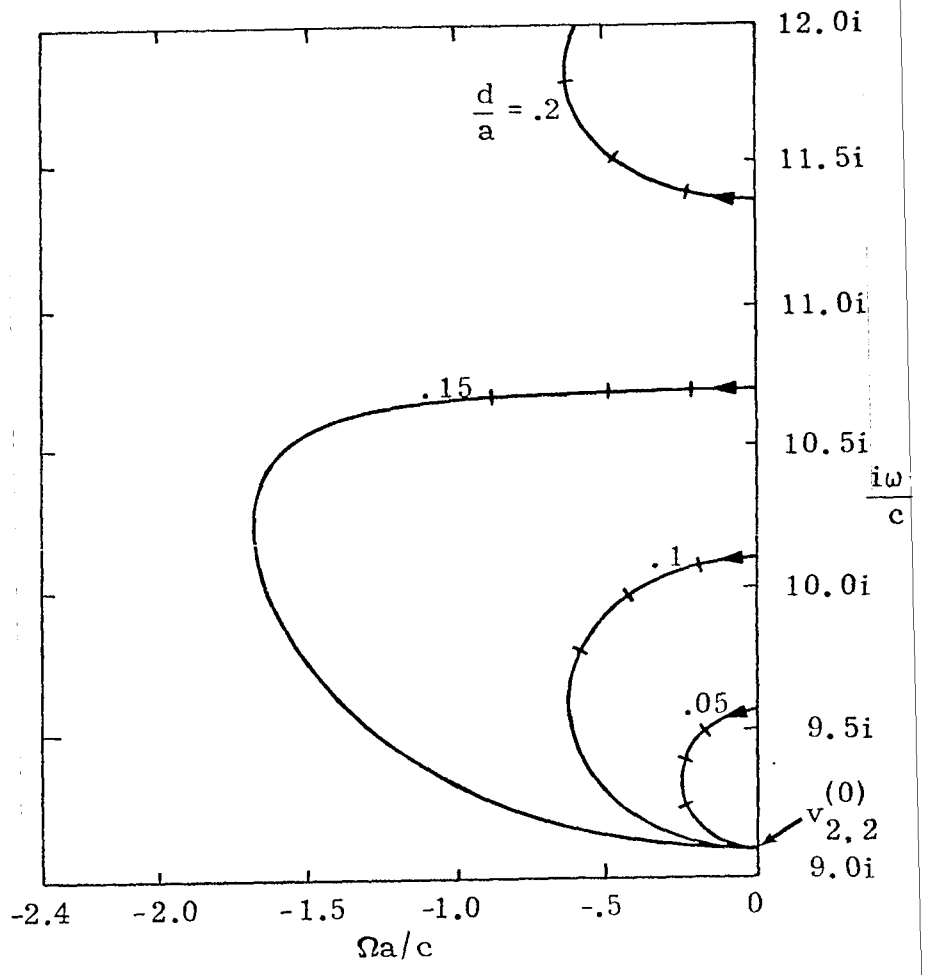

B. $v^{(1)}_{2,2}$

Figure 3.12. Trajectories from $v^{(1)}_{2,n}$ for Increasing z_s, $0 \leq z_s \leq \infty$, with d/a a Parameter

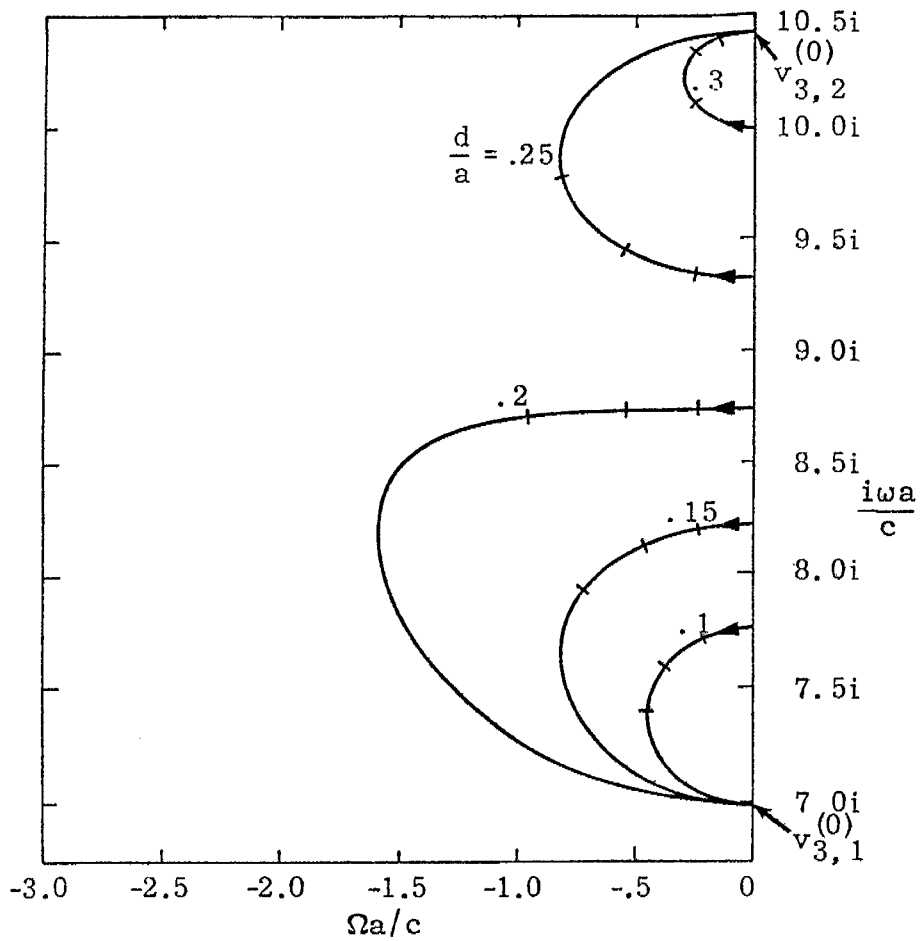

A. $v^{(1)}_{3,1}$

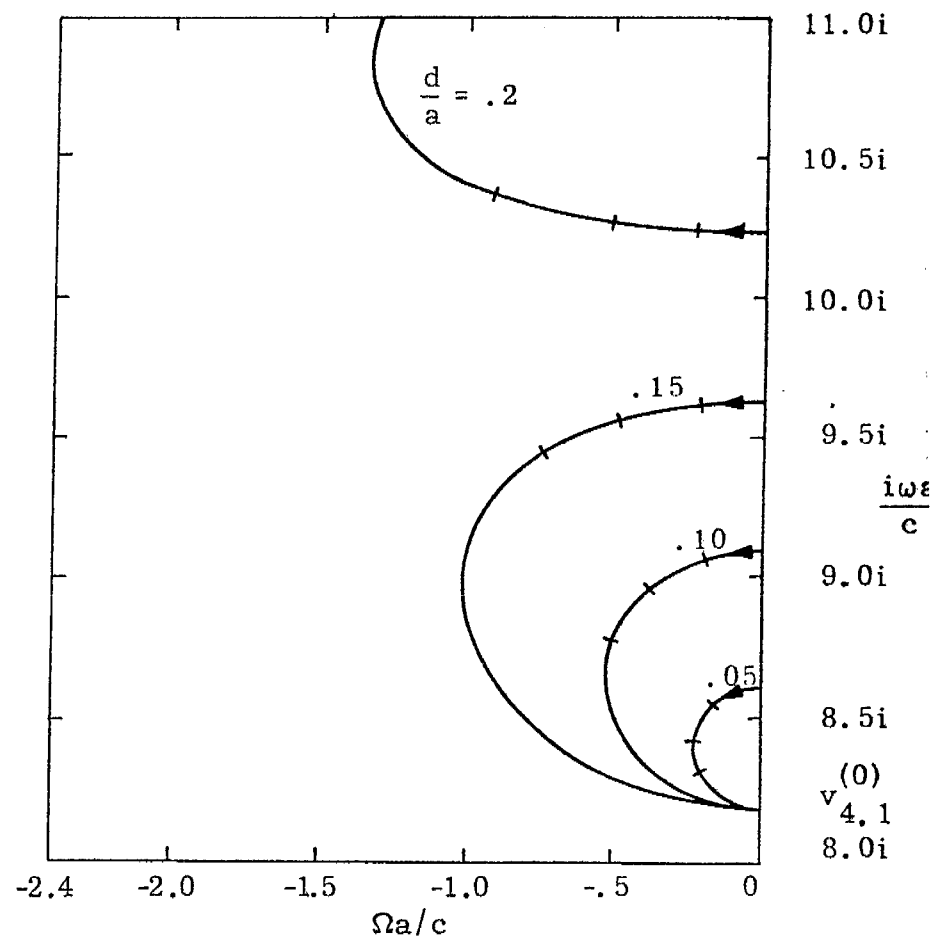

B. $v^{(1)}_{4,1}$

Figure 3.13. Trajectories from $v^{(1)}_{n,1}$ for Increasing z_s, $0 \leq z_s \leq \infty$, with d/a a Parameter

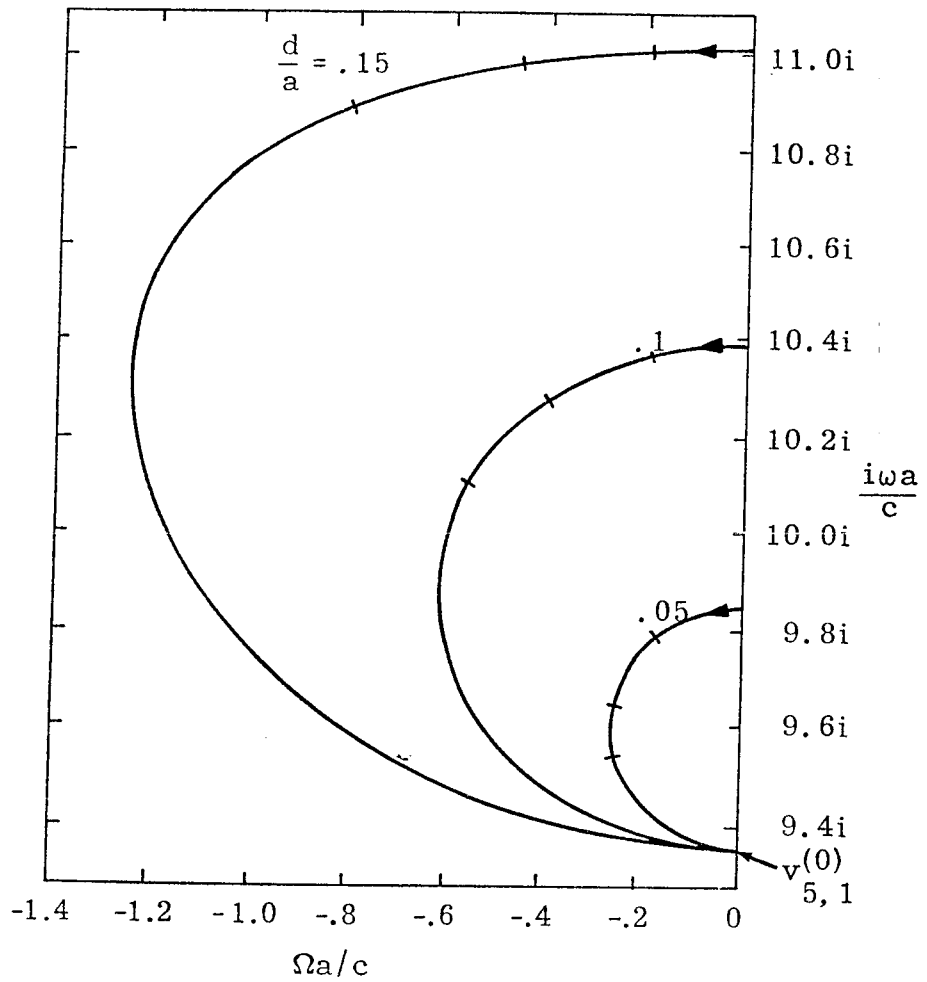

Figure 3.14. Trajectories from $v^{(1)}_{5,1}$ for Increasing z_s, $0 \leq z_s \leq \infty$, with d/a a Parameter

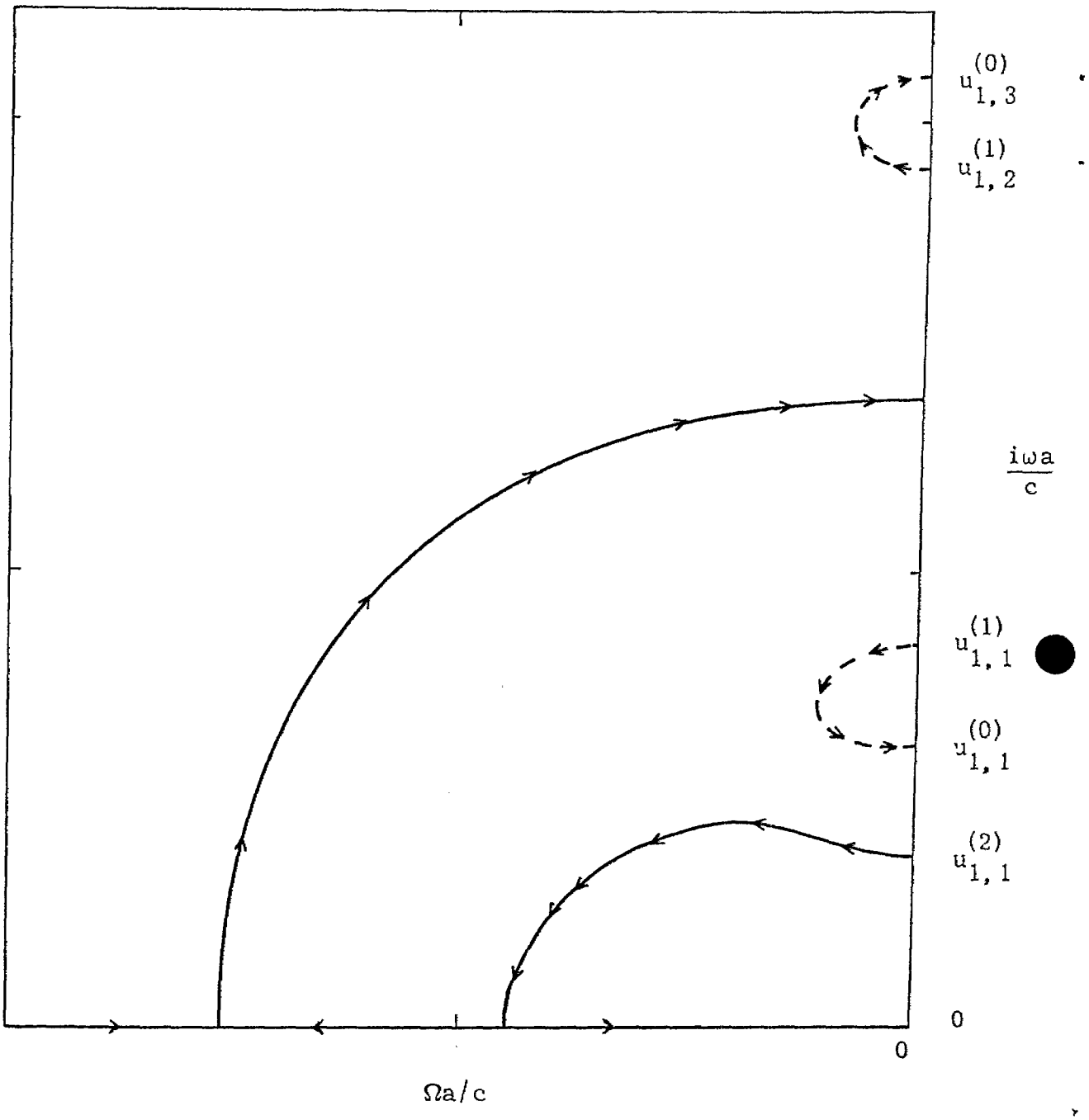

Figure 3.15. Movement Pattern for Coalescing Pole Loci Originating from $u_{1,1}^{(2)}$ for Increasing z_s $(0 \leq z_s \leq \infty)$ for $d/a = .27$, Dotted Lines Indicate Pole from $u_{1,n'}^{(1)}$

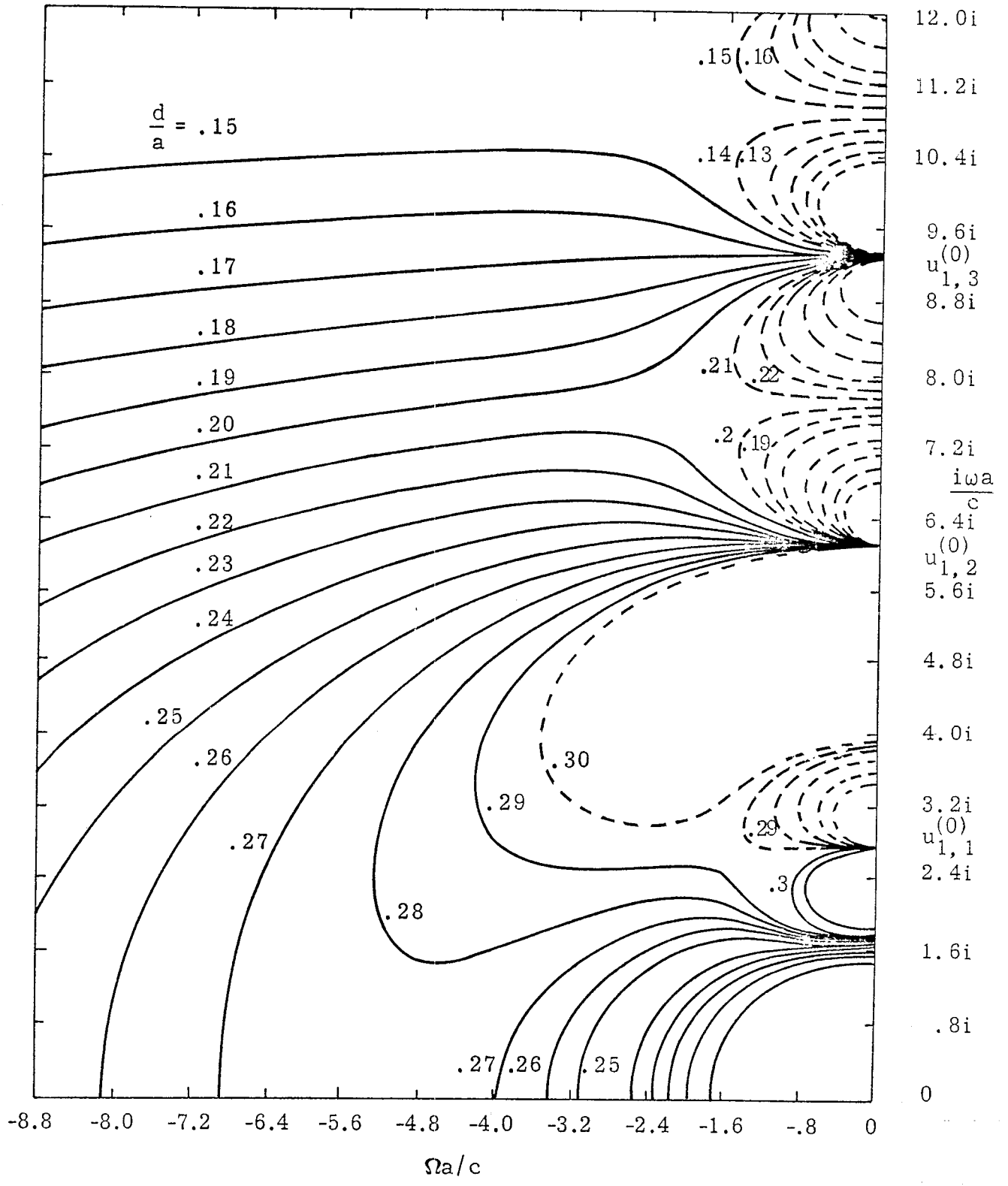

Figure 3.16. Inter-Connection of Pole Loci Originating from $u^{(2)}_{1,1}$ (Solid Lines) with those from $u^{(1)}_{1,n}$ (Dotted Lines) for Increasing z_s from 0 to ∞; $d/a \leq .3$

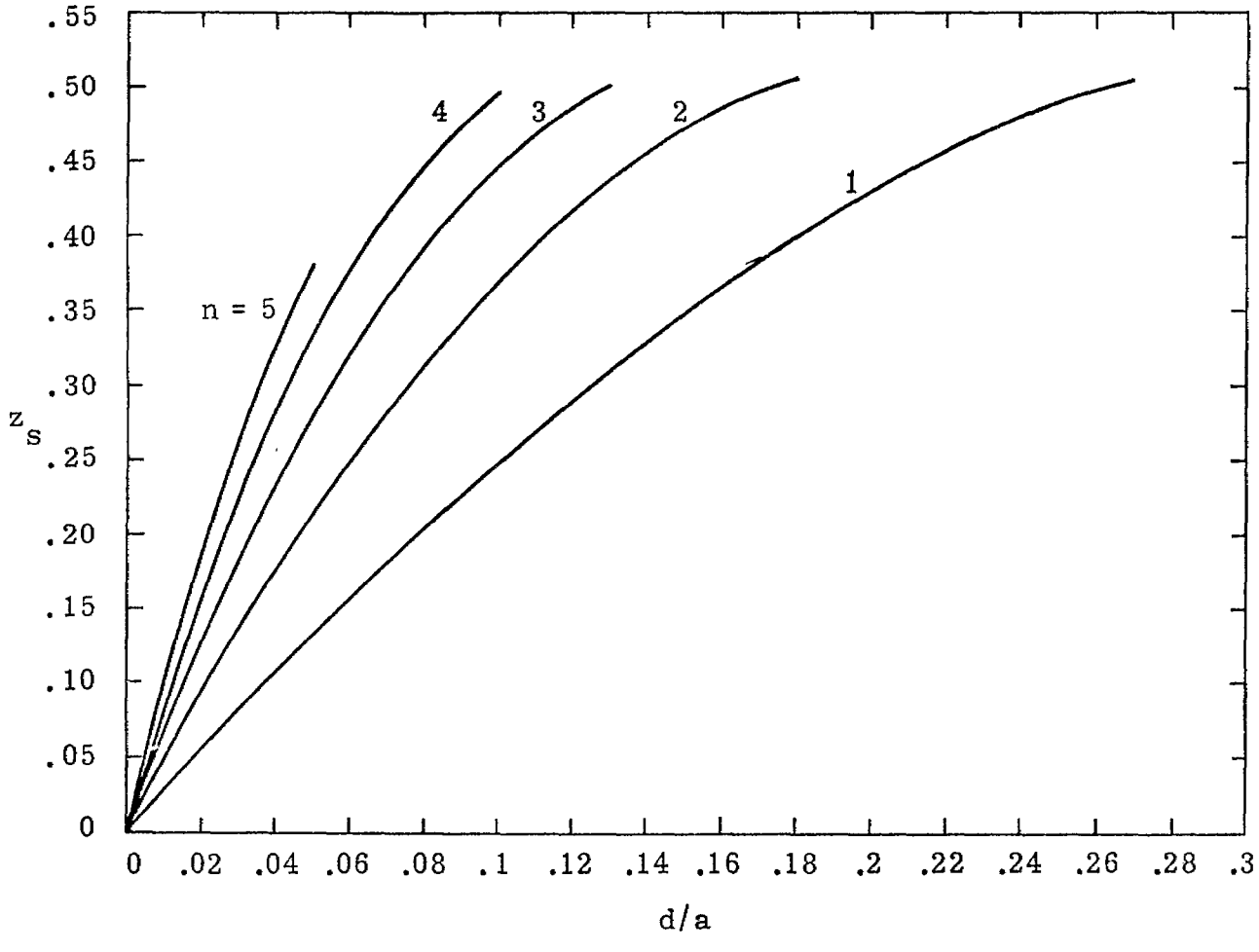

Figure 3.17. Resistive Sheet Loading Versus d/a for Critical Damping of the Lowest Order E-Mode ($u^{(2)}_{n,1}$), n a Parameter

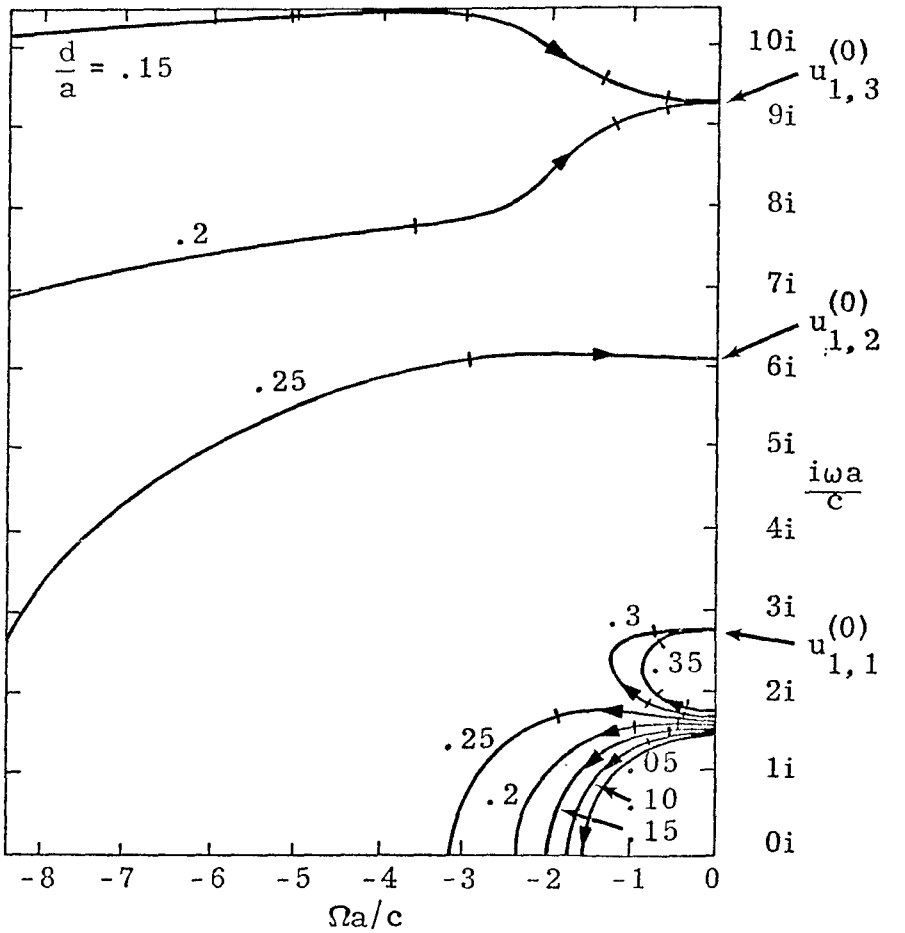

A. Values of $d/a \leq .35$ from $u^{(2)}_{1,1}$

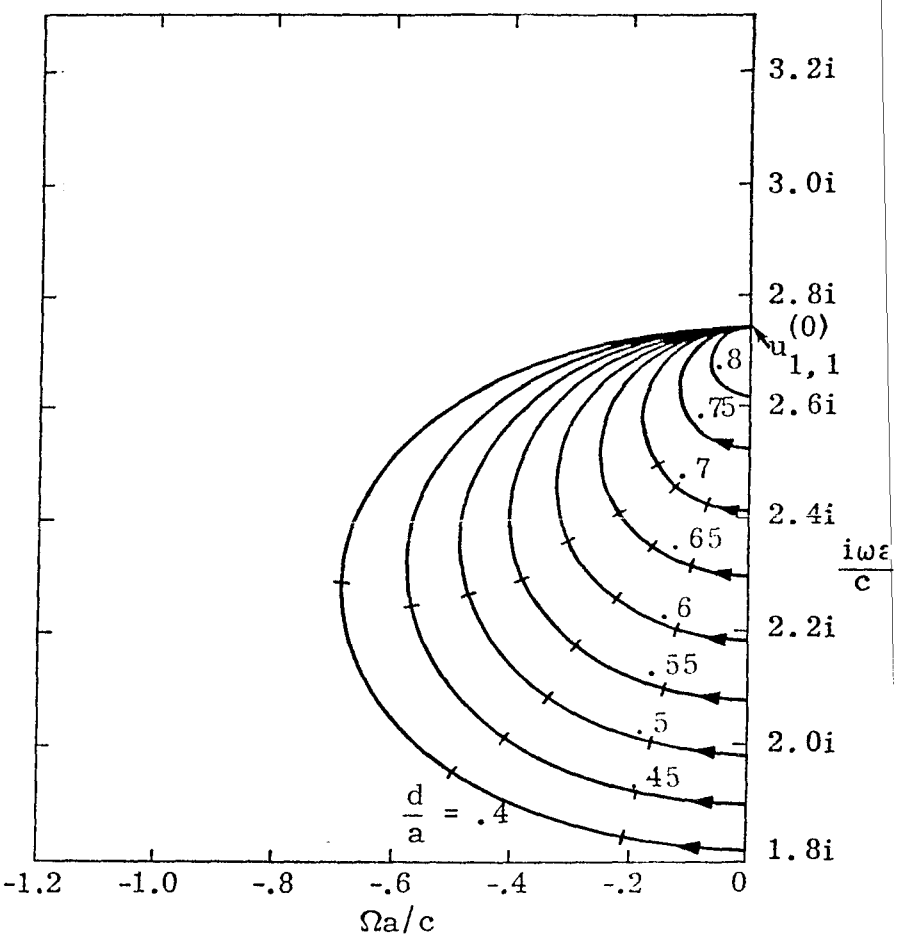

B. Values of $d/a \geq .4$ from $u^{(2)}_{1,1}$

Figure 3.18. Trajectories from $u^{(2)}_{1,1}$ for Increasing z_s, $0 \leq z_s \leq \infty$, with d/a a Parameter

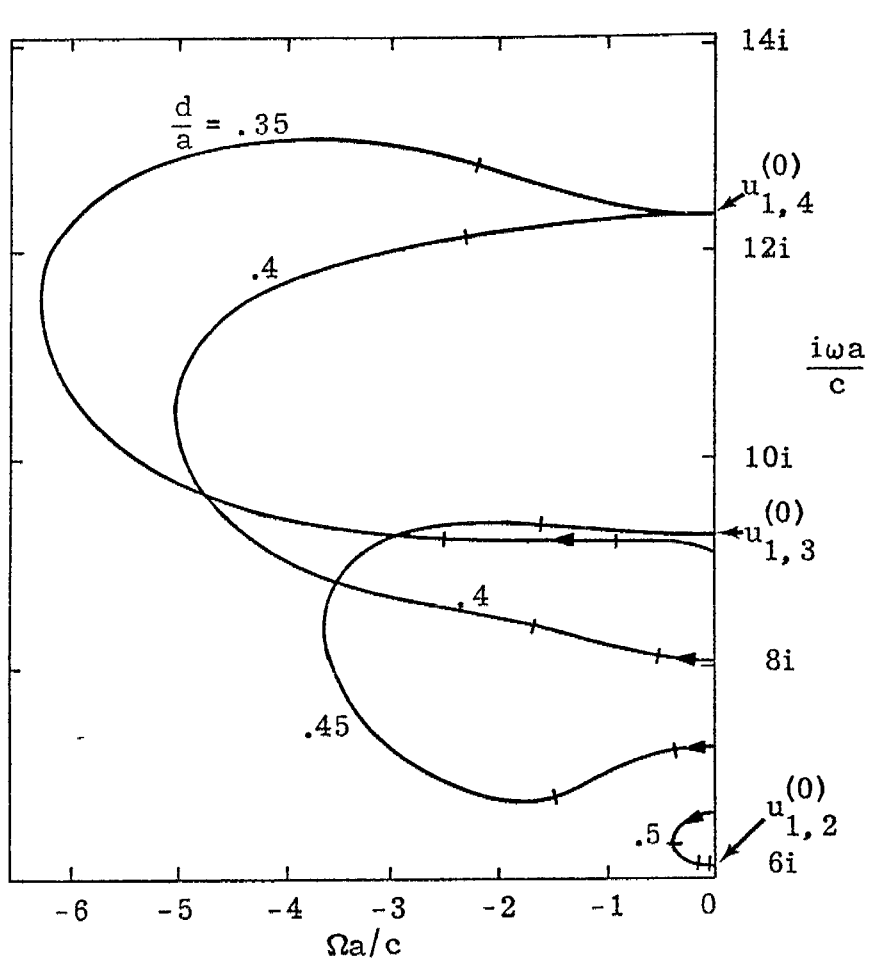

A. Values of $d/a \leq .5$ from $u^{(2)}_{1,2}$

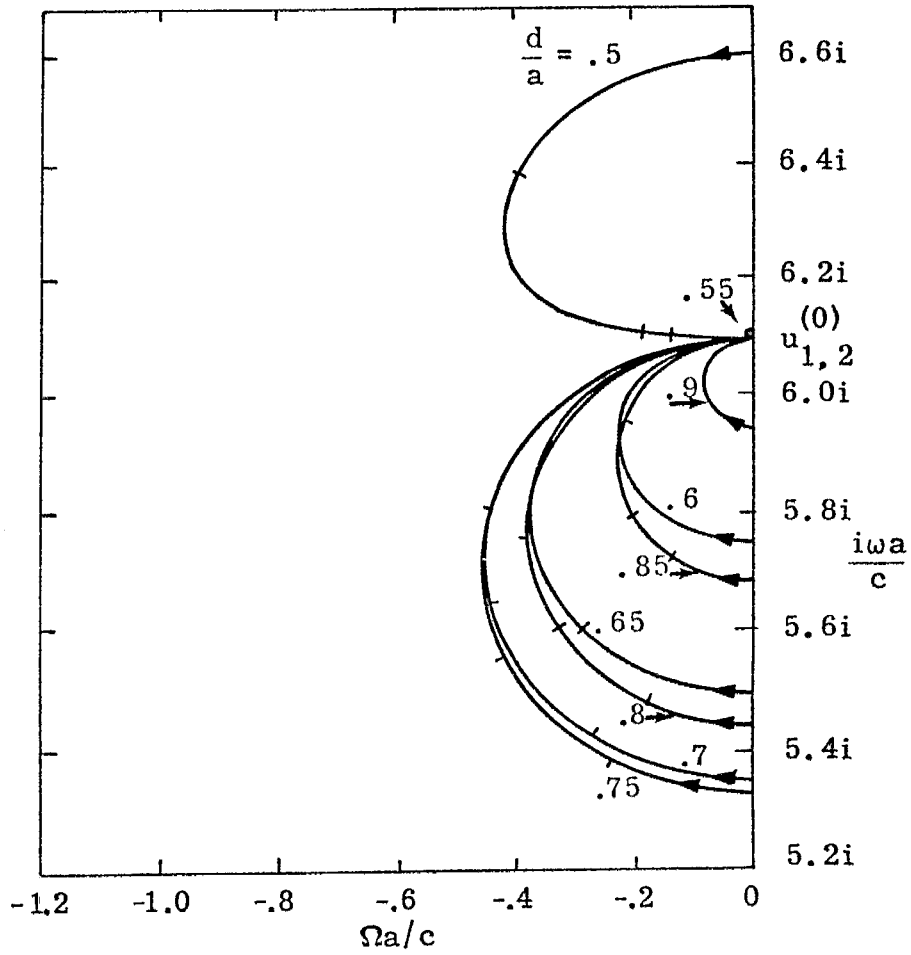

B. Values of $d/a \geq .5$ from $u^{(2)}_{1,2}$

Figure 3.19. Trajectories from $u^{(2)}_{1,2}$ for Increasing z_s, $0 \leq z_s \leq \infty$, with d/a a Parameter

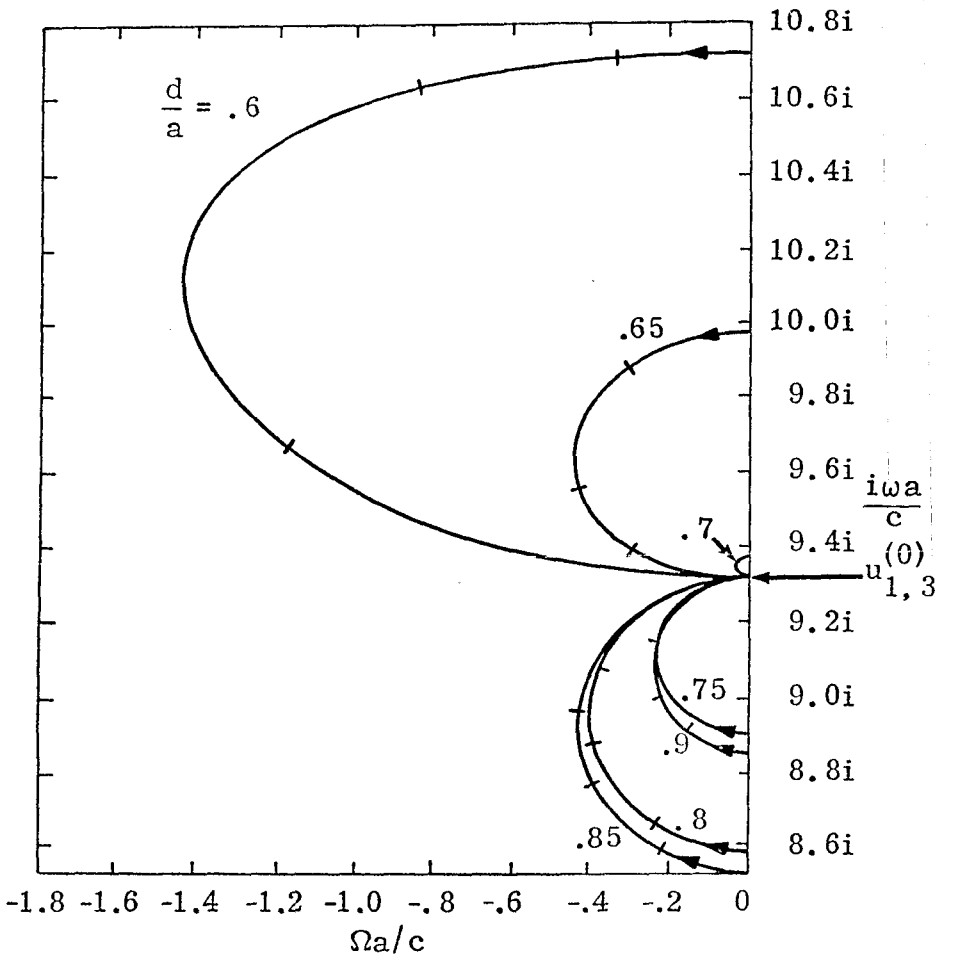

Figure 3.20. Trajectories from $u^{(2)}_{1,3}$ for Increasing z_s, $0 \leq z_s \leq \infty$, with d/a a Parameter

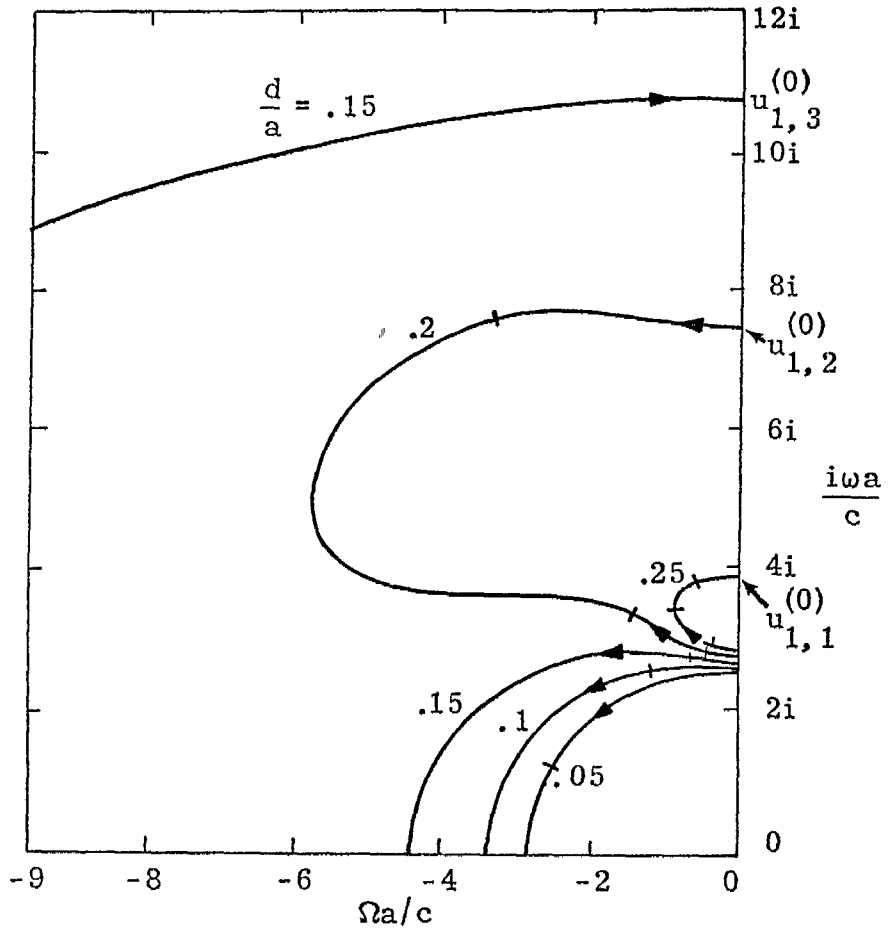

A. Values of $d/a \leq .25$ from $u^{(2)}_{2,1}$

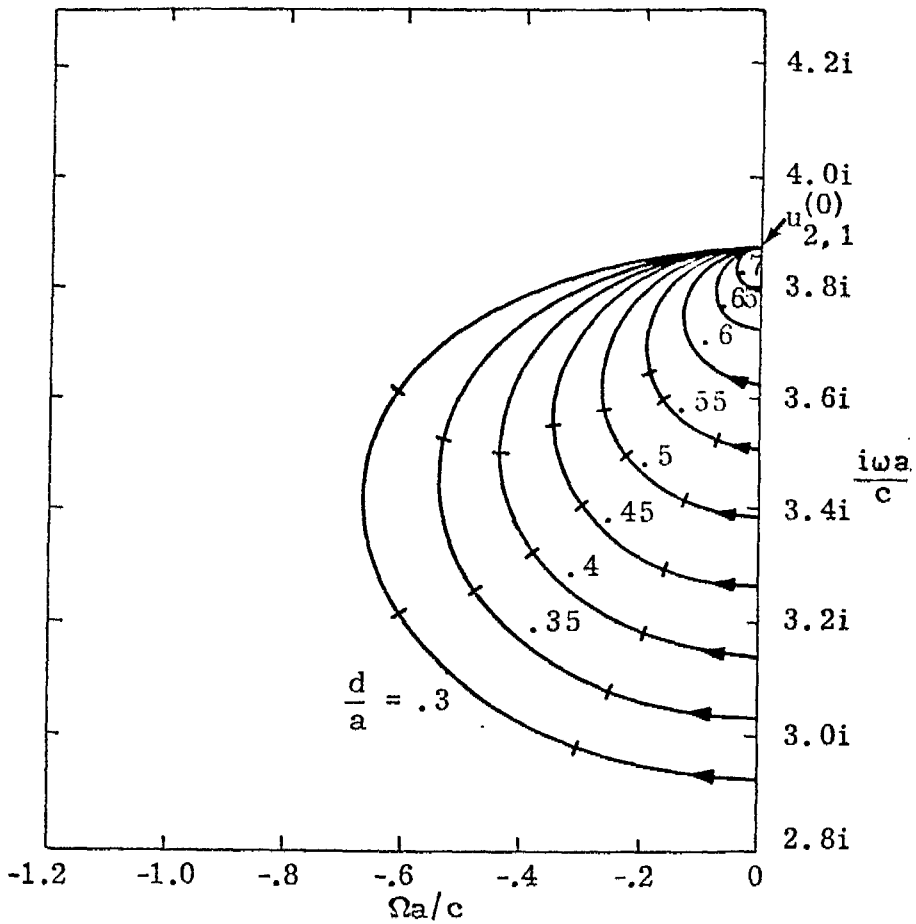

B. Values of $d/a \geq .3$ from $u^{(2)}_{2,1}$

Figure 3.21. Trajectories from $u^{(2)}_{2,1}$ for Increasing z_s, $0 \leq z_s \leq \infty$, with d/a a Parameter

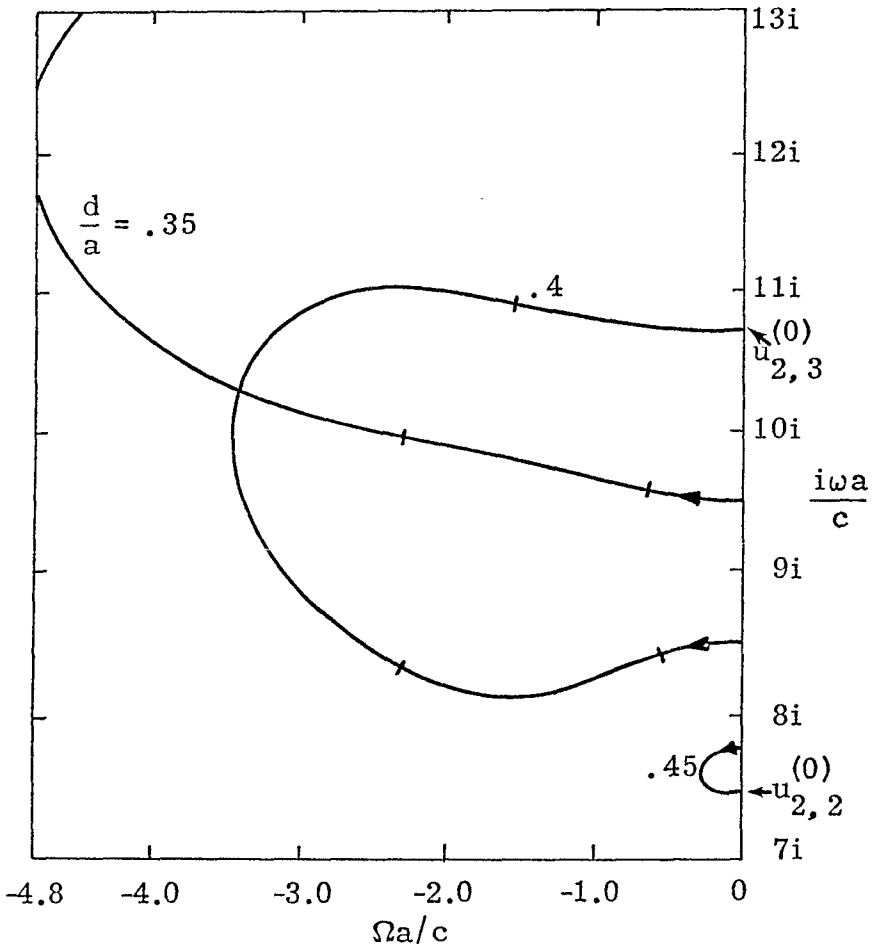

A. Values of $d/a \leq .45$ from $u^{(2)}_{2,2}$

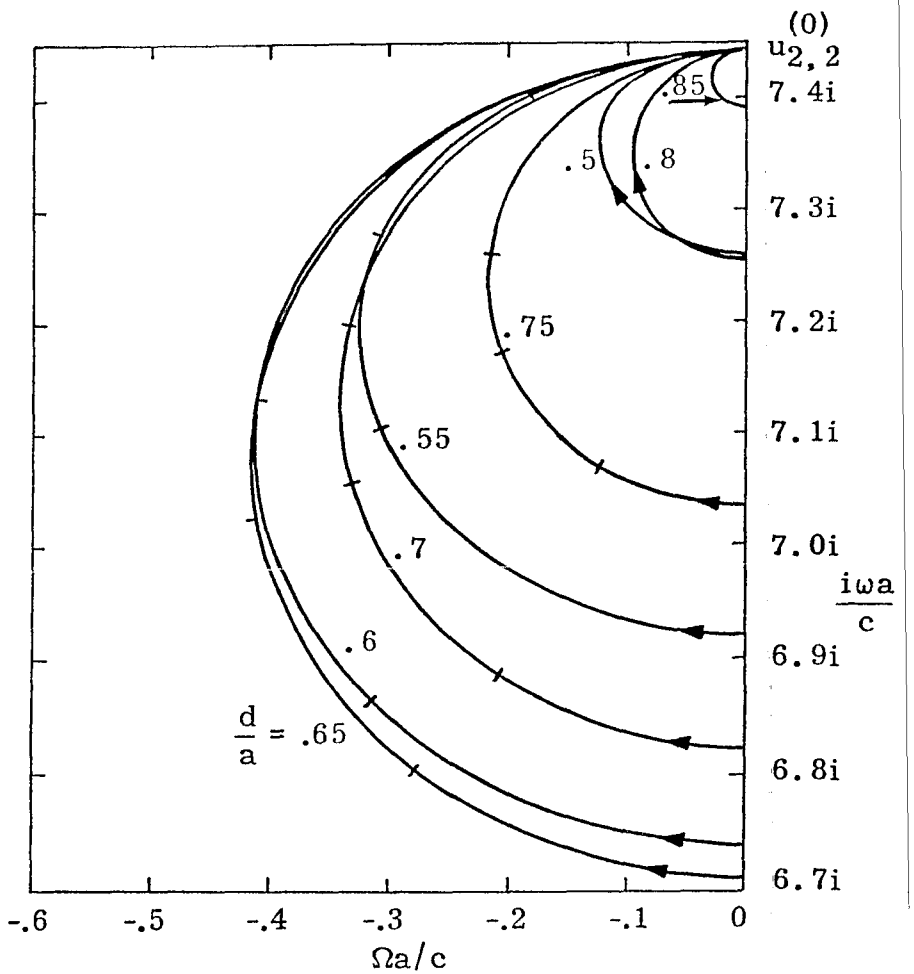

B. Values of $d/a \geq .5$ from $u^{(2)}_{2,2}$

Figure 3.22. Trajectories from $u^{(2)}_{2,2}$ for Increasing z_s, $0 \leq z_s \leq \infty$, with d/a a Parameter

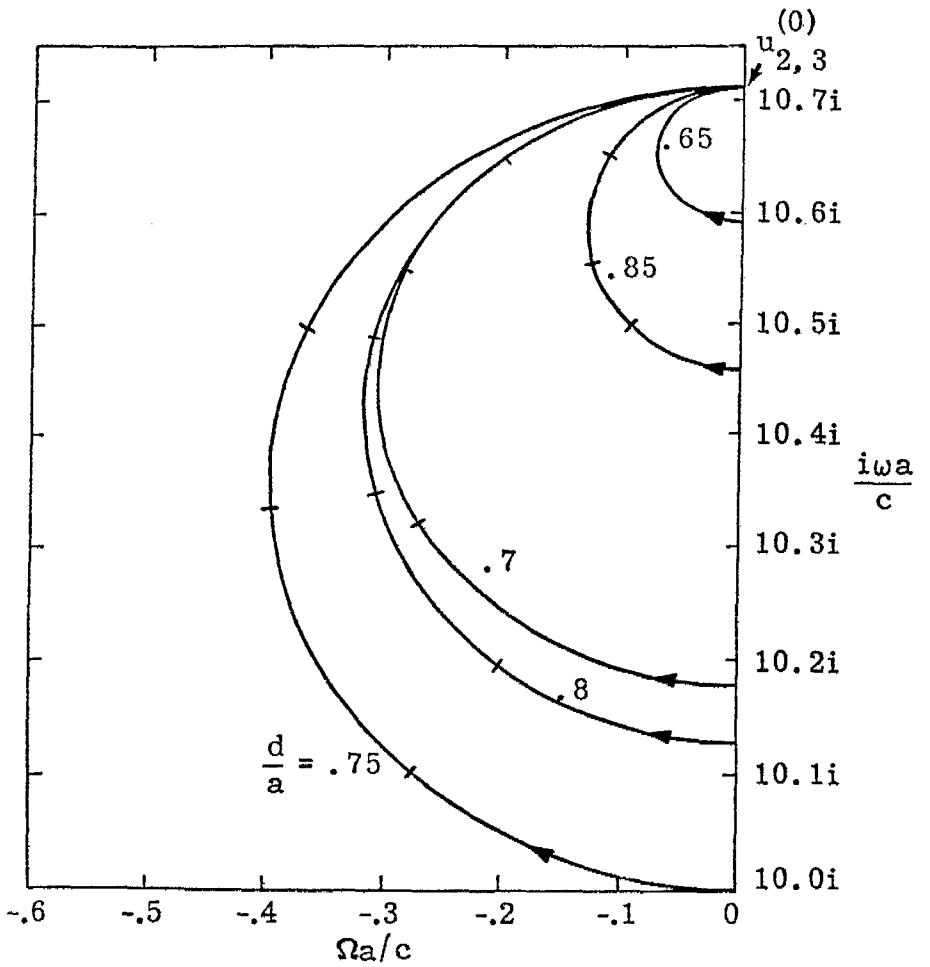

Figure 3.23. Trajectories from $u^{(2)}_{2,3}$ for Increasing z_s, $0 \leq z_s \leq \infty$, with d/a a Parameter

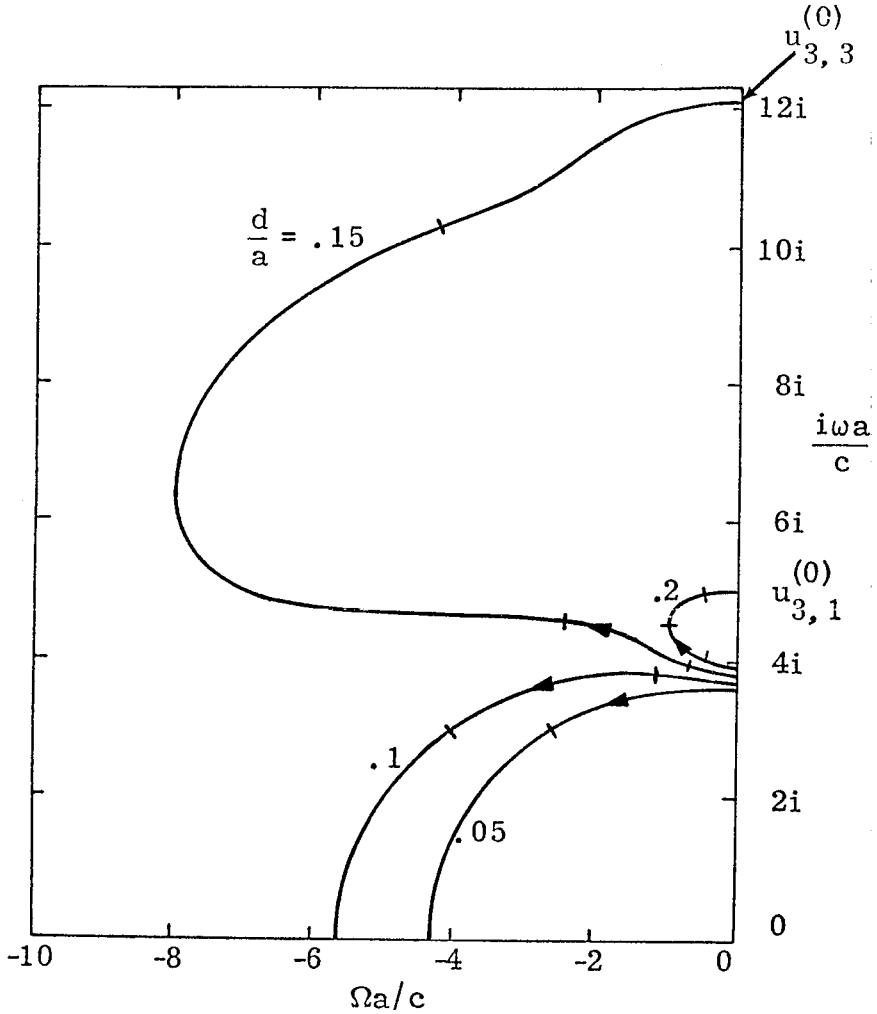

A. Values of $d/a \leq .2$ from $u^{(2)}_{3,1}$

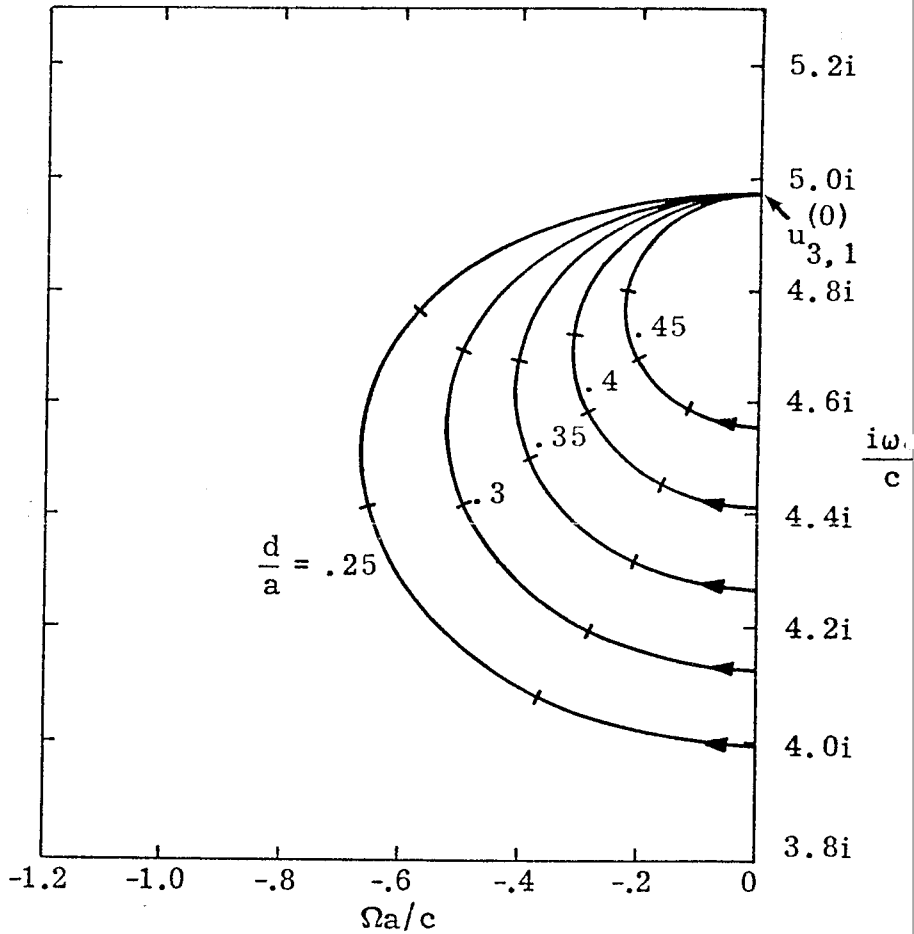

B. Values $.25 \leq d/a \leq .45$ from $u^{(2)}_{3,1}$

Figure 3.24. Trajectories from $u^{(2)}_{3,1}$ for Increasing z_s, $0 \leq z_s \leq \infty$, with d/a a Parameter

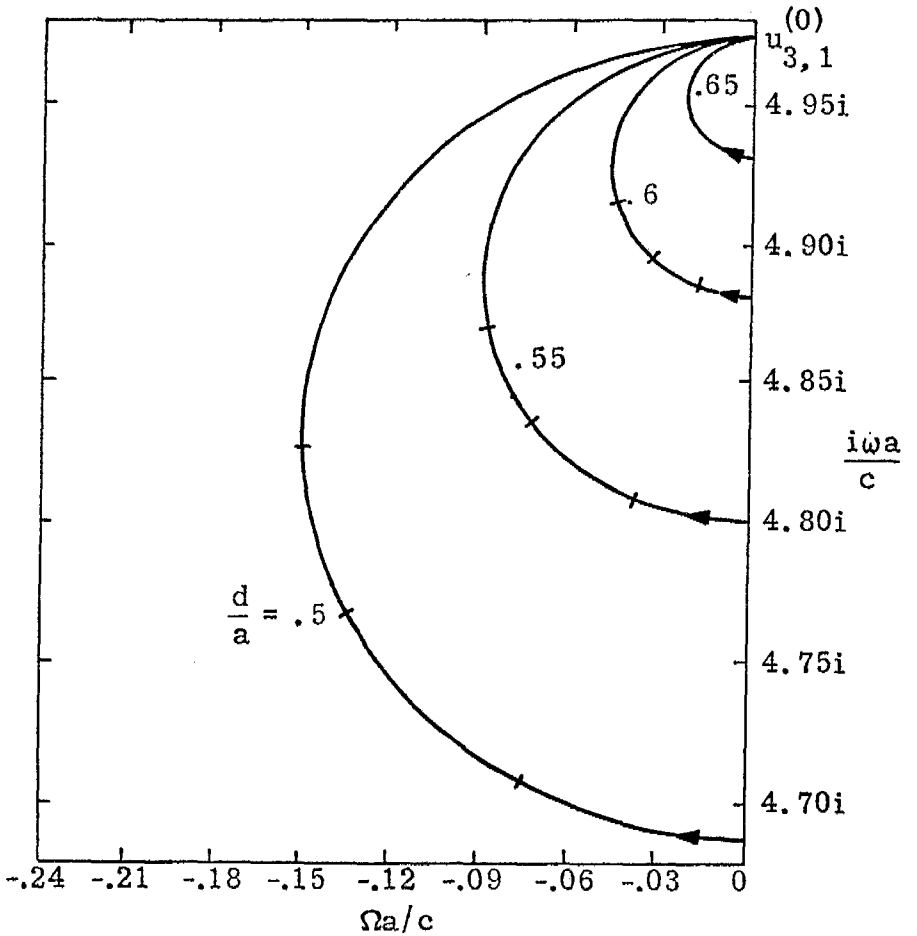

Figure 3.25. Trajectories from $u^{(2)}_{3,1}$ for Increasing z_s, $0 \leq z_s \leq \infty$, with d/a a Parameter; $d/a \geq .5$

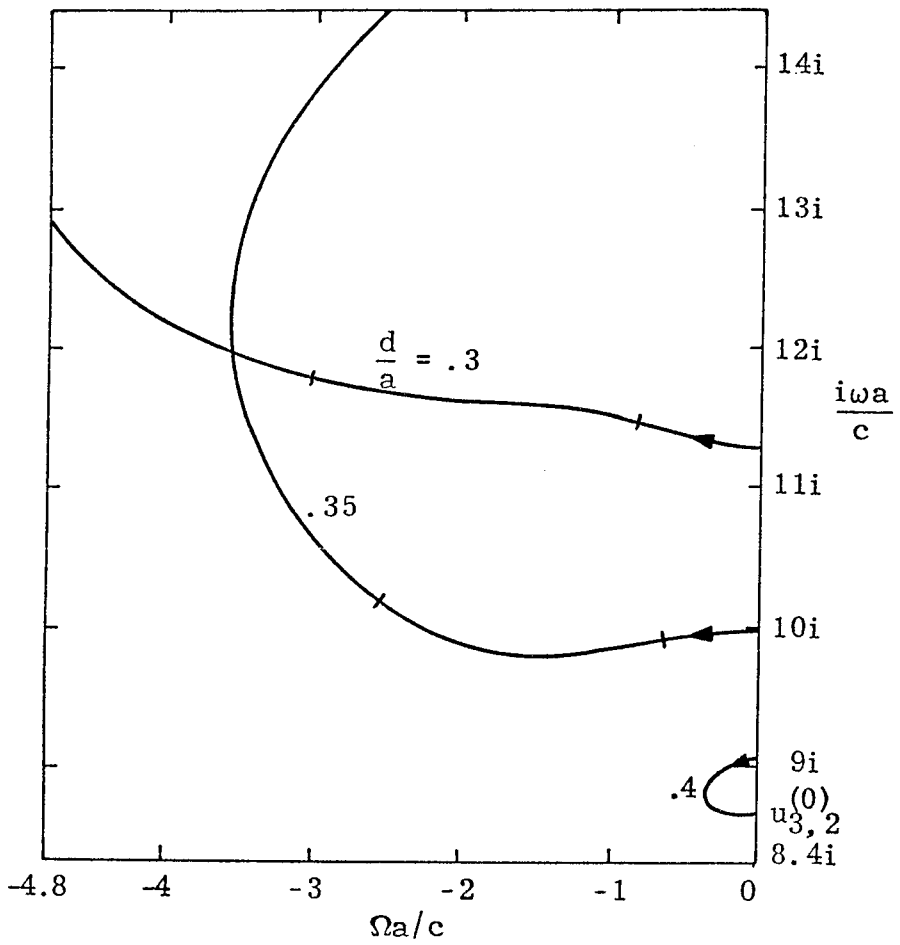

A. Values of $d/a \leq .4$ from $u_{3,2}^{(2)}$

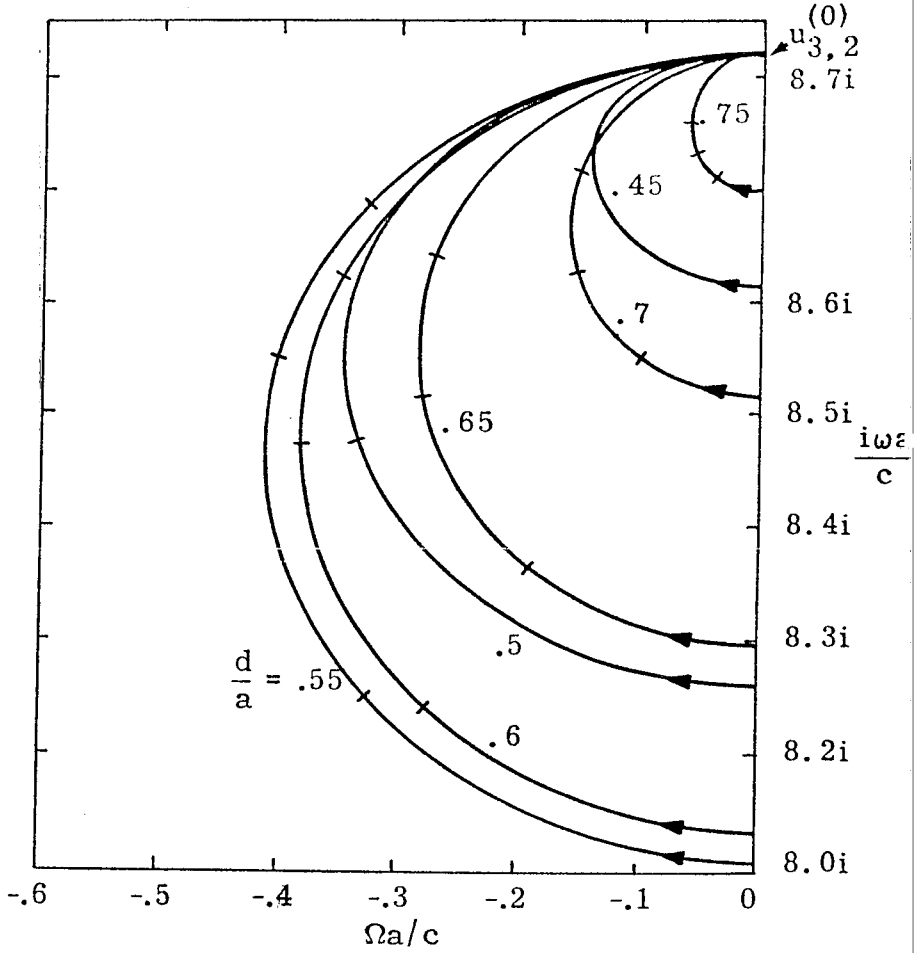

B. Values of $d/a \geq .45$ from $u_{3,2}^{(2)}$

Figure 3.26. Trajectories from $u_{3,2}^{(2)}$ for Increasing z_s, $0 \leq z_s \leq \infty$, with d/a a Parameter

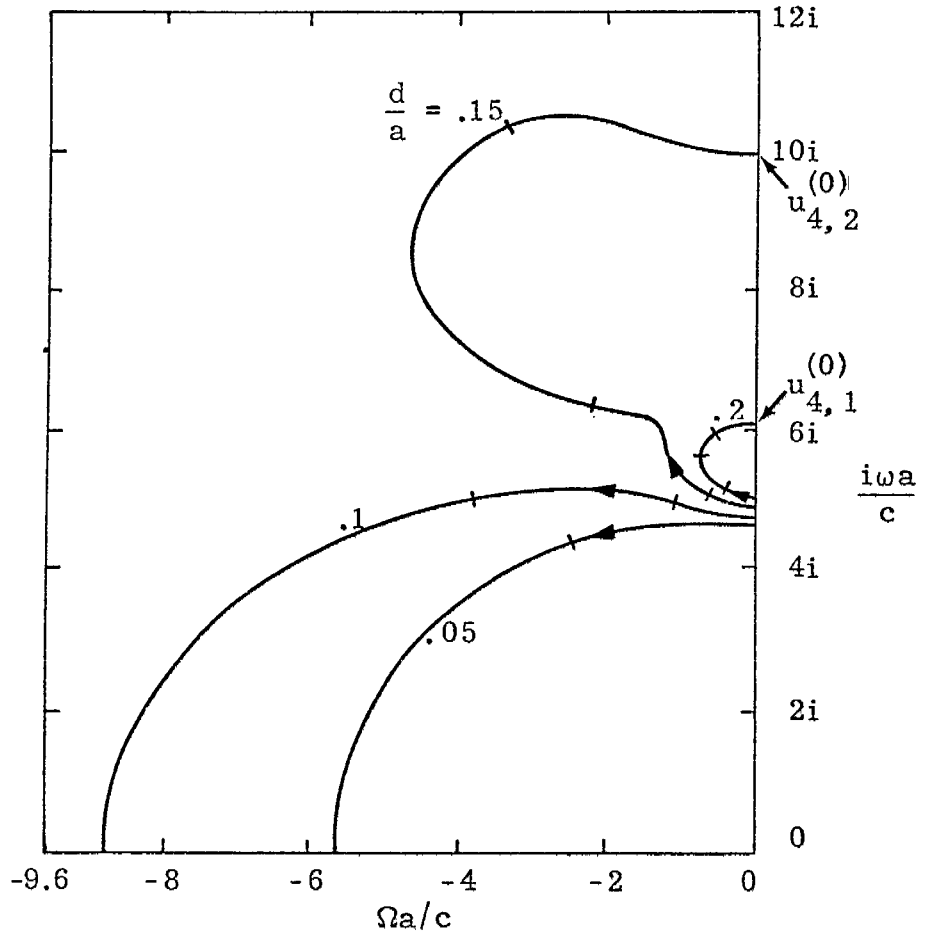

A. Values of $d/a \leq .2$ from $u^{(2)}_{4,1}$

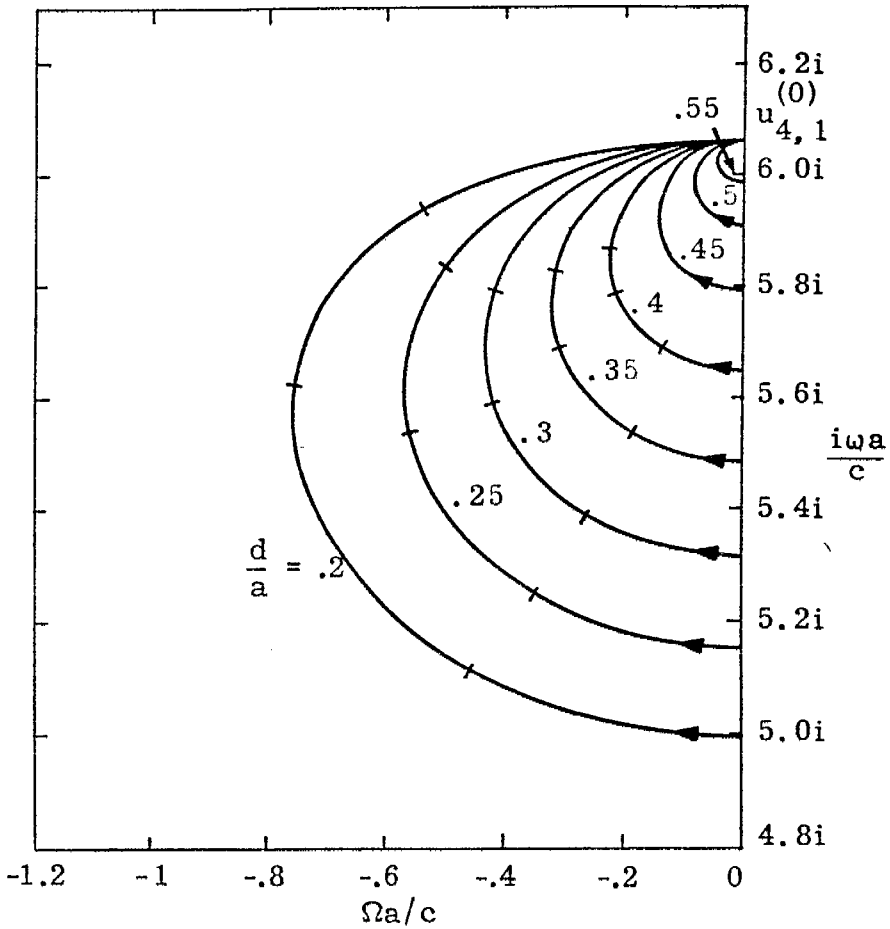

B. Values $.2 \leq d/a \leq .55$ from $u^{(2)}_{4,1}$

Figure 3.27. Trajectory from $u^{(2)}_{4,1}$ for Increasing z_s, $0 \leq z_s \leq \infty$, with d/a a Parameter

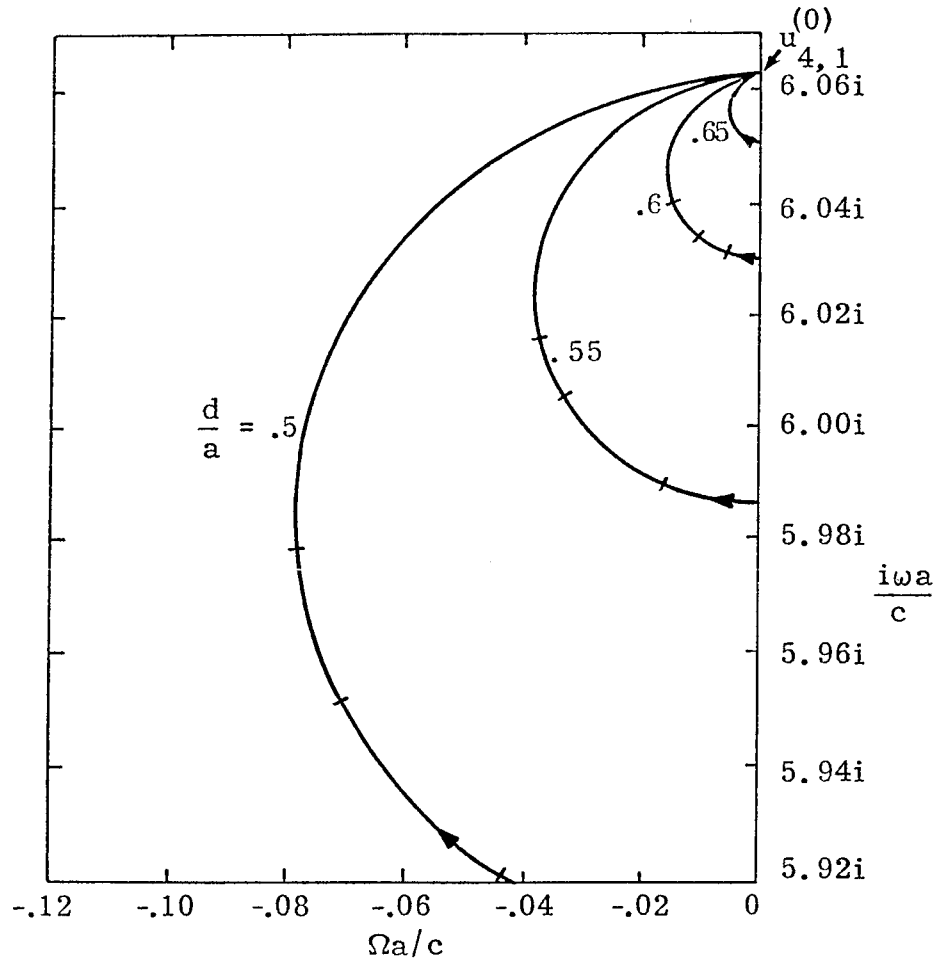

Figure 3.28. Trajectories from $u^{(2)}_{4,1}$ for Increasing z_s, $0 \leq z_s \leq \infty$, with d/a a Parameter; $d/a \geq .5$

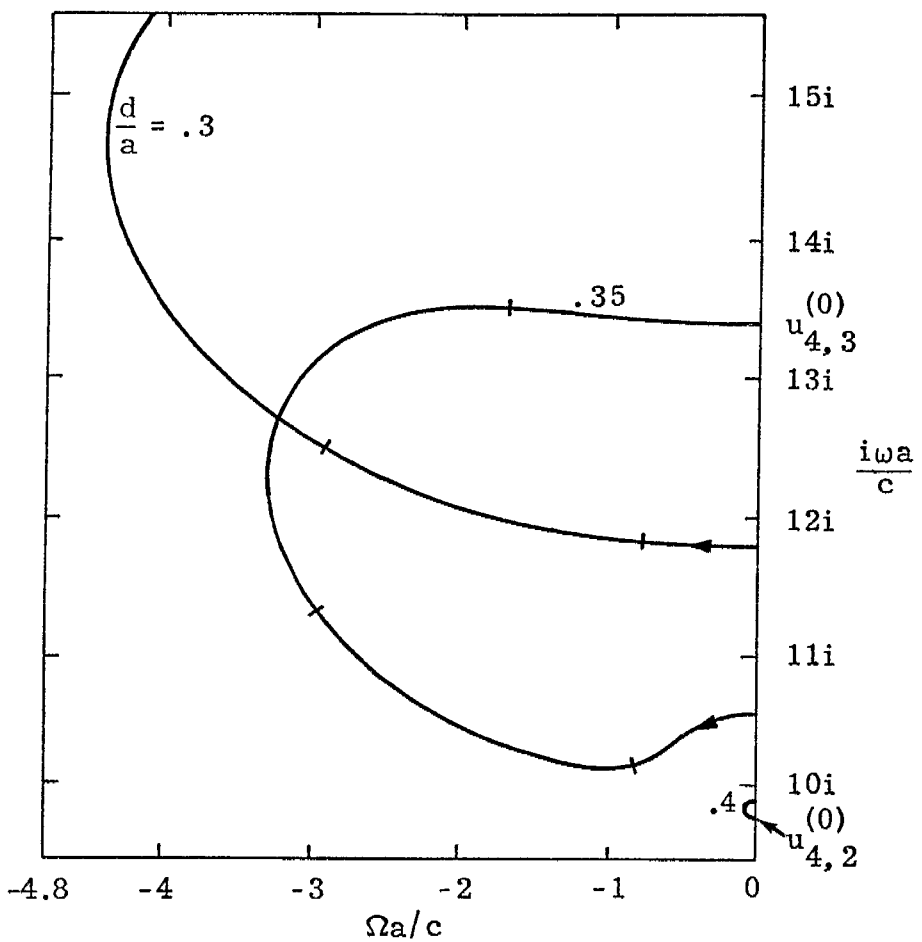

A. Values of $d/a \leq .4$ from $u^{(2)}_{4,2}$

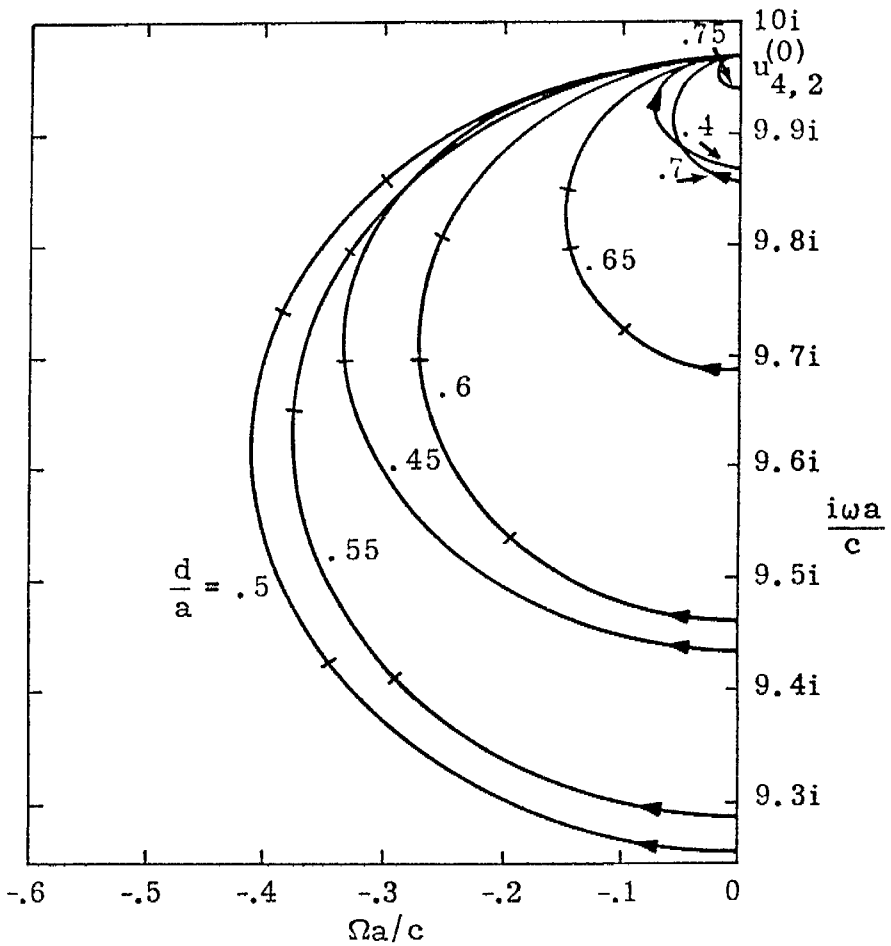

B. Values of $d/a \geq .4$ from $u^{(2)}_{4,2}$

Figure 3.29. Trajectories from $u^{(2)}_{4,2}$ for Increasing z_s, $0 \leq z_s \leq \infty$, with d/a a Parameter

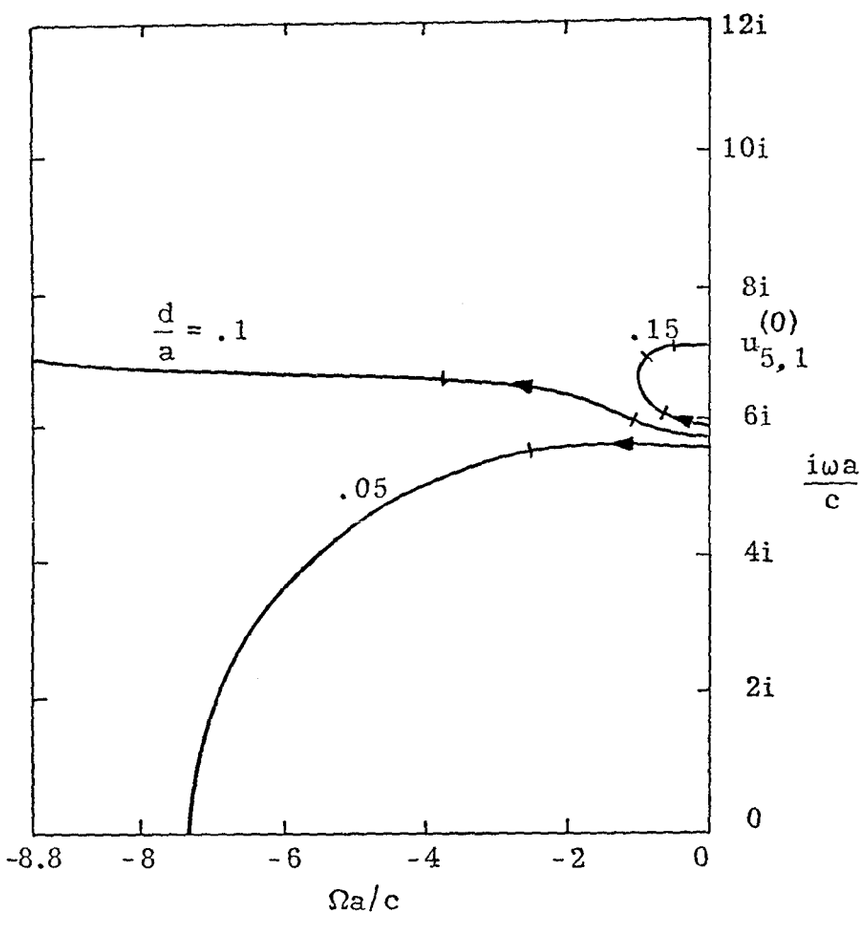

A. Values of $d/a \leq .15$ from $u_{5,1}^{(2)}$

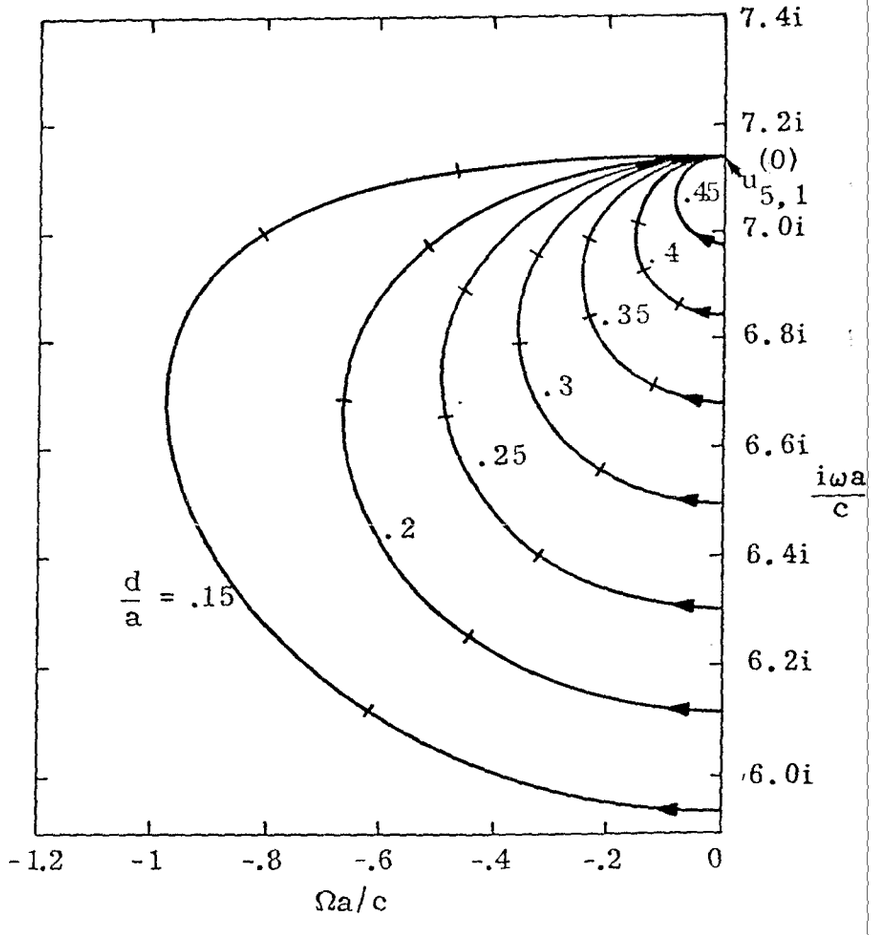

B. Values $.15 \leq d/a \leq .45$ from $u_{5,1}^{(2)}$

Figure 3.30. Trajectories from $u_{5,1}^{(2)}$ for Increasing z_s, $0 \leq z_s \leq \infty$, with d/a a Parameter

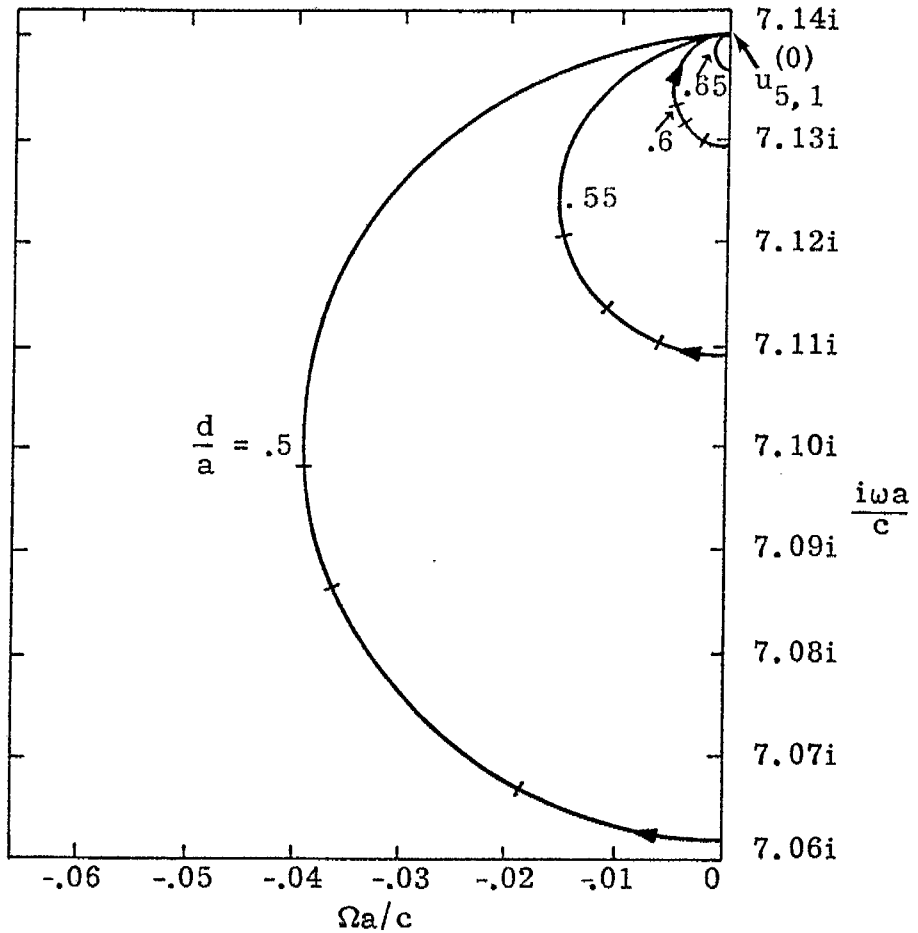

Figure 3.31 Trajectories from $u_{5,1}^{(2)}$ for Increasing z_s, $0 \leq z_s \leq \infty$, with d/a a Parameter; $d/a \geq .5$

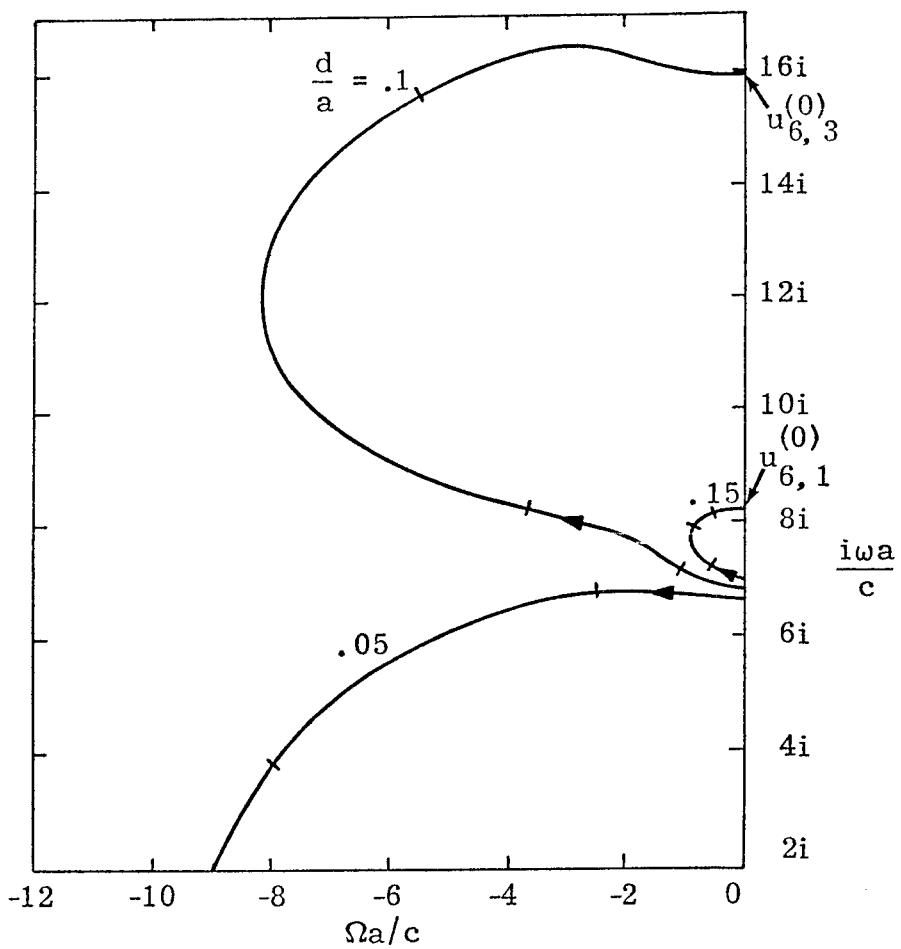

A. Values of $d/a \leq .15$ from $u^{(2)}_{6,1}$

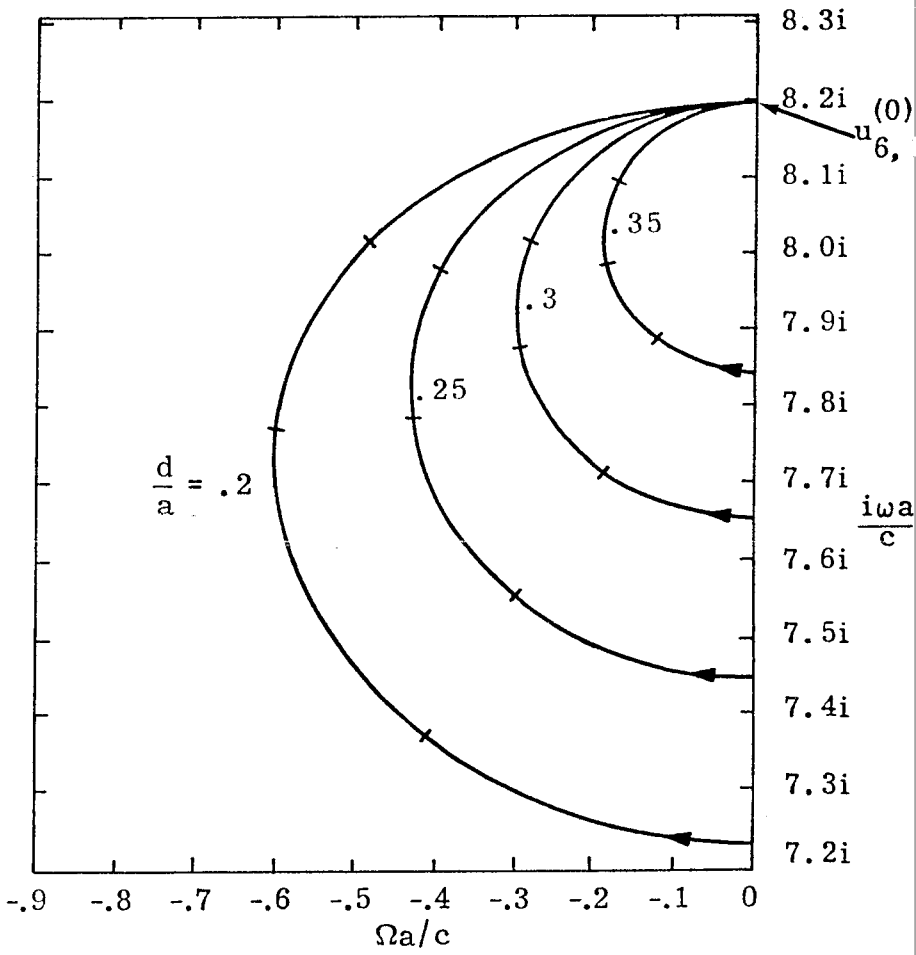

B. Values $.2 \leq d/a \leq .35$ from $u^{(2)}_{6,1}$

Figure 3.32. Trajectories from $u^{(2)}_{6,1}$ for Increasing z_s, $0 \leq z_s \leq \infty$, with d/a a Parameter

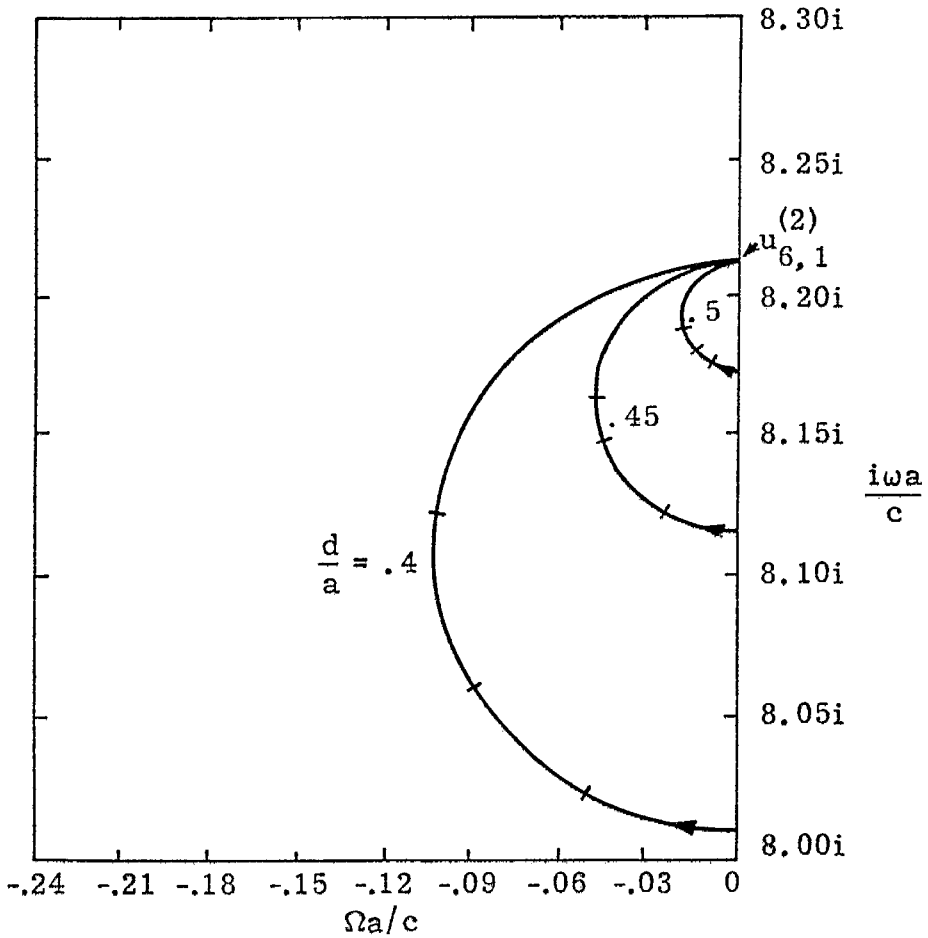

Figure 3.33. Trajectories from $u^{(2)}_{6,1}$ for Increasing z_s, $0 \leq z_s \leq \infty$, with d/a a Parameter; $d/a \geq .4$

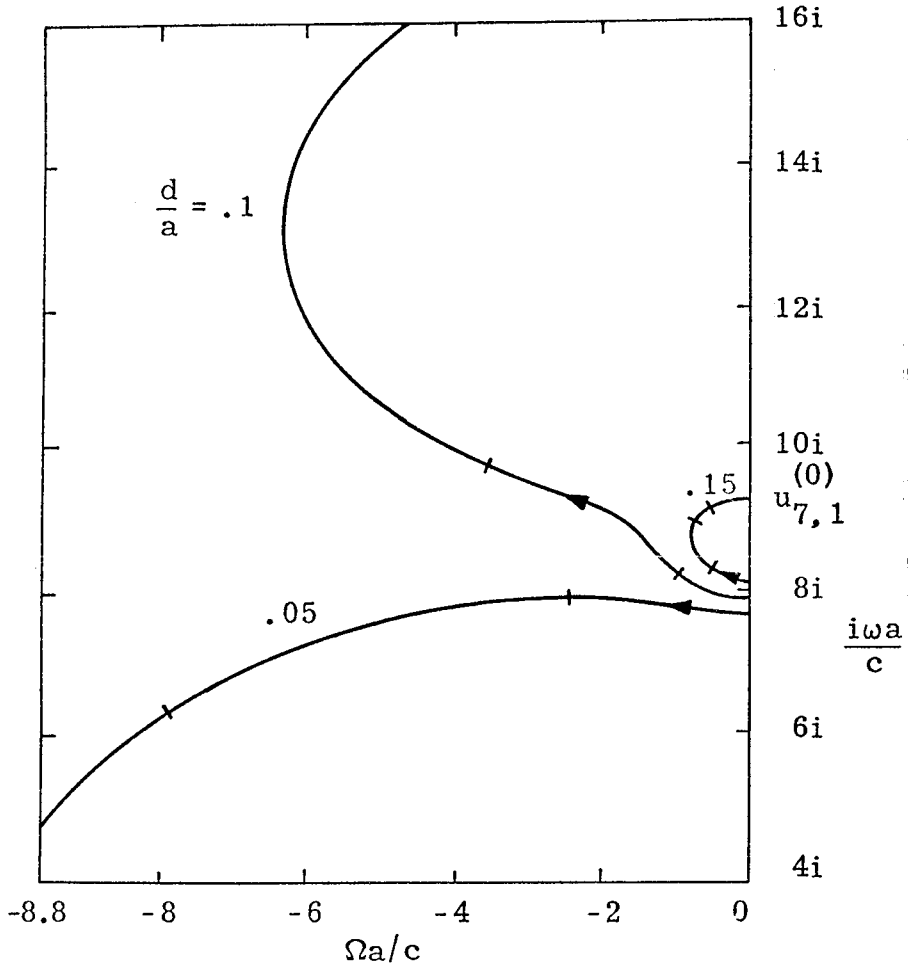

A. Values of $d/a \leq .15$ from $u_{7,1}^{(2)}$

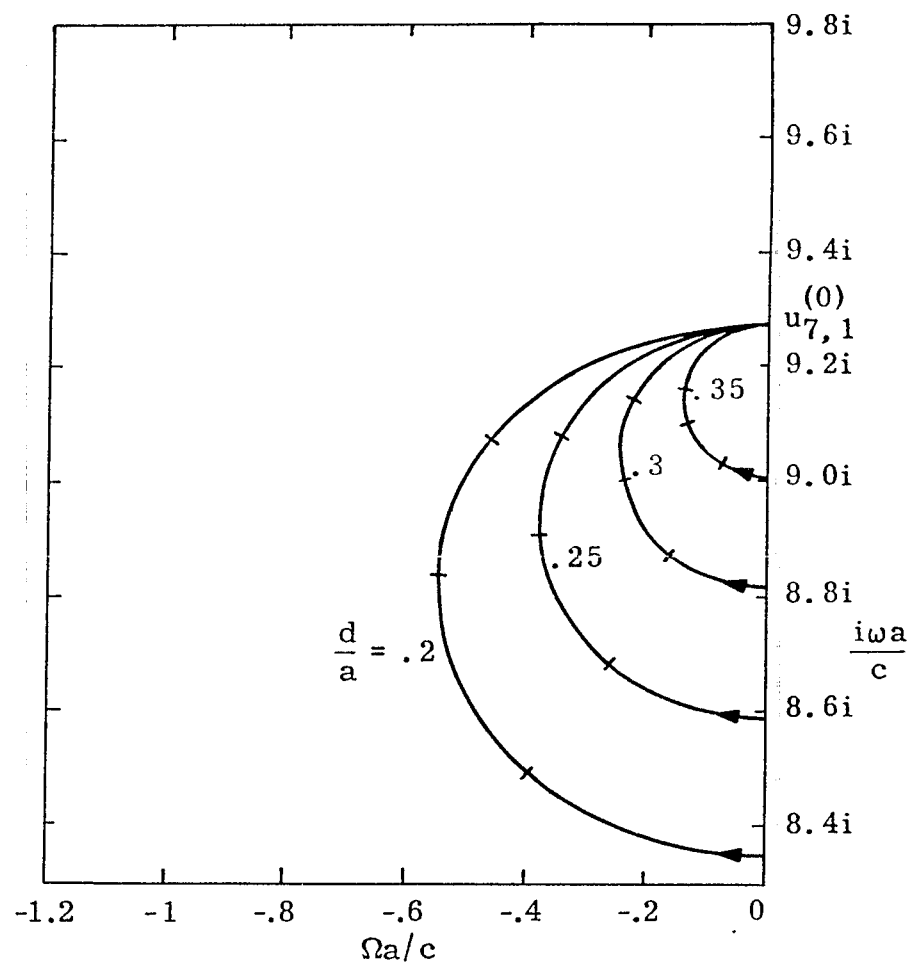

B. Values $.2 \leq d/a \leq .35$ from $u_{7,1}^{(2)}$

Figure 3.34. Trajectories from $u_{7,1}^{(2)}$ for Increasing z_s, $0 \leq z_s \leq \infty$, with d/a a Parameter

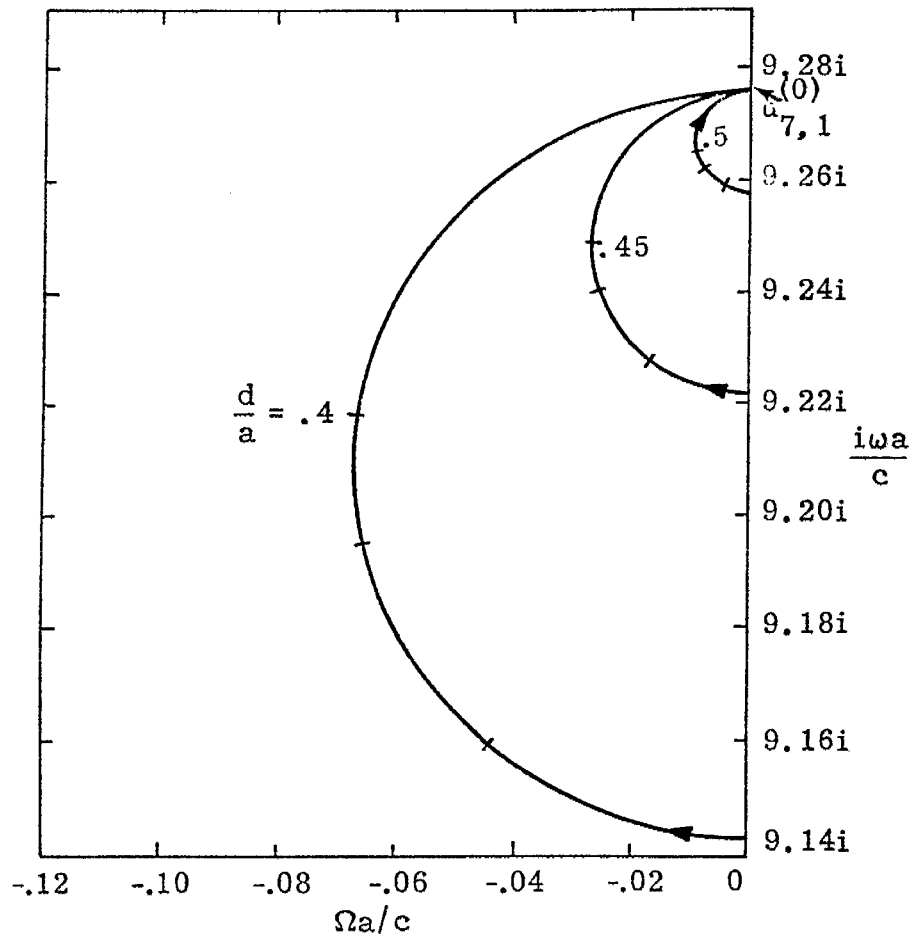

Figure 3.35. Trajectories from $u^{(2)}_{7,1}$ for Increasing z_s, $0 \leq z_s \leq \infty$, with d/a a Parameter; $d/a \geq .4$

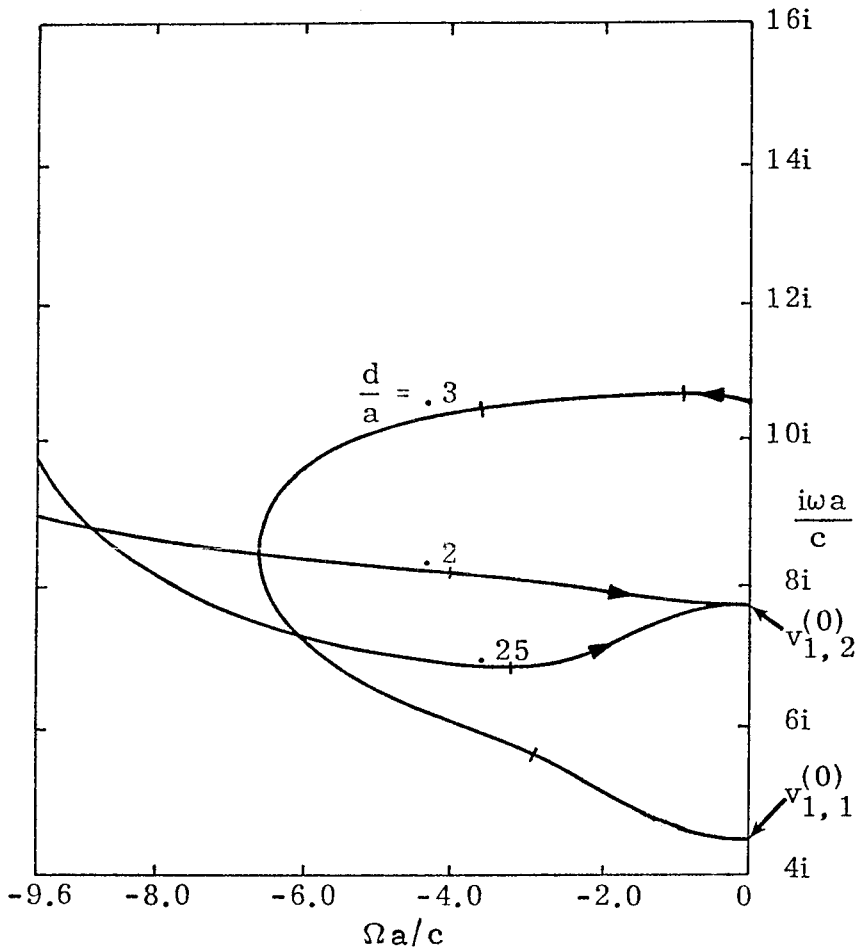

A. Values of $d/a \leq .3$ from $v_{1,1}^{(2)}$

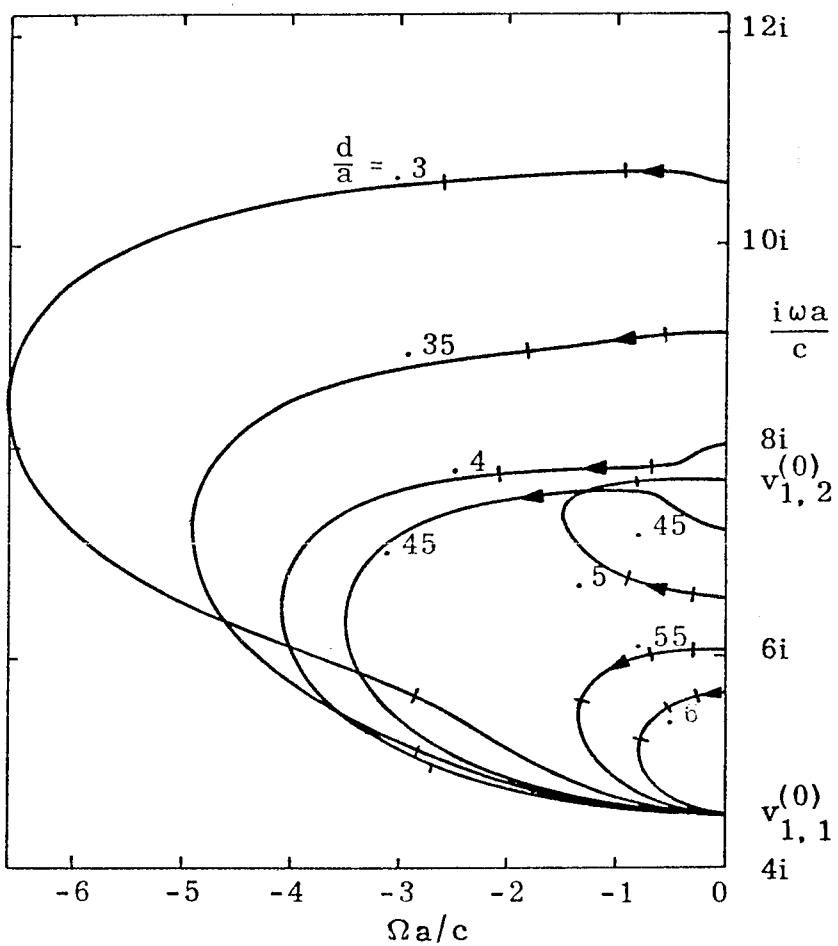

B. Values $.3 \leq d/a \leq .6$ from $v_{1,1}^{(2)}$

Figure 3.36. Trajectories from $v_{1,1}^{(2)}$ for Increasing z_s, $0 \leq z_s \leq \infty$, with d/a a Parameter

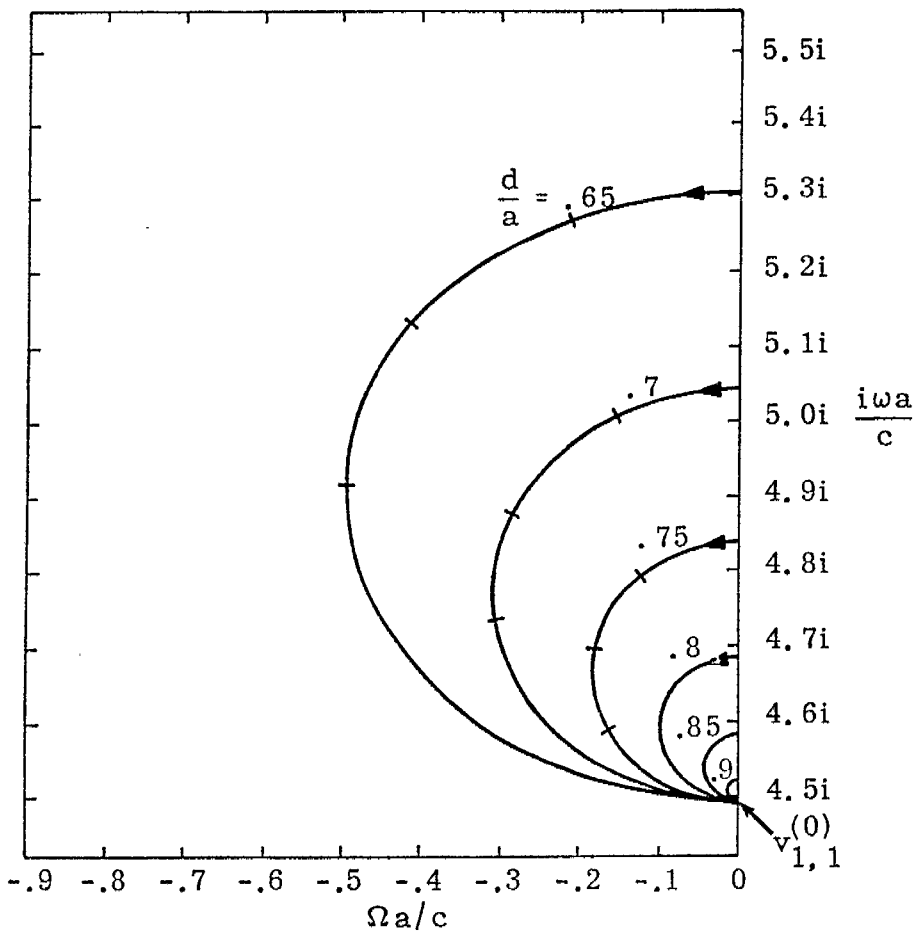

A. Values of $d/a \geq .65$ from $v_{1,1}^{(2)}$

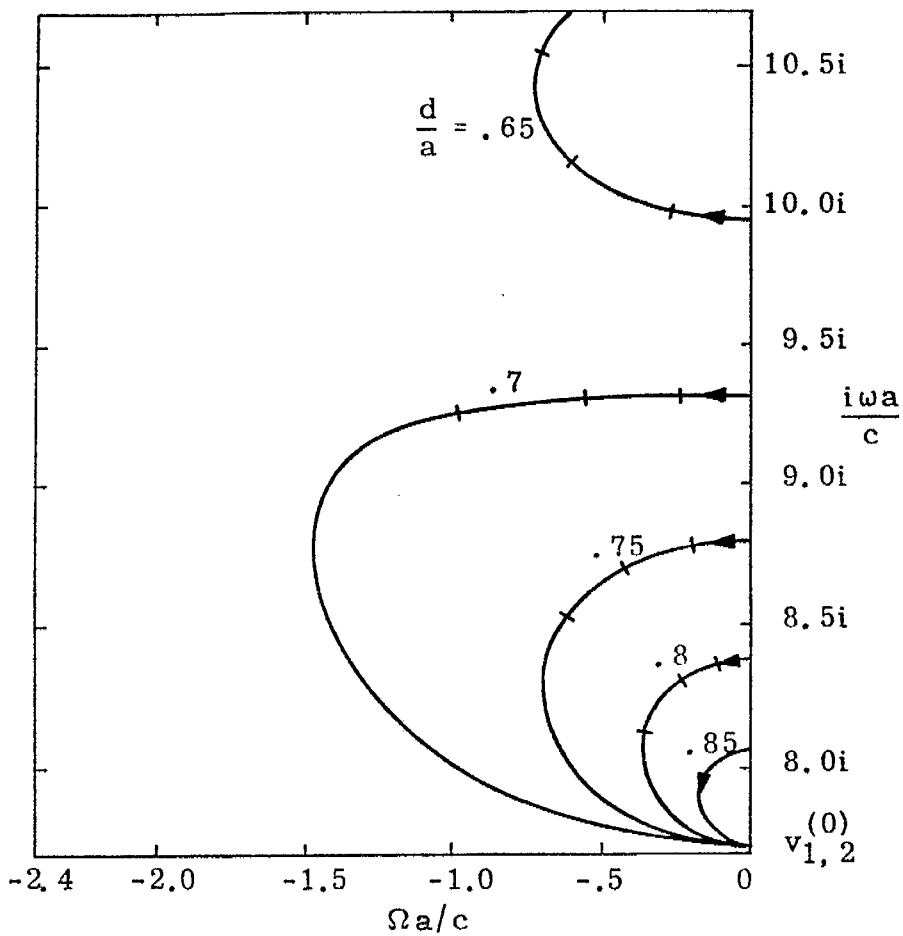

B. Values of $.65 \leq d/a \leq .85$ from $v_{1,2}^{(2)}$

Figure 3.37. Trajectories from $v_{1,n}^{(2)}$, for Increasing z_s, $0 \leq z_s \leq \infty$, with d/a a Parameter

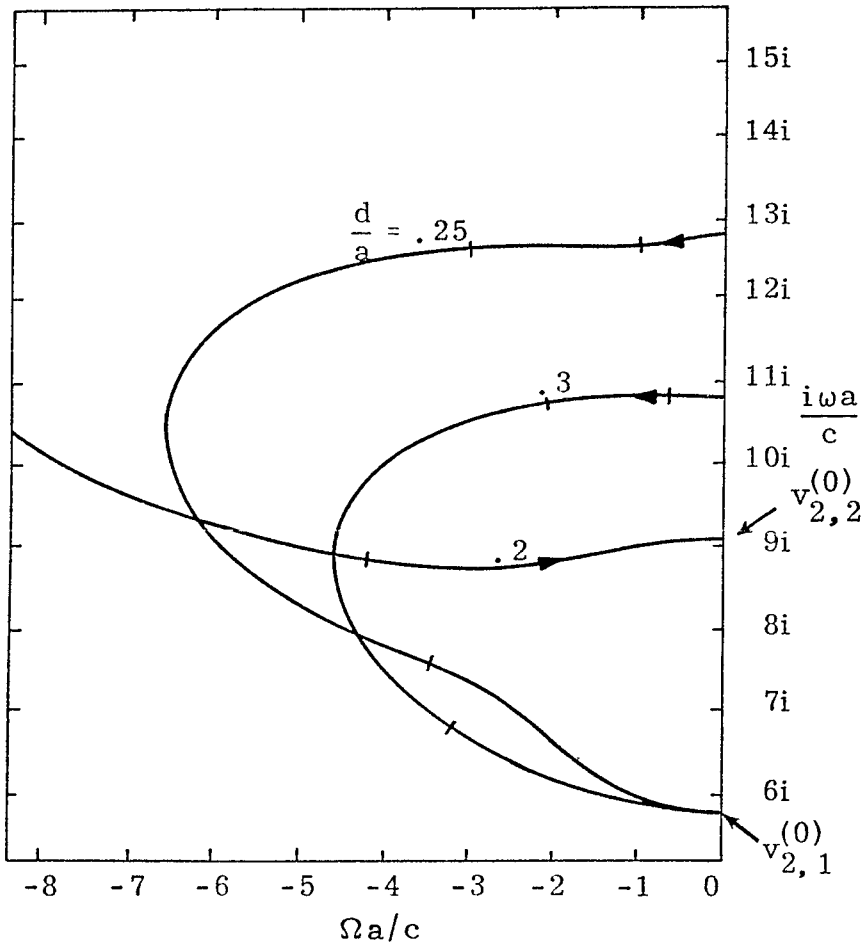

A. Values of $d/a \leq .2$ from $v_{2,1}^{(2)}$

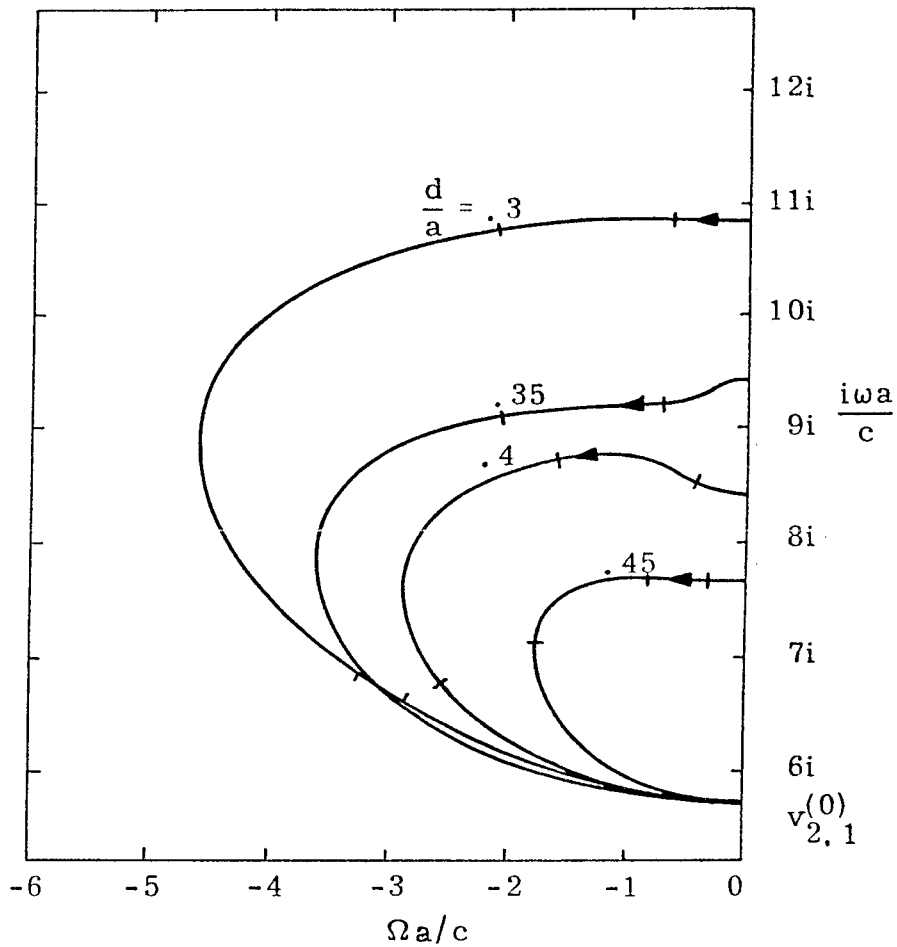

B. Values $.3 \leq d/a \leq .45$ from $v_{2,1}^{(2)}$

Figure 3.38. Trajectories from $v_{2,1}^{(2)}$ for Increasing z_s, $0 \leq z_s \leq \infty$, with d/a a Parameter

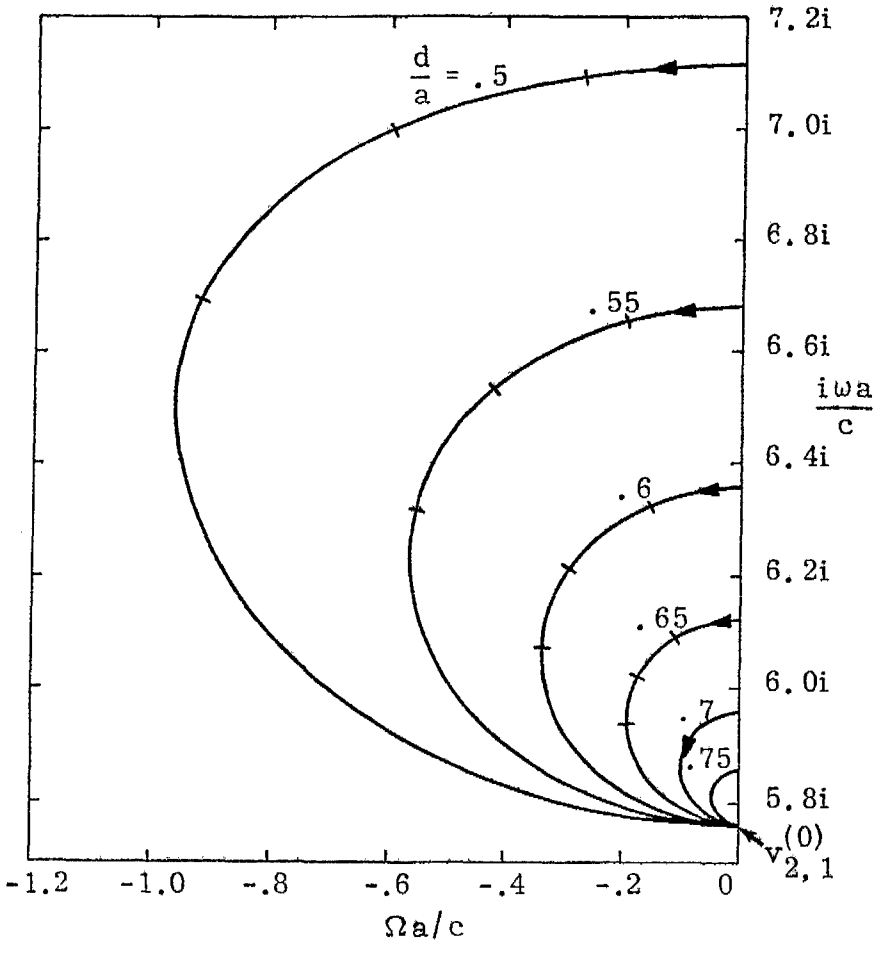

A. Values of $d/a \geq .5$ from $v_{2,1}^{(2)}$

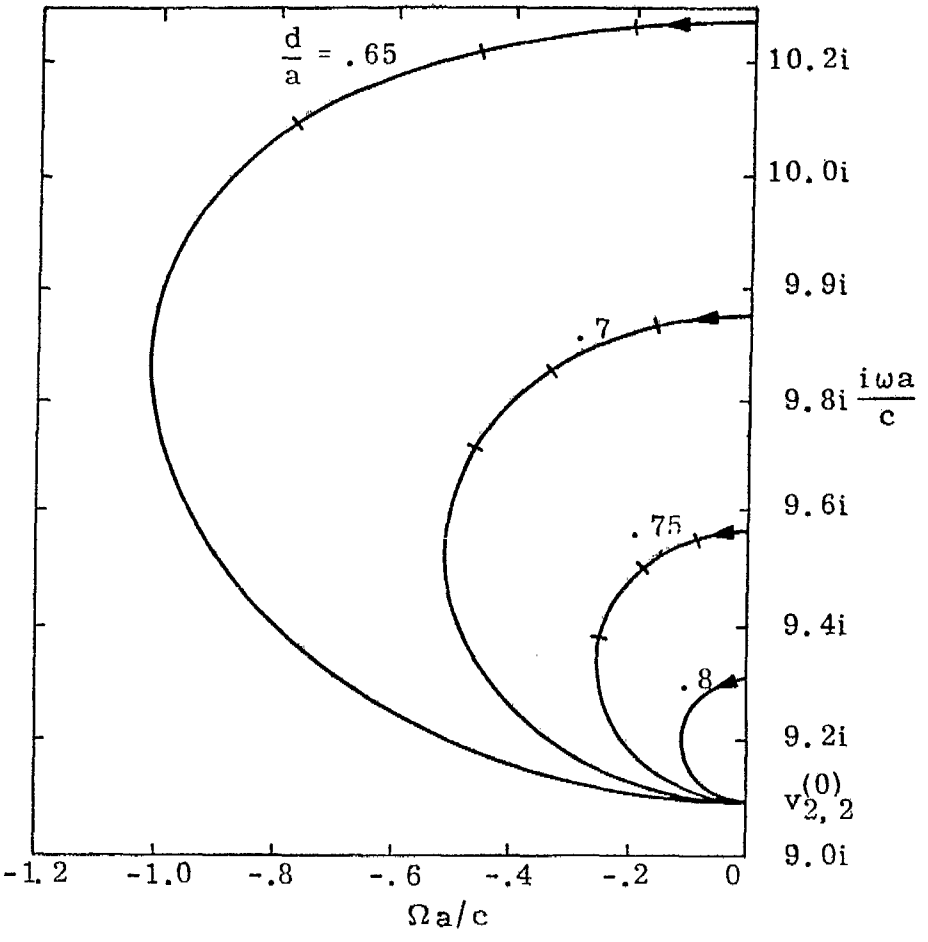

B. Values $.65 \leq d/a \leq .8$ from $v_{2,2}^{(2)}$

Figure 3.39. Trajectories from $v_{2,n}^{(2)}$, for Increasing z_s, $0 \leq z_s \leq \infty$, with d/a a Parameter

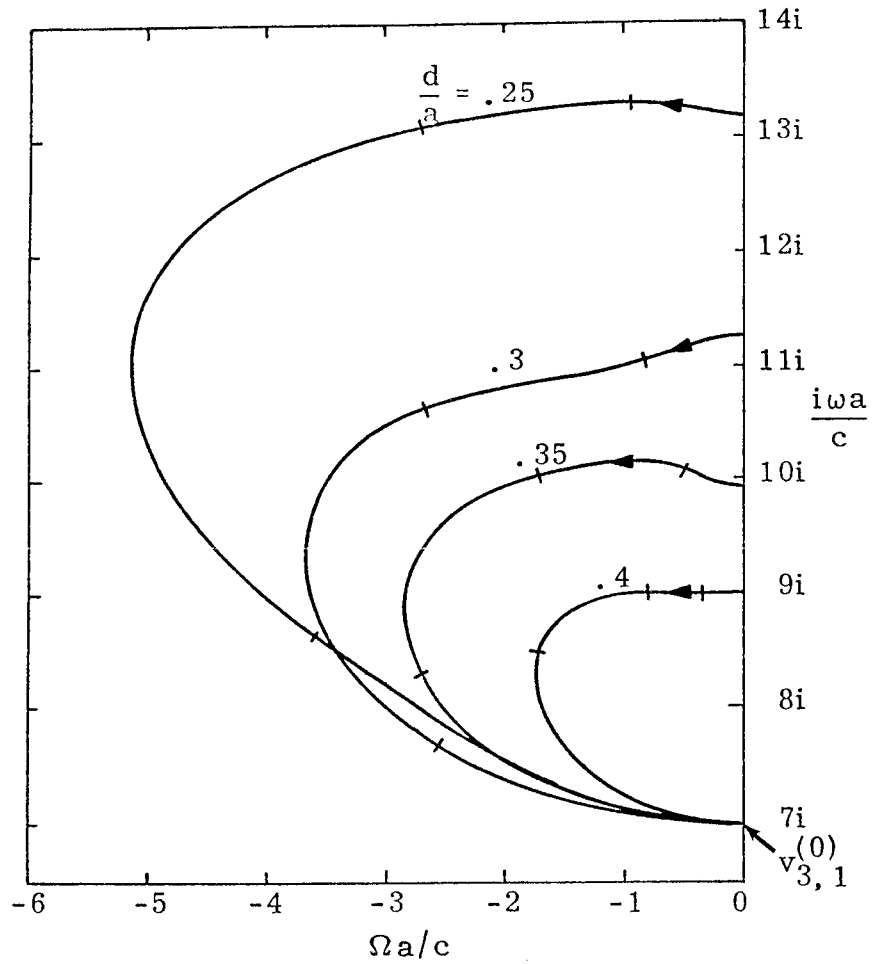

A. Values of $d/a \leq .4$ from $v_{3,1}^{(2)}$

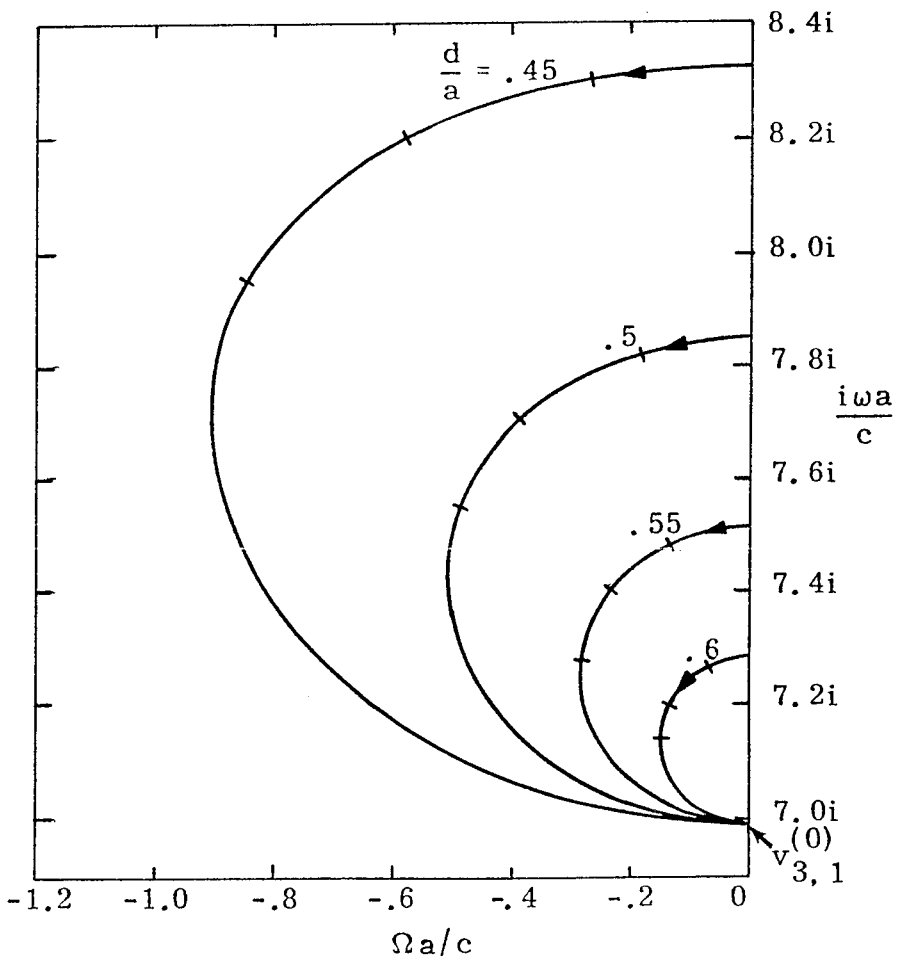

B. Values $.45 \leq d/a \leq .6$ from $v_{3,1}^{(2)}$

Figure 3.40. Trajectories from $v_{3,1}^{(2)}$ for Increasing z_s, $0 \leq z_s \leq \infty$, with d/a a Parameter

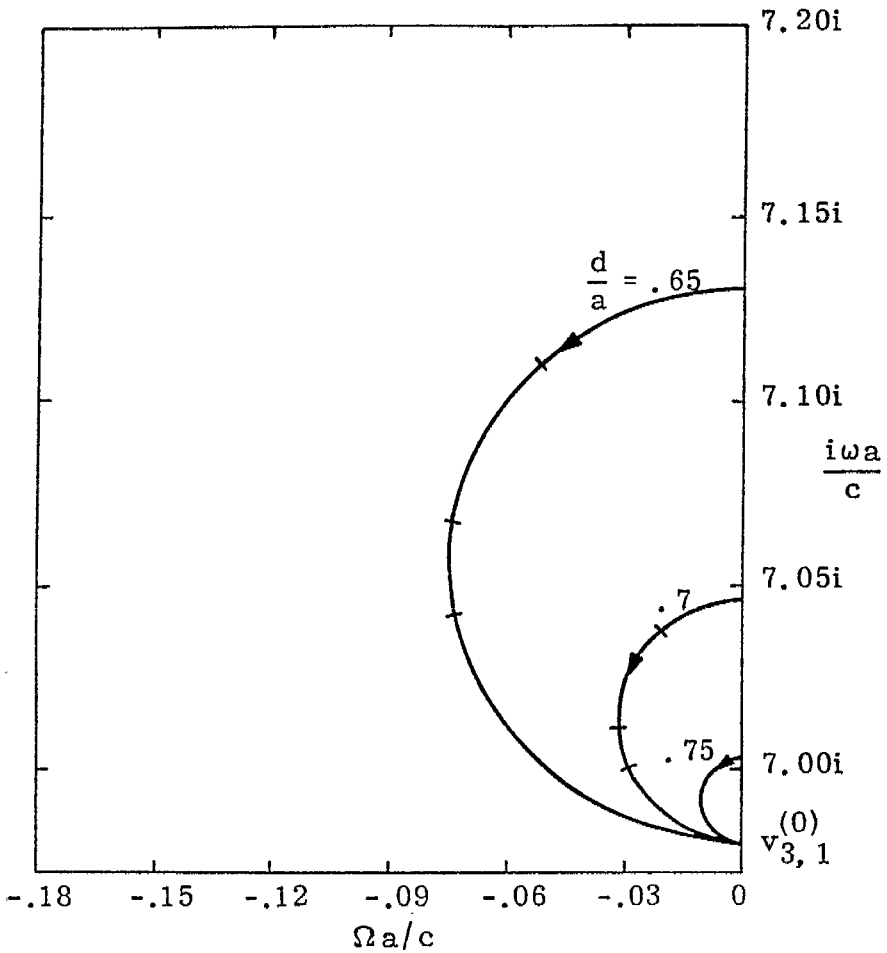

Figure 3.41. Trajectories from $v_{3,1}^{(2)}$ for Increasing z_s, $0 \leq z_s \leq \infty$, with d/a a Parameter; $d/a \geq .65$

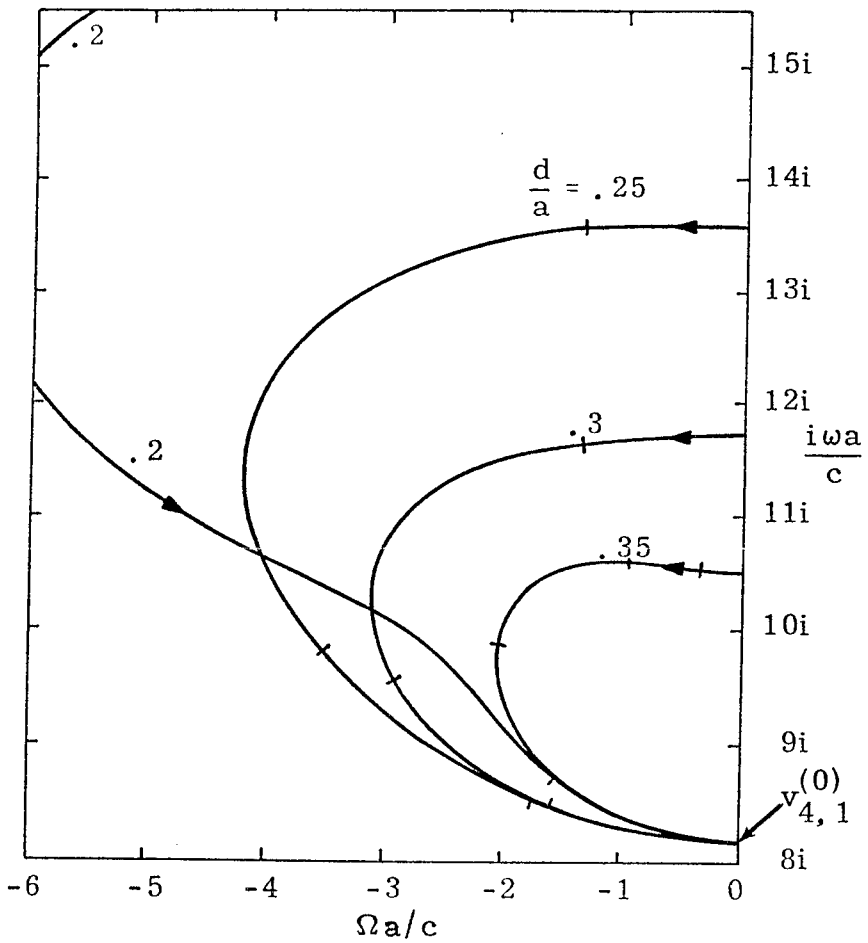

A. Values of $d/a \leq .35$ from $v_{4,1}^{(2)}$

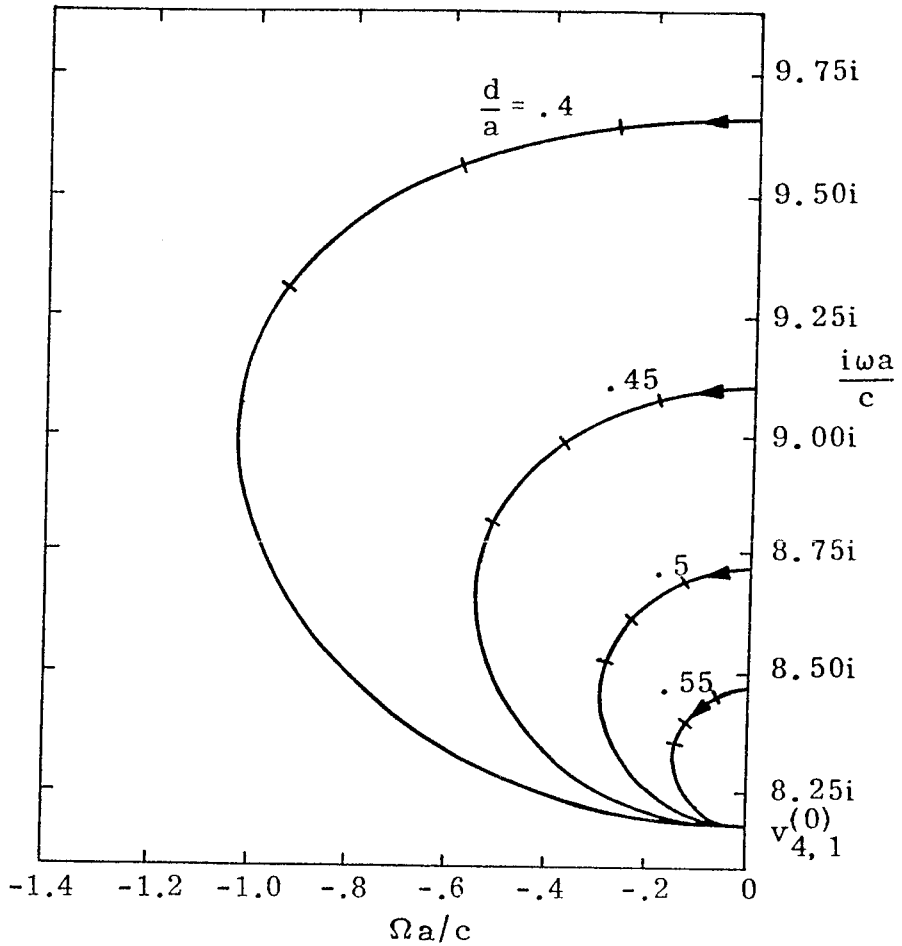

B. Values $.4 \leq d/a \leq .55$ from $v_{4,1}^{(2)}$

Figure 3.42. Trajectories from $v_{4,1}^{(2)}$ for Increasing z_s, $0 \leq z_s \leq \infty$, with d/a a Parameter

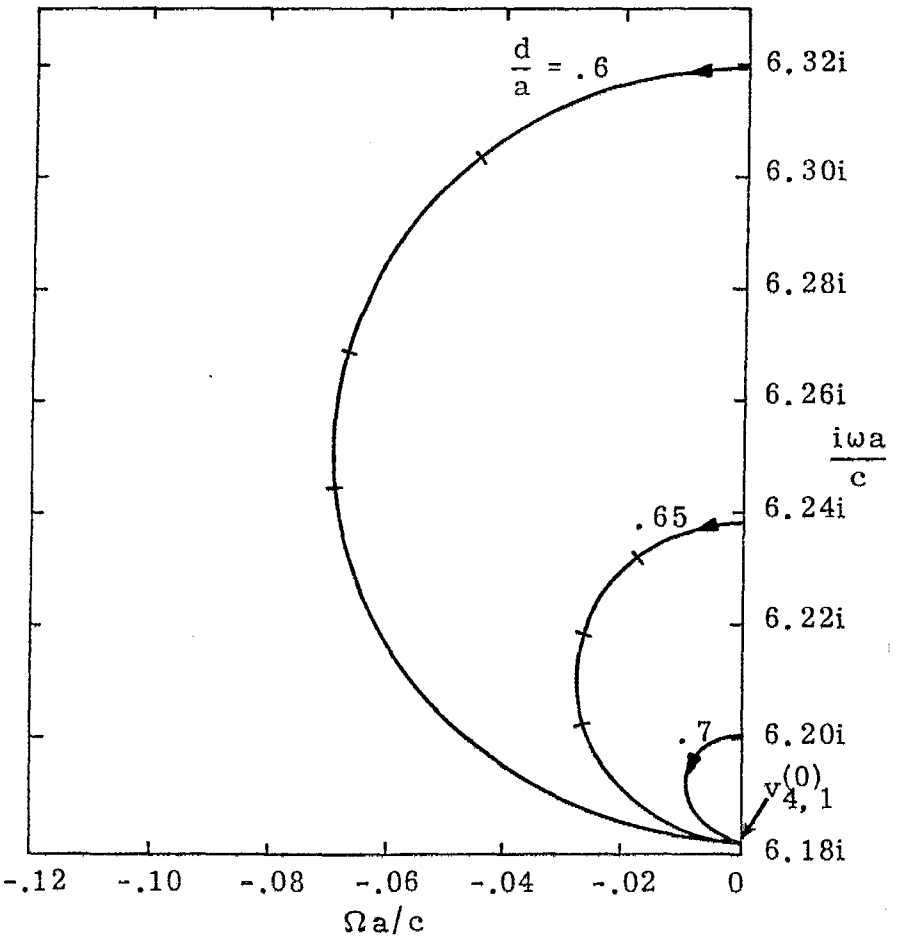

Figure 3.43. Trajectories from $v_{4,1}^{(2)}$ for Increasing z_s, $0 \leq z_s \leq \infty$, with d/a a Parameter; $d/a \geq .6$

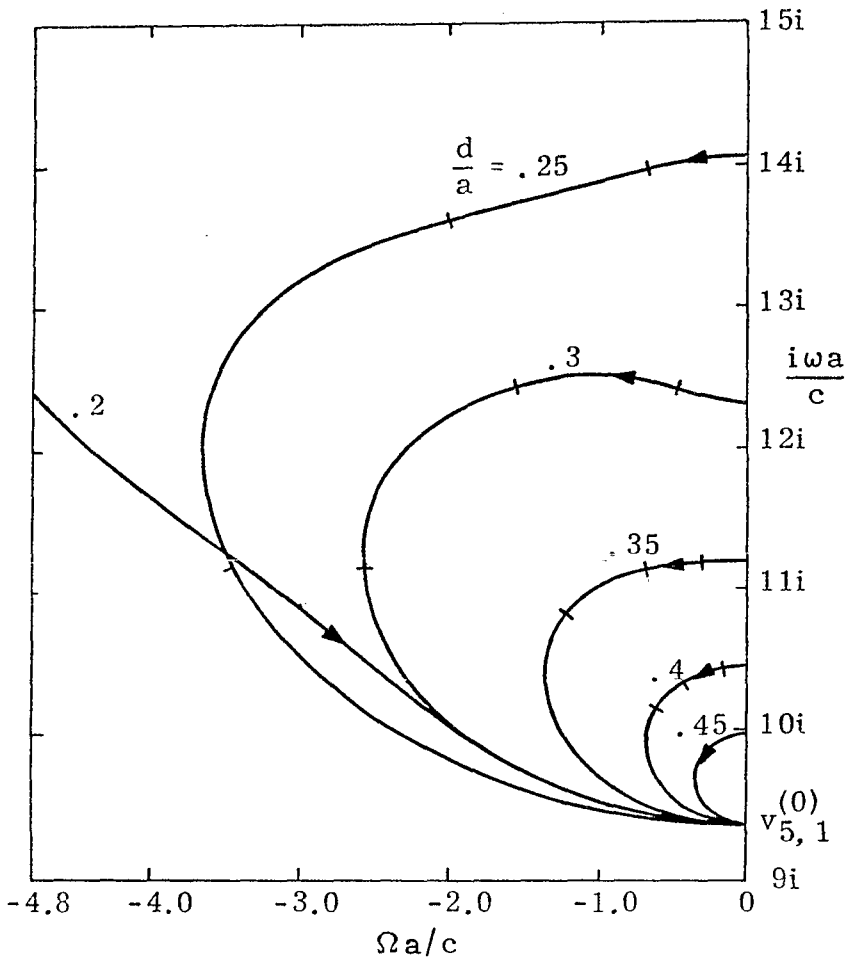

A. Values of $d/a \leq .45$ from $v_{5,1}^{(2)}$

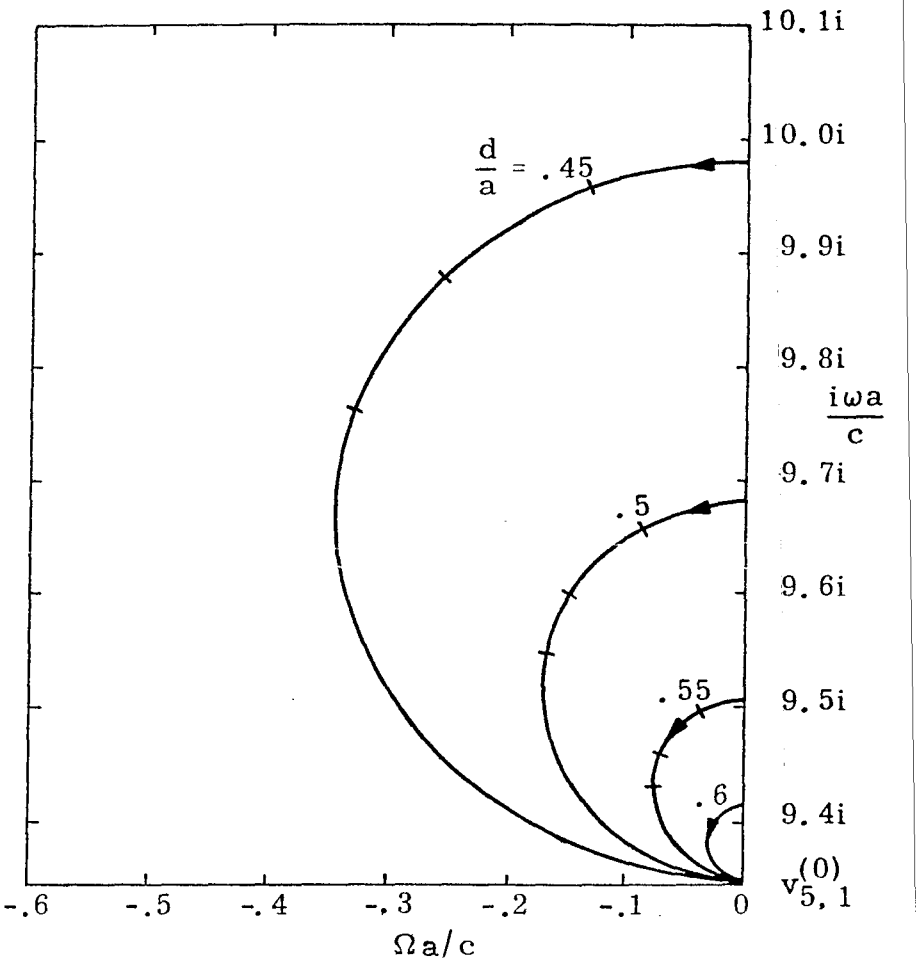

B. Values of $d/a \geq .45$ from $v_{5,1}^{(2)}$

Figure 3.44. Trajectories from $v_{5,1}^{(2)}$ for Increasing z_s, $0 \leq z_s \leq \infty$, with d/a a Parameter

IV. OPTIMUM DAMPING

For any given trajectory in the complex frequency plane, there exists a point and correspondingly the determining z_s in its path where maximum damping occurs. Naturally this maximum damping point shifts as d/a changes. In addition, the loading that produces an optimum or maximum damping for one particular pole is seldom the best value for another. Thus the selection of a d/a parameter within a given normalized frequency limit must consider not only the number of poles within this frequency limit, but where these poles are optimally damped. This fact becomes even more important when tradeoffs between which poles might be damped are considered. Moreover it has become obvious from figures 2.2 through 2.5 in conjunction with the trajectories in section III that as the parameter d/a increases the trajectories from $u^{(1)}_{n,n'}$ and $u^{(2)}_{n,n'}$ (and correspondingly those from $v^{(1)}_{n,n'}$ and $v^{(2)}_{n,n'}$) dramatically shift and eventually effect a complete interchange in position and consequent importance.

With the above information in mind then, the graphs in figures 4.2 through 4.11 are presented in an effort to show just how this optimum damping (position and loading) changes with d/a. The graphs are presented as pairs from $u^{(k)}_{n,n'}$ or $v^{(k)}_{n,n'}$ with $k = 1,2$ to represent the pole interchange around $u^{(0)}_{n,n'}$ and $v^{(0)}_{n,n'}$ as d/a increases. The resistive load is also plotted and labeled as $z^{(k)}_s$ with the superscript k representing pole type association. It might be noted that although the trajectories

make a smooth transition as d/a increases the optimum damping position does not. The reason for this stems from the coalescence that occurs between the interior (k = 2) and exterior (k = 1) poles. Typical discontinuities from coalescence are illustrated in figure 4.1.

It might be pointed out that a different definition from the outset and/or different combinations of poles presented on a graph could produce more continuous optimum damping curves. For example, consider loci from $u_{1,2}^{(2)}$ and $u_{1,1}^{(1)}$, two poles which coalesce around d/a = .47. Plotting the optimum damping of the pole from $u_{1,2}^{(2)}$ up to the point of coalescence and the optimum damping of the pole from $u_{1,1}^{(1)}$ after this point produces a continuous curve. This approach was not taken, however, to avoid the multitude of curves that would be necessary for some poles.

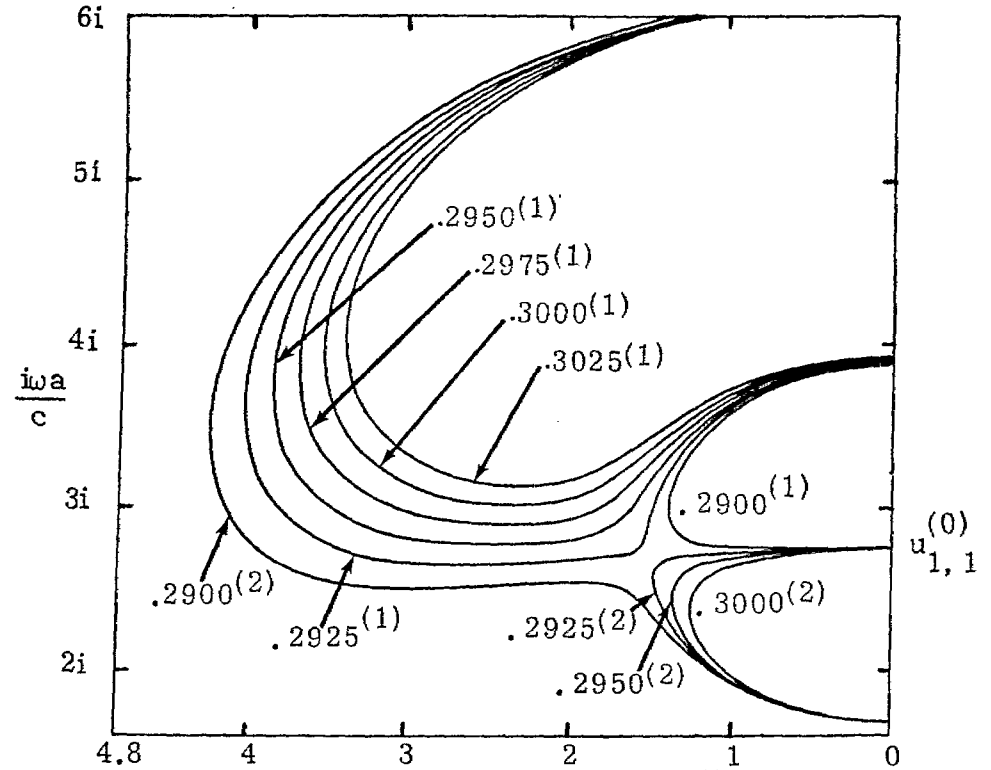

A. Trajectories Originating from $u^{(1)}_{1,1}$ and $u^{(2)}_{1,1}$ with d/a a Parameter and Increasing z_s, $0 \le z_s \le \infty$

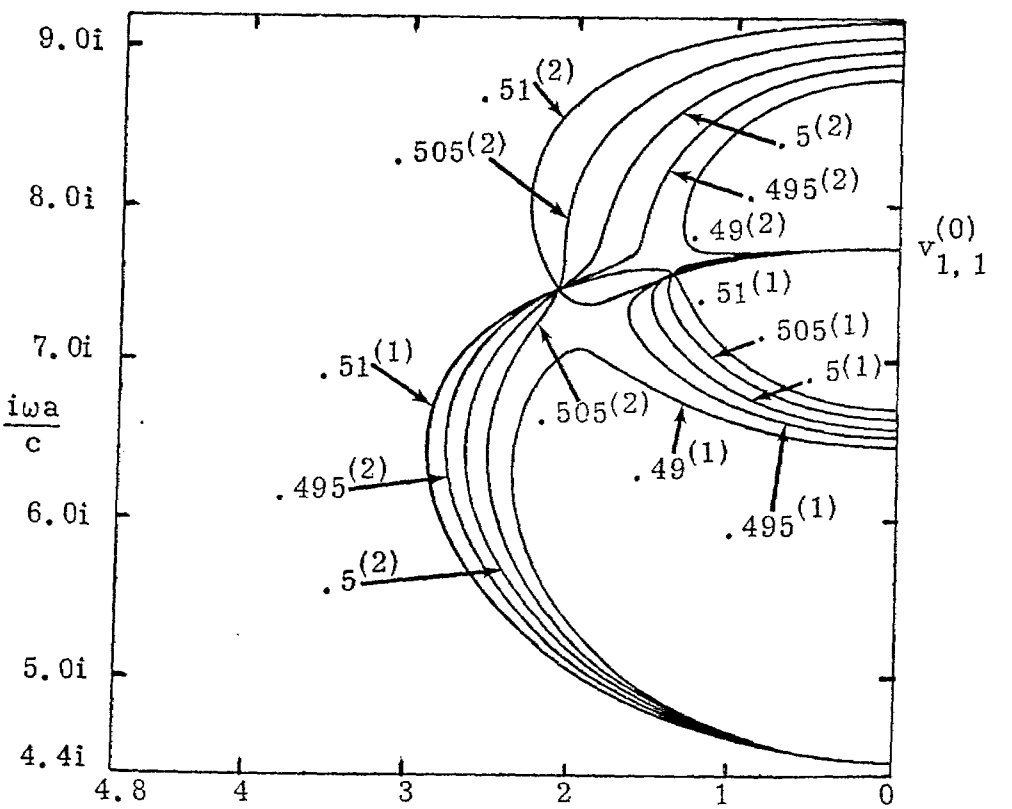

B. Trajectories Originating from $v^{(1)}_{1,1}$ and $v^{(2)}_{1,1}$ with d/a a Parameter and Increasing z_s, $0 \le z_s \le \infty$

Figure 4.1. Typical Exchange of Terminal Position at Coalescence of Trajectories (Superscript on d/a corresponds to k)

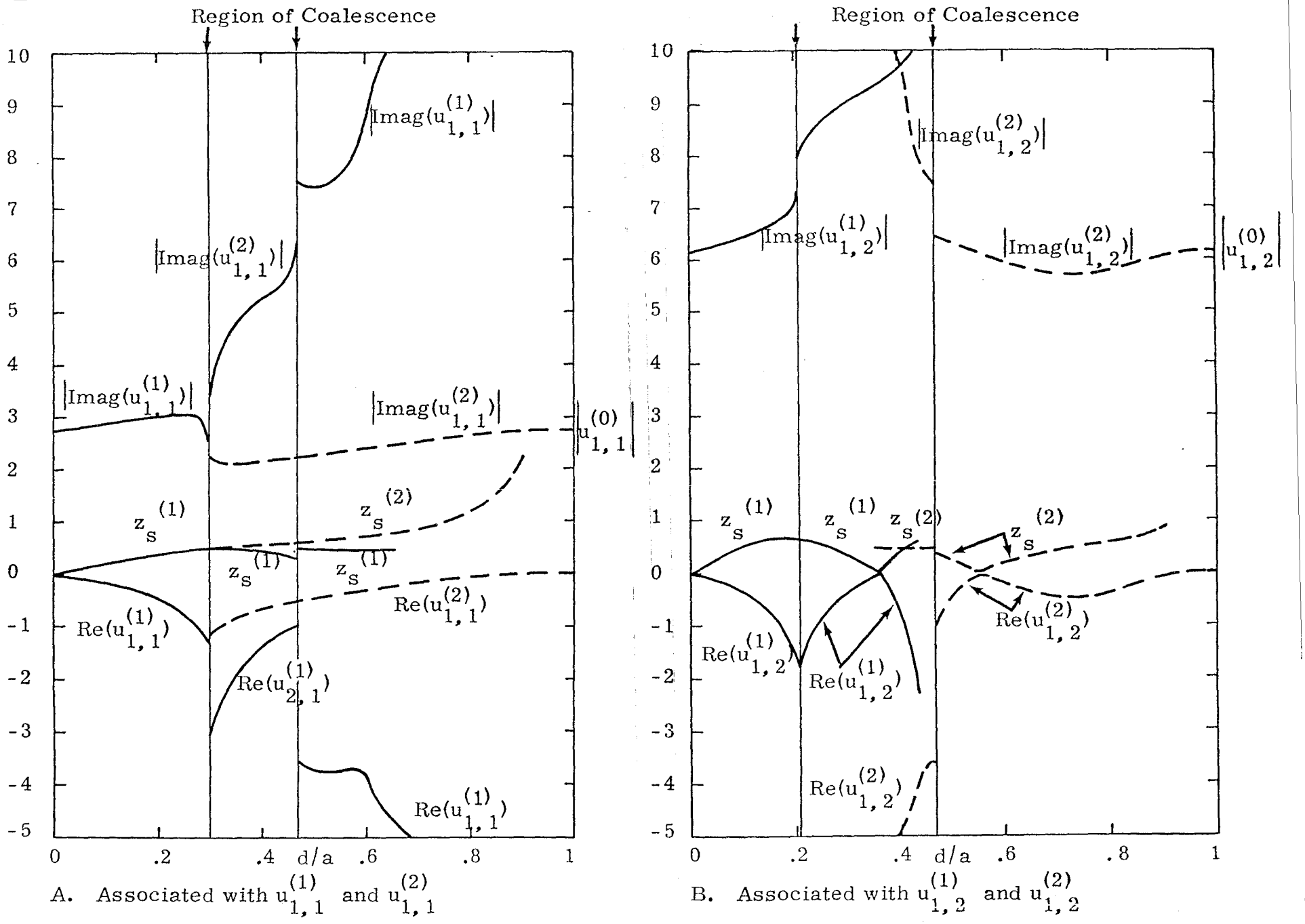

A. Associated with $u^{(1)}_{1,1}$ and $u^{(2)}_{1,1}$

B. Associated with $u^{(1)}_{1,2}$ and $u^{(2)}_{1,2}$

Figure 4.2. Optimum Damping ($Re(\gamma a)$, $|Imag(\gamma a)|$) and Resulting Loading ($z_s^{(k)}$) Versus d/a of Trajectories Originating from the Innermost Sphere (Solid Line, k = 1) and Between the Liner and Shell (Dotted Line, k = 2)

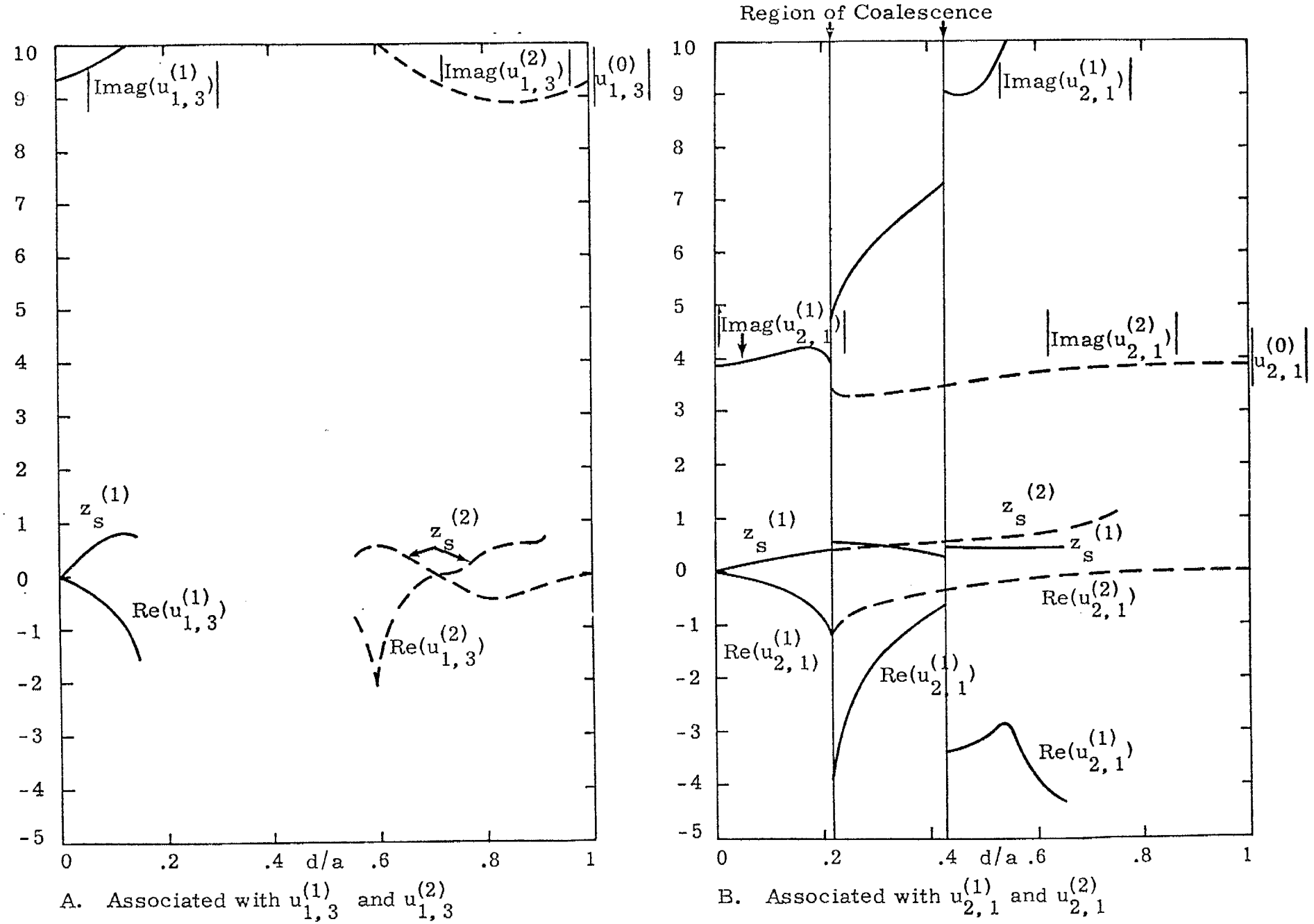

Figure 4.3. Optimum Damping (Re(γa), |Imag(γa)|) and Resulting Loading ($z_s^{(k)}$) Versus d/a of Trajectories Originating from the Innermost Sphere (Solid Line, k = 1) and Between the Liner and Shell (Dotted Line, k = 2)

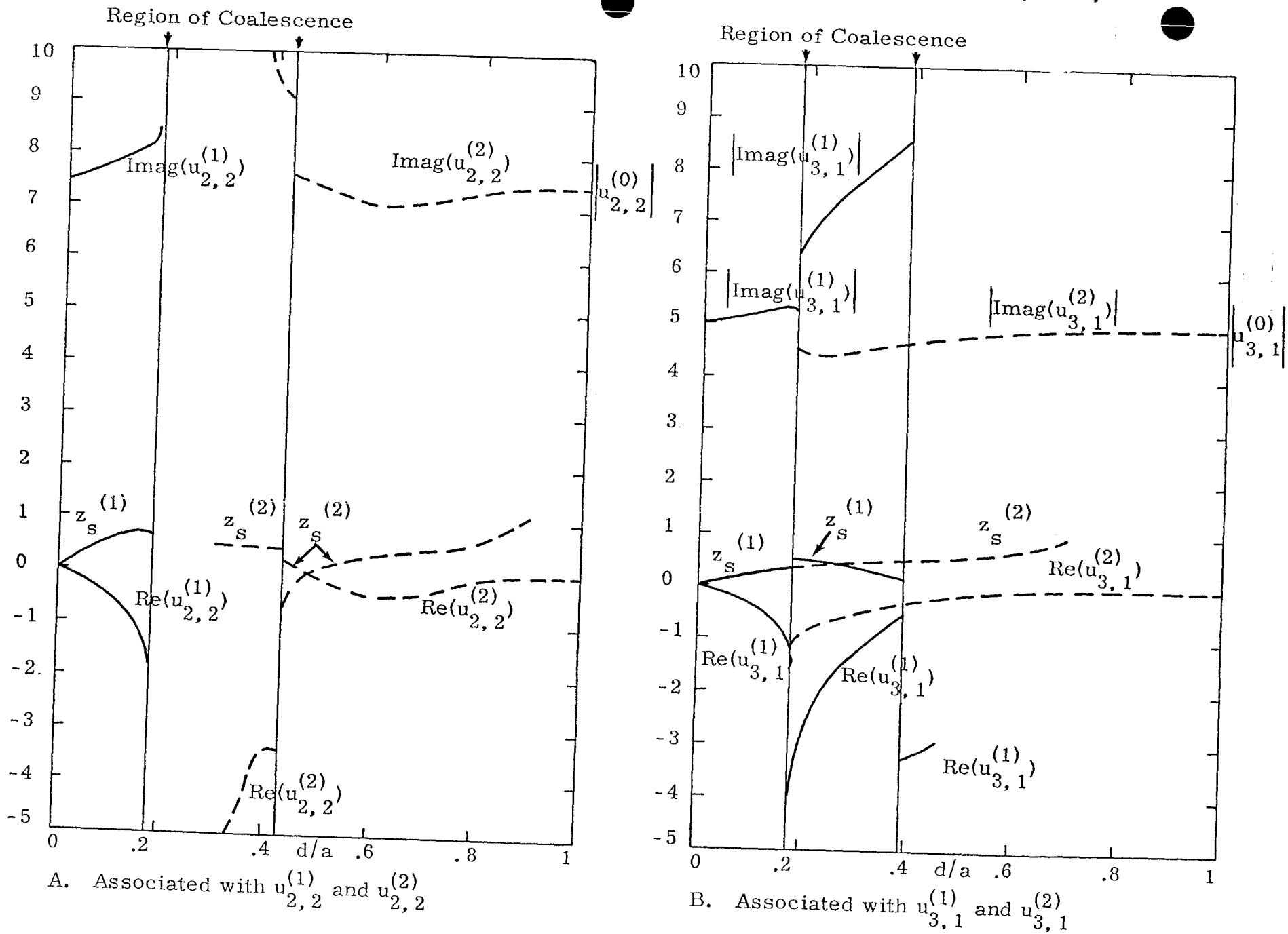

Figure 4.4. Optimum Damping (Re(γa), |Imag(γa)|) and Resulting Loading ($z_s^{(k)}$) Versus d/a of Trajectories Originating from the Innermost Sphere (Solid Line, k = 1) and Between the Liner and Shell (Dotted Line, k = 2)

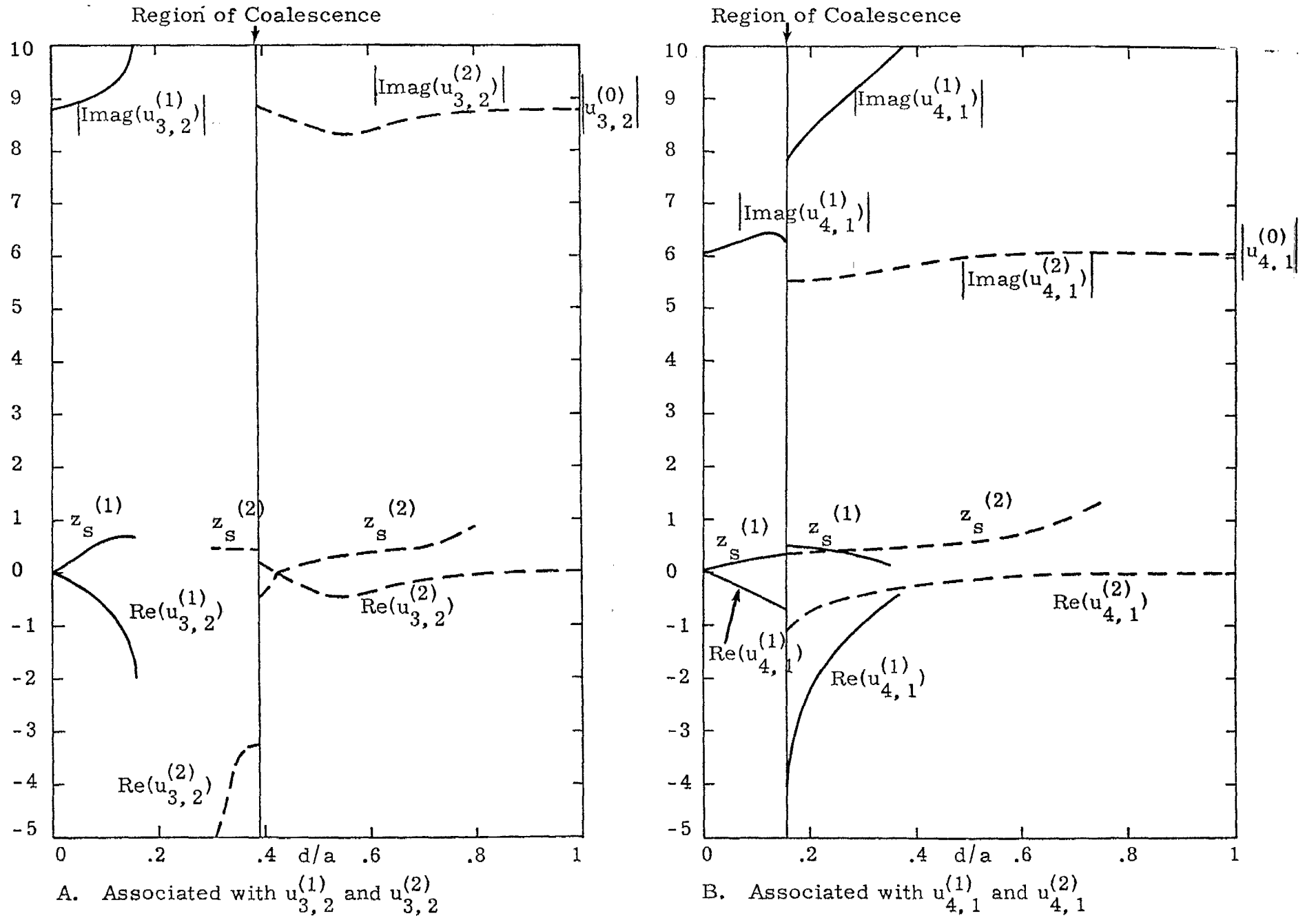

A. Associated with $u^{(1)}_{3,2}$ and $u^{(2)}_{3,2}$

B. Associated with $u^{(1)}_{4,1}$ and $u^{(2)}_{4,1}$

Figure 4.5. Optimum Damping (Re(γa), $|\text{Imag}(\gamma a)|$) and Resulting Loading ($z_s^{(k)}$) Versus d/a of Trajectories Originating from the Innermost Sphere (Solid Line, k = 1) and Between the Liner and Shell (Dotted Line, k = 2)

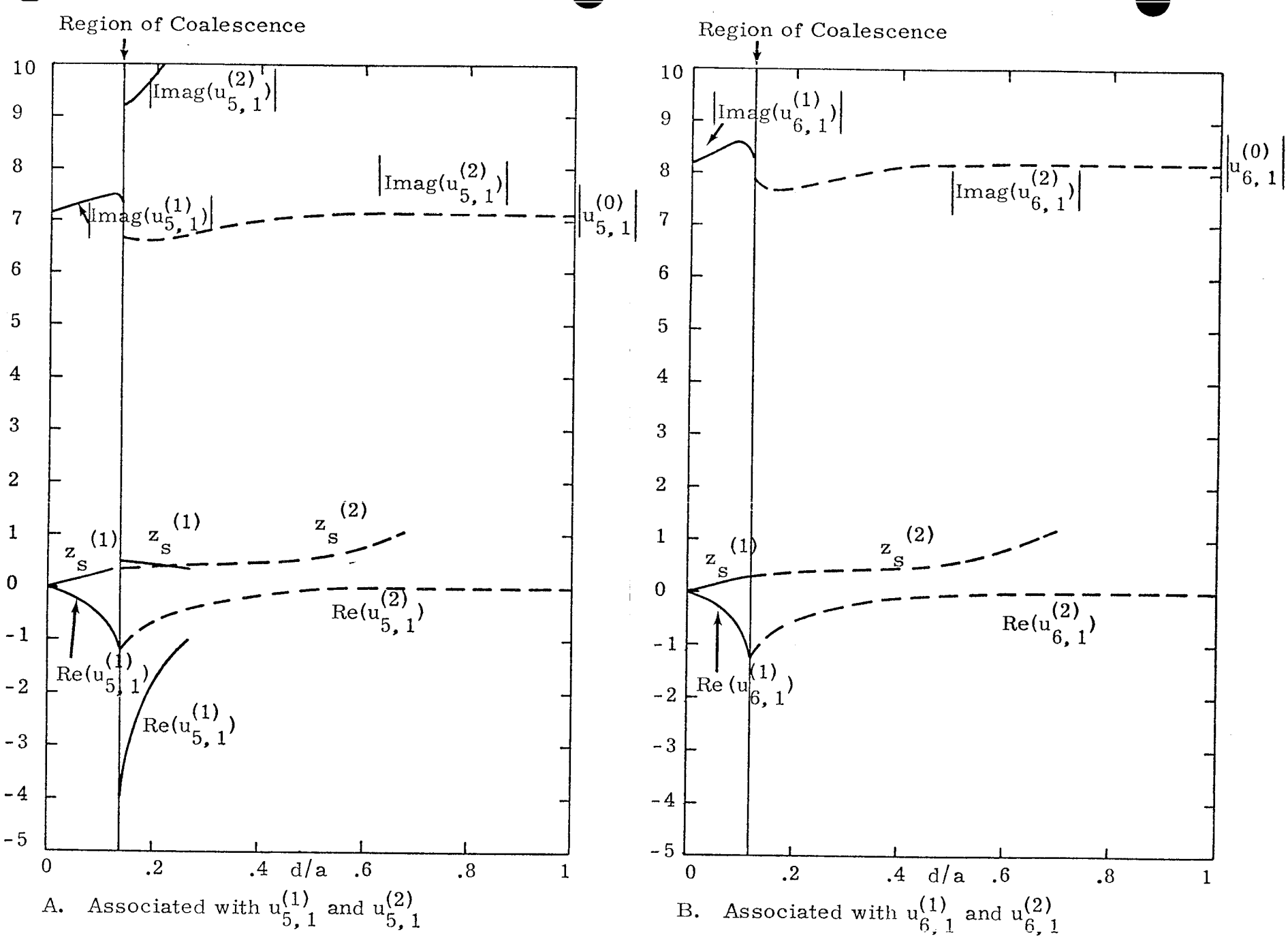

A. Associated with $u^{(1)}_{5,1}$ and $u^{(2)}_{5,1}$

B. Associated with $u^{(1)}_{6,1}$ and $u^{(2)}_{6,1}$

Figure 4.6. Optimum Damping (Re(γa), |Imag(γa)|) and Resulting Loading ($z_s^{(k)}$) Versus d/a of Trajectories Originating from the Innermost Sphere (Solid Line, k = 1) and Between the Liner and Shell (Dotted Line, k = 2)

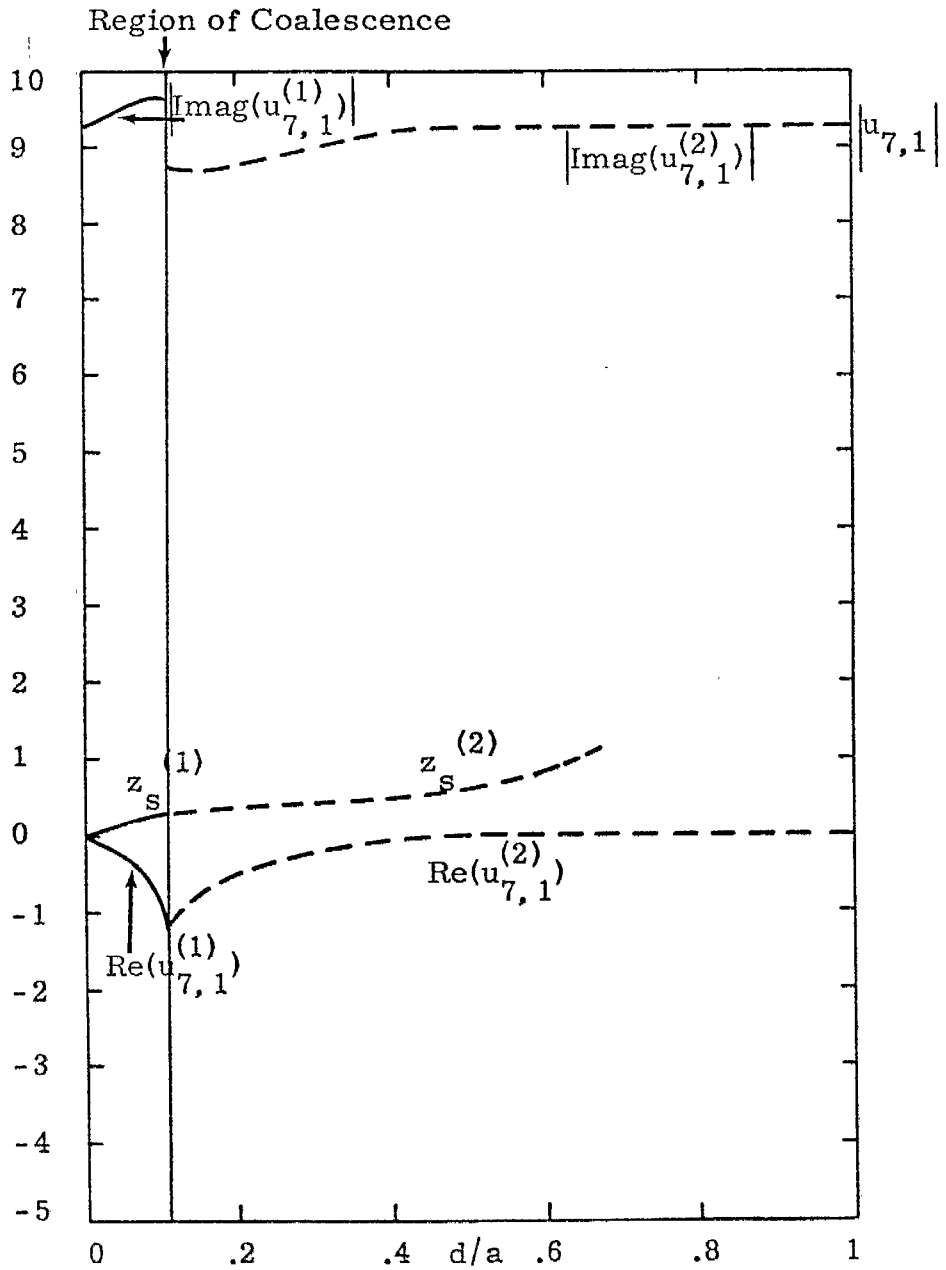

A. Associated with $u_{7,1}^{(1)}$ and $u_{7,1}^{(2)}$

Figure 4.7. Optimum Damping (Re(γa), |Imag(γa)|) and Resulting Loading ($z_s^{(k)}$) Versus d/a of Trajectories Originating from the Innermost Sphere (Solid Line, k = 1) and Between the Lines and Shell (Dotted Line, k = 2)

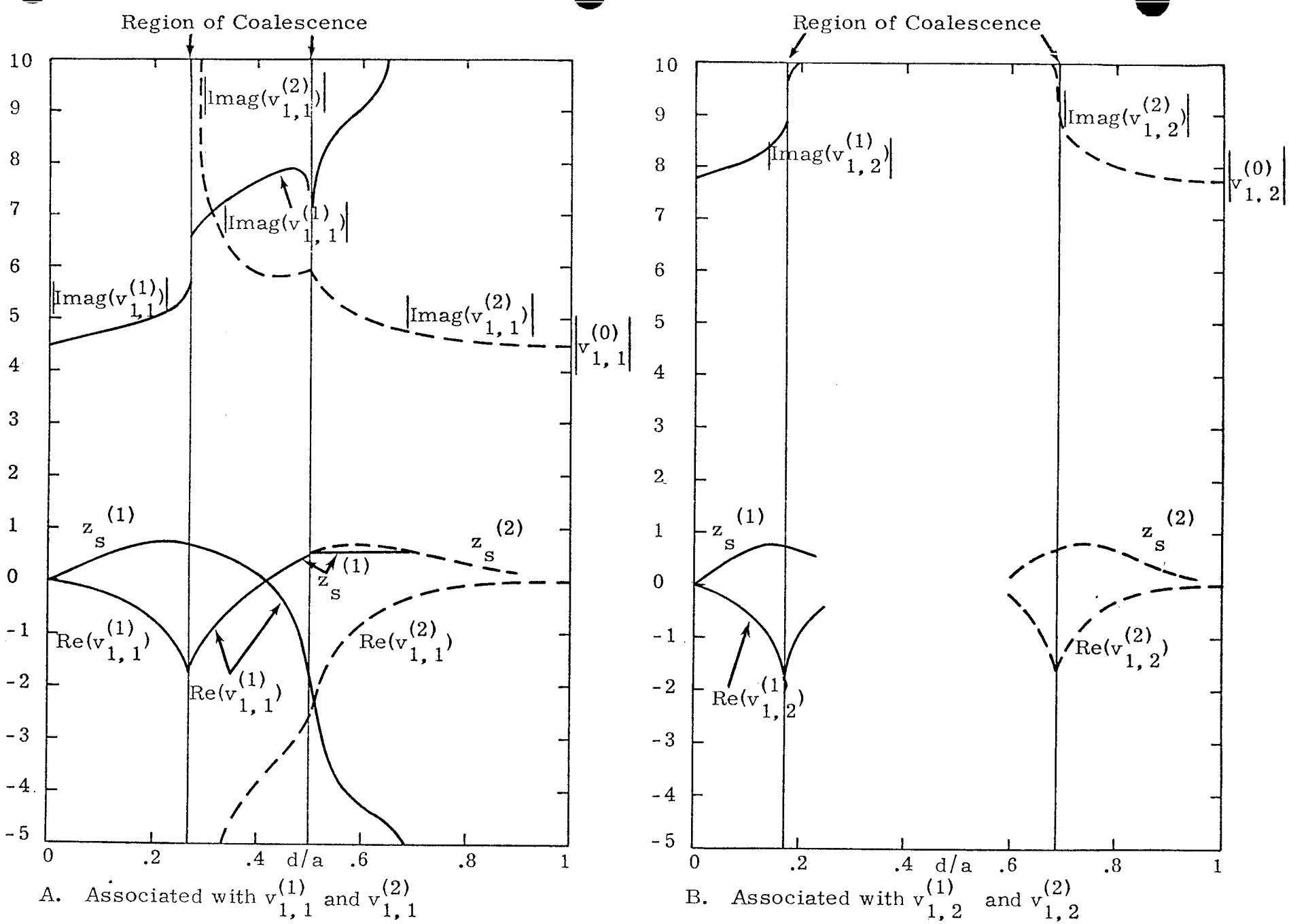

A. Associated with $v_{1,1}^{(1)}$ and $v_{1,1}^{(2)}$

B. Associated with $v_{1,2}^{(1)}$ and $v_{1,2}^{(2)}$

Figure 4.8. Optimum Damping ($\text{Re}(\gamma a)$, $|\text{Imag}(\gamma a)|$) and Resulting Loading ($z_s^{(k)}$) Versus d/a of Trajectories Originating from the Innermost Sphere (Solid Line, k = 1) and Between the Liner and Shell (Dotted Line, k = 2)

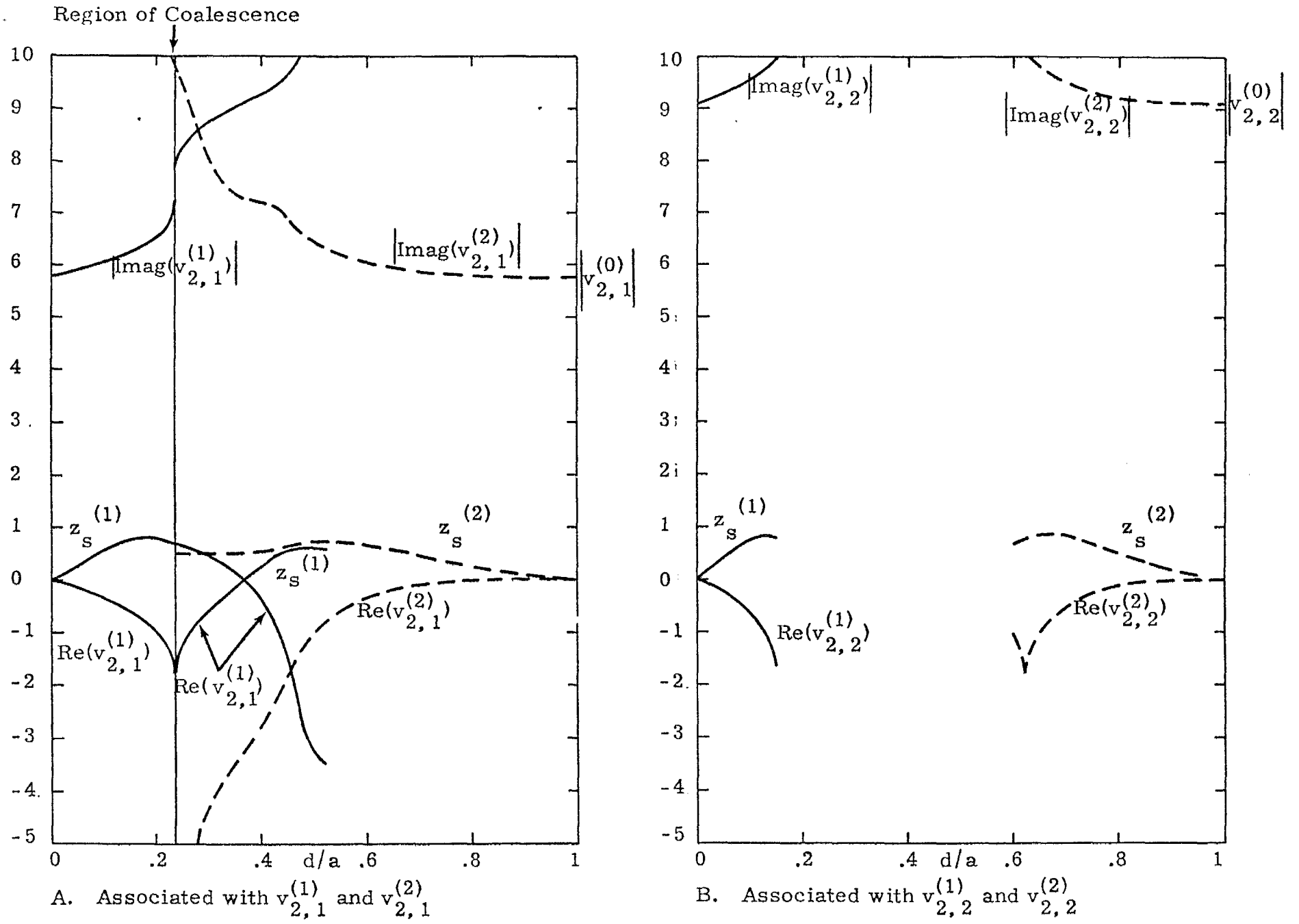

A. Associated with $v_{2,1}^{(1)}$ and $v_{2,1}^{(2)}$

B. Associated with $v_{2,2}^{(1)}$ and $v_{2,2}^{(2)}$

Figure 4.9. Optimum Damping ($\text{Re}(\gamma a)$, $|\text{Imag}(\gamma a)|$) and Resulting Loading ($z_s^{(k)}$) Versus d/a of Trajectories Originating from the Innermost Sphere (Solid Line, k = 1) and Between the Liner and Shell (Dotted Line, k = 2)

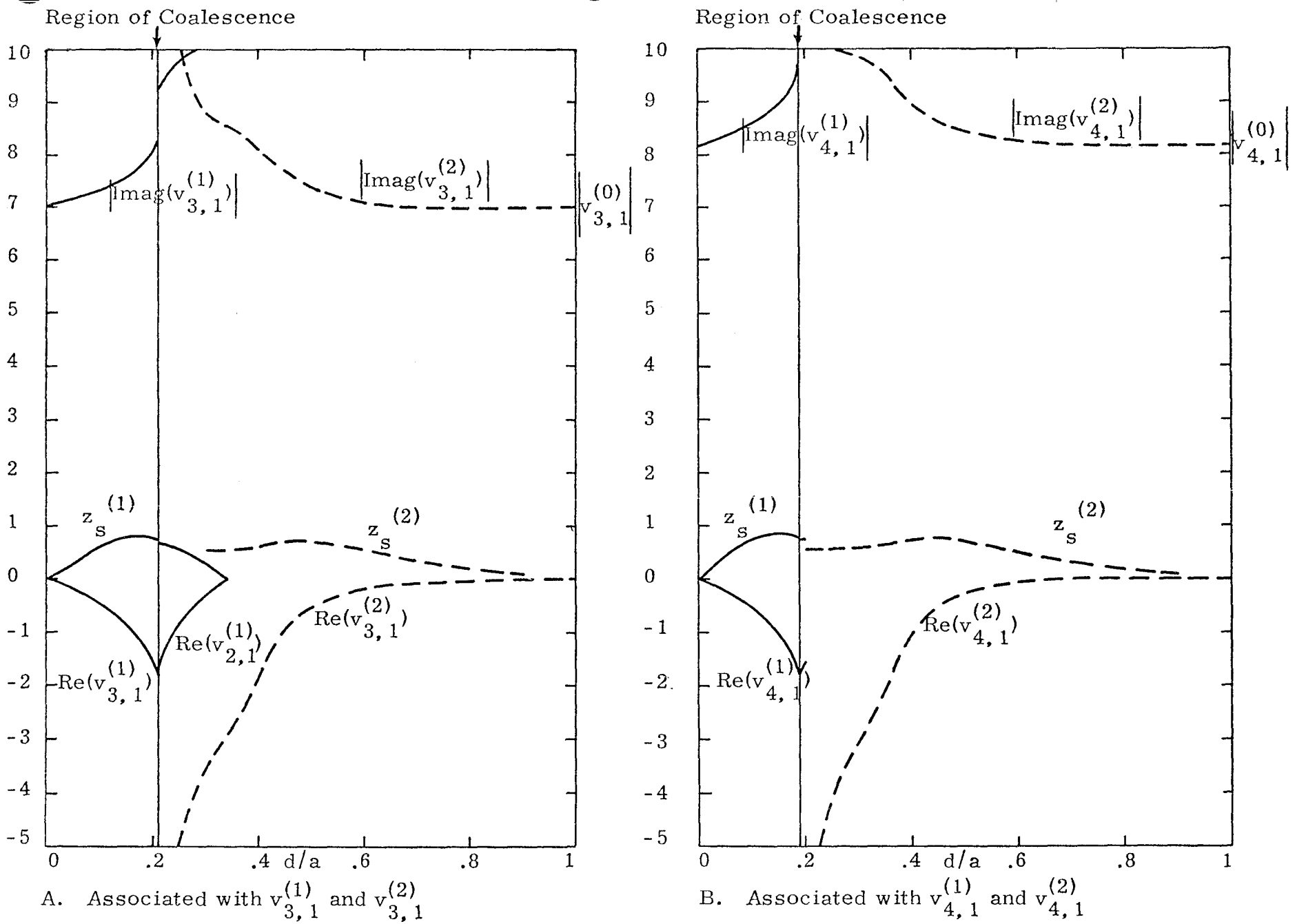

A. Associated with $v_{3,1}^{(1)}$ and $v_{3,1}^{(2)}$

B. Associated with $v_{4,1}^{(1)}$ and $v_{4,1}^{(2)}$

Figure 4.10. Optimum Damping ($\text{Re}(\gamma a)$, $|\text{Imag}(\gamma a)|$) and Resulting Loading ($z_s^{(k)}$) Versus d/a of Trajectories Originating from the Innermost Sphere (Solid Line, k = 1) and Between the Liner and Shell (Dotted Line, k = 2)

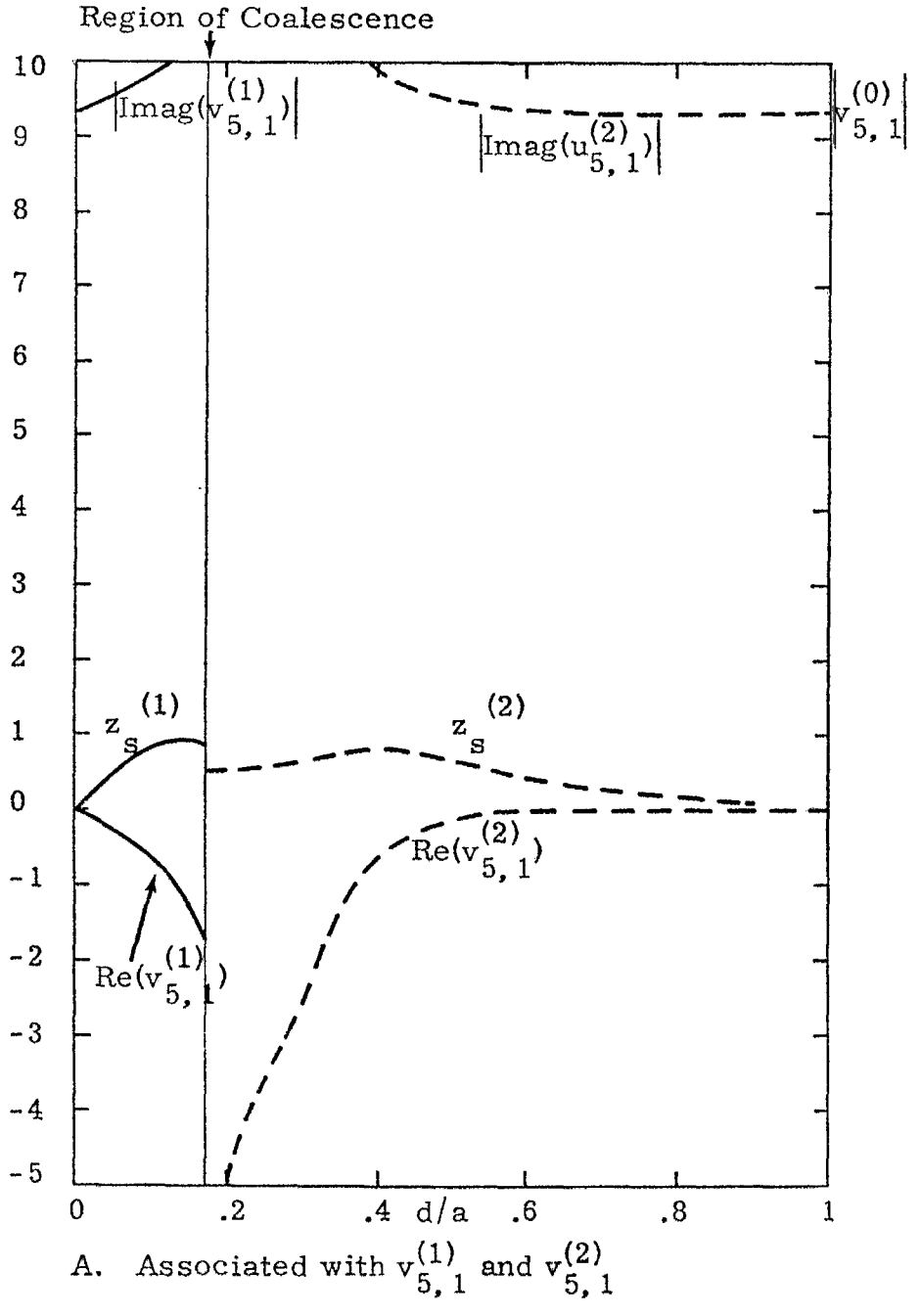

A. Associated with $v_{5,1}^{(1)}$ and $v_{5,1}^{(2)}$

Figure 4.11. Optimum Damping (Re(γa), |Imag(γa)|) and Resulting Loading ($z_s^{(k)}$) Versus d/a of Trajectories Originating from the Innermost Sphere (Solid Line, k = 1) and Between the Liner and Shell (Dotted Line, k = 2)

V. RESONANT FREQUENCY SHIFT RESULTING FROM THE SHEET LINER LOCATION WITH FIXED RESISTANCE

If the sheet liner is allowed to vary from the shell wall to the sphere center ($0 \leq d/a \leq 1$) while holding its resistance (z_s) constant, the resonant frequencies shift in a manner quite different from those illustrated in section III. With the addition of these trajectories the entire pole reaction to parameter alteration is provided.

For very small z_s the trajectory of a particular resonant frequency must move approximately as $u^{(1)}_{n,n'}$ or $v^{(1)}_{n,n'}$ as discussed in section II. Large z_s trajectories must approach $u^{(0)}_{n,n'}$ or $v^{(0)}_{n,n'}$ as shown in the asymptotic form in reference 1.

The trajectories of the resonant frequencies (E and H) as the constant resistance sheet liner moves through the range $0 \leq d/a \leq 1$ are given in figures 5.1 through 5.6. The curves are not identified as far as kind ($k = 1$ or $k = 2$) since a smooth transition is made from one to the other and this distinction is not the utmost interest here. In general, however, the upper movement of the loci represents poles from $u^{(1)}_{n,n'}$ ($v^{(1)}_{n,n'}$) while the descending loci tend to be poles from $u^{(2)}_{n,n'}$ ($v^{(2)}_{n,n'}$) for increasing d/a. One exception is the trajectory from $u^{(2)}_{n,1}$ which has an upward mobility with increasing d/a.

The graphs are arranged according to increasing mode with some modes broken into two graphs--one with $z_s = .2, .4$ and the other with $z_s = .5, .6$. This arrangement is solely to avoid crowding. The values

of constant z_s selected for parameters are those that cut through interesting portions of the damping versus loading graphs in the previous section.

As mentioned in connection with tables 3.1 through 3.7, one pole exits each $u^{(0)}_{n,n'}$ for each pole entry. The seemingly disjointed trajectory loops seen in the upper portion of the graphs (e.g., $z_s = .4$ for loci from $u^{(k)}_{1,n'}$ in figure 5.1A) are the results of the smooth transition of the trajectory from $u^{(2)}_{n,n'}$ into the trajectory from $u^{(1)}_{n,n'}$ as mentioned above.

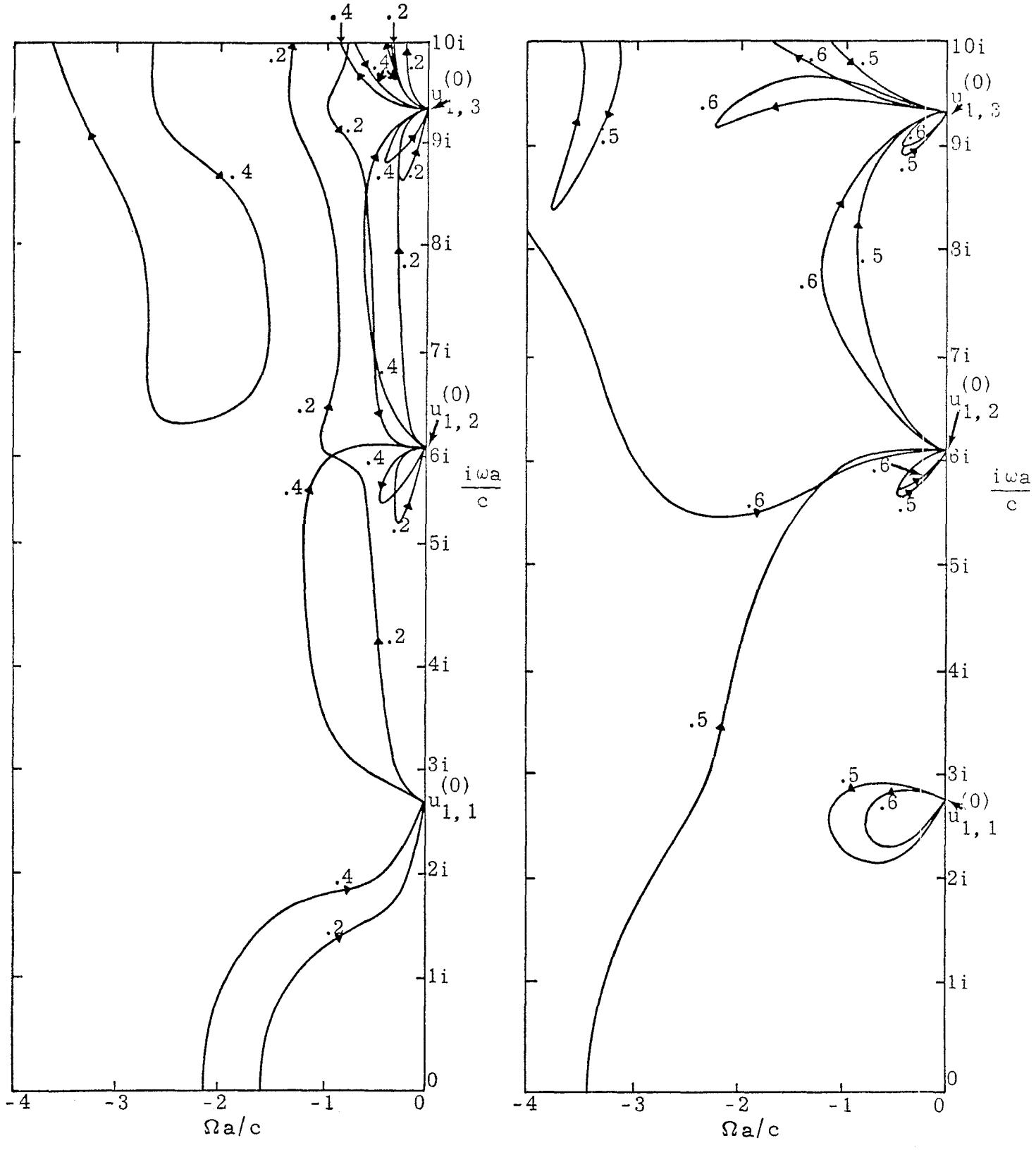

A. $z_s = .2, .4$

B. $z_s = .5, .6$

Figure 5.1. Trajectories from $u^k_{1,n'}$ for Varying d/a with z_s a Parameter Arrows Indicate Increasing d/a

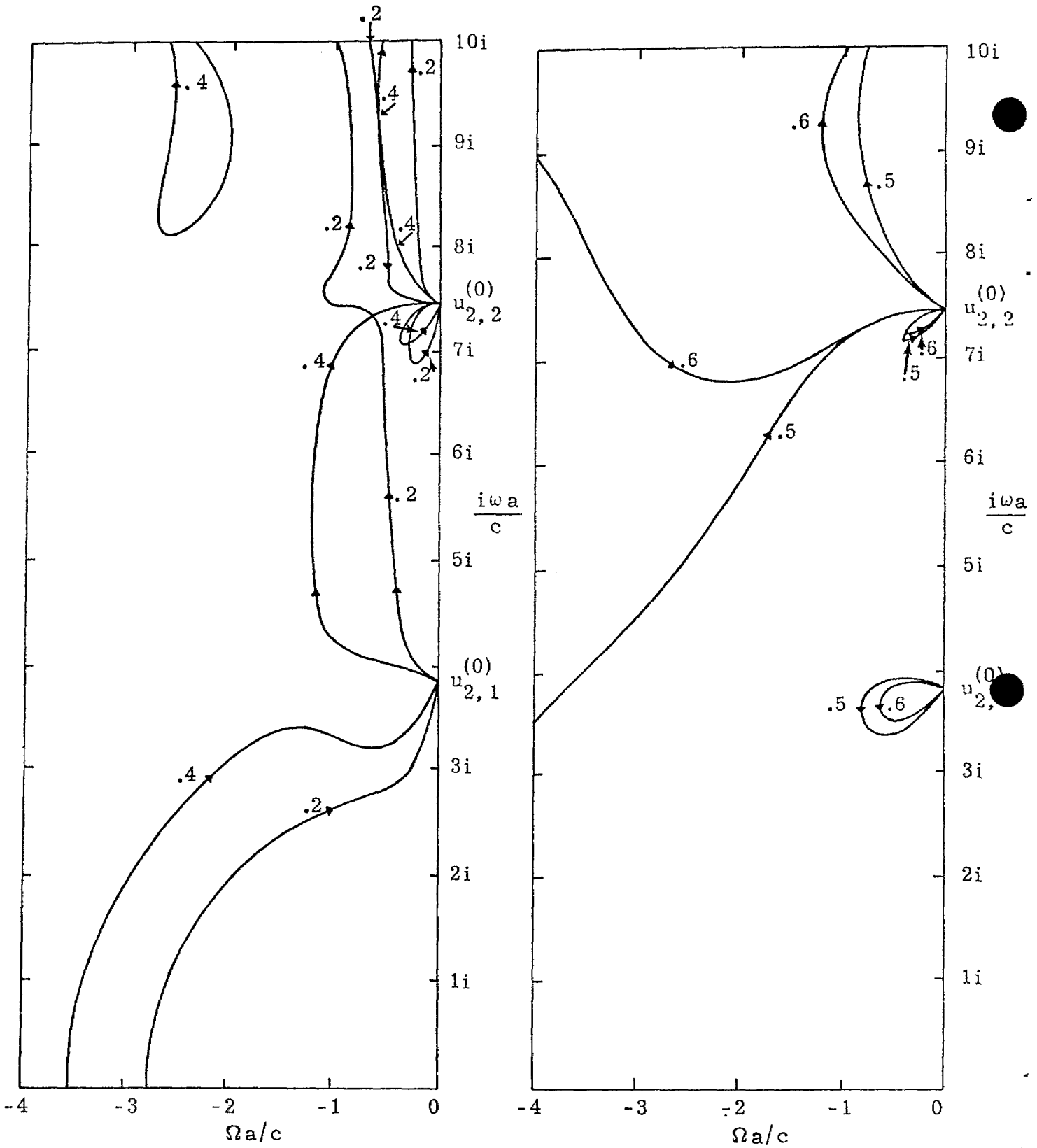

A. $z_s = .2, .4$

B. $z_s = .5, .6$

Figure 5.2. Trajectories from $u^k_{2,n'}$ for Varying d/a with z_s a Parameter
Arrows Indicate Increasing d/a

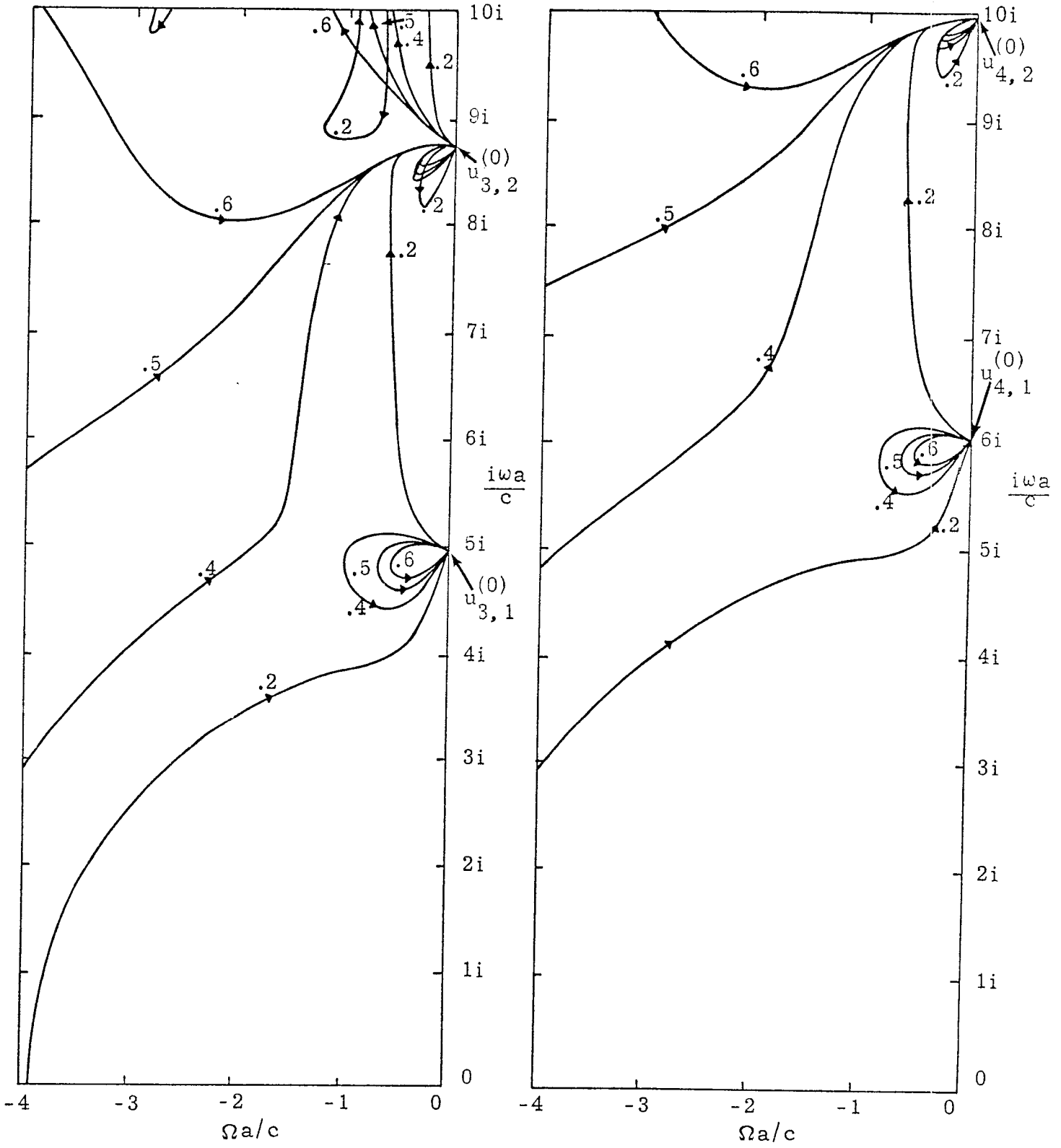

A. z_s = .2, .3, .4, .5; n = 3

B. z_s = .2, .3, .4, .5; n = 4

Figure 5.3. Trajectories from $u^k_{n,n'}$ for Varying d/a with z_s a Parameter, n = 3, 4. Arrows indicate Increasing d/a

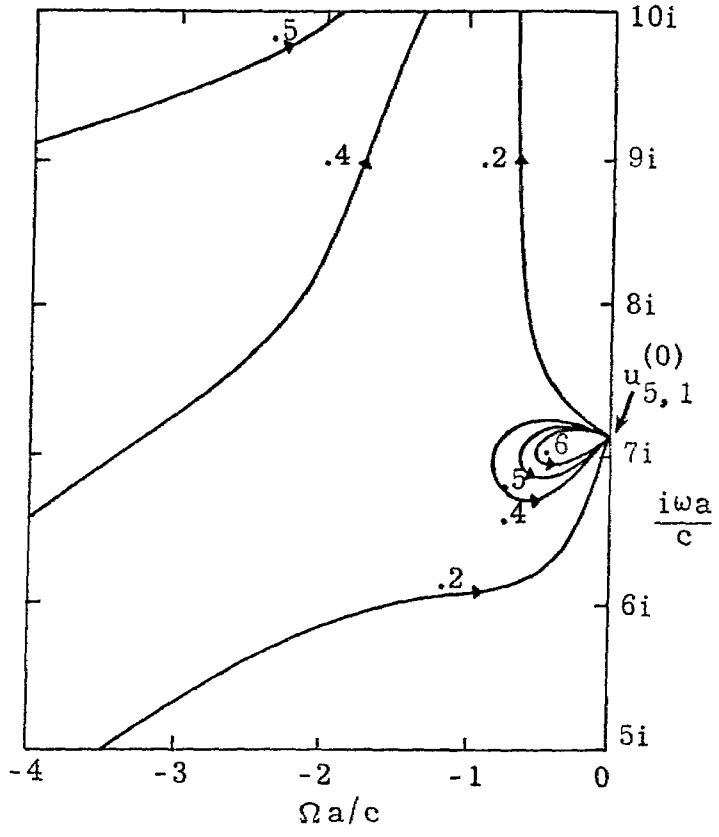

A. z_s = .2, .4, .5, .6; n = 5

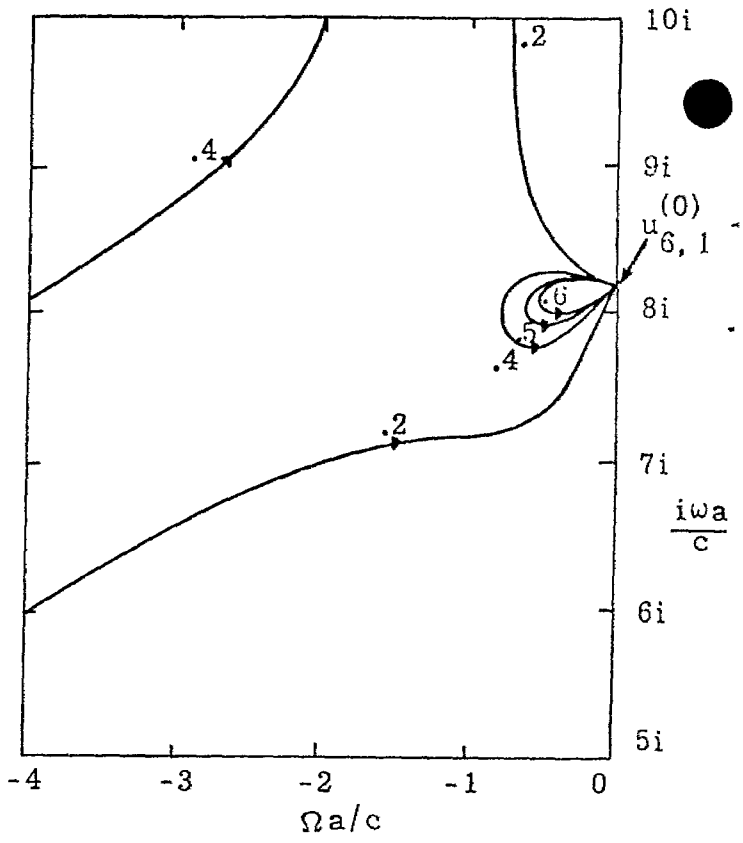

B. z_s = .2, .4, .5, .6; n = 6

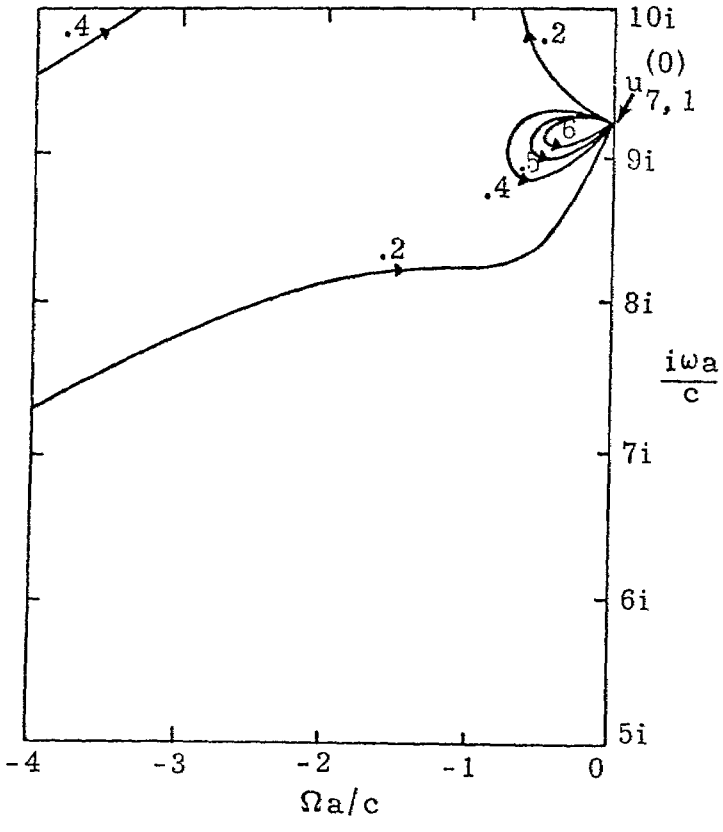

C. z_s = .2, .4, .5, .6; n = 7

Figure 5.4. Trajectories from $u^k_{n,n'}$ for Varying d/a with z_s a Parameter, n = 5, 6, 7. Arrows indicate Increasing d/a

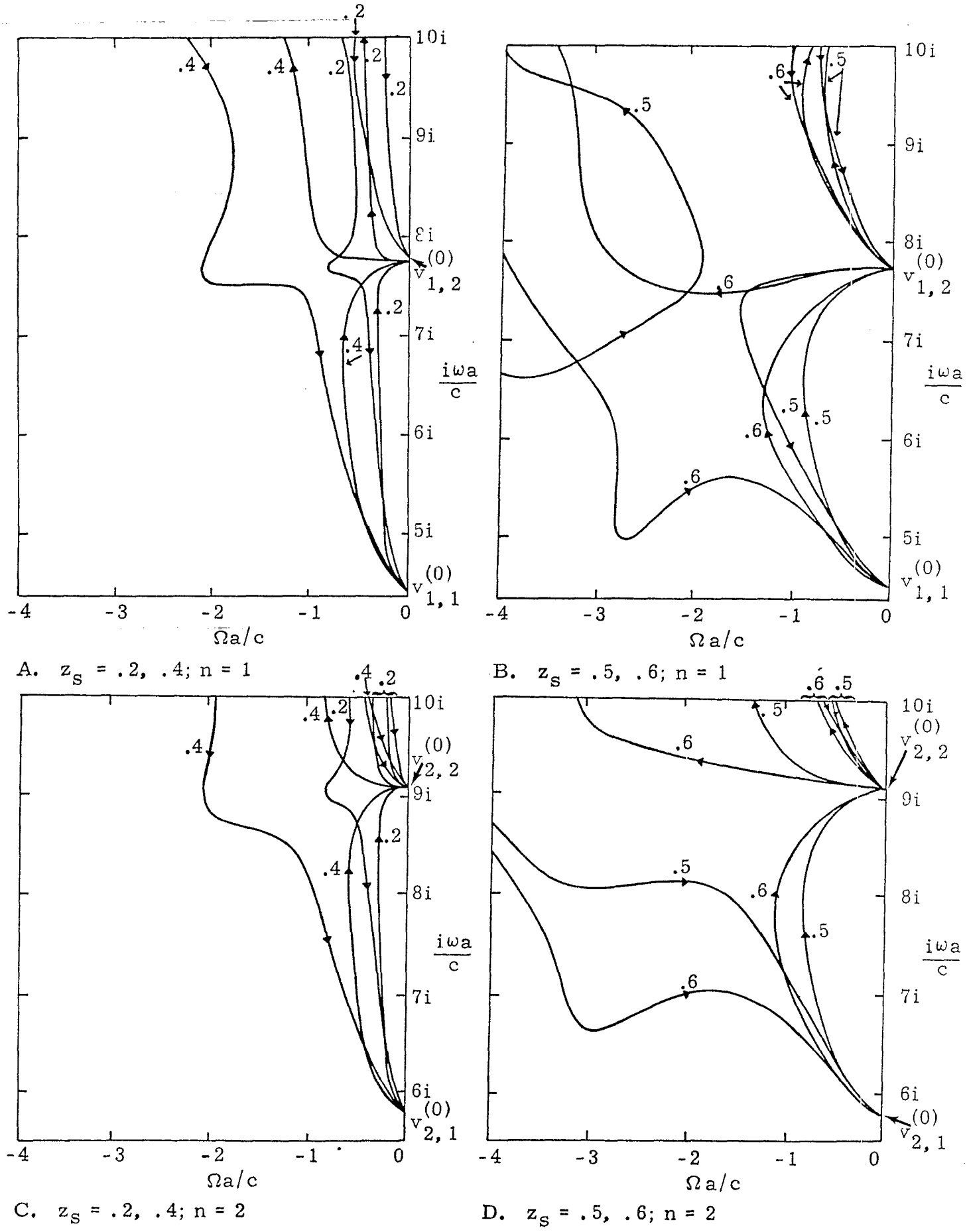

A. z_s = .2, .4; n = 1

B. z_s = .5, .6; n = 1

C. z_s = .2, .4; n = 2

D. z_s = .5, .6; n = 2

Figure 5.5. Trajectories from $v_{1,n'}^{k}$ and $v_{2,n'}^{k}$ for Varying d/a with z_s a Parameter. Arrows indicate Increasing d/a

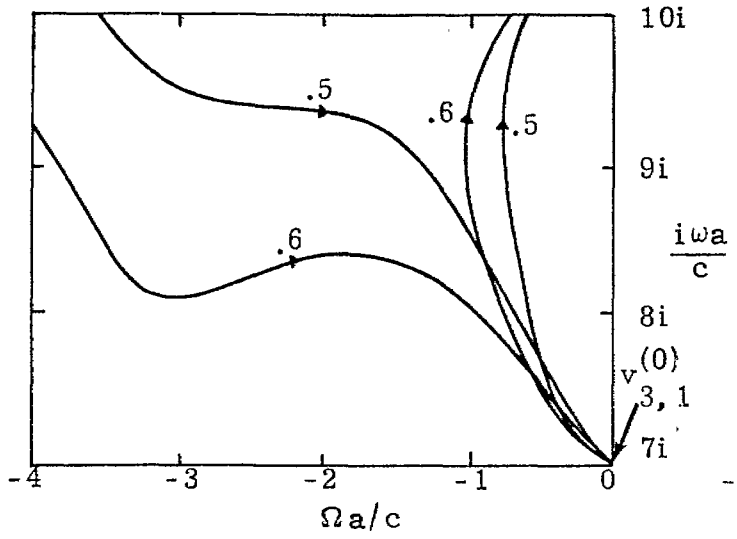

A. $z_s = .5, .6; n = 3$

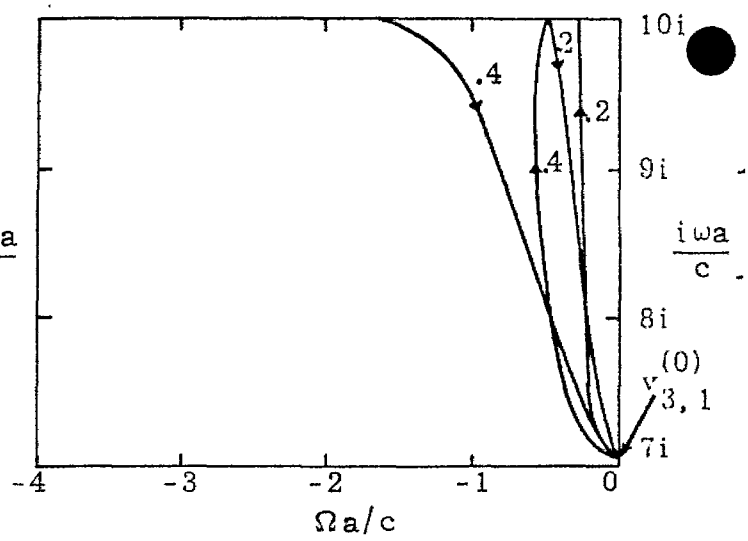

B. $z_s = .2, .4; n = 3$

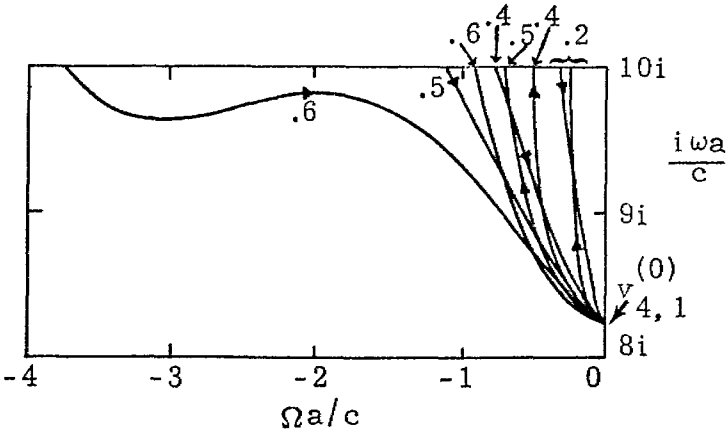

C. $z_s = .2, .4, .5, .6; n = 4$

Figure 5.6. Trajectories from $v^k_{3,n'}$ and $v^k_{4,n'}$ for Varying d/a with z_s a Parameter. Arrows Indicate Increasing d/a

VI. COMBINED RESONANT DAMPING

From the graphs of pole trajectories in section III it is evident that some interior resonances will damp, while others will not, for the same d/a and z_s. Of course it is this damping and the damping of as many resonant frequencies as possible that are of interest. It is not enough to damp an individual resonance and in addition the individual modes cannot be segregated to determine optimum parameters.

The graphs in this section are presented by mode with all the normalized damping ($|\Omega_\alpha|/|\omega_\alpha|$) of each resonant frequency of that mode plotted against z_s with d/a a parameter. Since the higher order modes become increasingly difficult to damp as d/a increases the concentration of this parameter will be restricted to the range $0 \leq d/a \leq .6$. Of course the number of resonant frequencies for any one mode and d/a is determined by the normalized frequency bound ($i\omega a/c \approx 10.5$) stated at the outset. These plots demonstrate the resistive loading (z_s) that best damps the individual poles from $u^{(k)}_{n,n'}$ and $v^{(k)}_{n,n'}$ as well as all the resonances grouped by mode (n). This arrangement should prove to be very useful if some of the higher frequencies (n') of a particular mode were deleted or scaled according to their importance in the normalized frequency range.

Determining an optimum loading for a given d/a for all seven E modes and correspondingly an optimum loading for all five H modes is a challenge. Several questions come to mind immediately. First, should

the higher resonant frequencies be scaled down in importance? Should all modes be treated equally, that is, should the modes be scaled? If the resonant frequencies and/or modes are scaled what method should be used?

Although intuitively the answer to the first two questions is yes, it is not the intent here to delve into these areas. Hopefully, ample information is contained here so questions of relative importance concerning frequencies and modes can be answered.

Assigning a resistive loading for a given d/a value can be achieved simply by combining all the modes for that d/a parameter. This oversimplification results in loss of much information. Keeping in mind that the lower order modes should (in some way) dominate, tables 6.1 and 6.2 list the optimum loading as progressive modes are considered. The first number in the tables gives the optimum loading (z_s) and the second number is the least amount of normalized damping for all the poles for the modes considered. It should be noted that the approach resulting in these tables places equal emphasis on all the resonant frequencies (within the frequency bound) of the various modes. In addition it should be stressed that interpolation in this table is nontrivial.

Modes (n) Considered	d/a = .1 z_s	.1 $\frac{\lvert\Omega_\alpha\rvert}{\lvert\omega_\alpha\rvert}$	.2 z_s	.2 $\frac{\lvert\Omega_\alpha\rvert}{\lvert\omega_\alpha\rvert}$	.3 z_s	.3 $\frac{\lvert\Omega_\alpha\rvert}{\lvert\omega_\alpha\rvert}$	.4 z_s	.4 $\frac{\lvert\Omega_\alpha\rvert}{\lvert\omega_\alpha\rvert}$	.5 z_s	.5 $\frac{\lvert\Omega_\alpha\rvert}{\lvert\omega_\alpha\rvert}$	.6 z_s	.6 $\frac{\lvert\Omega_\alpha\rvert}{\lvert\omega_\alpha\rvert}$
1	.38	.05	.60	.11	.32	.04	.40	.08	.22	.07	.22	.04
1,2	.39	.04	.59	.11	.32	.04	.40	.08	.08	.02	.34	.03
1,2,3	.39	.04	.57	.07	.32	.04	.15	.03	.14	.01	.85	.01
1,2,3,4	.39	.04	.57	.07	.32	.04	.05	.006	.18	.008	.85	.002
1,2,3,4,5	.39	.04	.57	.07	.32	.04	.06	.005	.25	.004	.85	.0008
1,2,3,4,5,6	.39	.04	.51	.07	.45	.04	.08	.003	.60	.002	.85	.0002
1,2,3,4,5,6,7	.39	.04	.42	.06	.42	.02	.08	.003	.70	.001	.85	5×10^{-5}

Table 6.1. Resistive Loading for Optimum Damping of All E Mode Resonances (n') in the Frequency Bounded Solution

Modes (n) Considered	d/a = .1 z_s	.1 $\frac{\lvert\Omega_\alpha\rvert}{\lvert\omega_\alpha\rvert}$	.2 z_s	.2 $\frac{\lvert\Omega_\alpha\rvert}{\lvert\omega_\alpha\rvert}$	.3 z_s	.3 $\frac{\lvert\Omega_\alpha\rvert}{\lvert\omega_\alpha\rvert}$	.4 z_s	.4 $\frac{\lvert\Omega_\alpha\rvert}{\lvert\omega_\alpha\rvert}$	.5 z_s	.5 $\frac{\lvert\Omega_\alpha\rvert}{\lvert\omega_\alpha\rvert}$	.6 z_s	.6 $\frac{\lvert\Omega_\alpha\rvert}{\lvert\omega_\alpha\rvert}$
1	.49	.06	.68	.09	.6	.16	.13	.02	.49	.20	.68	.16
1, 2	.52	.06	.68	.09	.48	.07	.14	.02	.55	.12	.65	.06
1, 2, 3	.52	.06	.68	.09	.25	.03	.14	.02	.76	.07	.55	.02
1, 2, 3, 4	.52	.06	.68	.09	.25	.03	.14	.02	.71	.05	.50	.008
1, 2, 3, 4, 5	.58	.05	.68	.09	.25	.03	.17	.02	.65	.02	.48	.003

Table 6.2. Resistive Loading for Optimum Damping of All H Mode Resonances (n') in the Frequency Bounded Solution

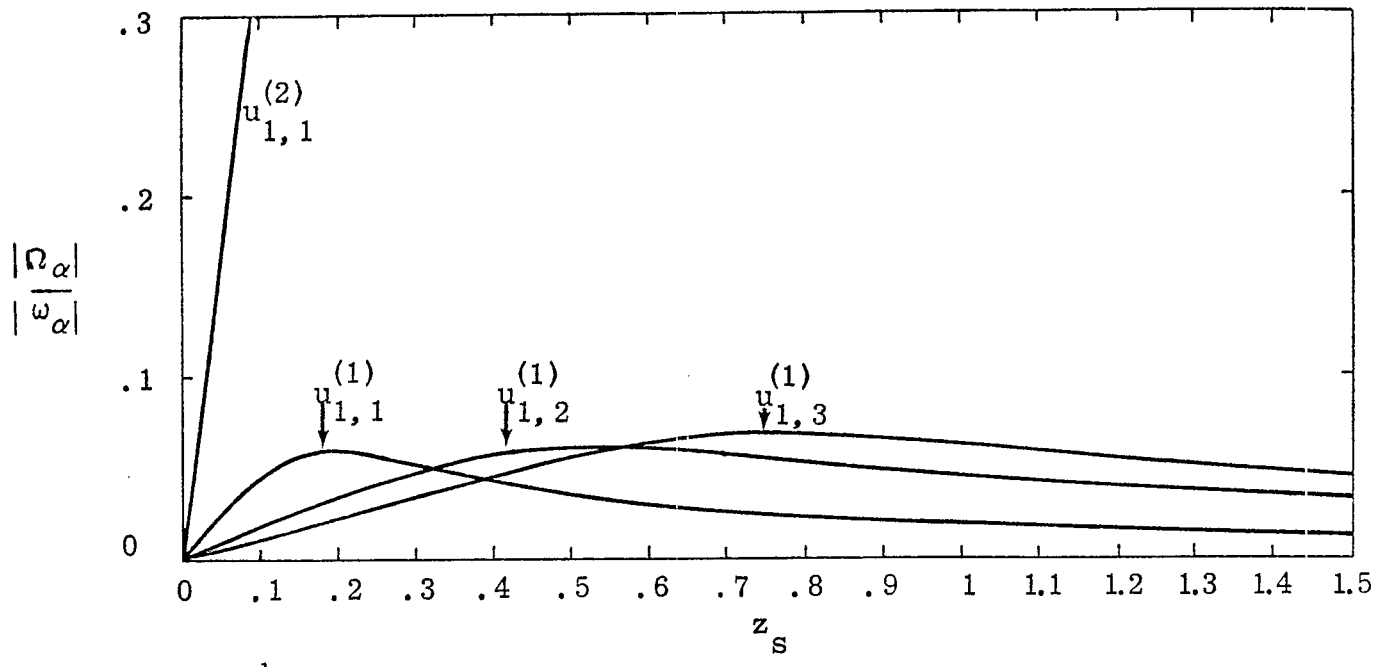

B. $\frac{d}{a} = .1$

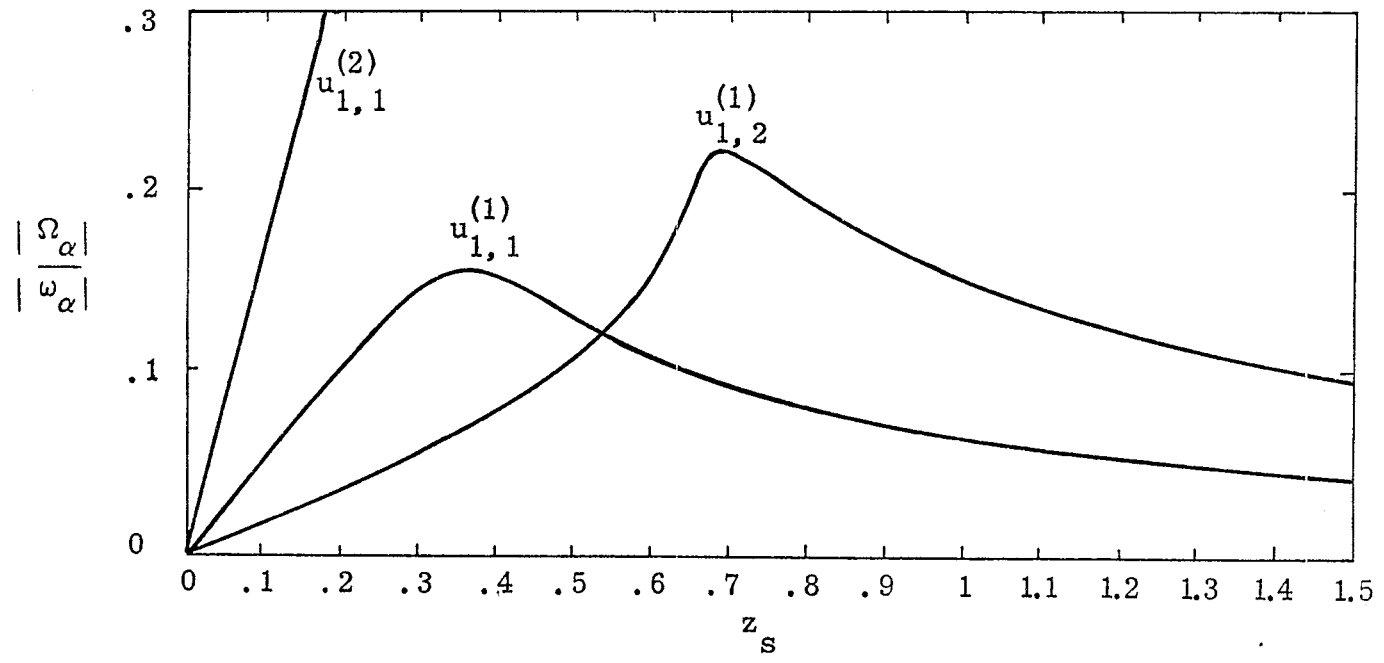

B. $\frac{d}{a} = .2$

Figure 6.1. E-Mode Damping vs. Normalized Loading, n = 1
Curve Label Indicates Origin of Pole Loci

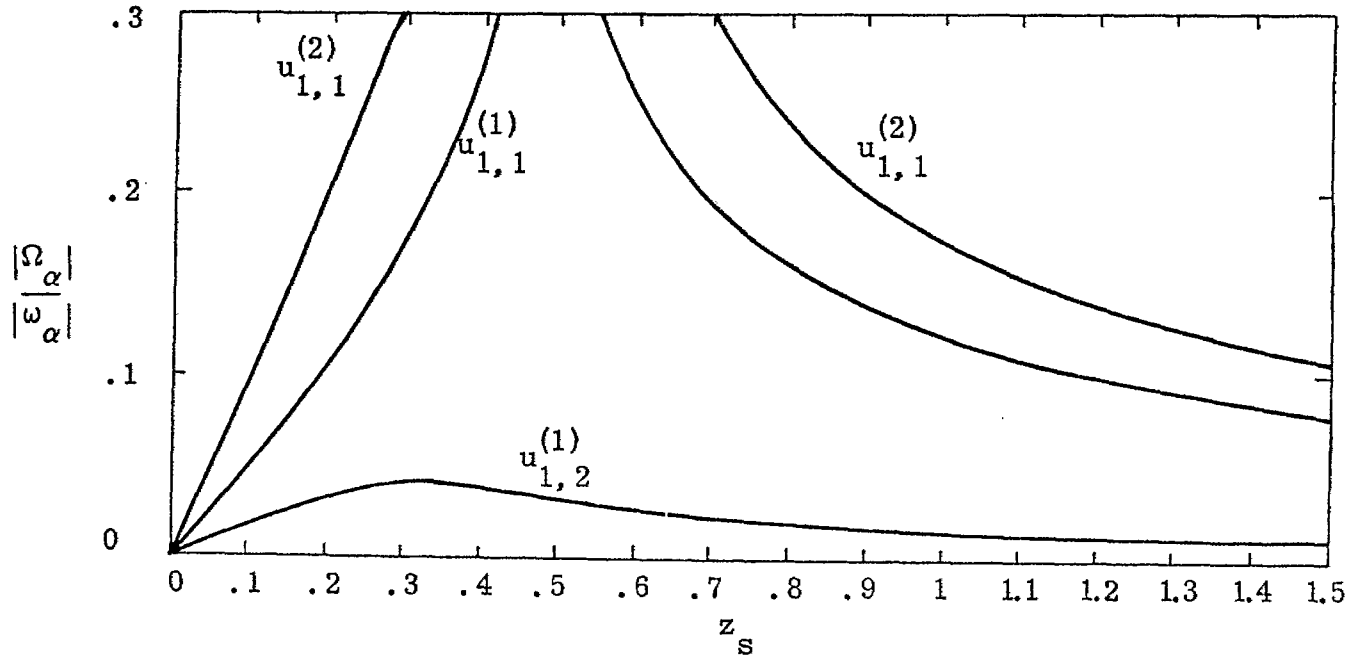

A. $\frac{d}{a} = .3$

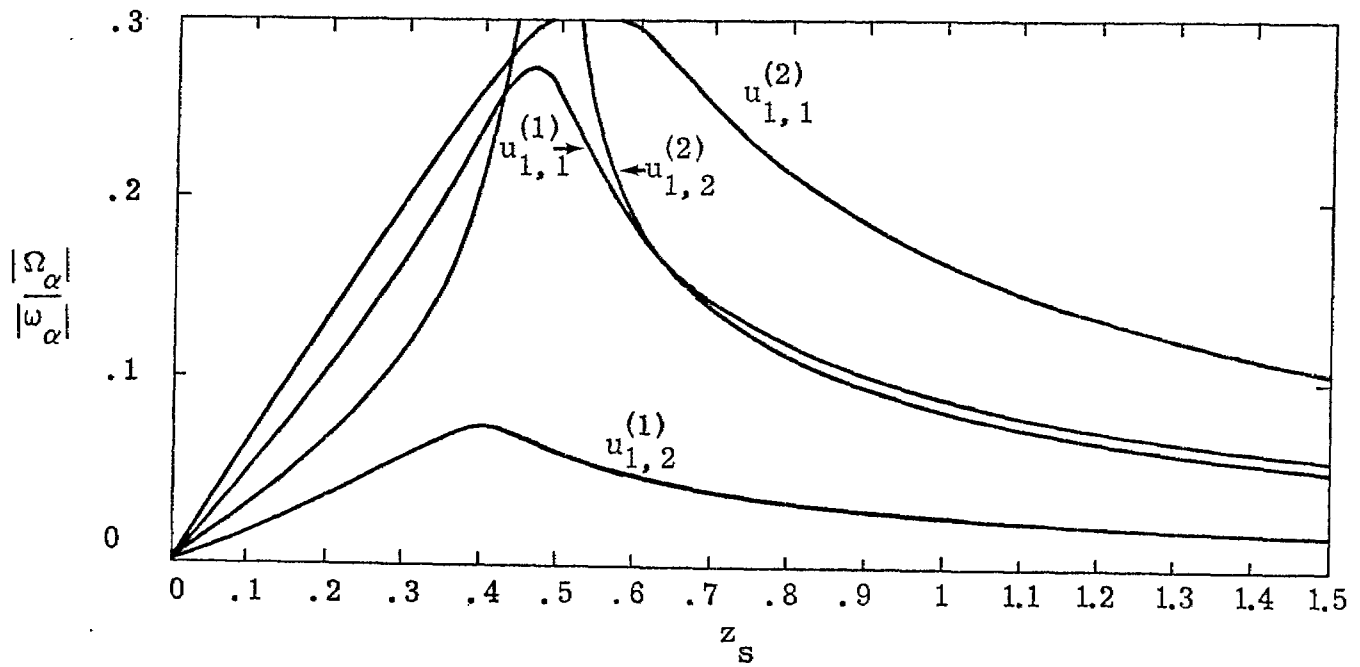

B. $\frac{d}{a} = .4$

Figure 6.2. E-Mode Damping vs. Normalized Loading, n = 1
Curve Label Indicates Origin of Pole Loci

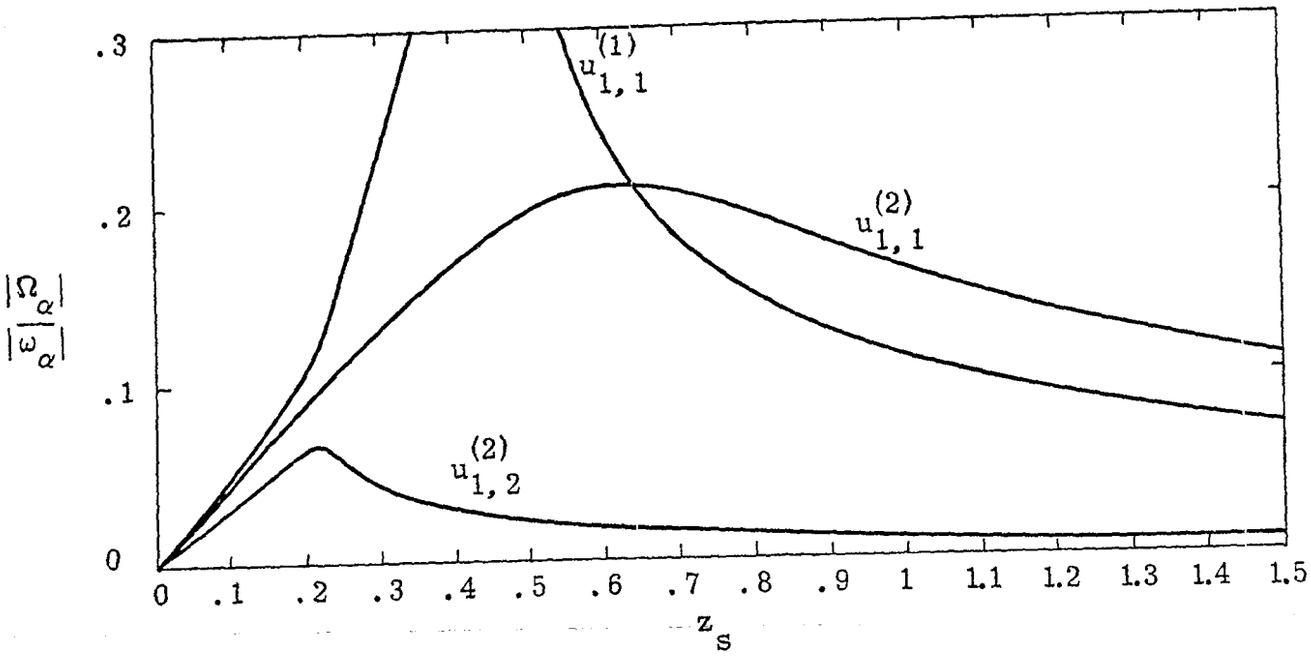

A. $\frac{d}{a} = .5$

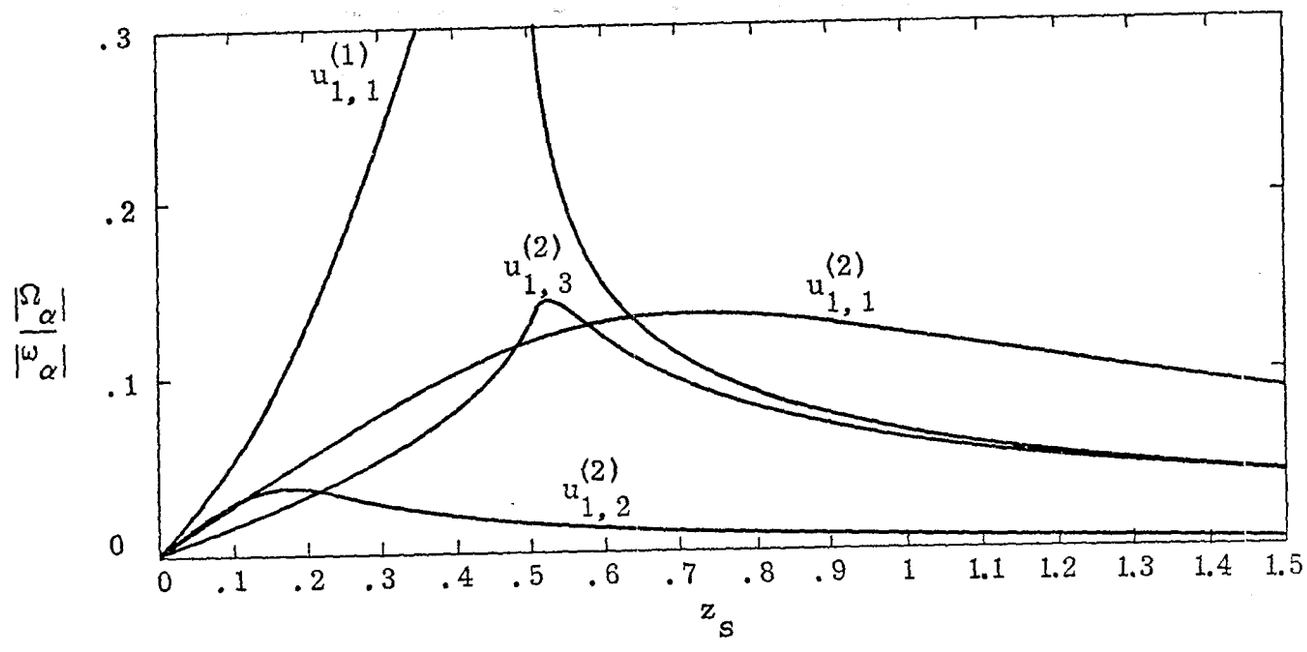

B. $\frac{d}{a} = .6$

Figure 6.3. E-Mode Damping vs. Normalized Loading, n = 1
Curve Label Indicates Origin of Pole Loci

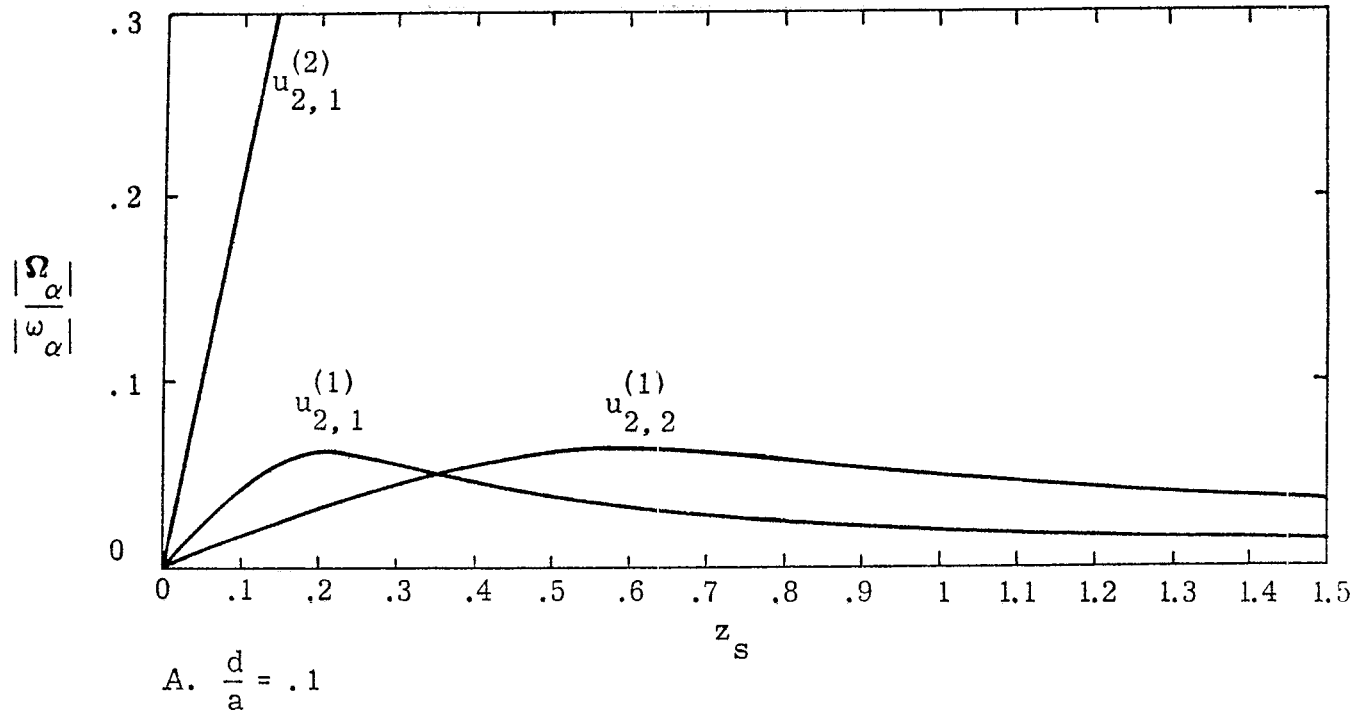

A. $\frac{d}{a} = .1$

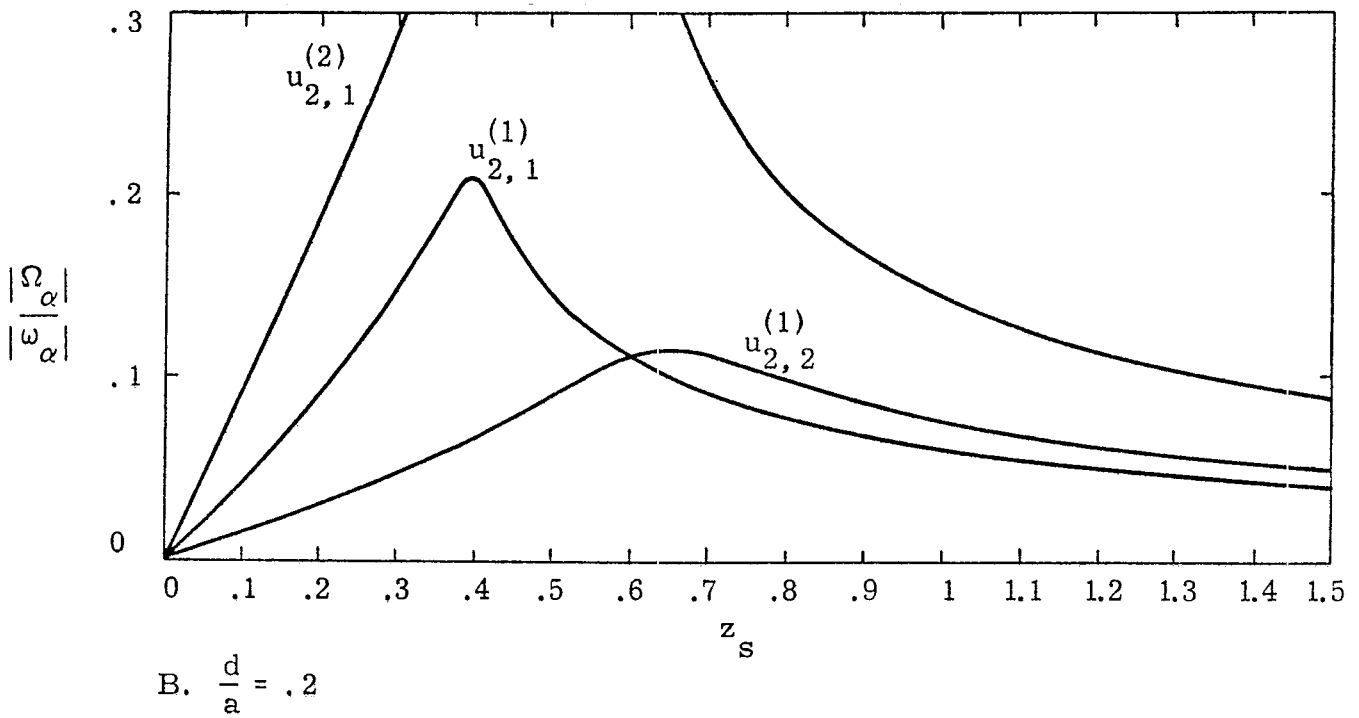

B. $\frac{d}{a} = .2$

Figure 6.4. E-Mode Damping vs. Normalized Loading, n = 2
Curve Label Indicates Origin of Pole Loci

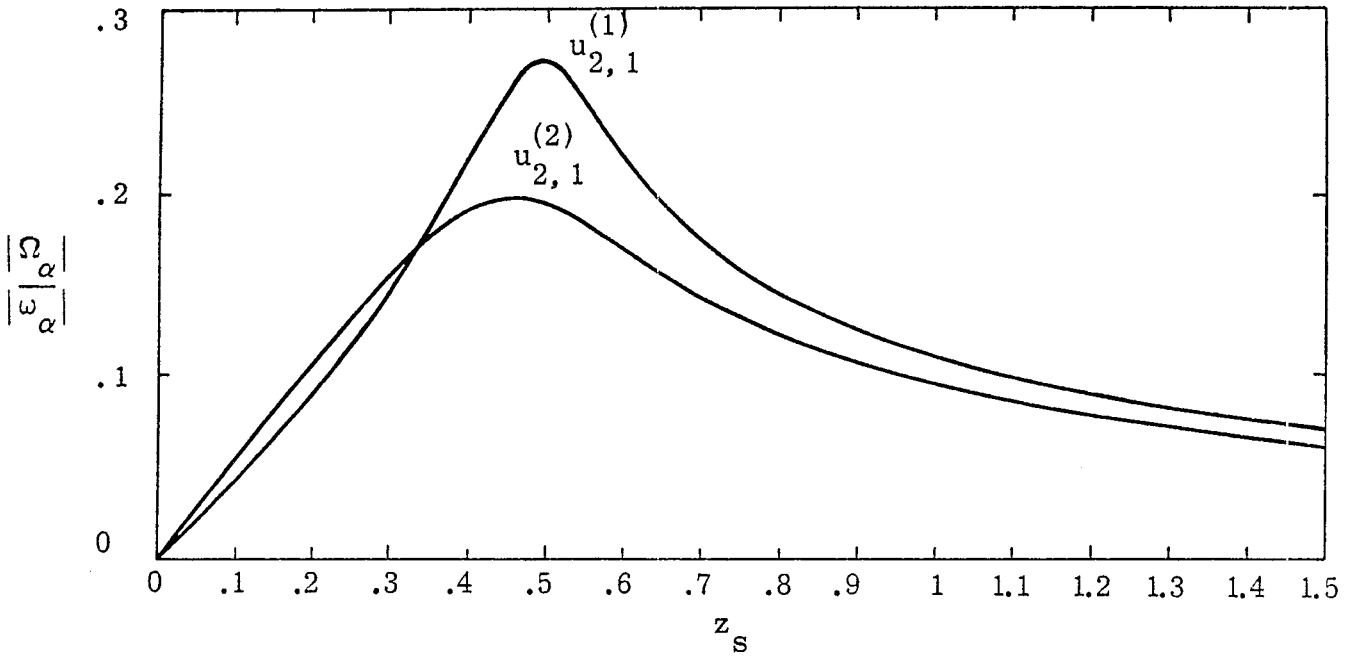

A. $\frac{d}{a} = .3$

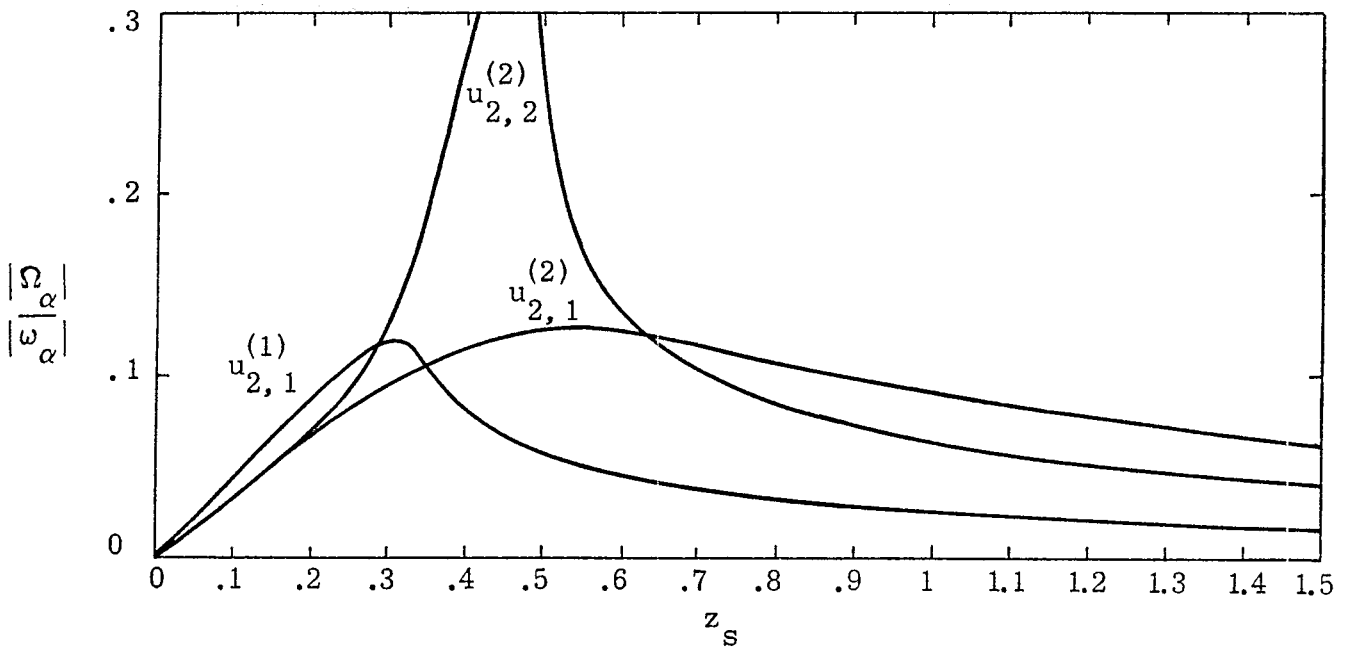

B. $\frac{d}{a} = .4$

Figure 6.5. E-Mode Damping vs. Normalized Loading, n = 2
Curve Label Indicates Origin of Pole Loci

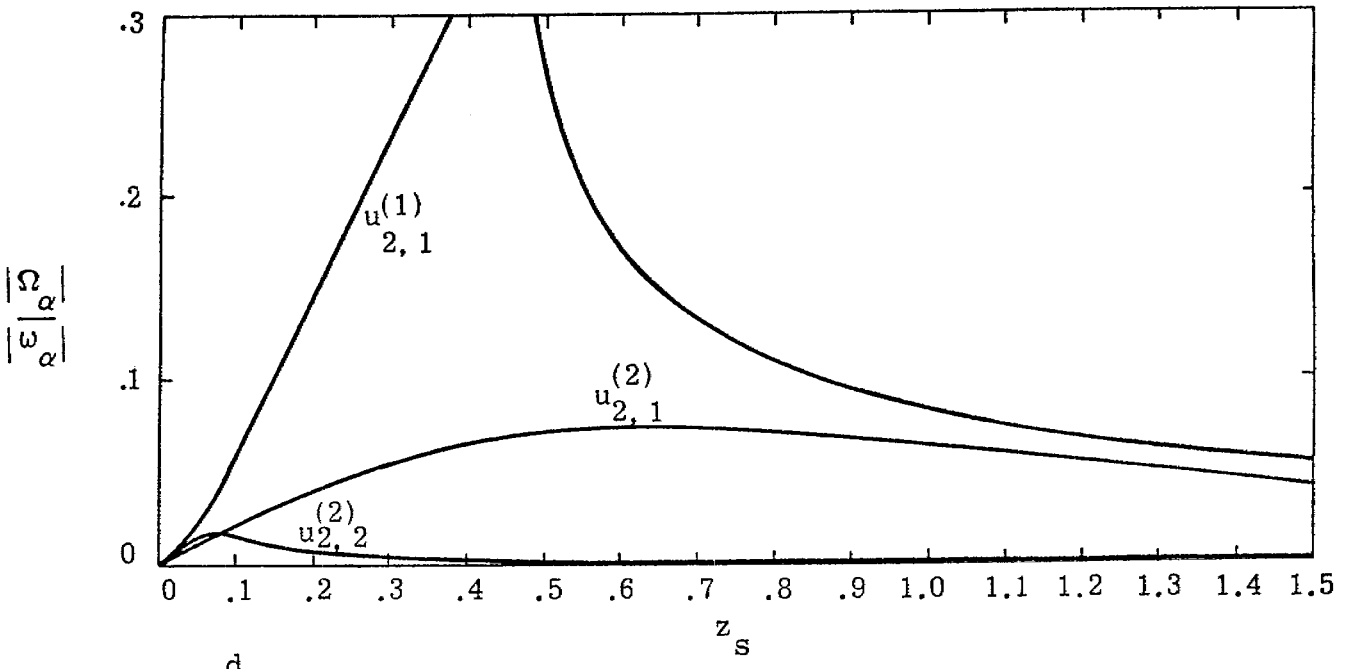

A. $\frac{d}{a} = .5$

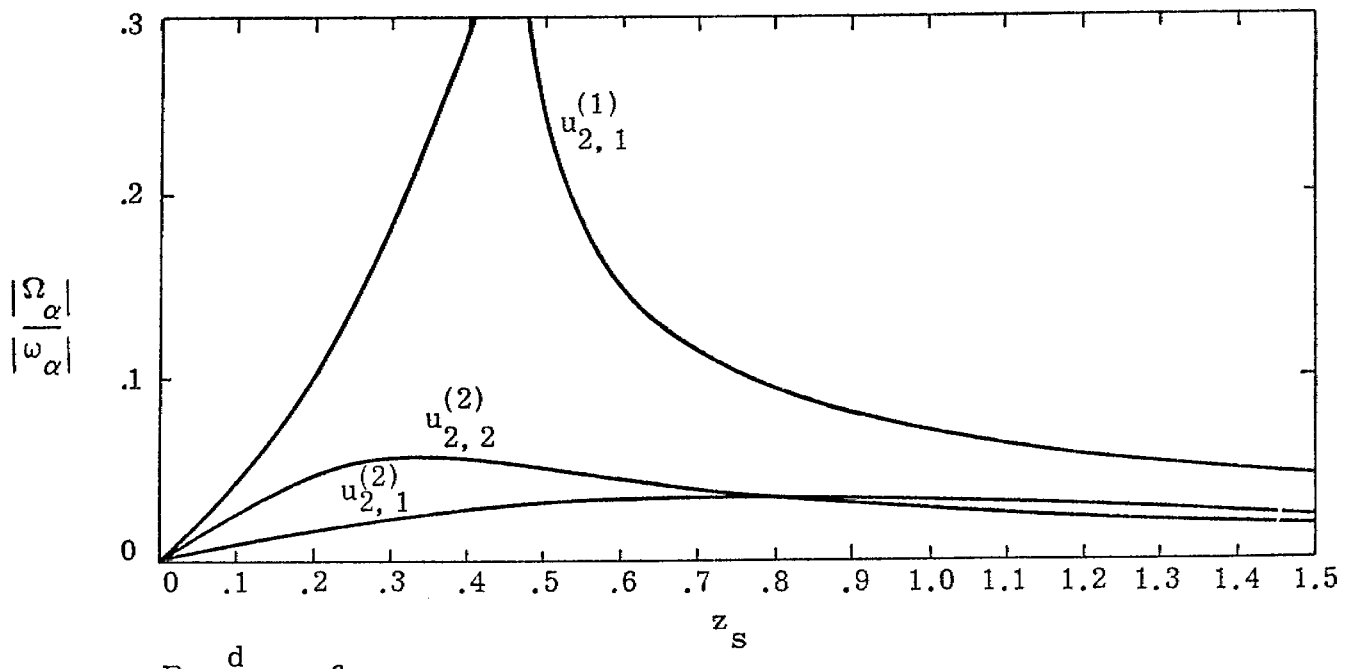

B. $\frac{d}{a} = .6$

Figure 6.6. E-Mode Damping vs. Normalized Loading, n = 2
Curve Label Indicates Origin of Pole Loci

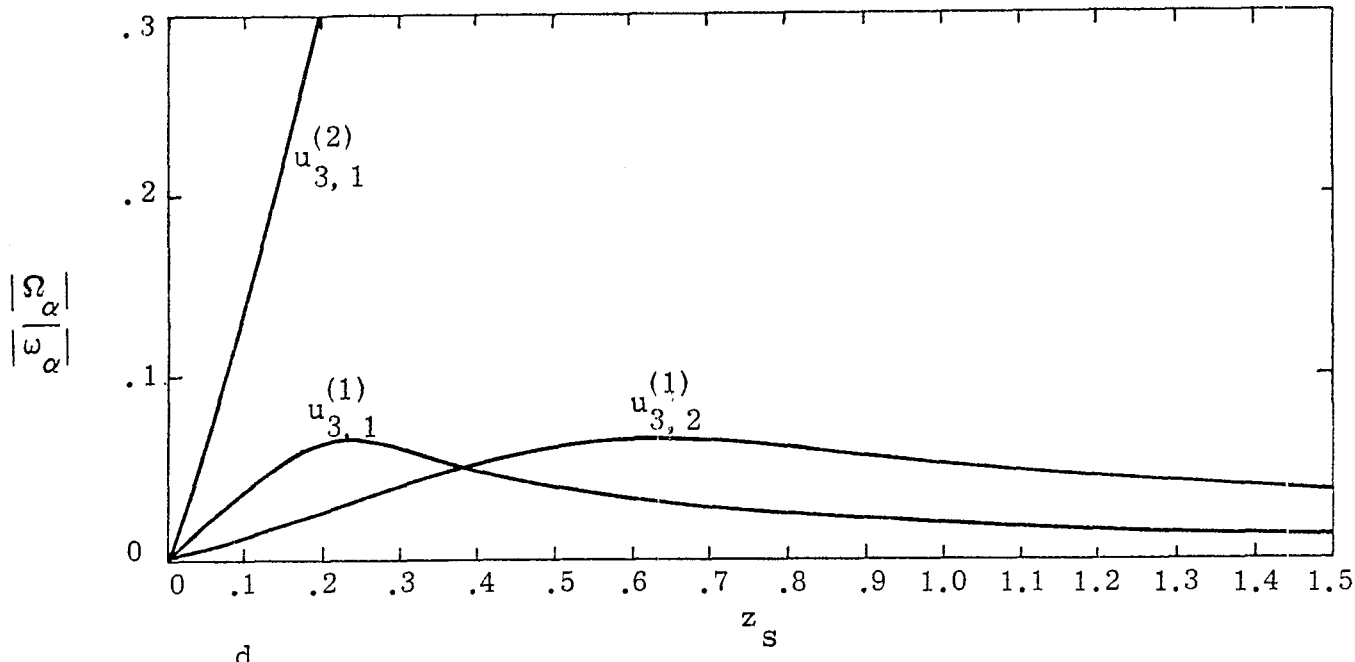

A. $\frac{d}{a} = .1$

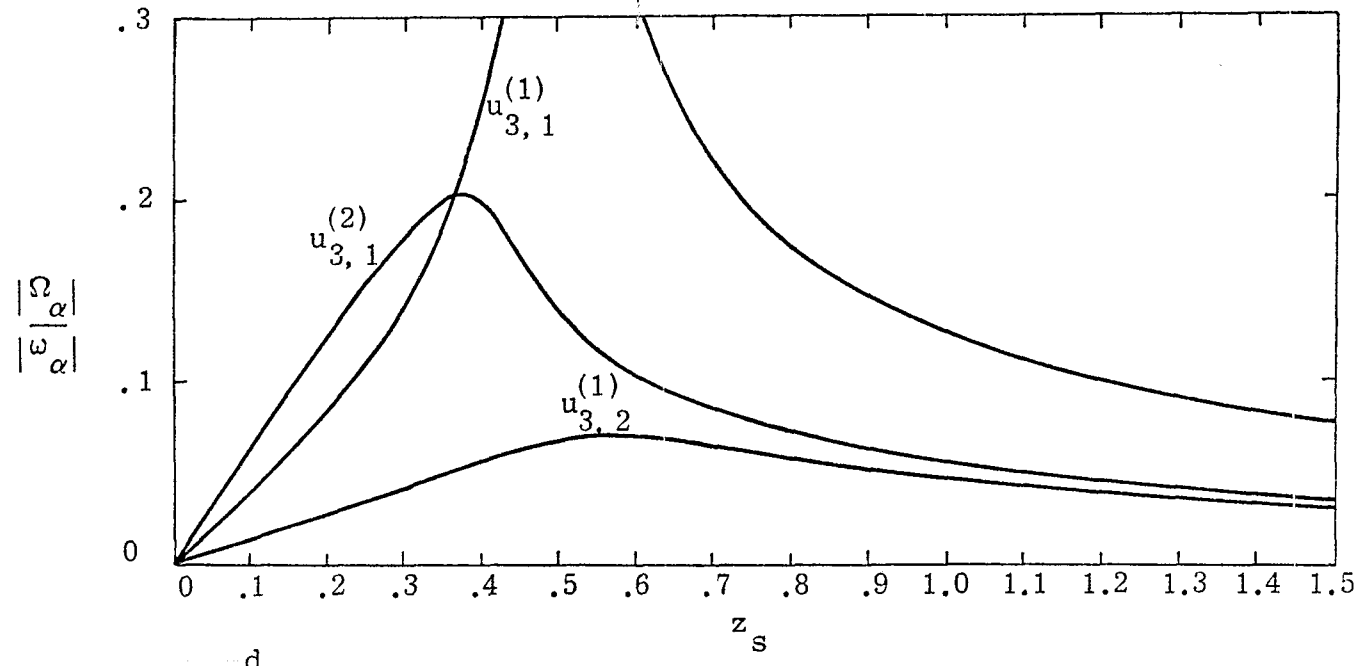

B. $\frac{d}{a} = .2$

Figure 6.7. E-Mode Damping vs. Normalized Loading, n = 3
Curve Label Indicates Origin of Pole Loci

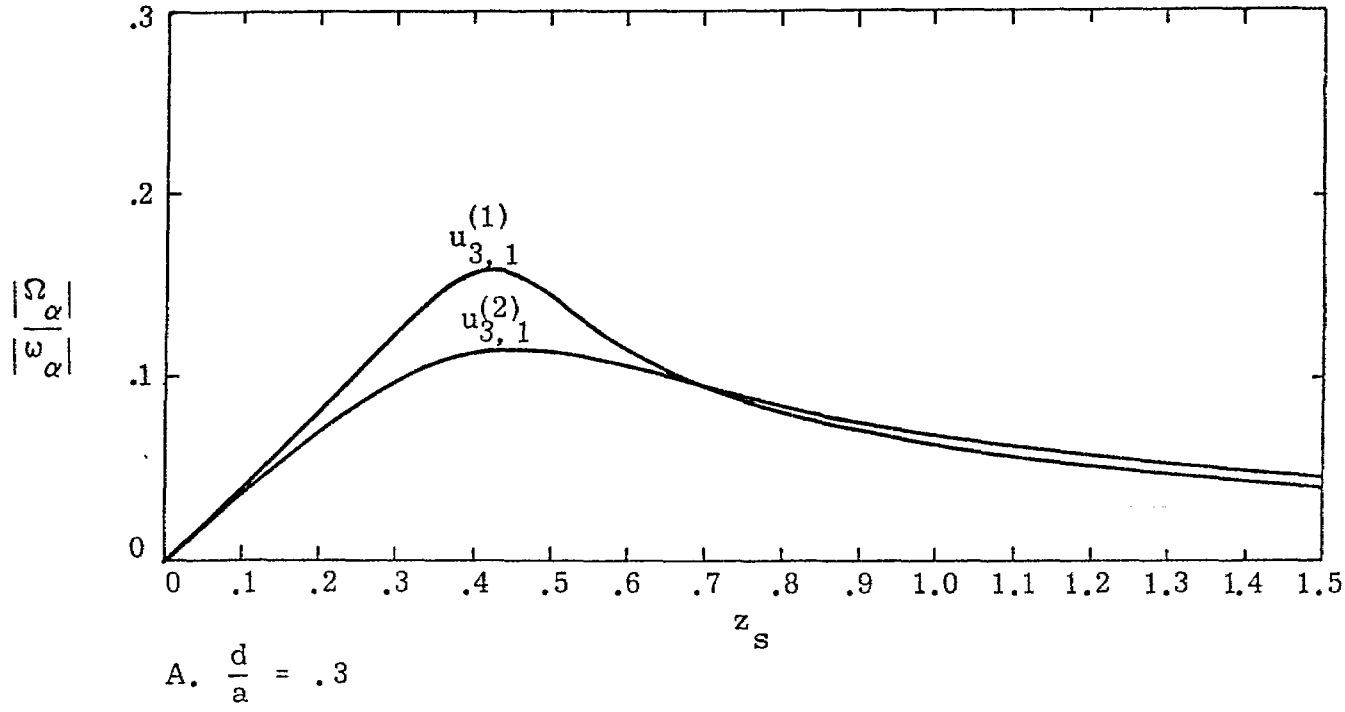

A. $\frac{d}{a} = .3$

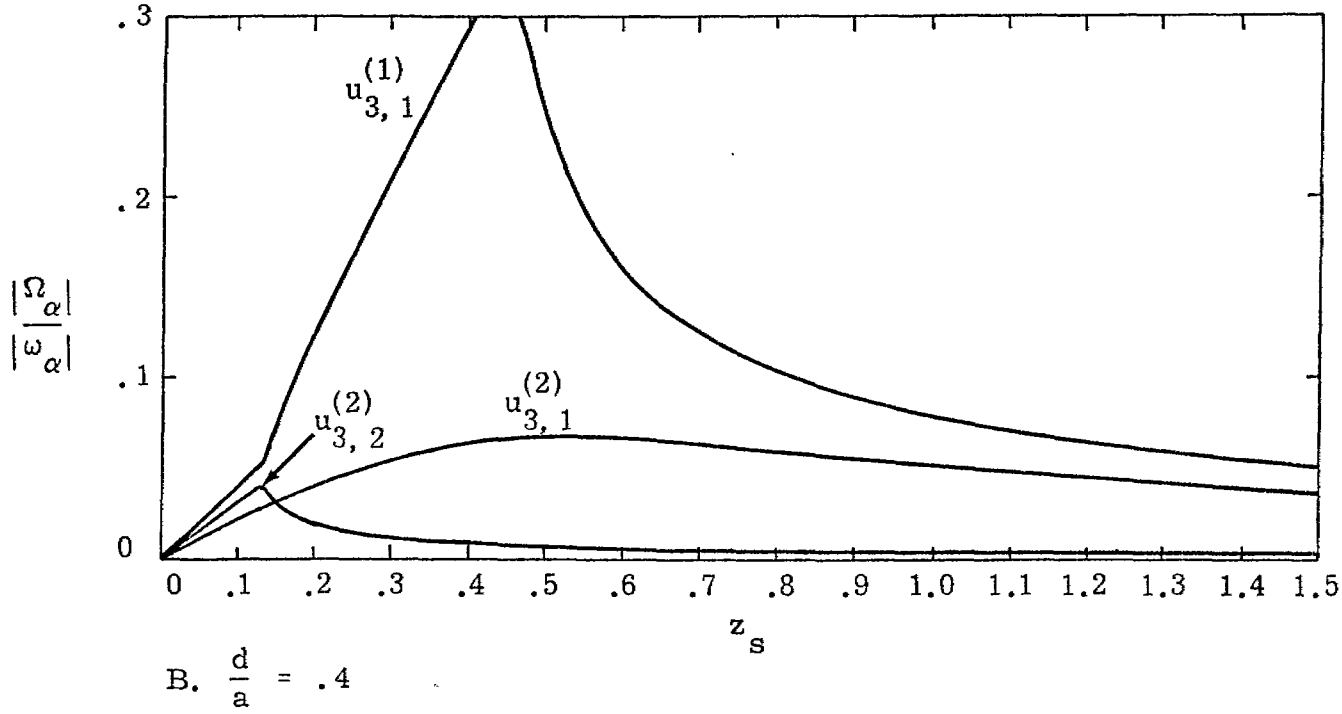

B. $\frac{d}{a} = .4$

Figure 6.8. E-Mode Damping vs. Normalized Loading, n = 3
Curve Label Indicates Origin of Pole Loci

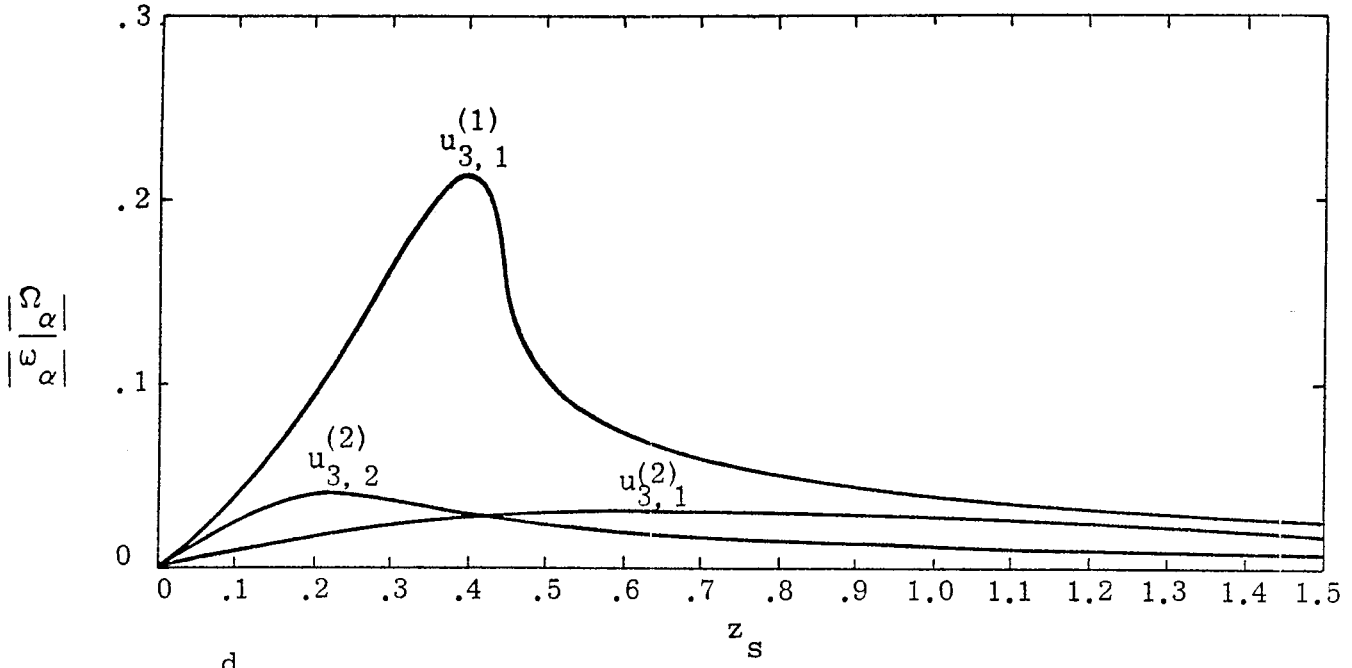

A. $\frac{d}{a} = .5$

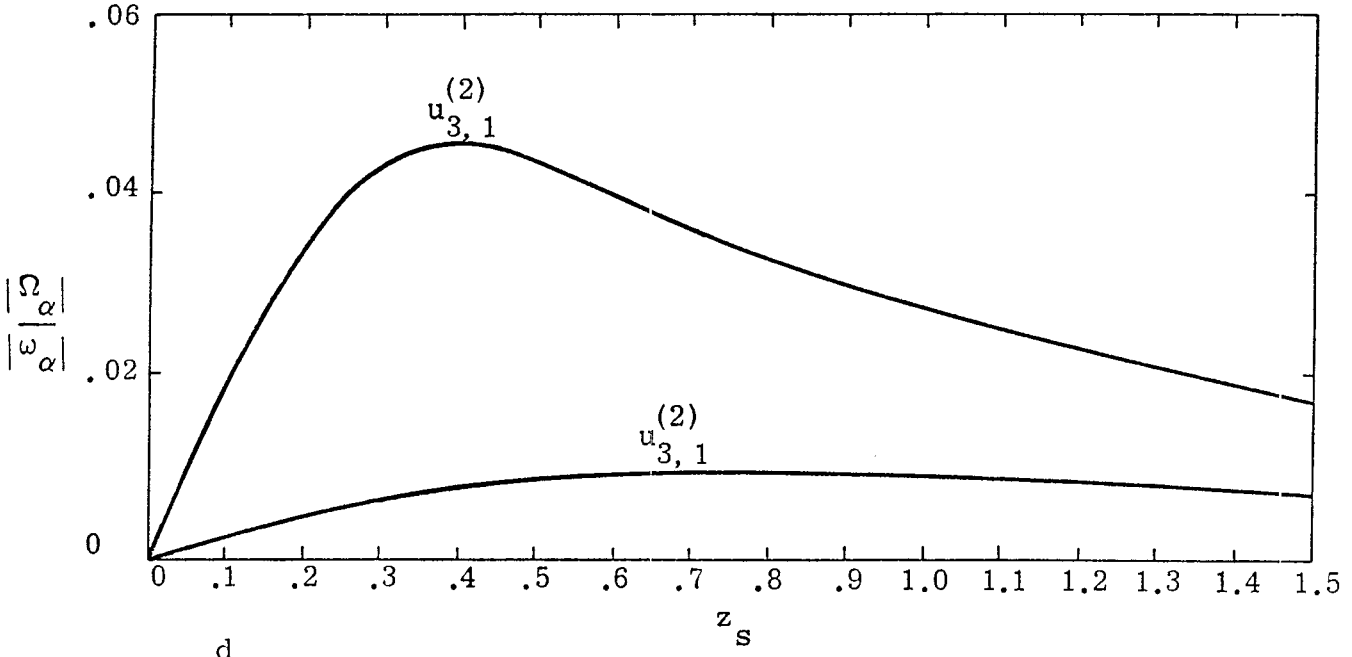

B. $\frac{d}{a} = .6$

Figure 6.9. E-Mode Damping vs. Normalized Loading, n = 3
Curve Label Indicates Origin of Pole Loci

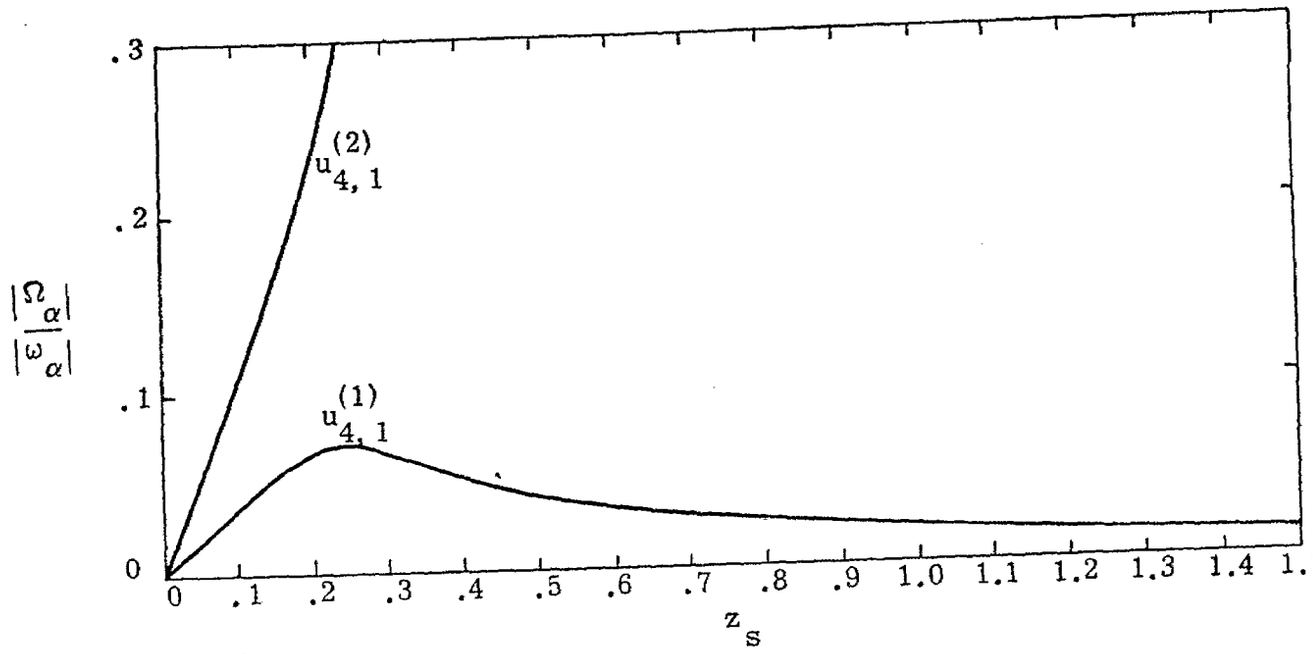

A. $\frac{d}{a} = .1$

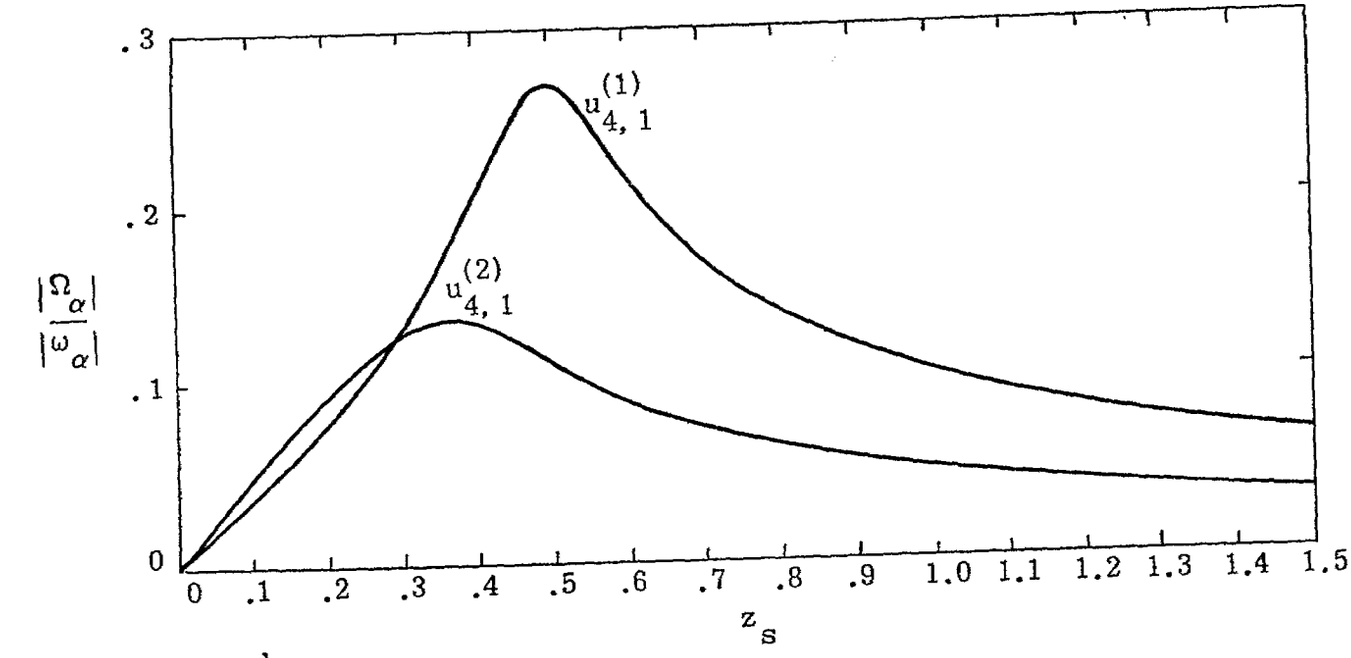

B. $\frac{d}{a} = .2$

Figure 6.10. E-Mode Damping vs. Normalized Loading, n = 4
Curve Label Indicates Origin of Pole Loci

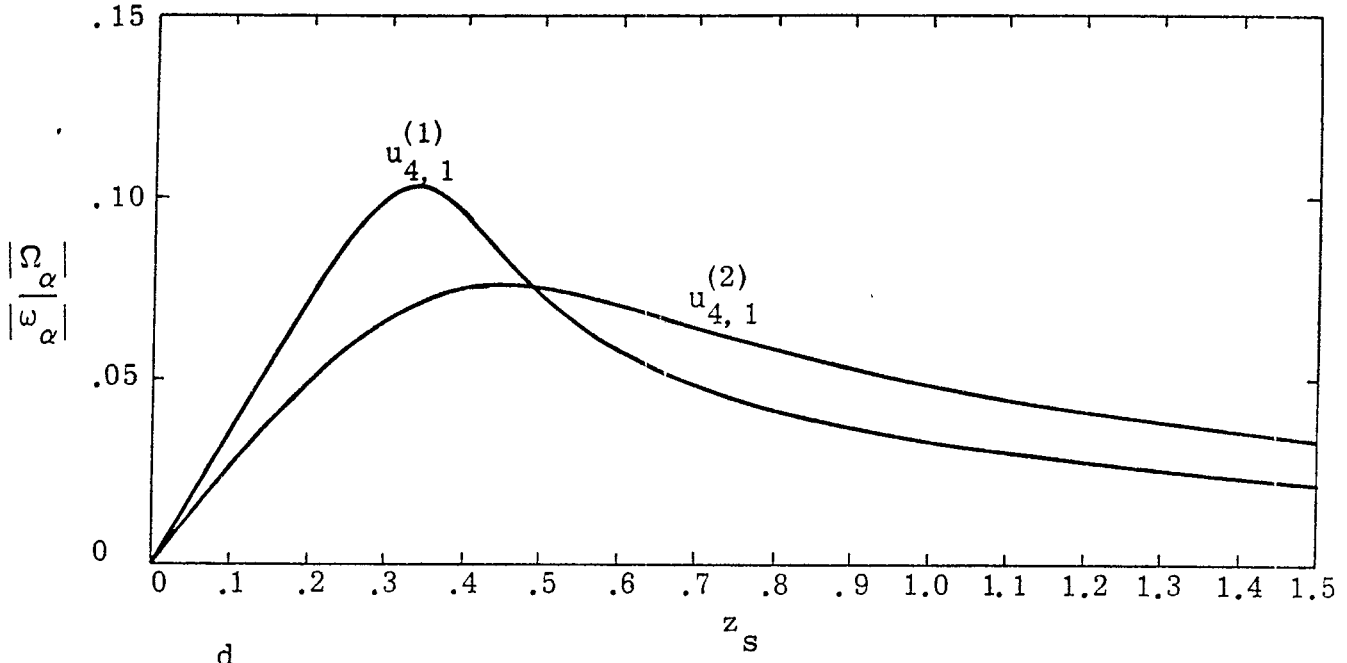

A. $\frac{d}{a} = .3$

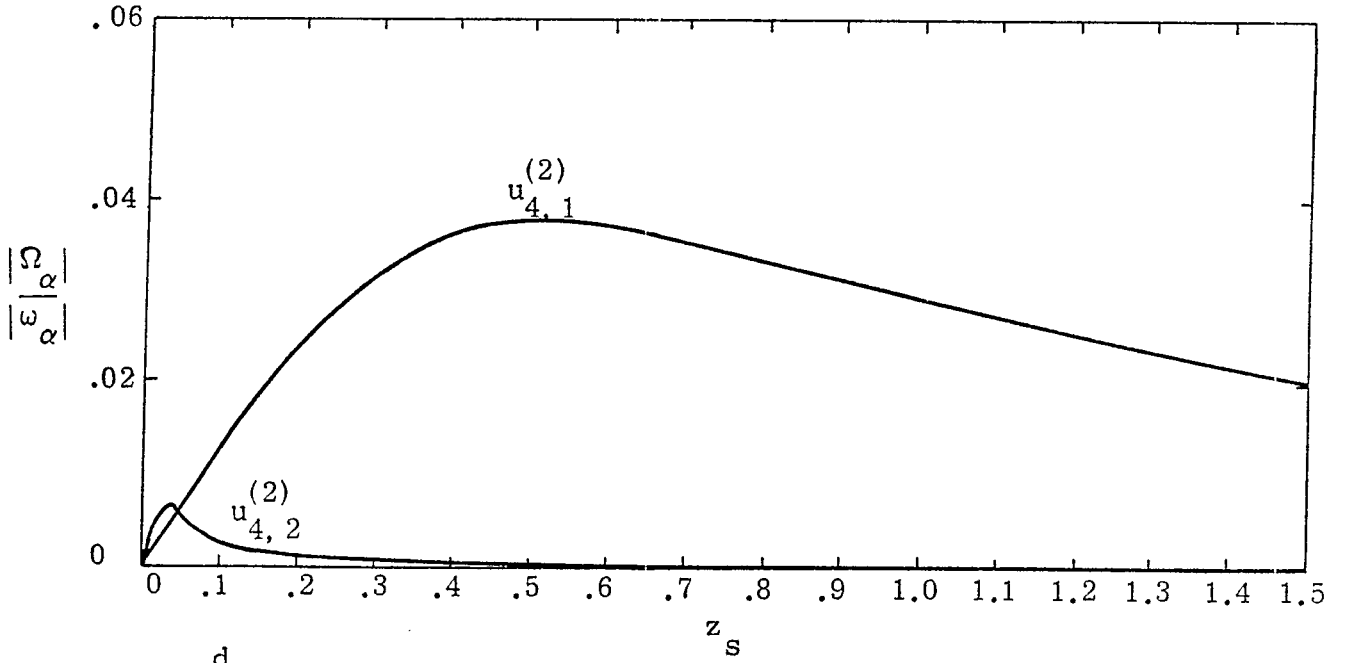

B. $\frac{d}{a} = .4$

Figure 6.11. E-Mode Damping vs. Normalized Loading, n = 4
Curve Label Indicates Origin of Pole Loci

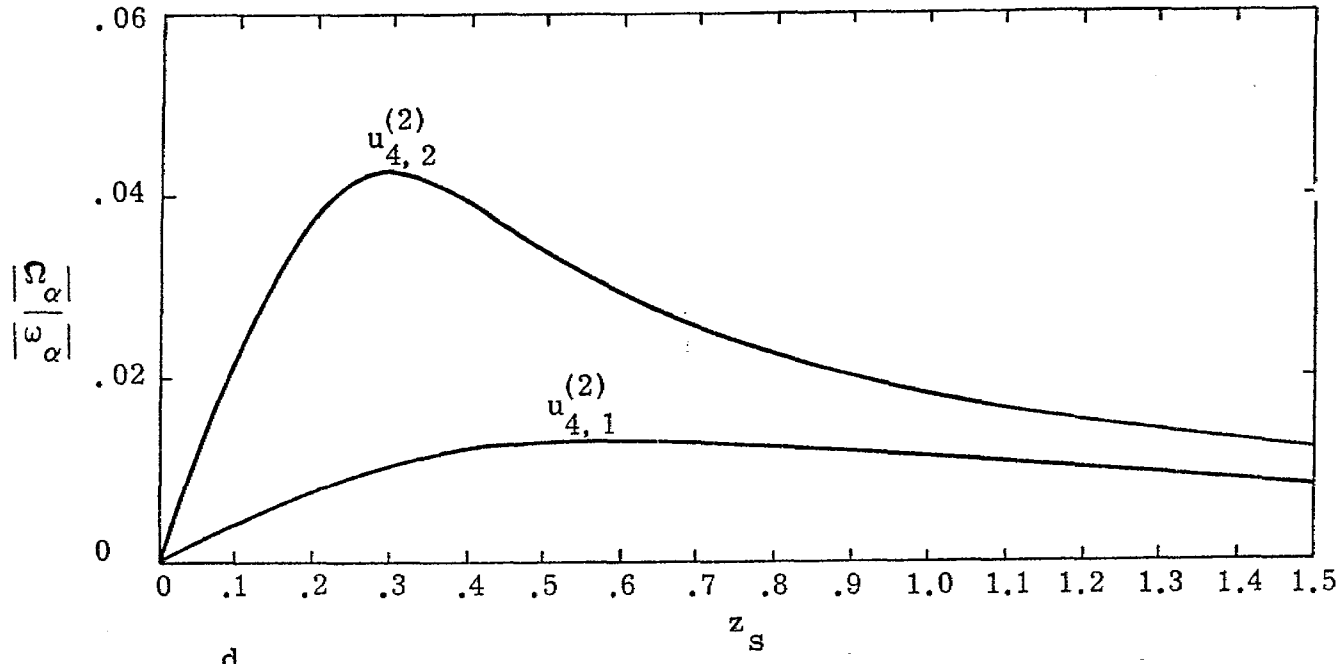

A. $\frac{d}{a} = .5$

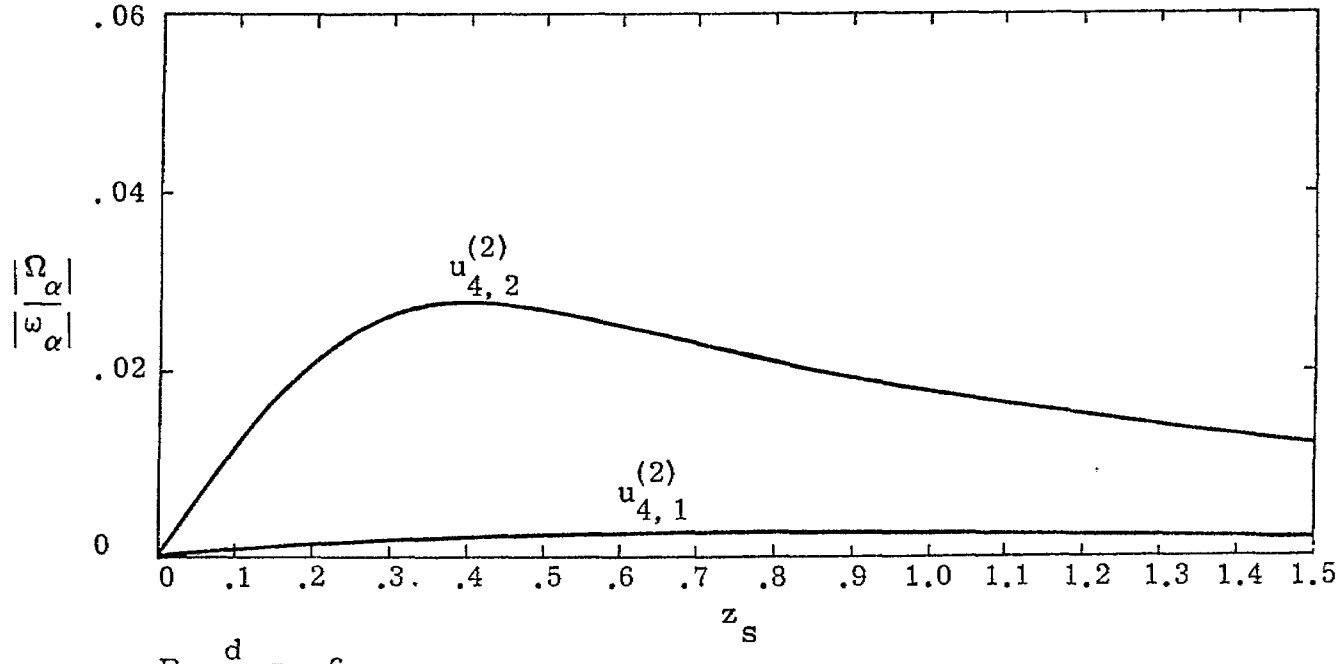

B. $\frac{d}{a} = .6$

Figure 6.12. E-Mode Damping vs. Normalized Loading, n = 4
Curve Label Indicates Origin of Pole Loci

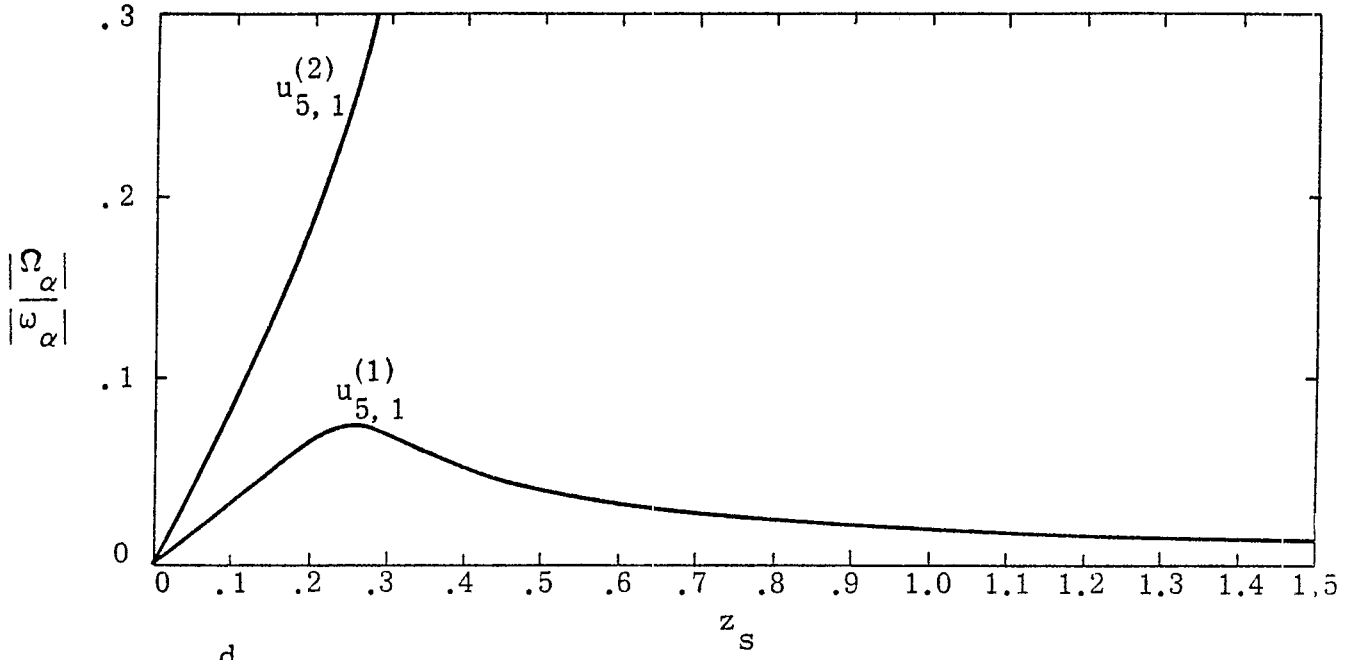

A. $\frac{d}{a} = .1$

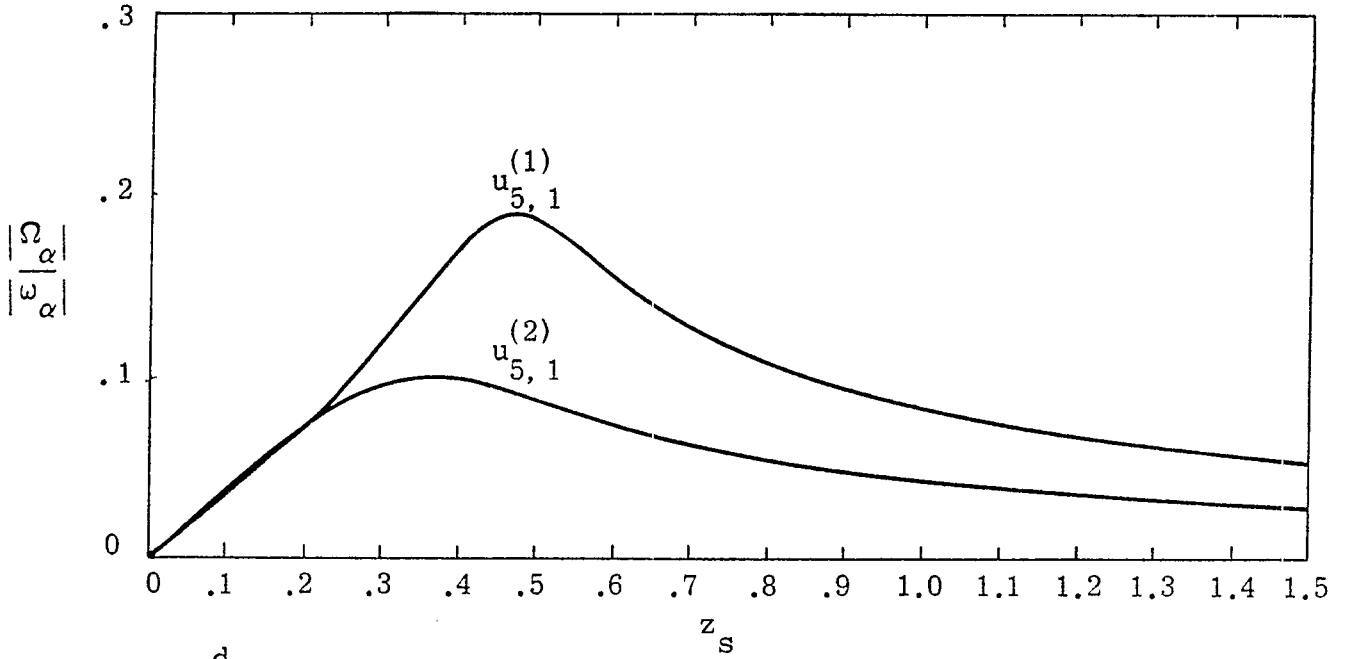

B. $\frac{d}{a} = .2$

Figure 6.13. E-Mode Damping vs. Normalized Loading, n = 5
Curve Label Indicates Origin of Pole Loci

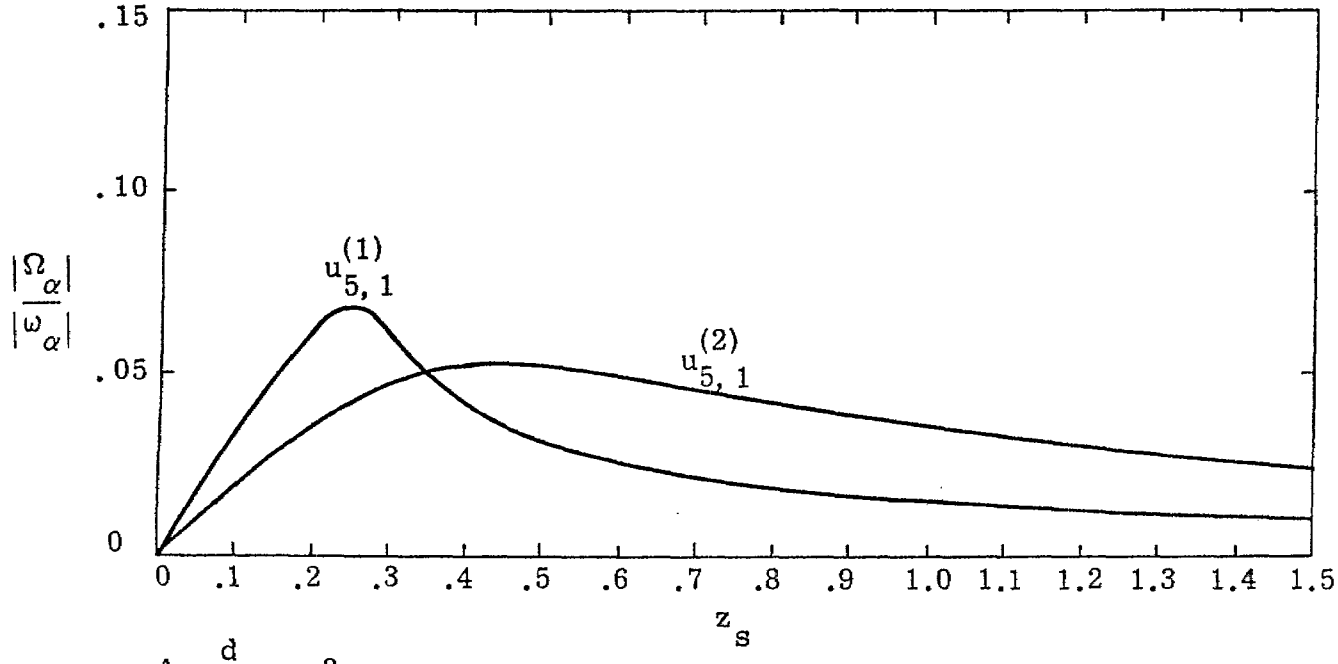

A. $\frac{d}{a} = .3$

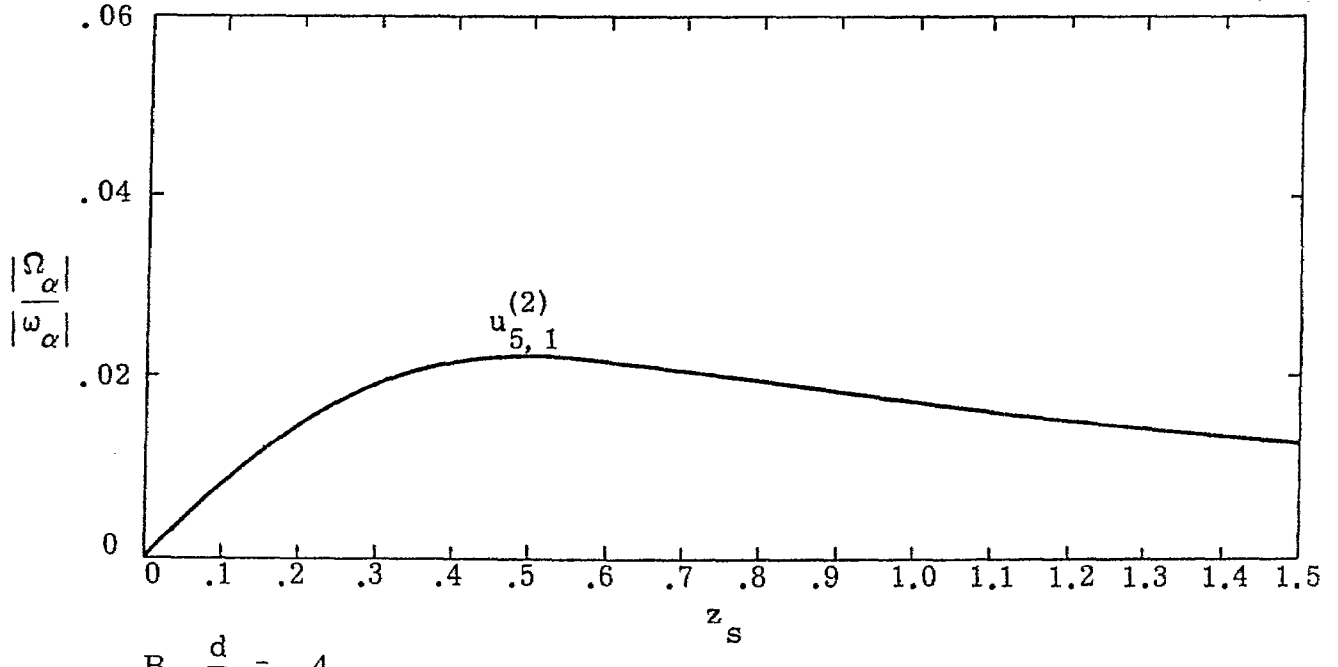

B. $\frac{d}{a} = .4$

Figure 6.14. E-Mode Damping vs. Normalized Loading, n = 5
Curve Label Indicates Origin of Pole Loci

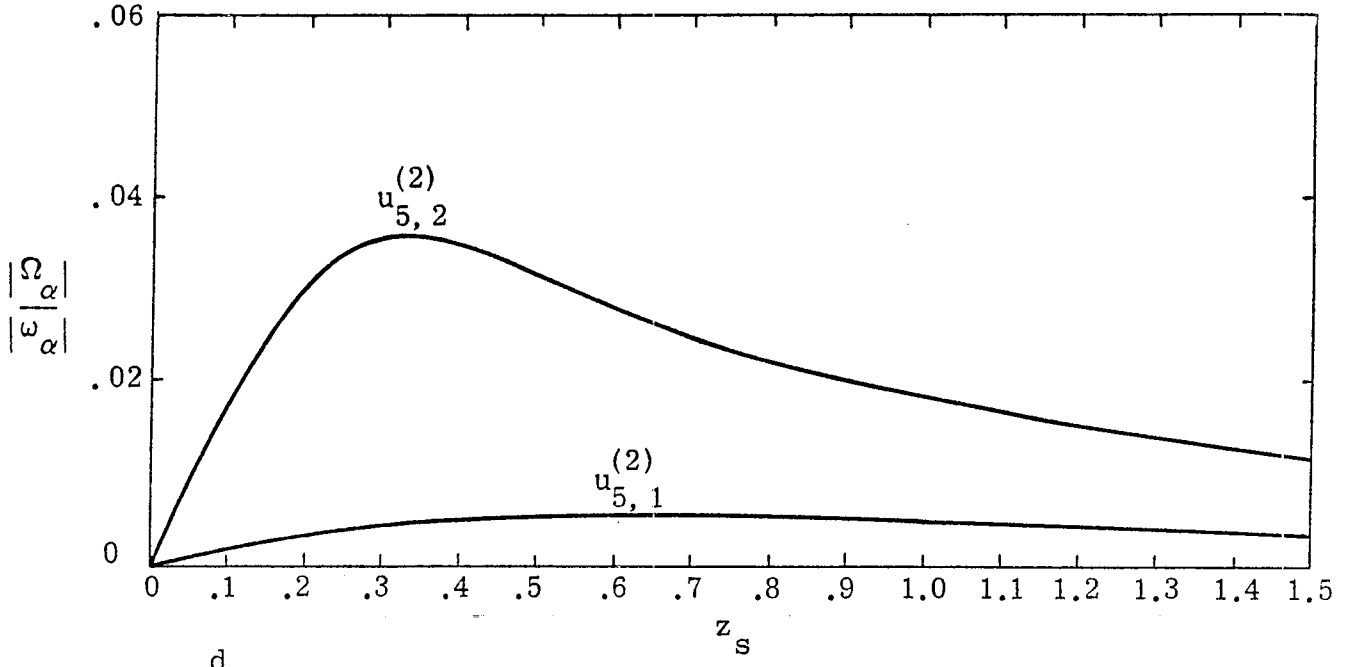

A. $\frac{d}{a} = .5$

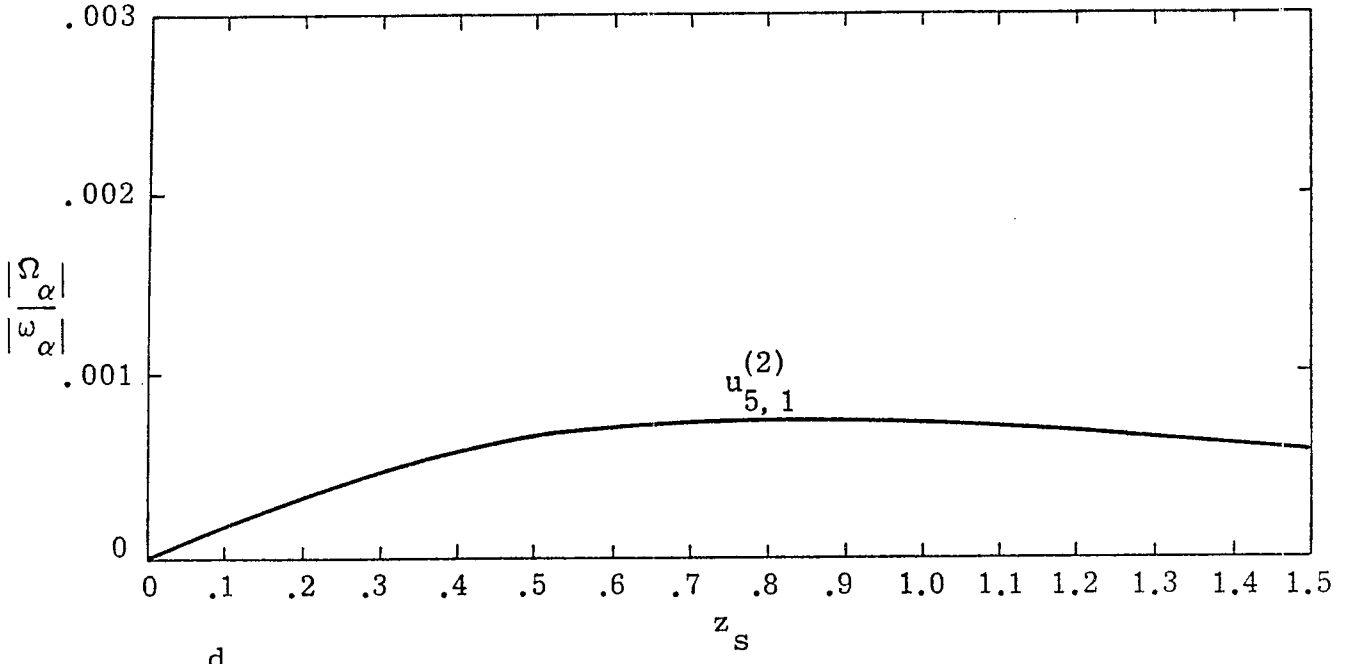

B. $\frac{d}{a} = .6$

Figure 6.15. E-Mode Damping vs. Normalized Loading, n = 5
Curve Label Indicates Origin of Pole Loci

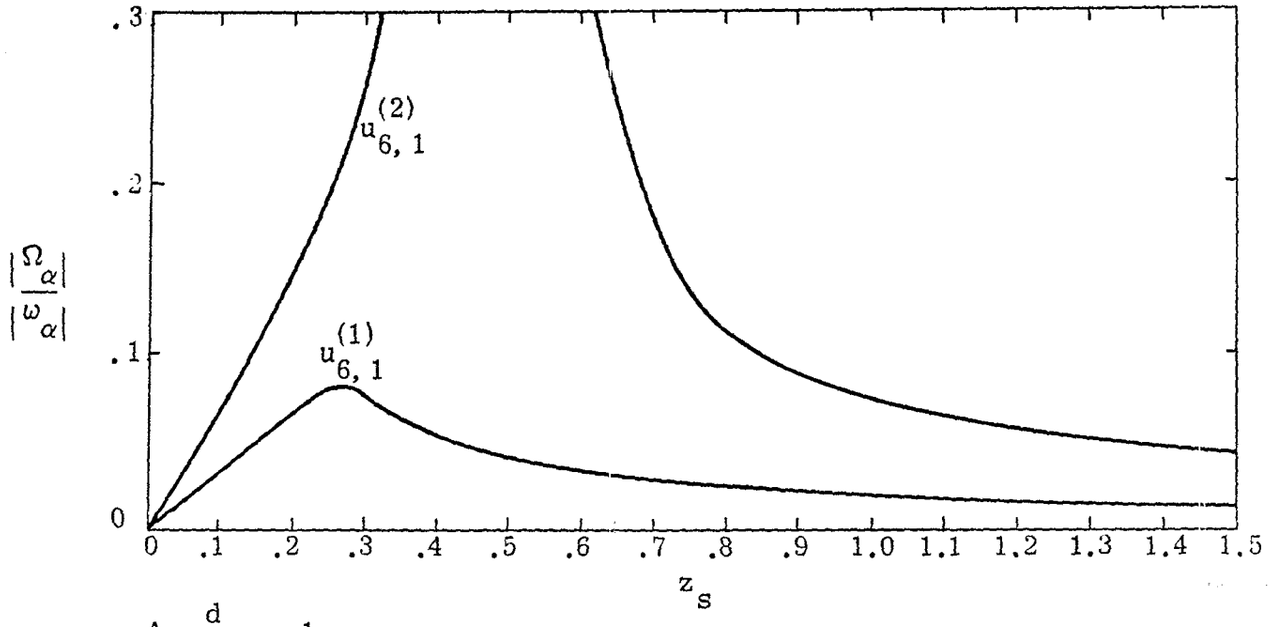

A. $\frac{d}{a} = .1$

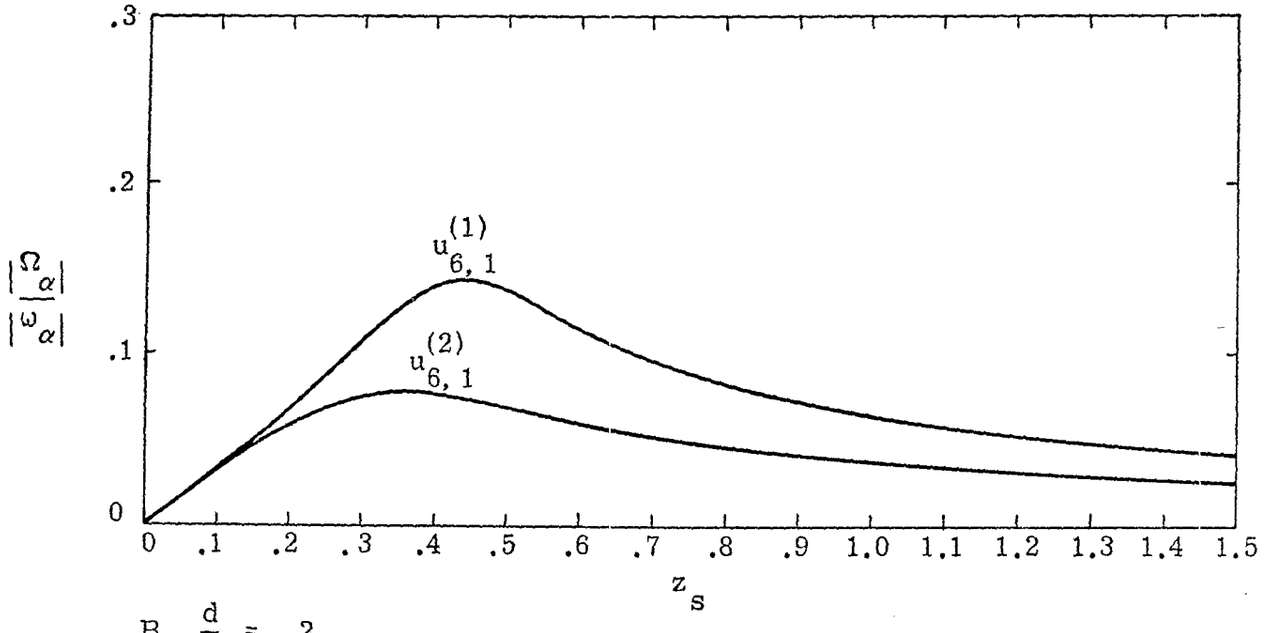

B. $\frac{d}{a} = .2$

Figure 6.16. E-Mode Damping vs. Normalized Loading, n = 6
Curve Label Indicates Origin of Pole Loci

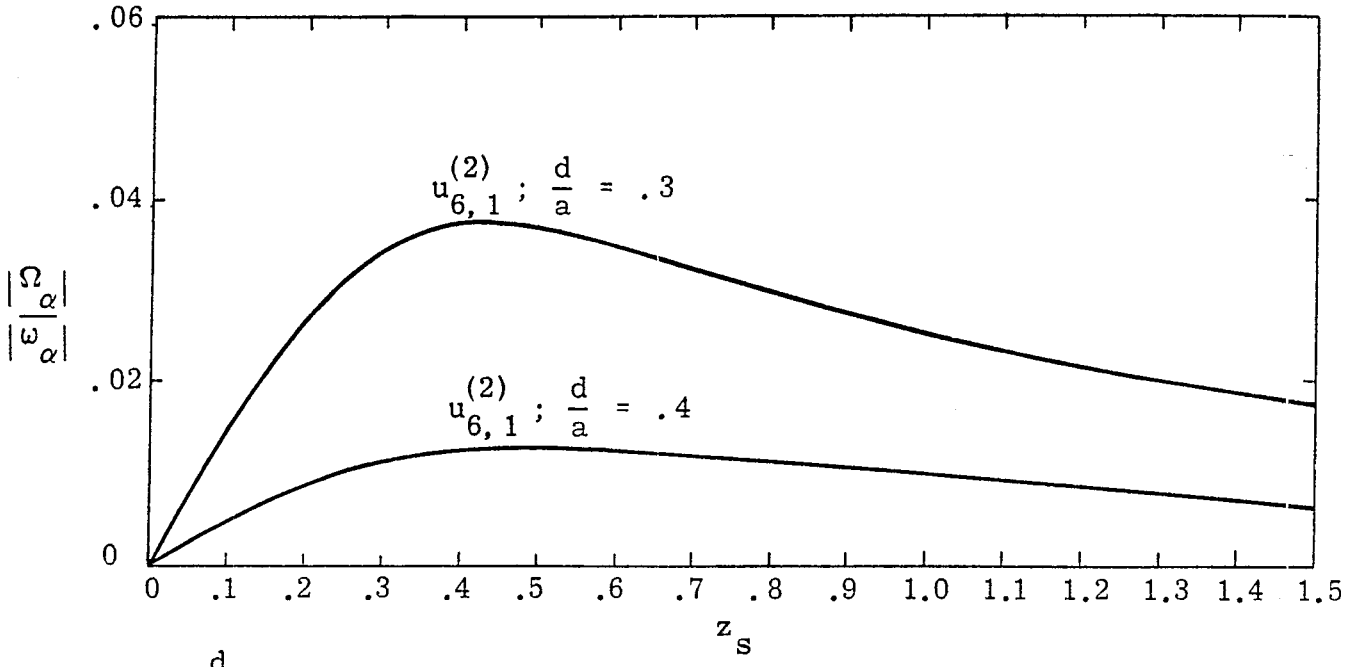

A. $\frac{d}{a}$ = .3, .4

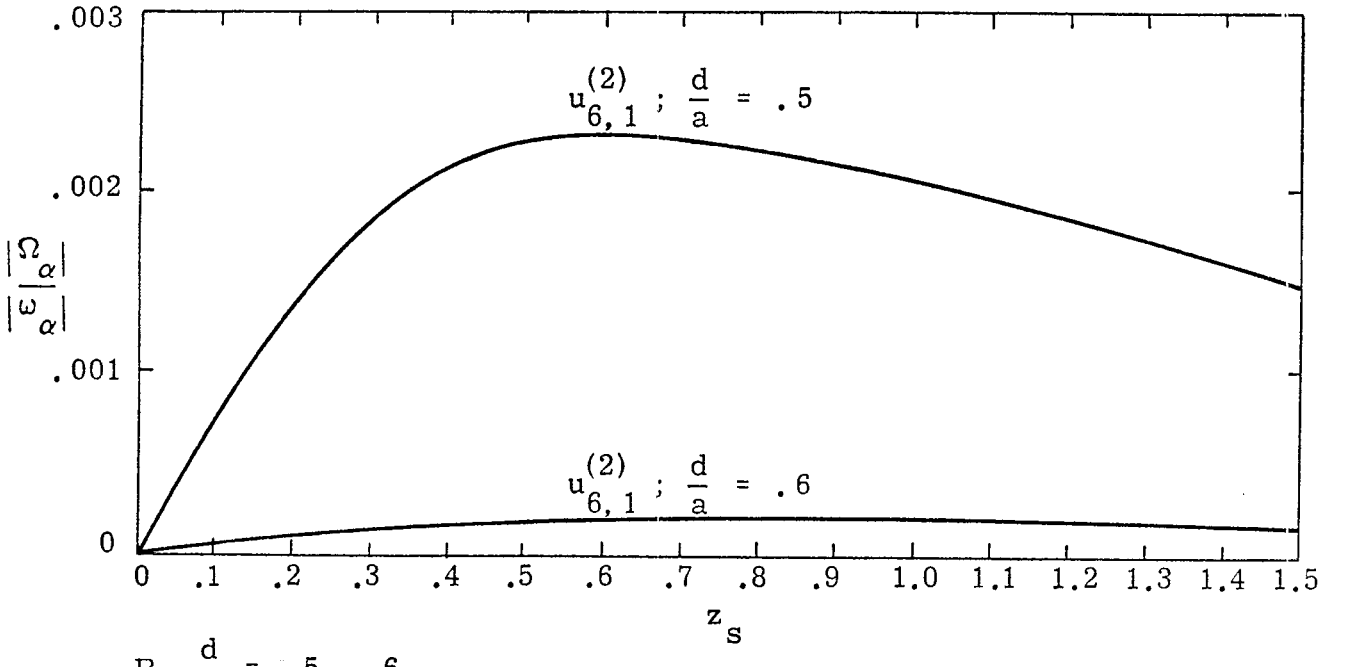

B. $\frac{d}{a}$ = .5, .6

Figure 6.17. E-Mode Damping vs. Normalized Loading, n = 6
Curve Label Indicates Origin of Pole Loci and d/a

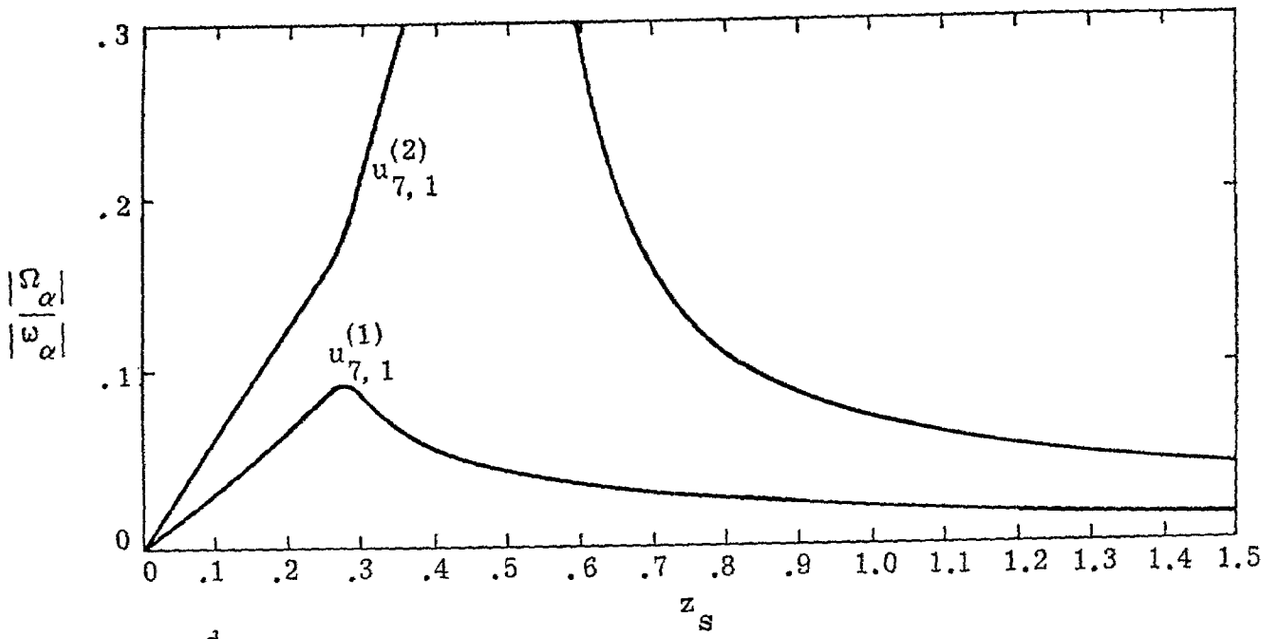

A. $\frac{d}{a} = .1$

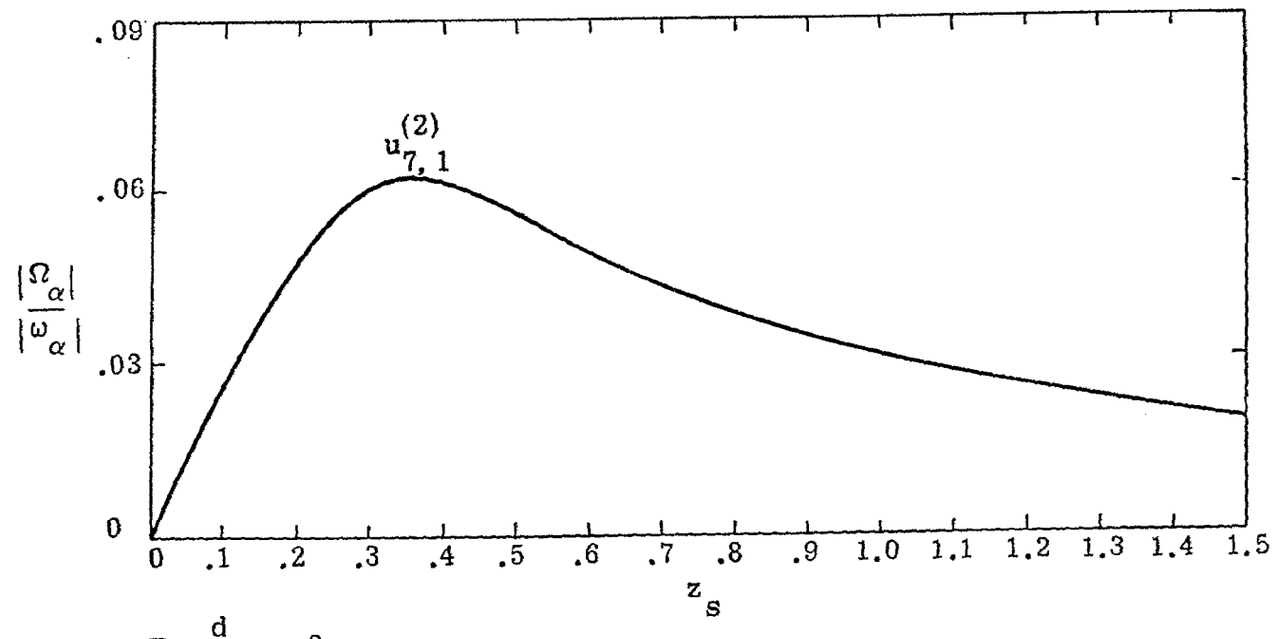

B. $\frac{d}{a} = .2$

Figure 6.18. E-Mode Damping vs. Normalized Loading, n = 7
Curve Label Indicates Origin of Pole Loci

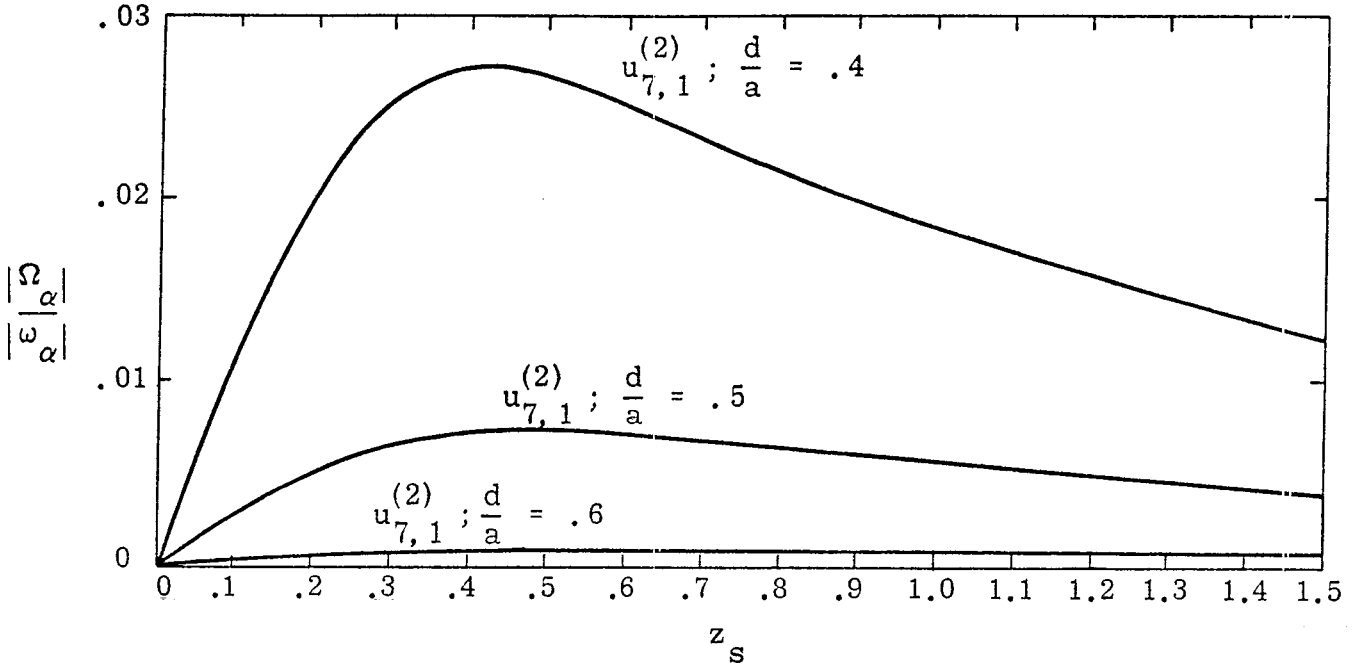

Figure 6.19. E-Mode Damping vs. Normalized Loading, n = 7 with d/a a Parameter. Curve Label Indicates Origin of Pole Loci

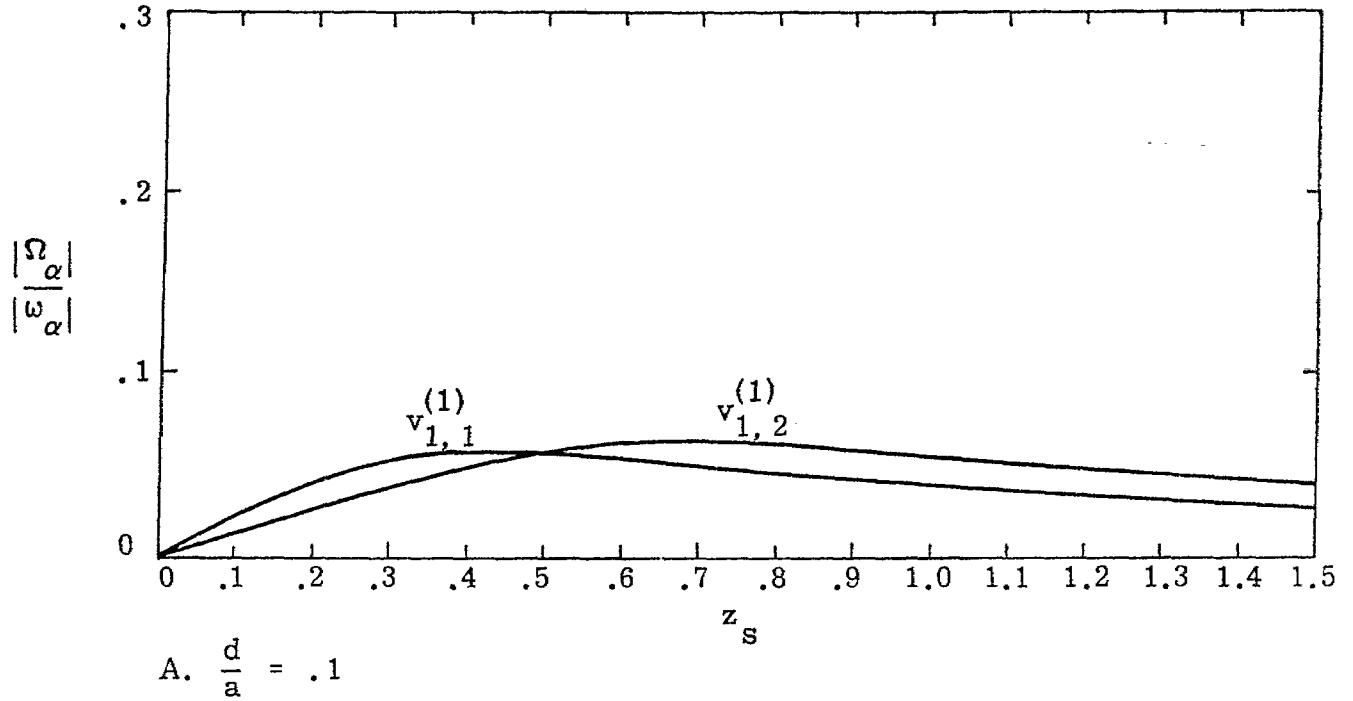

A. $\frac{d}{a} = .1$

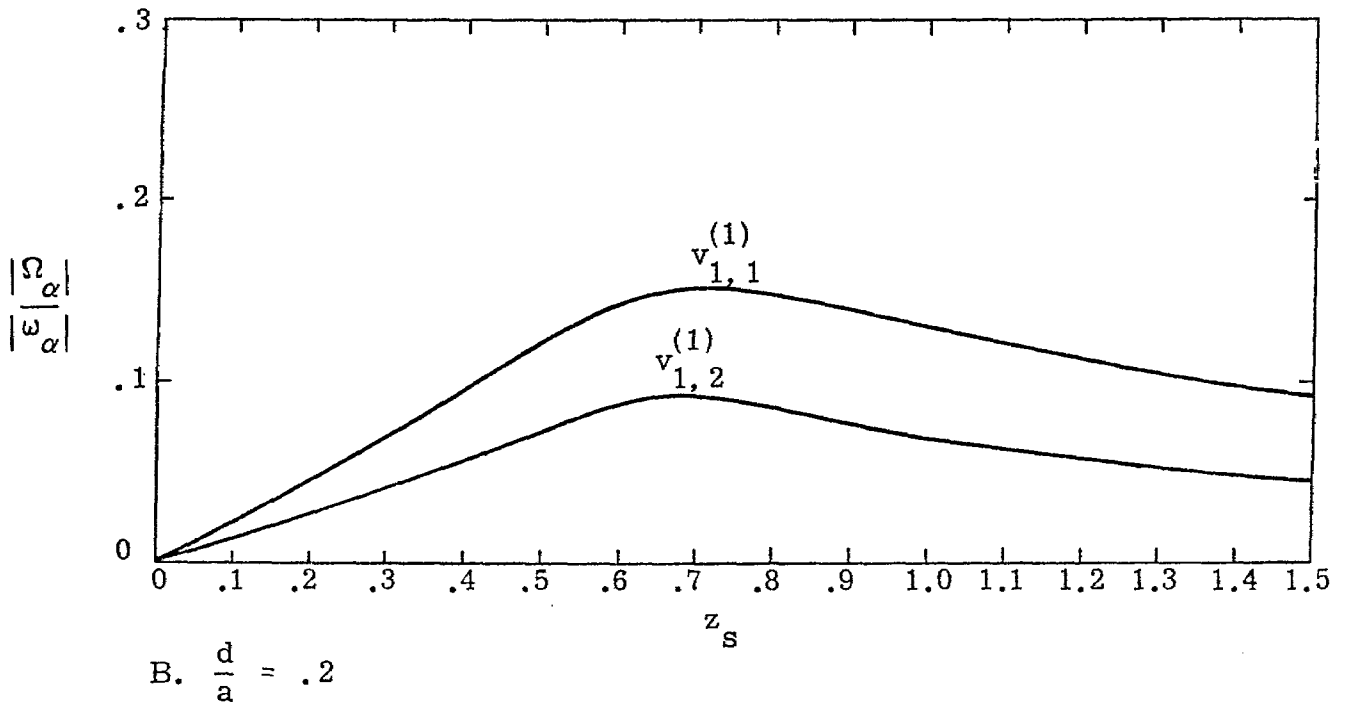

B. $\frac{d}{a} = .2$

Figure 6.20. H-Mode Damping vs. Normalized Damping, n = 1
Curve Label Indicates Origin of Pole Loci

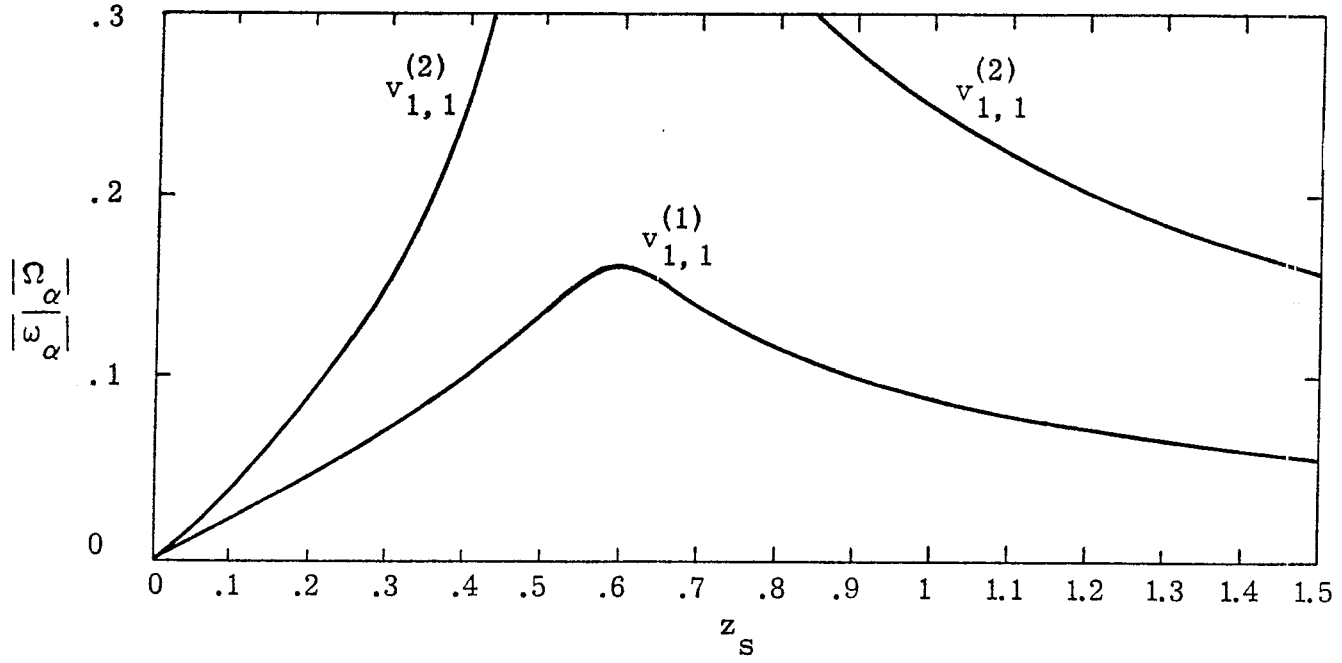

A. $\frac{d}{a} = .3$

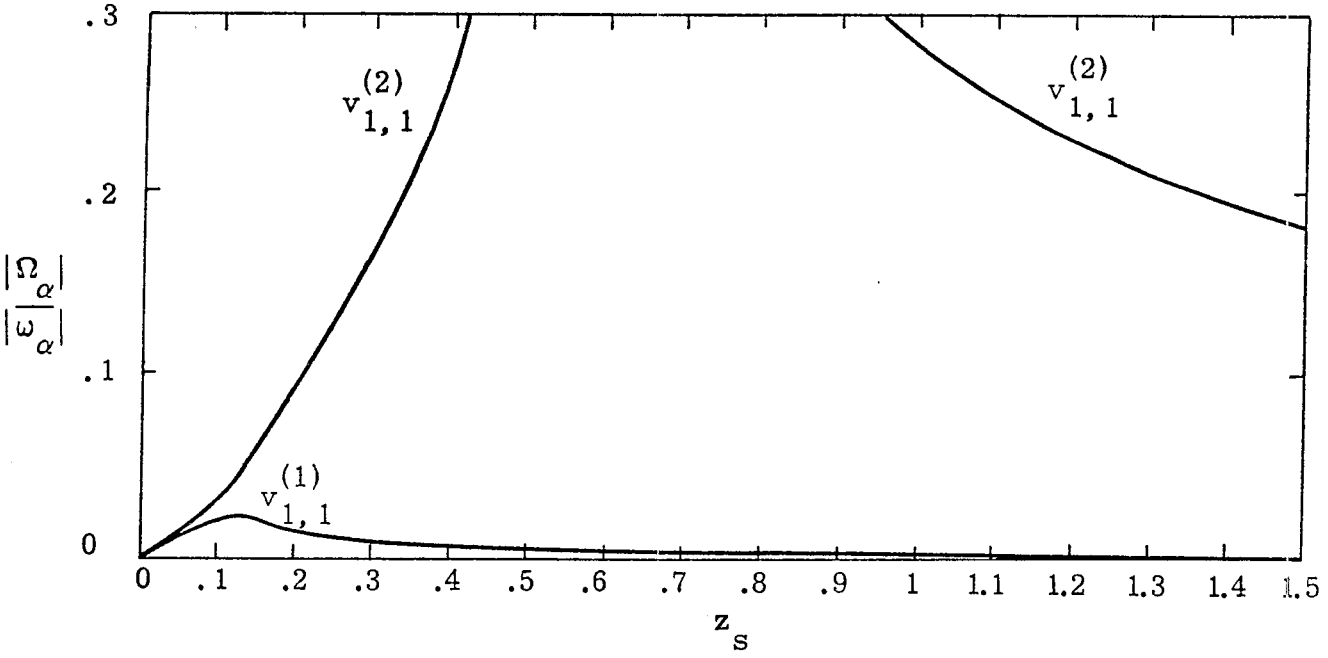

B. $\frac{d}{a} = .4$

Figure 6.21. H-Mode Damping vs. Normalized Loading, n = 1
Curve Label Indicates Origin of Pole Loci

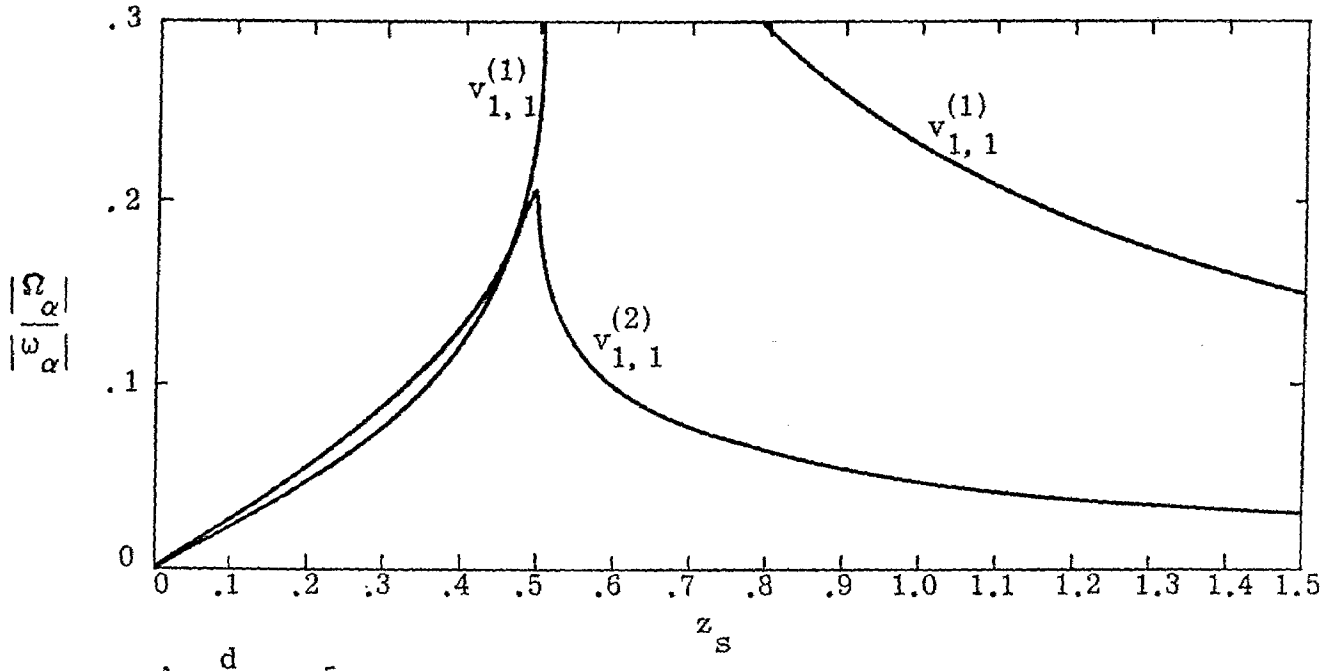

A. $\frac{d}{a} = .5$

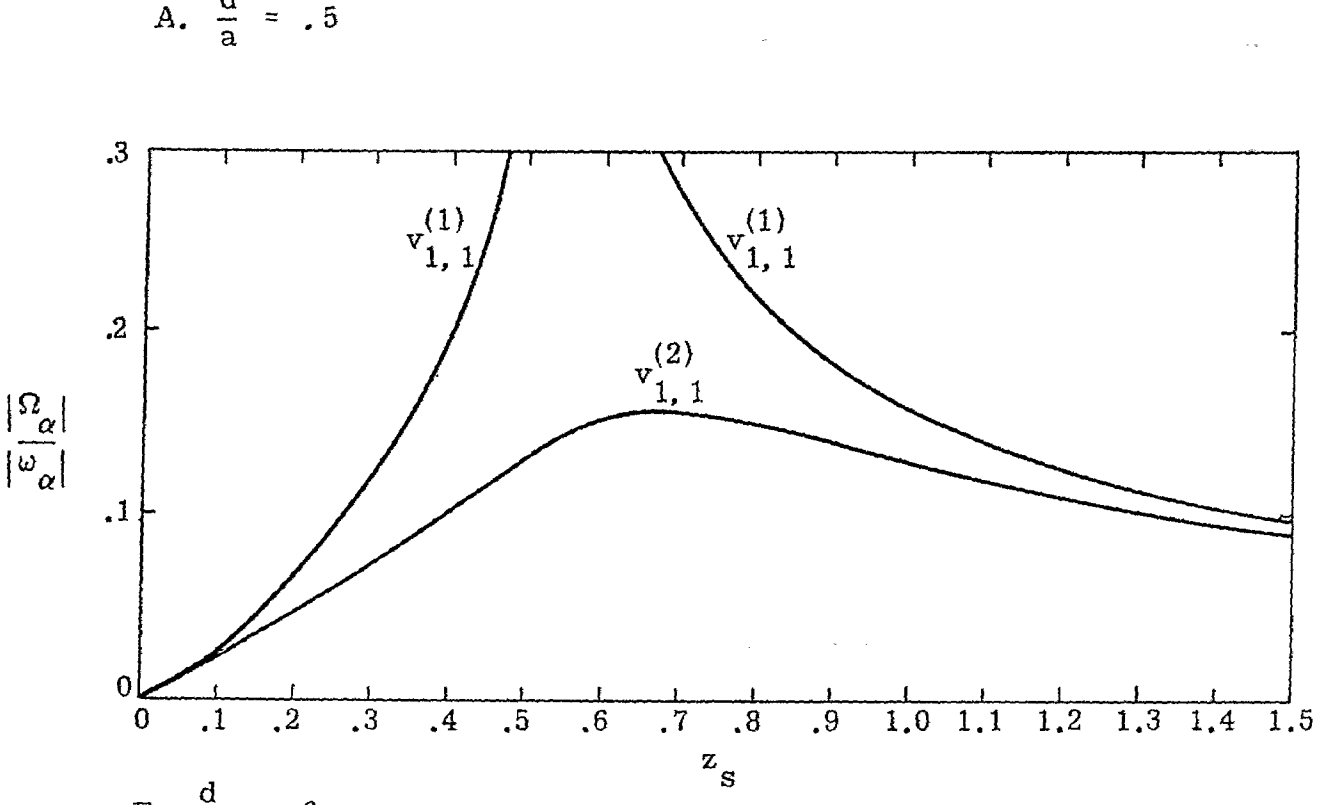

B. $\frac{d}{a} = .6$

Figure 6.22. H-Mode Damping vs. Normalized Loading, n = 1
Curve Label Indicates Origin of Pole Loci

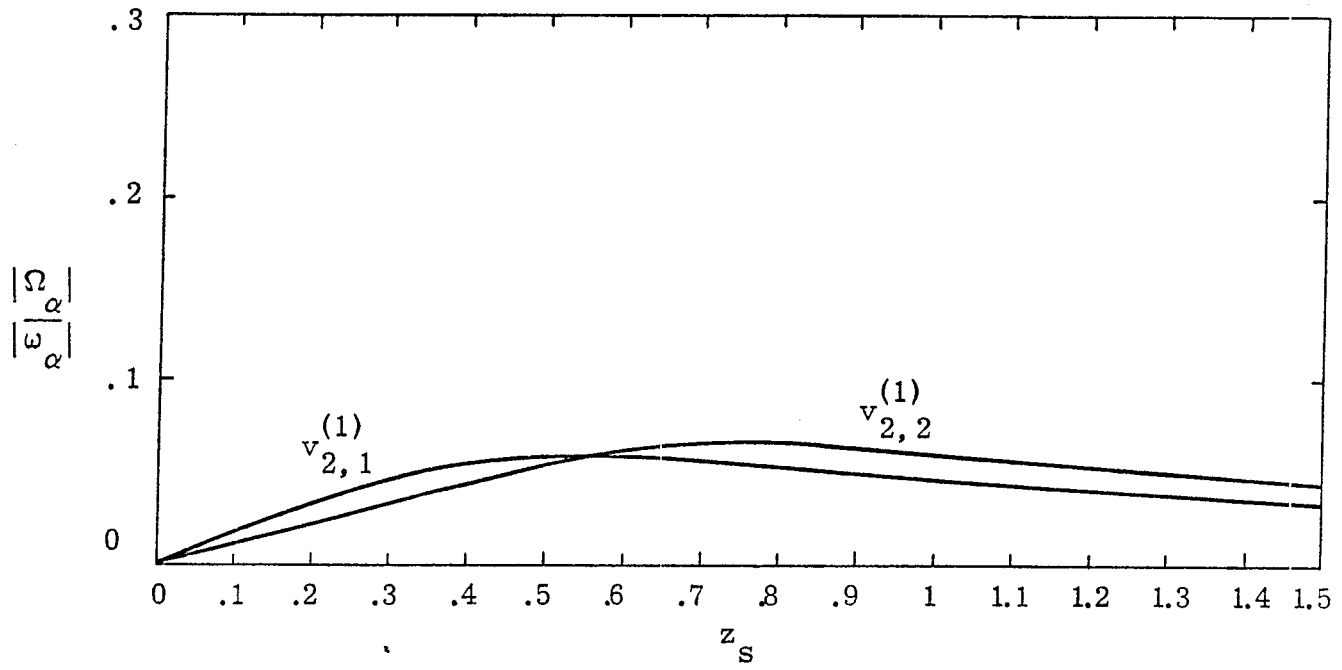

A. $\frac{d}{a} = .1$

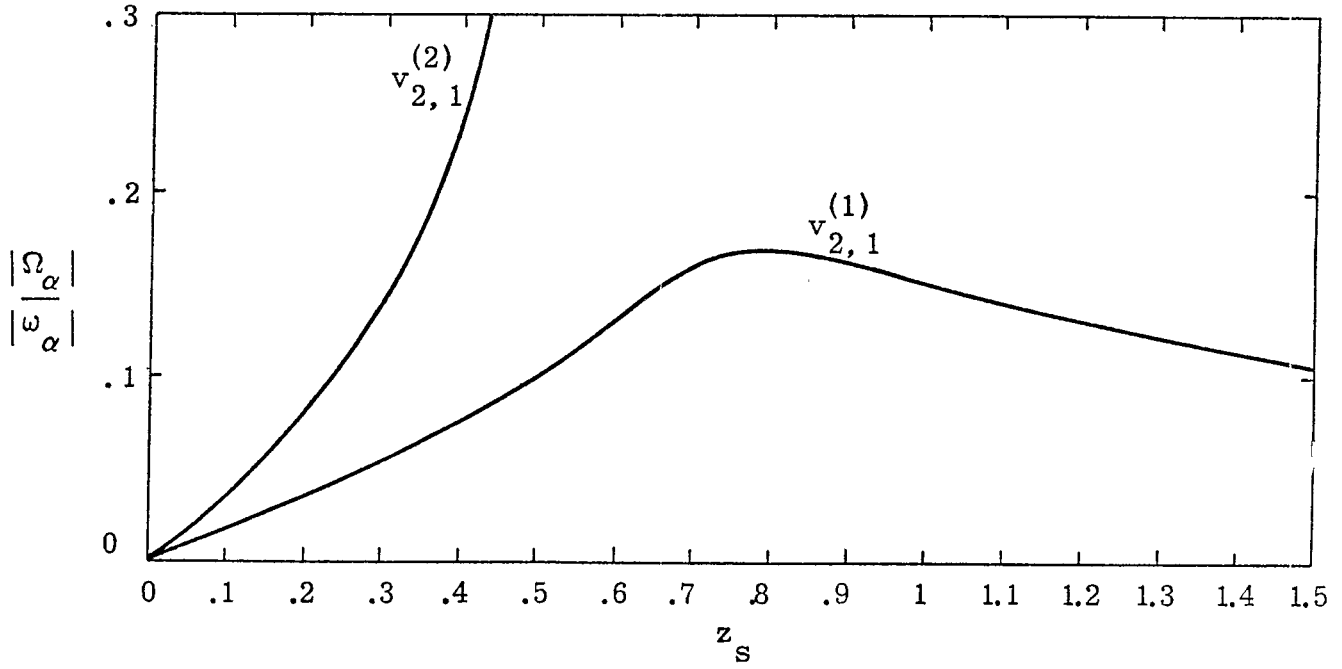

B. $\frac{d}{a} = .2$

Figure 6.23. H-Mode Damping vs. Normalized Loading, n = 2
Curve Label Indicates Origin of Pole Loci

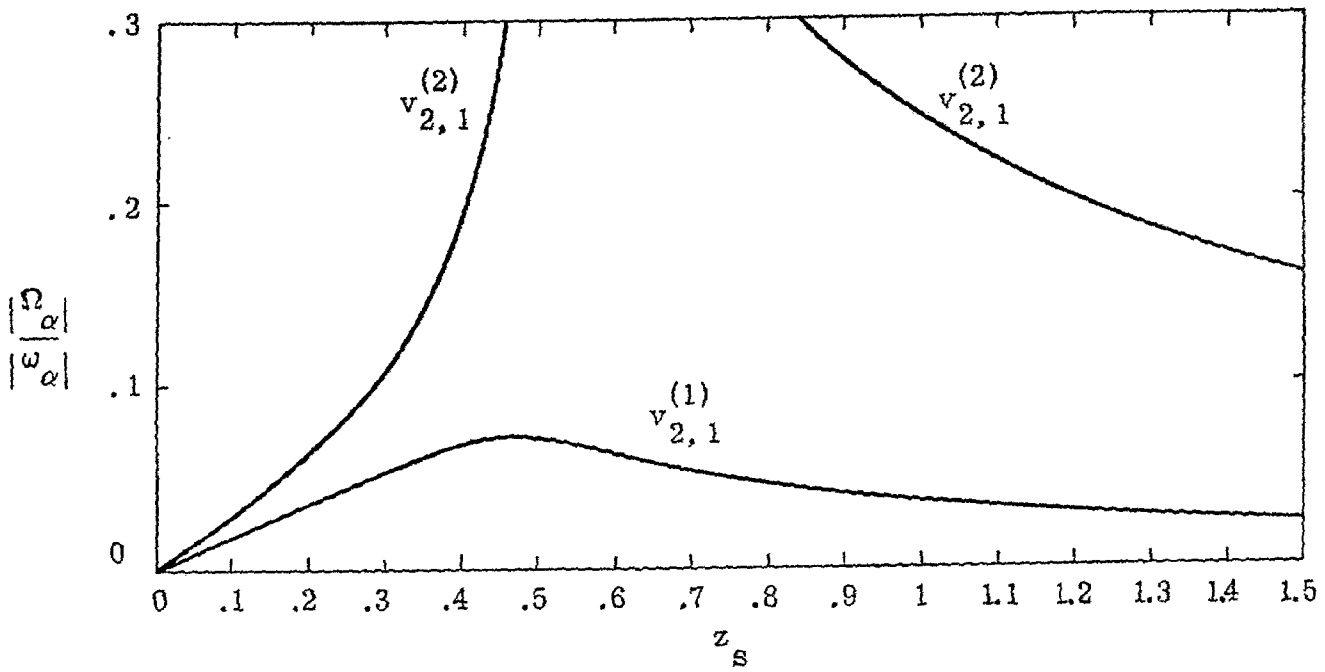

A. $\frac{d}{a} \approx .3$

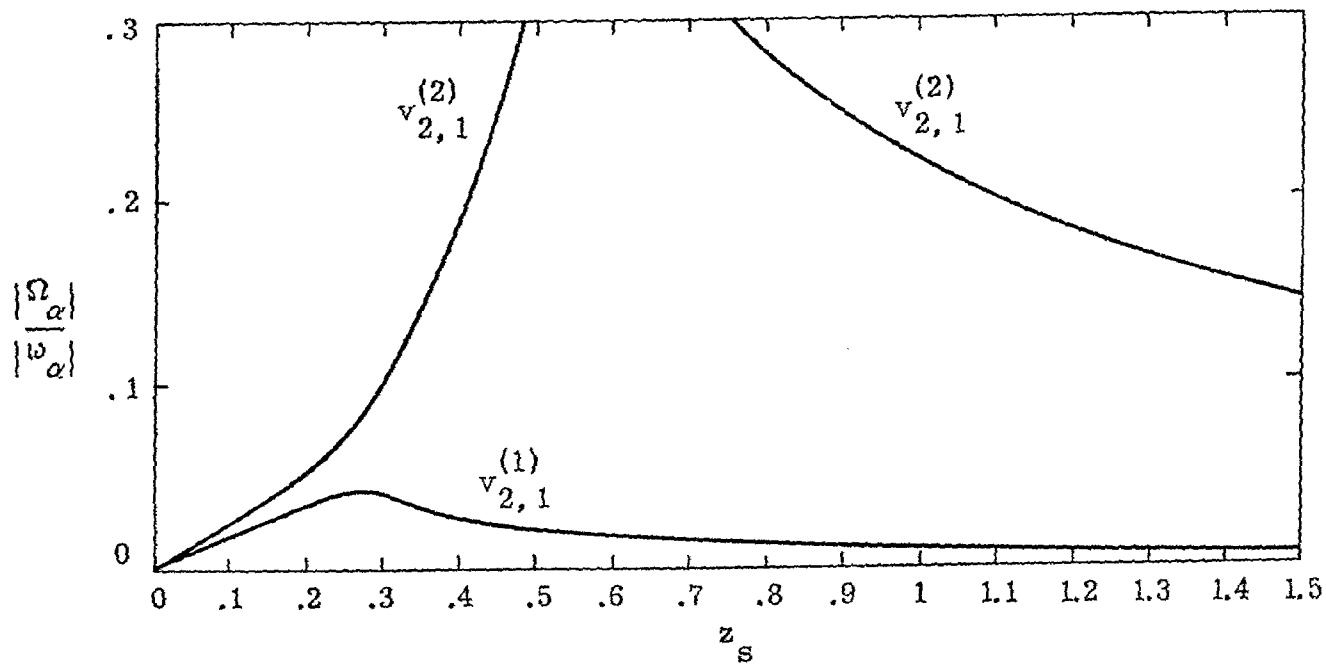

B. $\frac{d}{a} = .4$

Figure 6.24. H-Mode Damping vs. Normalized Loading, n = 2
Curve Label Indicates Origin of Pole Loci

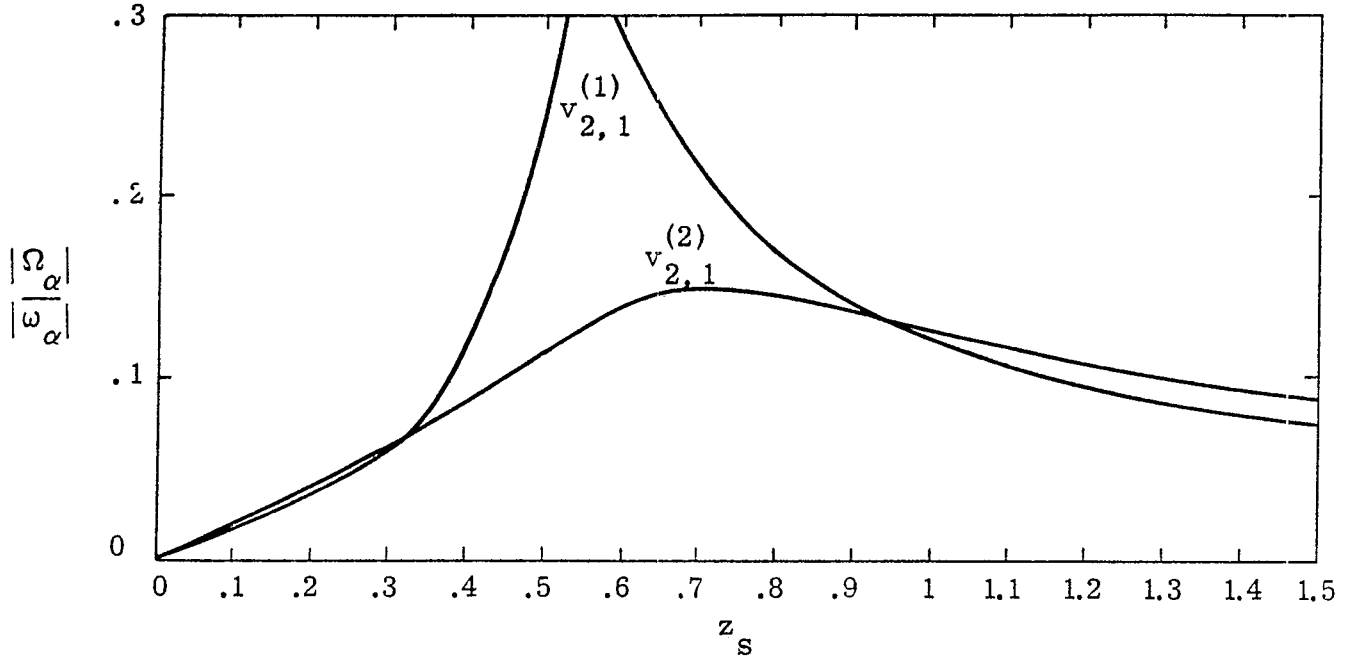

A. $\frac{d}{a} = .5$

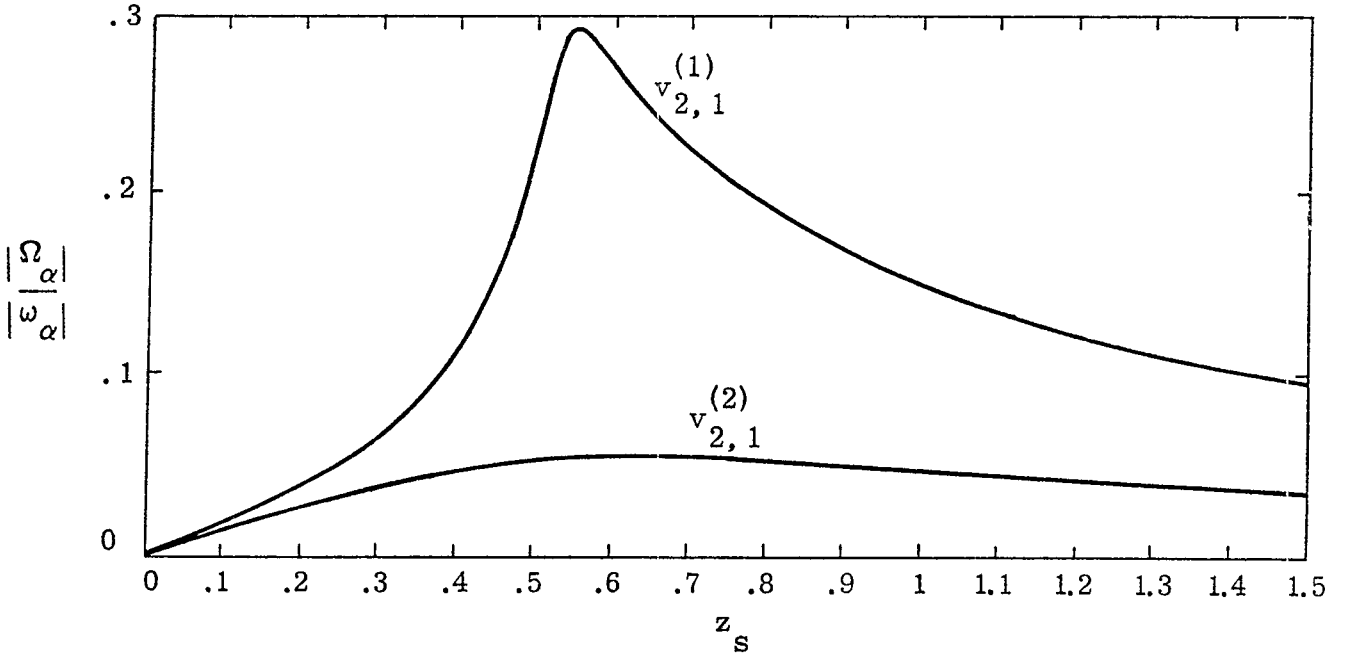

B. $\frac{d}{a} = .6$

Figure 6.25. H-Mode Damping vs. Normalized Loading, n = 2
Curve Label Indicates Origin of Pole Loci

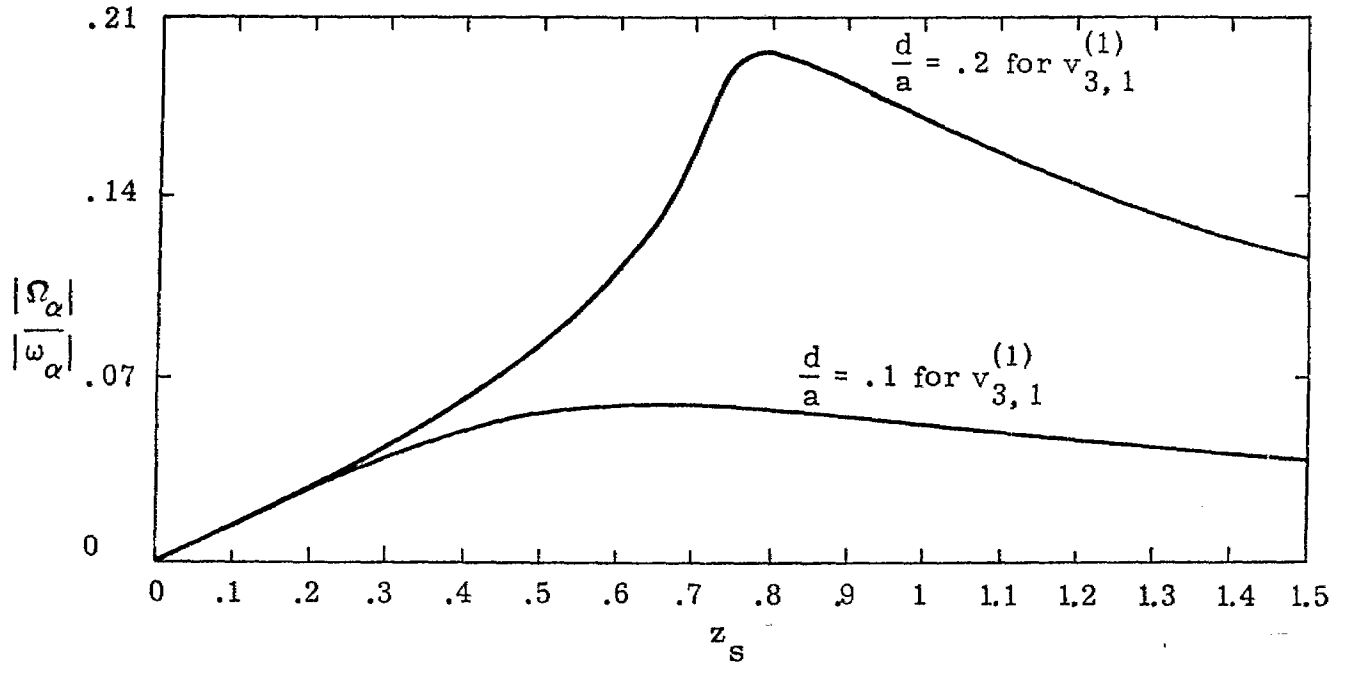

A. $\frac{d}{a}$ = .1, .2

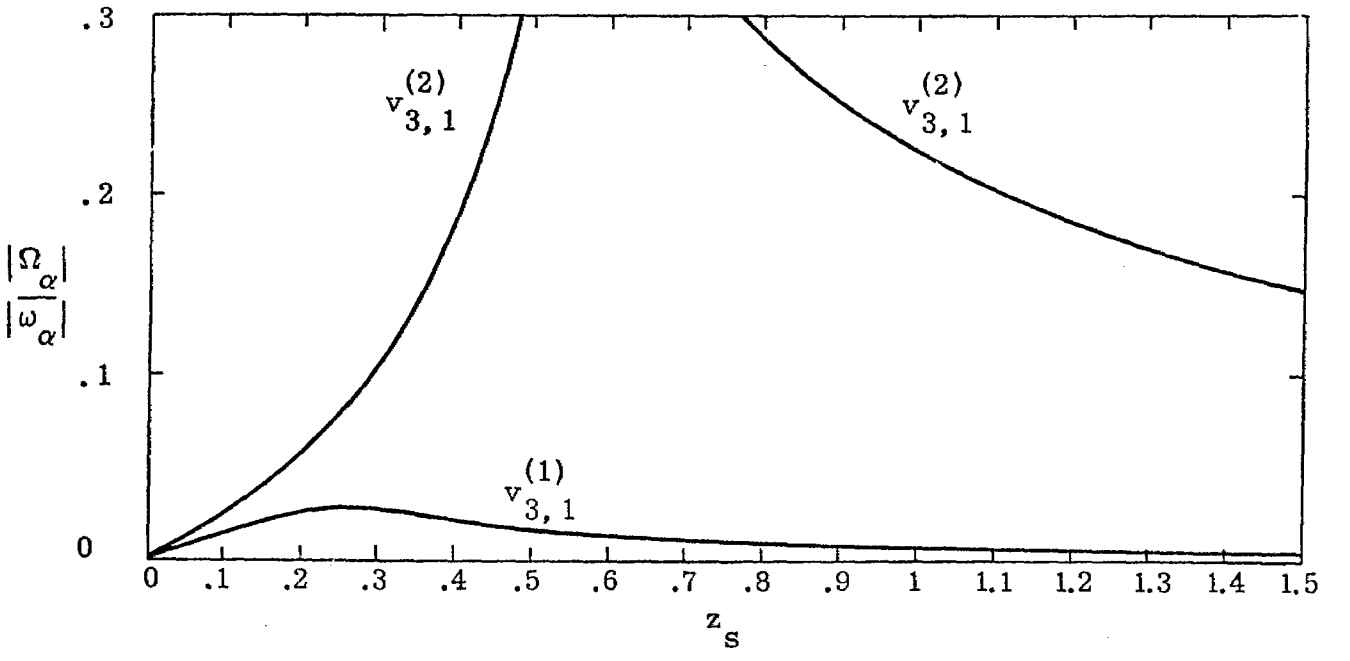

B. $\frac{d}{a}$ = .3

Figure 6.26. H-Mode Damping vs. Normalized Loading, n = 3
Curve Label Indicates Origin of Pole Loci

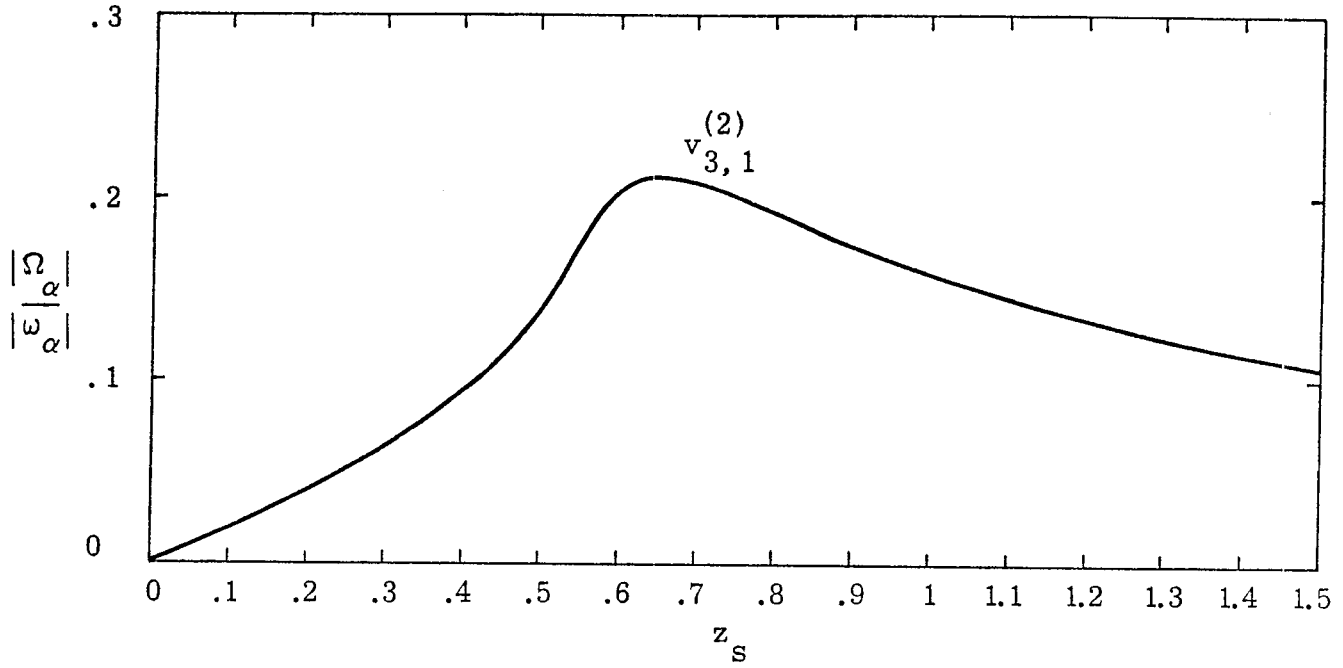

A. $\frac{d}{a} = .4$

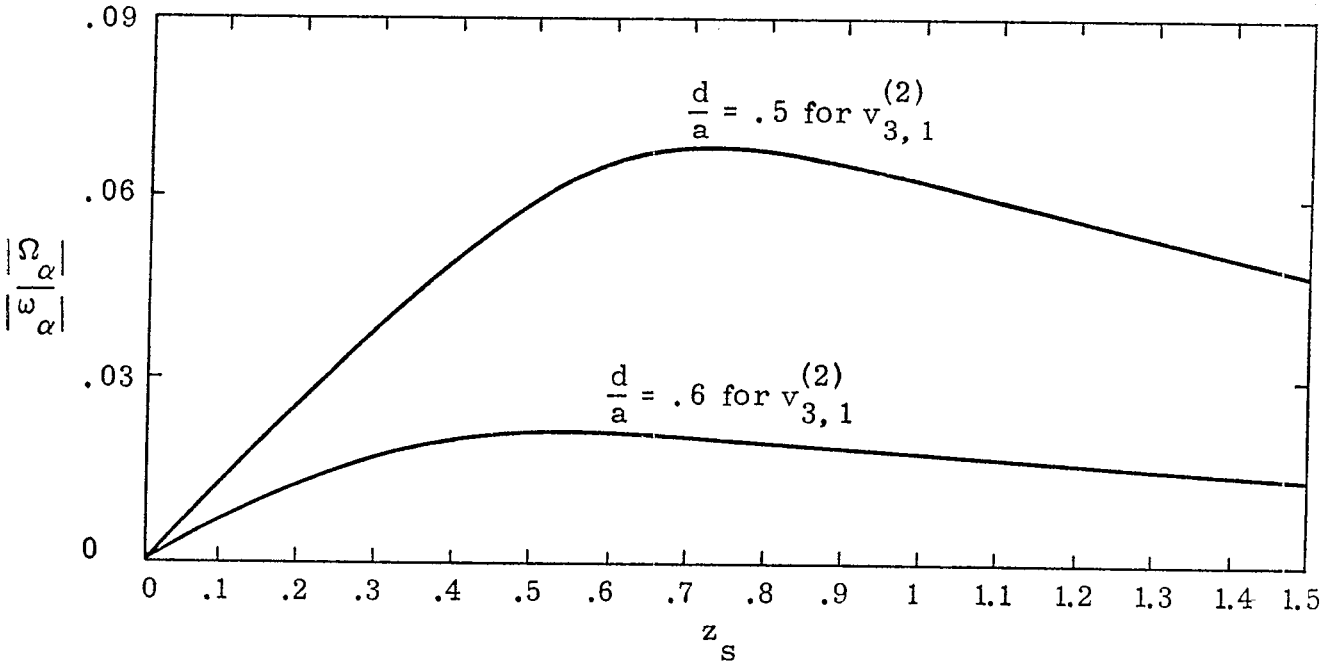

B. $\frac{d}{a} = .5, .6$

Figure 6.27. H-Mode Damping vs. Normalized Loading, n = 3
Curve Label Indicates Origin of Pole Loci

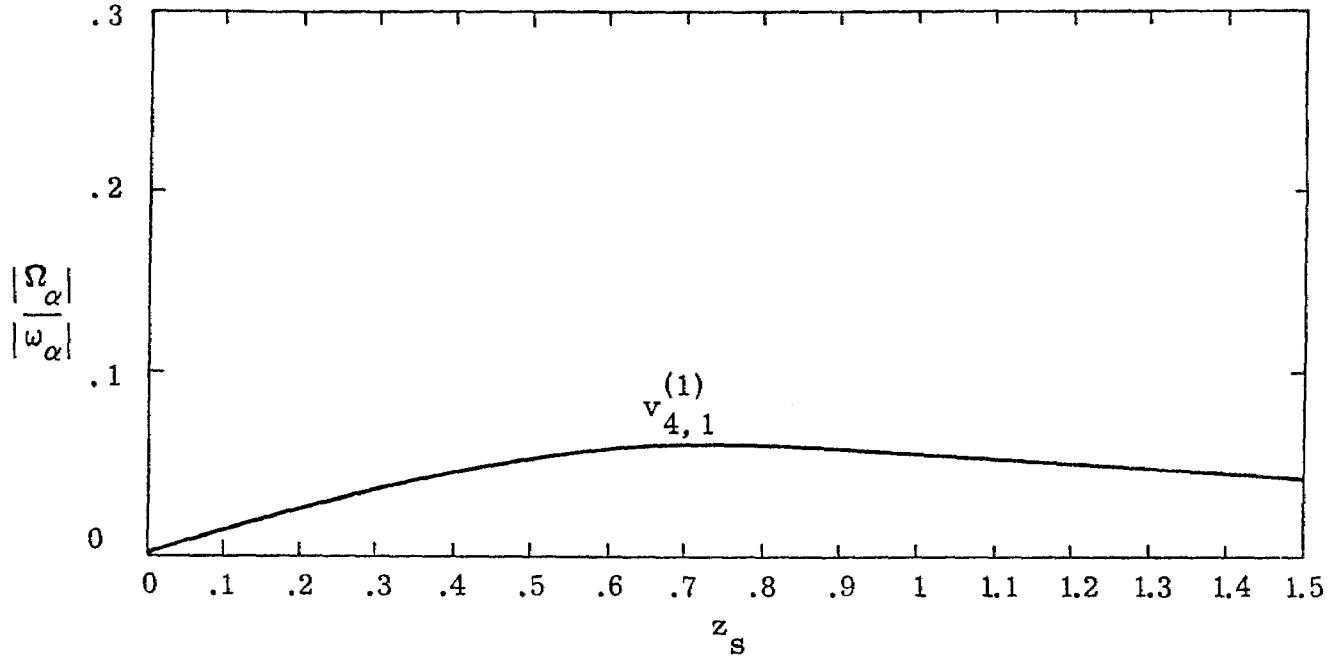

A. $\frac{d}{a} = .1$

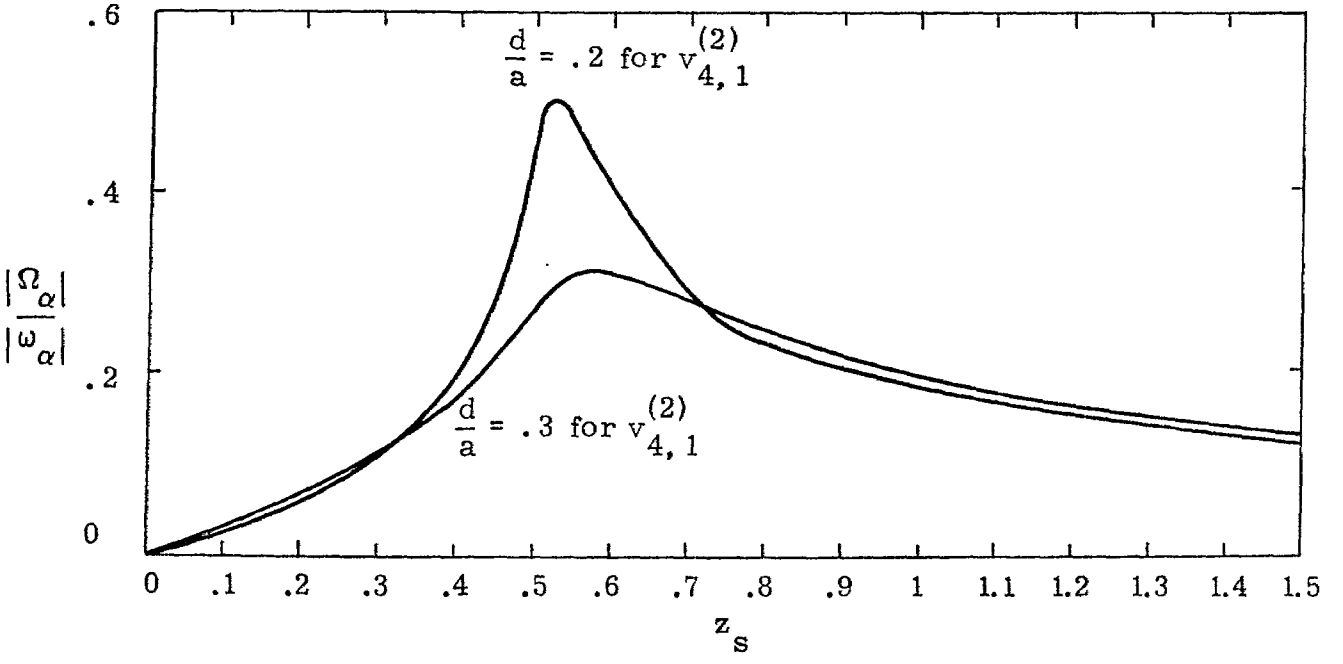

B. $\frac{d}{a} = .2, .3$

Figure 6.28. H-Mode Damping vs. Normalized Loading, n = 4
Curve Label Indicates Origin of Pole Loci

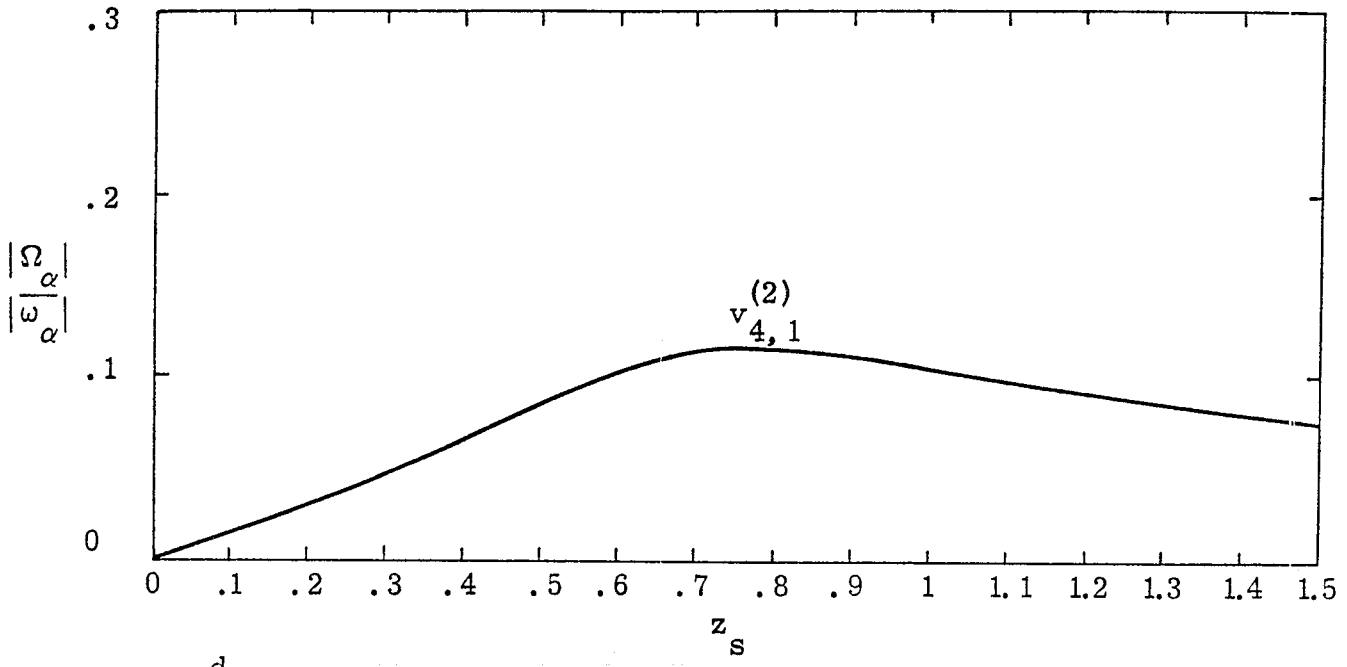

A. $\frac{d}{a} = .4$

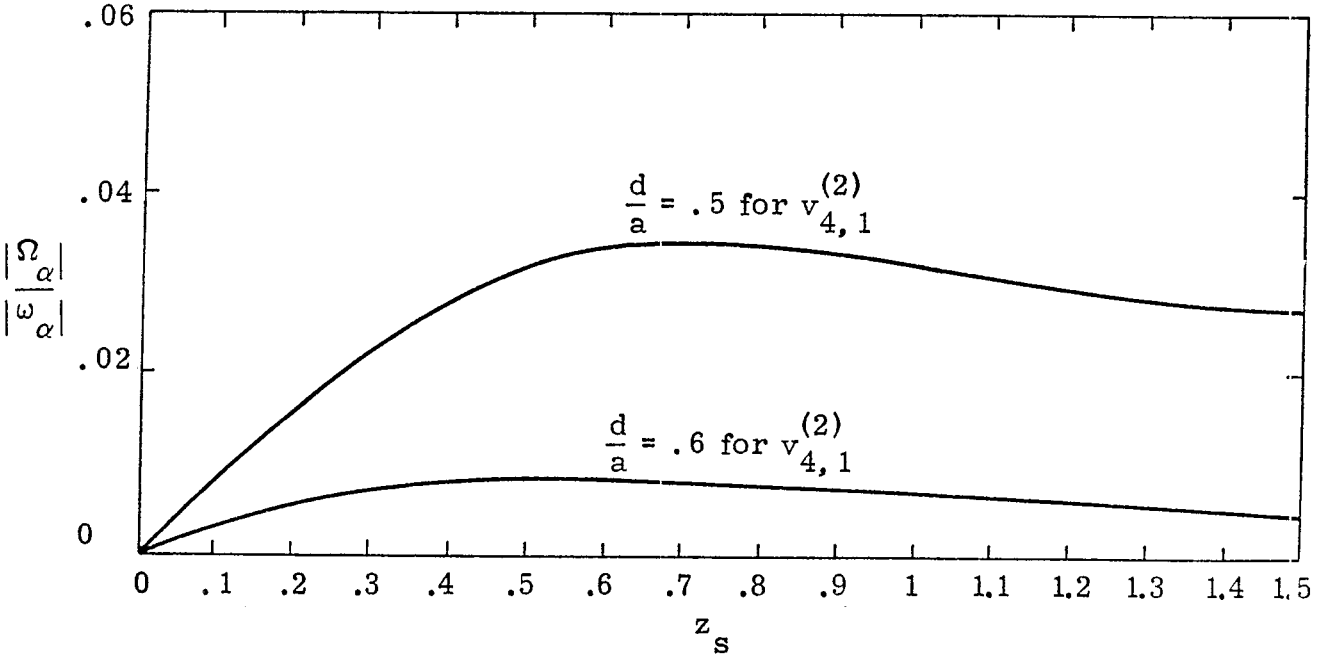

B. $\frac{d}{a} = .5, .6$

Figure 6.29. H-Mode Damping vs. Normalized Loading, n =4
Curve Label Indicates Origin of Pole Loci

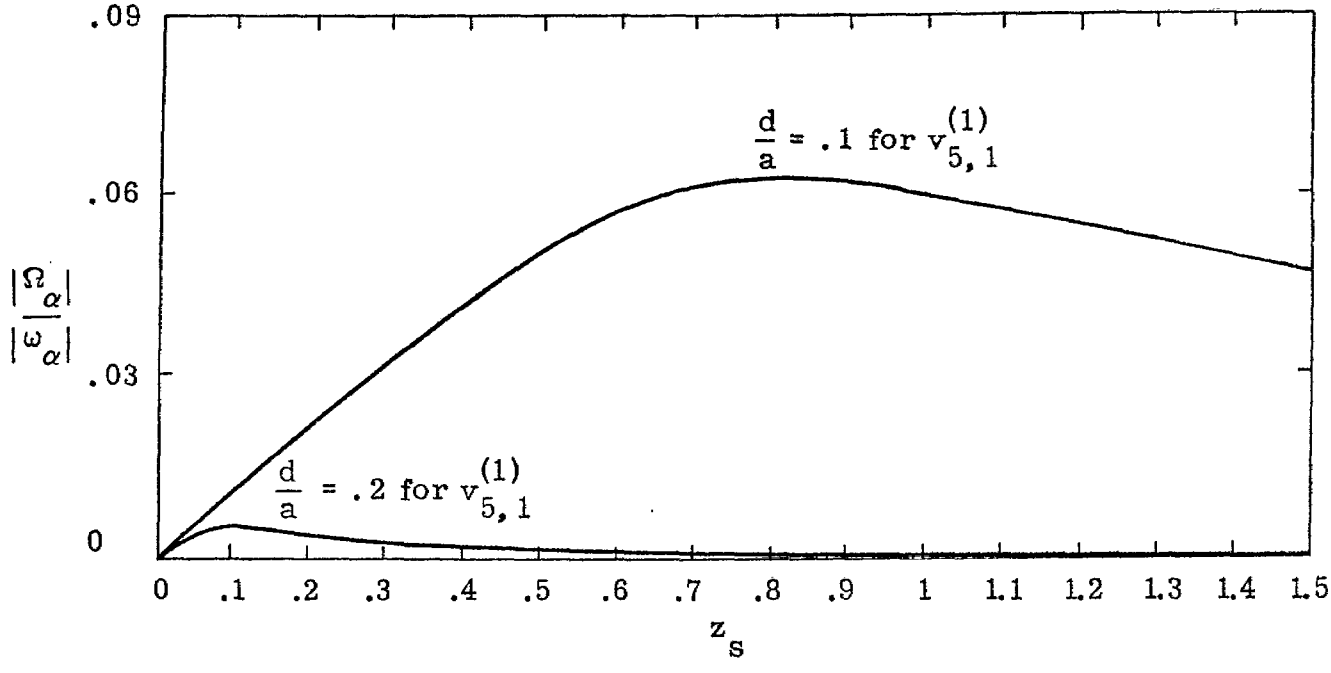

A. $\frac{d}{a}$ = .1, .2

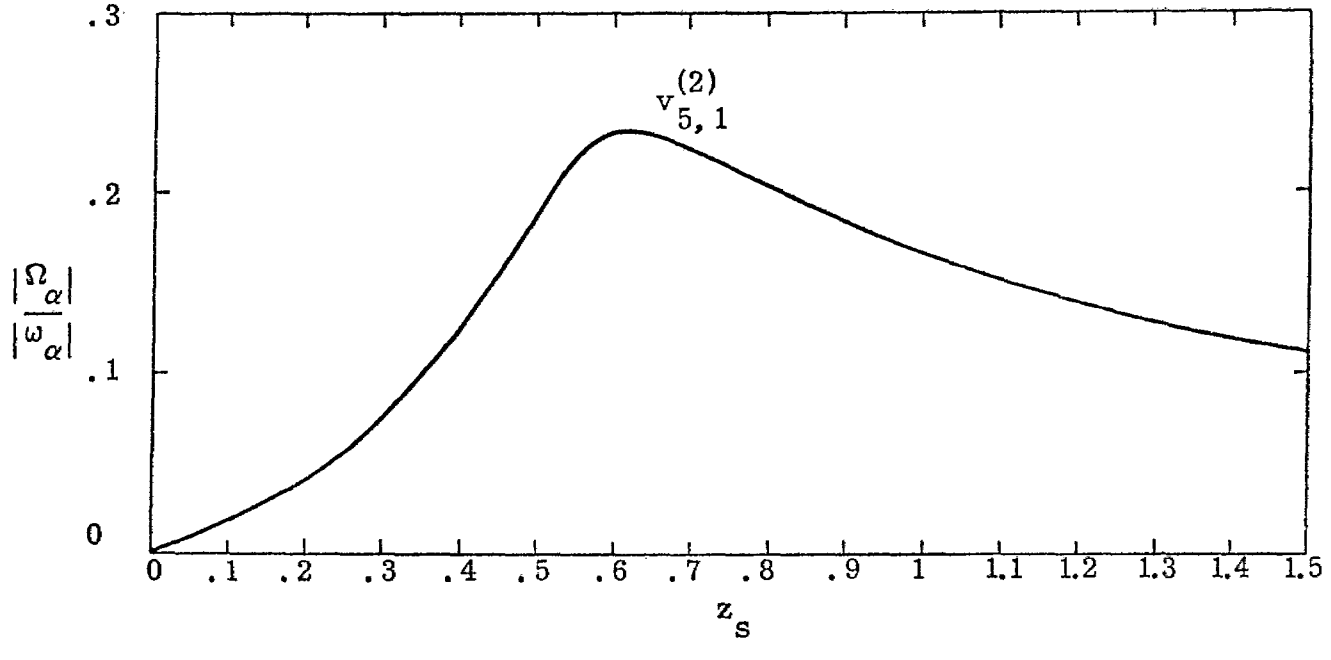

B. $\frac{d}{a}$ = .3

Figure 6.30. H-Mode Damping vs. Normalized Loading, n =5
Curve Label Indicates Origin of Pole Loci

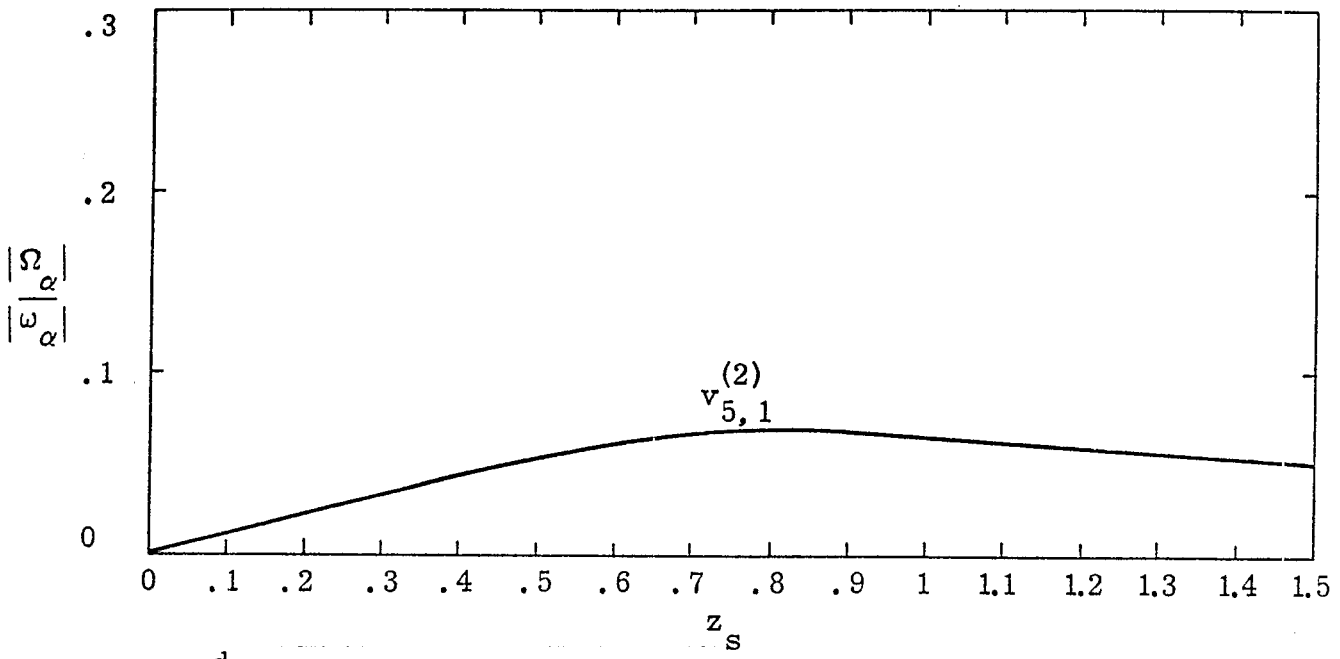

A. $\frac{d}{a} = .4$

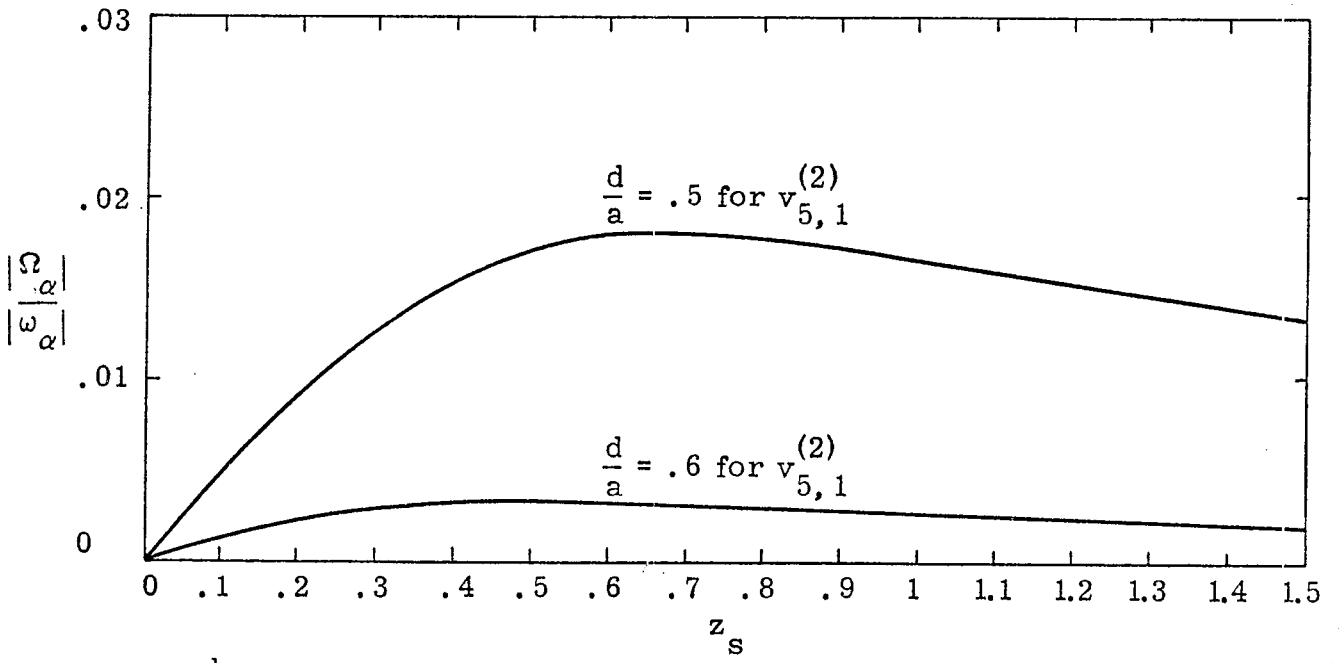

B. $\frac{d}{a} = .5, .6$

Figure 6.31. H-Mode Damping vs. Normalized Loading, n = 5
Curve Label Indicates Origin of Pole Loci

VII. LOADING THE SHEET LINER WITH OTHER THAN PURE RESISTANCE

If R, X_L and X_C represent some resistance, inductive reactance, and capacitive reactance, then any complex impedance, $Z = R + i(X_L + X_C)$, can be written in terms of the magnitude ($r_m = |Z|$) and phase ($\arg(Z)$, i.e., $\theta = \tan^{-1}[(X_L + X_C)/R]$)

$$Z = r_m e^{i\theta} \tag{7.1}$$

For the purpose here the natural log is taken as

$$\ell n(Z) = \ell n(r_m) + i\theta_o \tag{7.2}$$

with the phase angle given its principal value θ_o, $-\pi < \theta_o \leq \pi$ to avoid the multiple-valueness of $\ell n(Z)$. This is a very useful form for the impedance for the approach used below.

Now consider an E and H mode impedance function which can be written by solving equations 2.5 and 2.6, respectively, for $-z_s$ as

$$f_n^E(S) = -\Big\{[Sbk_n(Sb)]'[Si_n(S)]'[Sbi_n(Sb)]' -$$

$$[Sk_n(S)]'\big([Sbi_n(Sb)]'\big)^2\Big\}\big([Si_n(S)]'\big)^{-1} \tag{7.3}$$

and

$$f_n^H(S) = -\left\{Sk_n(S)[Sbi_n(Sb)]^2 - Si_n(S)Sbk_n(Sb)Sbi_n(Sb)\right\}[Si_n(S)]^{-1} \quad (7.4)$$

Obviously then $z_s + f_n^E(S) = 0$ for the E modes and $z_s + f_n^H(S) = 0$ for the H modes will, for a fixed geometry (i.e., d/a), describe the natural resonances of the spherical cavity regardless of the complex nature of z_s. The two functions actually represent all solution of z_s in the complex S plane with the exception of the trivial solution.

The scheme to be used here is to present $f_n^E(S)$ and $f_n^H(S)$ in the same form as equation 7.2. The natural log of the negative impedance functions is written as

$$\ell n\left(f_n^E(S)\right) = \ell n\left(\left|f_n^E(S)\right|\right) + i \arg\left(f_n^E(S)\right) \quad (7.5a)$$

and

$$\ell n\left(f_n^H(S)\right) = \ell n\left(\left|f_n^H(S)\right|\right) + i \arg\left(f_n^H(S)\right) \quad (7.5b)$$

Now a subdivision of the complex frequency plane can be made by simply plotting constant magnitude and phase contours to produce an orthogonal mapping such that each intersection defines a particular impedance configuration. By applying the same magnitude and phase constraint around all poles and zeros of concern the resonant shift and consequently the damping can be determined.

For the negative impedance function, $f_n^E(S)$ and $f_n^H(S)$, presented in this section the phase contours have been plotted[7] with values such that

$$C_{phase} = \pi\left(\frac{n}{2N} - 1\right), \quad n = 0, \pm1, \pm2, \cdots, \pm N; \quad N = 6 \tag{7.6}$$

The magnitude contours are taken in the same increments to produce curvilinear squares in the complex S plane. A somewhat truncated series of contour values is used for the phase from that described for the principal value since the entire phase map is mirrored across the imaginary axis as $\pi + C_{phase}$. As many magnitude contours

$$C_{mag} = \frac{n\pi}{2N}, \quad n = 0, \pm1, \pm2, \cdots \tag{7.7}$$

are taken as needed to define regions around the zeros and poles.

Note that the phase lines exist along the axes. In particular along the ordinate the phase is either $-\pi/2$ (where $n = N$) or $\pi/2$ (where $n = -N$) alternating between poles and zeros. The phase line extending in the positive $i\omega a/c$ direction from any $u^{(0)}_{n,n'}$ ($v^{(0)}_{n,n'}$) is $-\pi/2$ while the phase line extending in the negative $i\omega a/c$ direction (but not across $i\omega a/c = 0$) is $\pi/2$.

Vividly shown in the contour map are the zeros and poles of the impedance function. These points have previously been defined. The zeros correspond to $u^{k}_{n,n'}$ ($v^{k}_{n,n'}$) and the poles correspond to $u^{(0)}_{n,n'}$ ($v^{(0)}_{n,n'}$). The relationship to the zeros is obvious when the numerators of $f_n^E(S)$ and

$f_n^H(S)$ are factored and compared with equations 2.9 through 2.11. The poles of the negative impedance functions stem from equations 2.7 and 2.8.

Although it might be expected from line integral theorems (of the Cauchy and Rouche type) concerning poles and zeros in the complex plane, it is nonetheless interesting to note some of the constant phase patterns; for example the pole-zero phase line connection. A quite different pattern is present about two zeros or two poles. The two-pole or two-zero configuration is not as obvious in the impedance function presented here as it will be in a forthcoming report by R. F. Blackburn on the impedance loaded loop. In addition each pole has M phase lines radiating from it where $\Delta_{phase} = 2\pi/M$ (here M = 24 with 12 in each half plane). The number of constant phase lines coming from a pole or zero is directly related to its order, that is, a second order pole would have 2M phase lines for the same Δ_{phase}. All poles and zeros of the functions f_n^E and f_n^H presented here, however, are of the first order.

Of special interest is the particular phase contour

$$C_{phase_\Sigma} = \arg\left(f_n^E(S_\Sigma)\right) \tag{7.8a}$$

and

$$C_{phase_\Sigma} = \arg\left(f_n^H(S_\Sigma)\right) \tag{7.8b}$$

where s_Σ is defined as

$$\left[f_n^H(s_\Sigma)\right]' = 0$$

$$\left[f_n^E(s_\Sigma)\right]' = 0 \qquad (7.9)$$

That is, simple the saddles of $f_n^E(s)$ and $f_n^H(s)$. By plotting $C_{phase\Sigma}$ only through the saddle point s_Σ with which it is associated (even though it may exist in other parts of the plane) affords a convenient method for subdividing the plane into pole or zero regions. Saddle argument contours from pole to pole encompass the associated zeros while argument contours from zero to zero determine regions of associated poles. A complete discussion of the use of phase and magnitude mapping as an approach to solutions to impedance functions including saddle argument contours is given in a recent note by Baum[8].

Figures 7.1 through 7.12 give the constant magnitude and phase contours of f_n^E and f_n^H. The saddle argument contours are represented as dotted lines. Poles, zeros and saddle are indicated on the graphs as p, z and Σ, respectively.

An obvious contour to be noted in the graphs is the $-\pi$ phase line which corresponds to the purely resistive loading. In this case $-z_s = -R + 0i$ and has a constant phase of $-\pi$. Since the phase is independent of the magnitude in this case the $-\pi$ phase contour is actually the

trajectory of the resonance frequency as presented in section III. As in section III the intersection along its path measures various magnitudes of $|-z_s| = |R|$. Of course for other than pure resistive loading the contour map defines discrete or interpolated points of magnitude and phase at the curve intersection since magnitude and phase are interrelated.

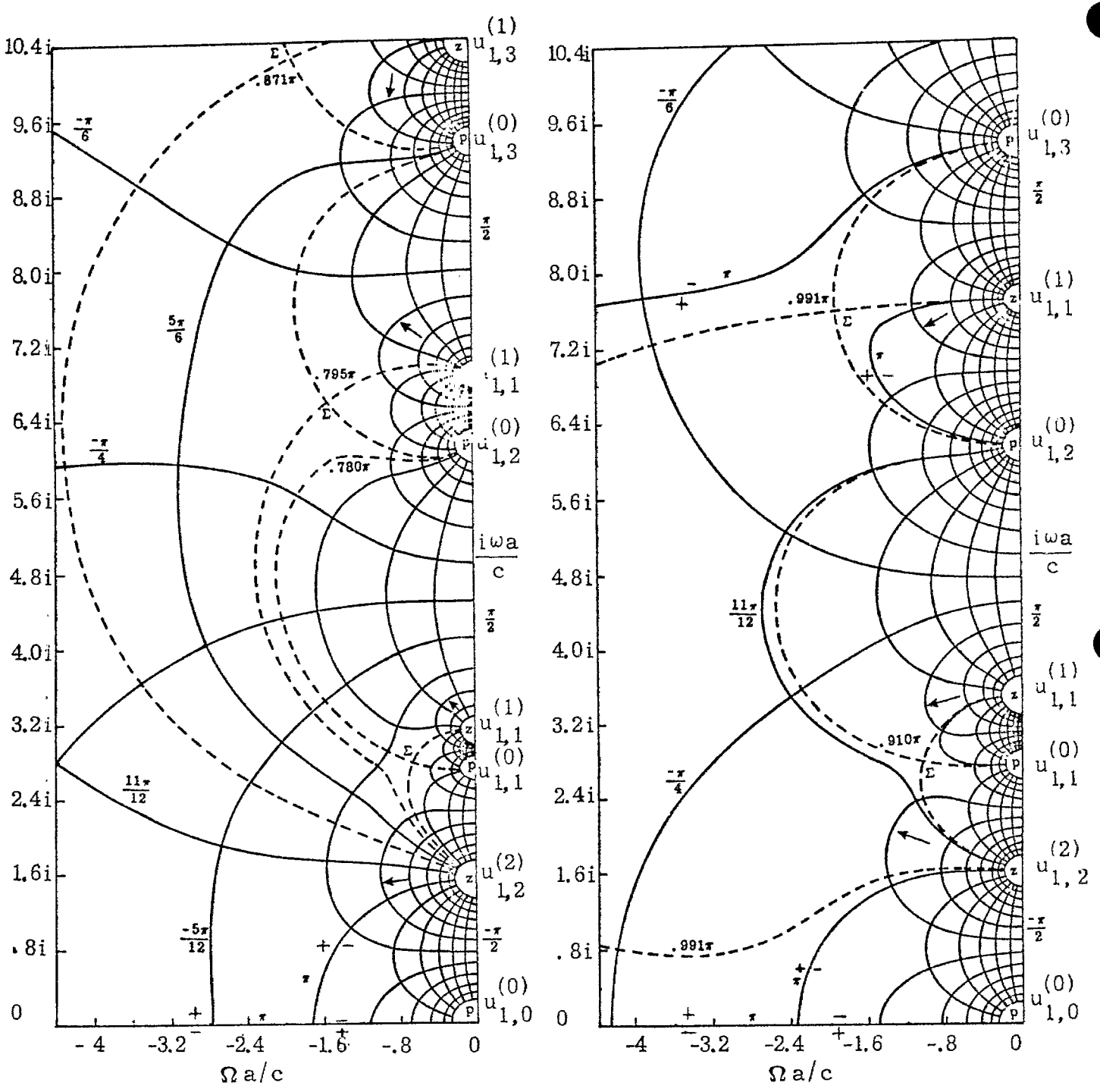

A. d/a = .1

B. d/a = .2

Figure 7.1. Constant Log Magnitude ($\ell n\,|\,f_n^E(S)|$) and Phase ($\arg[f_n^E(S)]$) Contours of the Negative Complex E-Mode Impedance Function, n = 1. Saddle Argument Contours are Represented as Dotted Lines. Arrows (←) Indicate Direction of Increasing Magnitude, $\Delta_{phase} = \Delta_{mag} = \pi/12$.

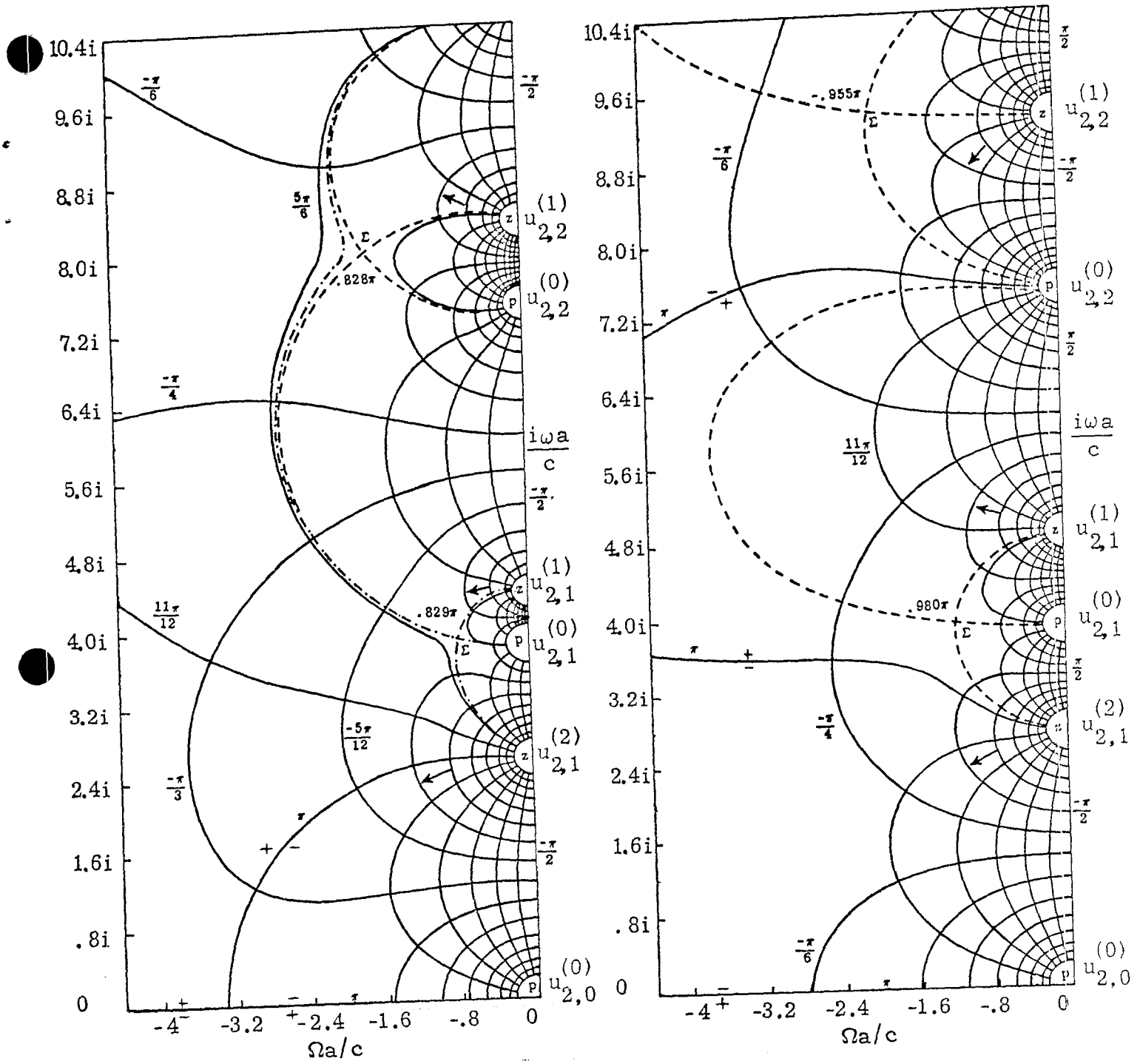

A. d/a = .1

B. d/a = .2

Figure 7.2. Constant Log Magnitude ($\ell n|f_n^E(S)|$) and Phase ($\arg[f_n^E(S)]$) Contours of the Negative Complex E-Mode Impedance Function, n = 2. Saddle Argument Contours are Represented as Dotted Lines. Arrows (←) Indicate Direction of Increasing Magnitude, $\Delta_{phase} = \Delta_{mag} = \pi/12$.

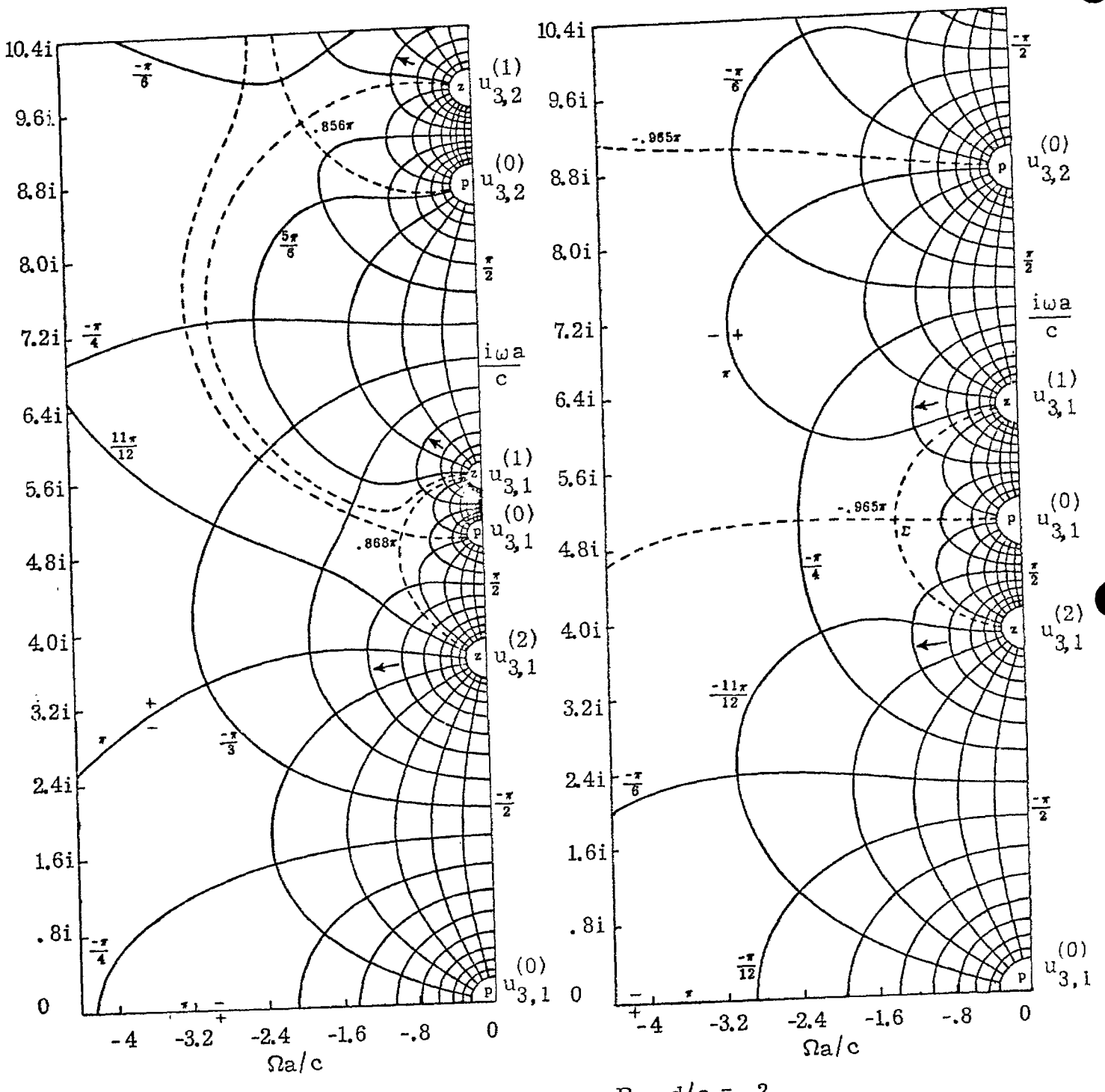

A. d/a = .1

B. d/a = .2

Figure 7.3. Constant Log Magnitude ($\ell n|f_n^E(S)|$) and Phase ($\arg[f_n^E(S)]$) Contours of the Negative Complex E-Mode Impedance Function, n = 3. Saddle Argument Contours are Represented as Dotted Lines. Arrows (←) Indicate Direction of Increasing Magnitude, $\Delta_{phase} = \Delta_{mag} = \pi/12$.

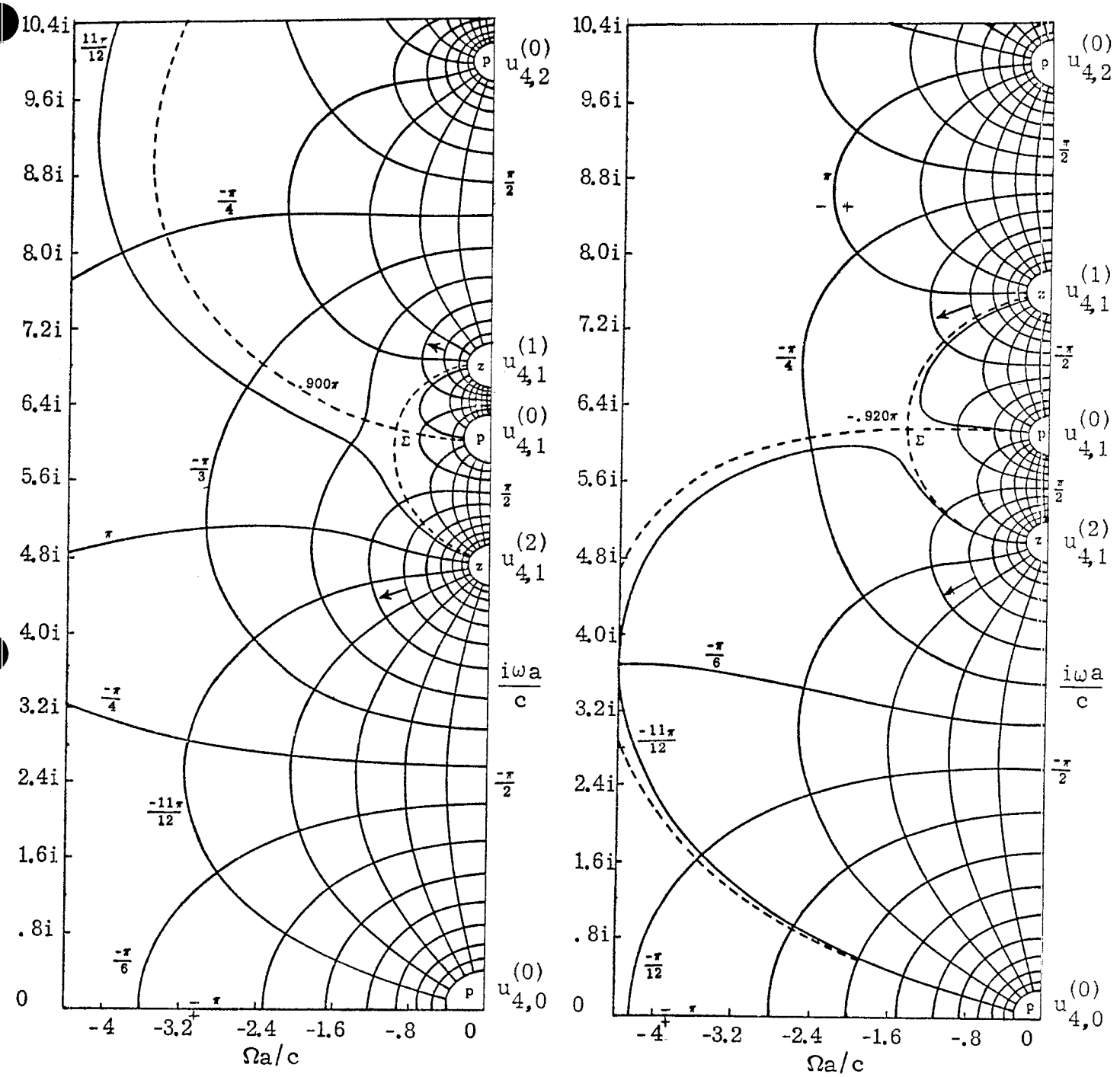

A. d/a = .1

B. d/a = .2

Figure 7.4. Constant Log Magnitude ($\ell n|f_n^E(S)|$) and Phase ($\arg[f_n^E(S)]$) Contours of the Negative Complex E-Mode Impedance Function, n = 4. Saddle Argument Contours are Represented as Dotted Lines. Arrows (←) Indicate Direction of Increasing Magnitude, $\Delta_{phase} = \Delta_{mag} = \pi/12$.

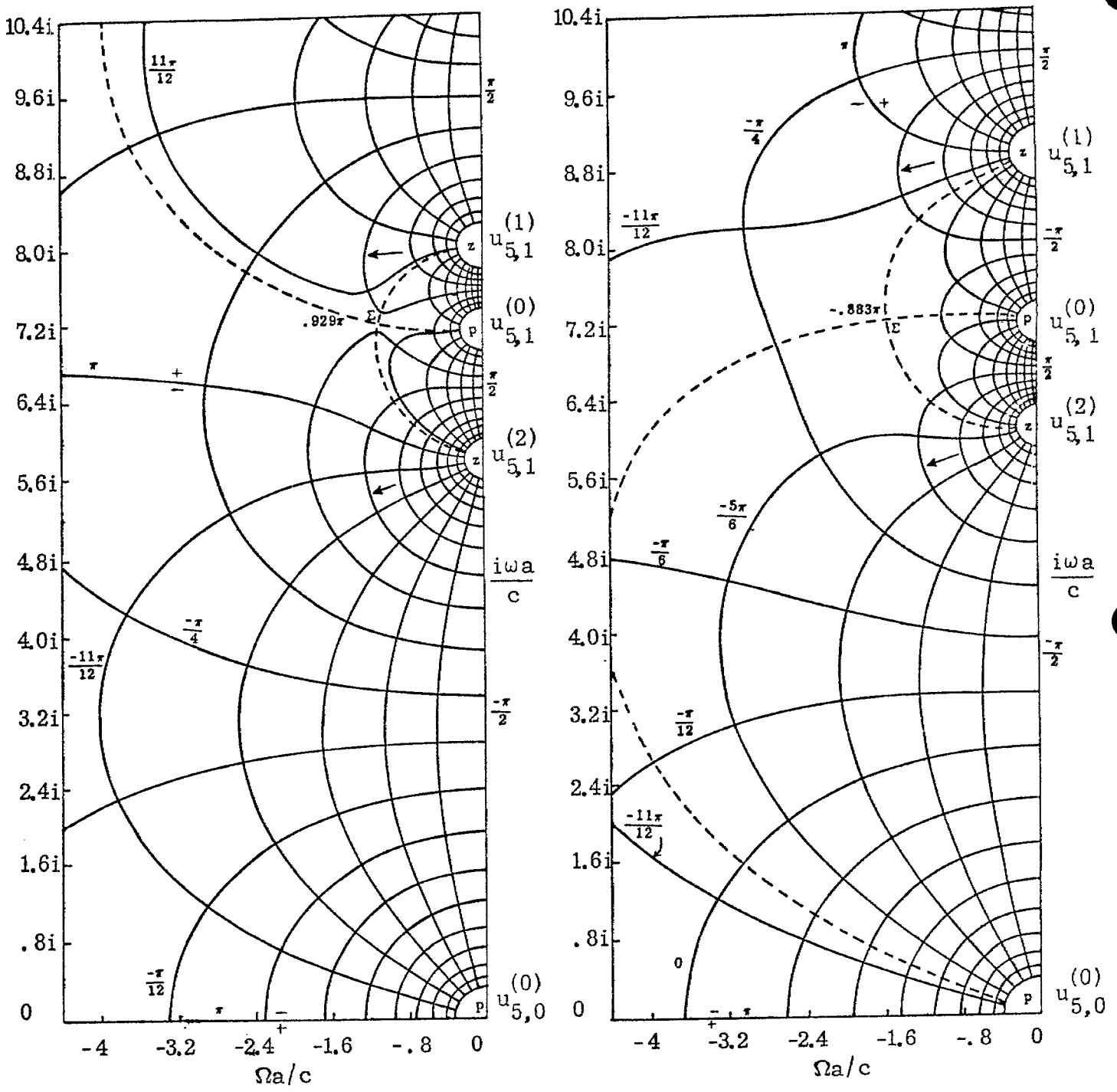

Figure 7.5. Constant Log Magnitude ($\ell n|f_n^E(S)|$) and Phase ($\arg[f_n^E(S)]$) Contours of the Negative Complex E-Mode Impedance Function, n = 5. Saddle Argument Contours are Represented as Dotted Lines. Arrows (←—) Indicate Direction of Increasing Magnitude, $\Delta_{phase} = \Delta_{mag} = \pi/12$.

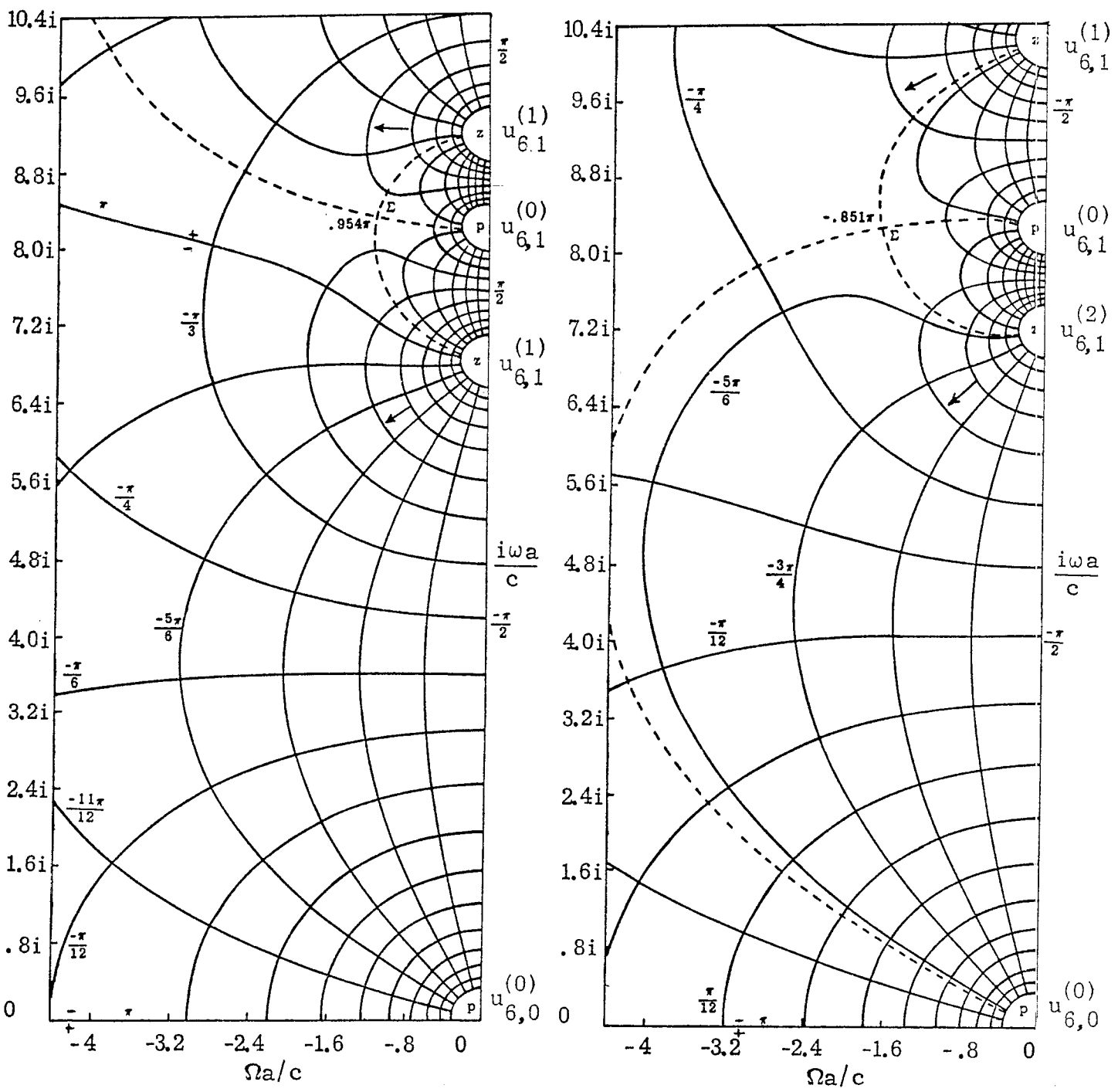

A. d/a = .1

B. d/a = .2

Figure 7.6. Constant Log Magnitude ($\ell n|f_n^E(S)|$) and Phase ($\arg[f_n^E(S)]$) Contours of the Negative Complex E-Mode Impedance Function, n = 6. Saddle Argument Contours are Represented as Dotted Lines. Arrows (←) Indicate Direction of Increasing Magnitude, $\Delta_{phase} = \Delta_{mag} = \pi/12$.

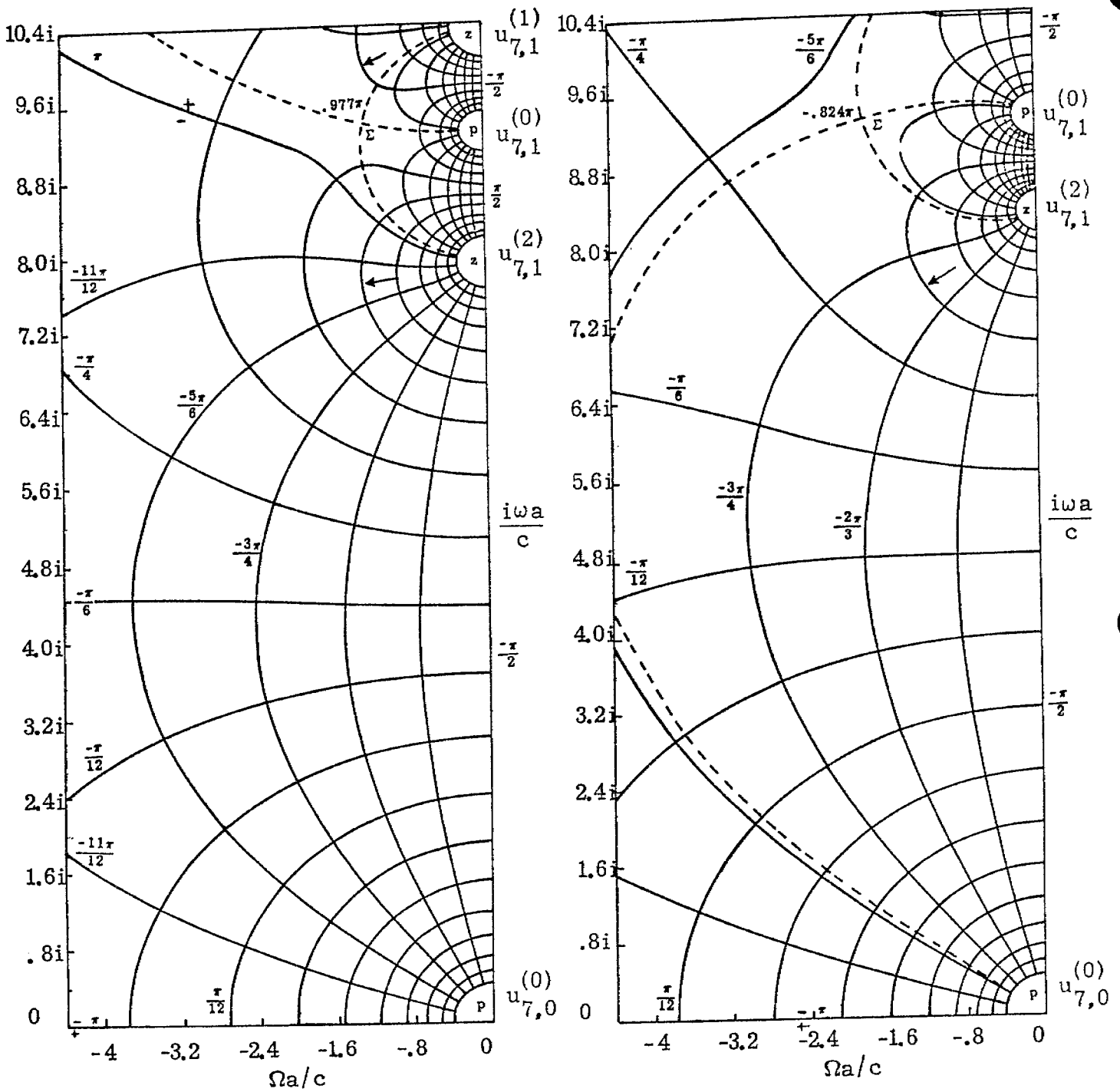

Figure 7.7. Constant Log Magnitude ($\ell n|f_n^E(S)|$) and Phase ($\arg[f_n^E(S)]$) Contours of the Negative Complex E-Mode Impedance Function, n = 7. Saddle Argument Contours are Represented as Dotted Lines. Arrows (←) Indicate Direction of Increasing Magnitude, $\Delta_{phase} = \Delta_{mag} = \pi/12$.

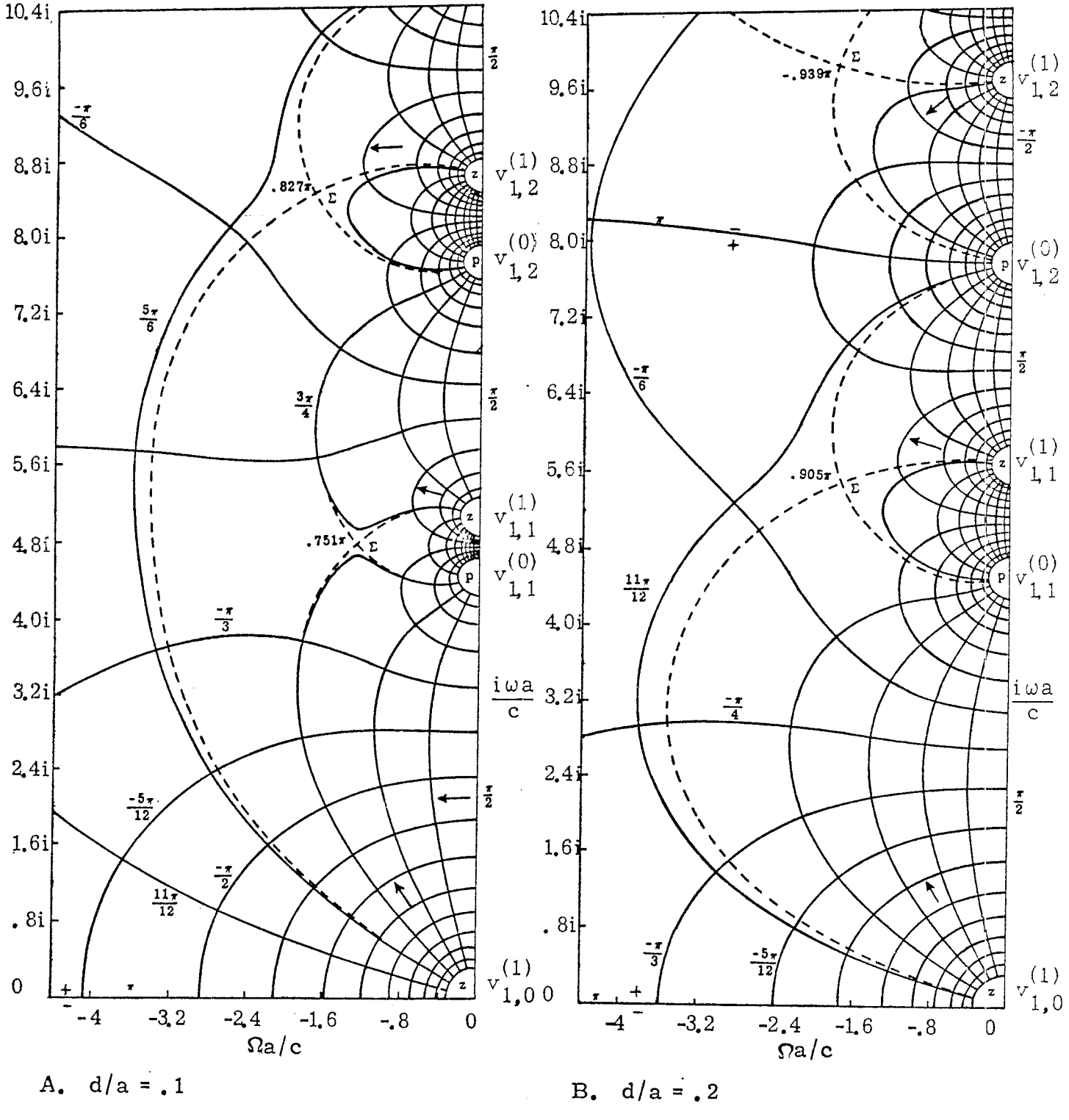

A. d/a = .1

B. d/a = .2

Figure 7.8. Constant Log Magnitude ($\ell n|f_n^H(S)|$) and Phase ($\arg[f_n^H(S)]$) Contours of the Negative Complex H-Mode Impedance Function, n = 1. Saddle Argument Contours are Represented as Dotted Lines. Arrows (←) Indicate Direction of Increasing Magnitude, $\Delta_{phase} = \Delta_{mag} = \pi/12$.

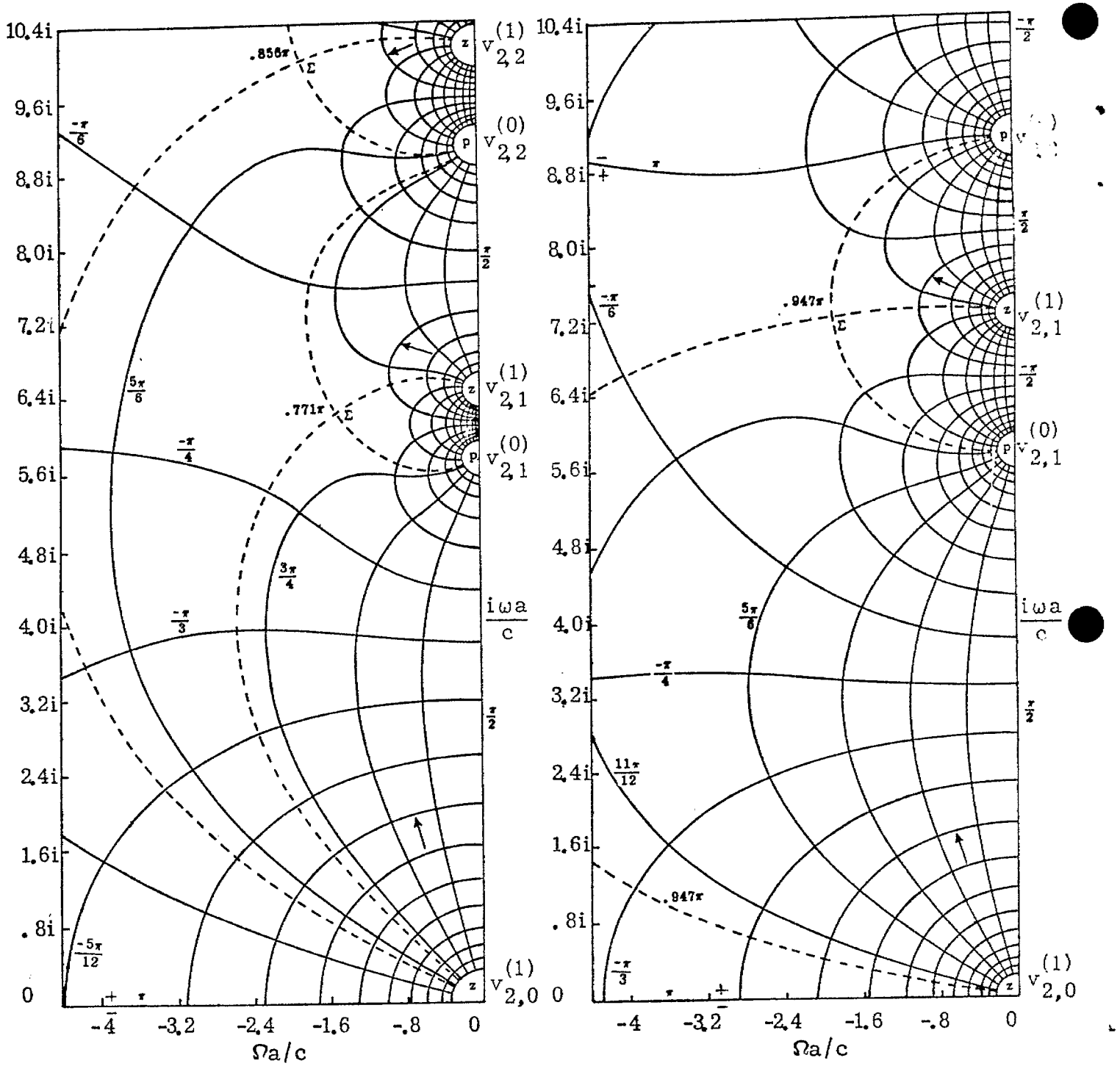

A. d/a = .1

B. d/a = .2

Figure 7.9. Constant Log Magnitude ($\ell n|f_n^H(S)|$) and Phase ($\arg[f_n^H(S)]$) Contours of the Negative Complex H-Mode Impedance Function, n = 2. Saddle Argument Contours are Represented as Dotted Lines. Arrows (←) Indicate Direction of Increasing Magnitude, $\Delta_{phase} = \Delta_{mag} = \pi/12$.

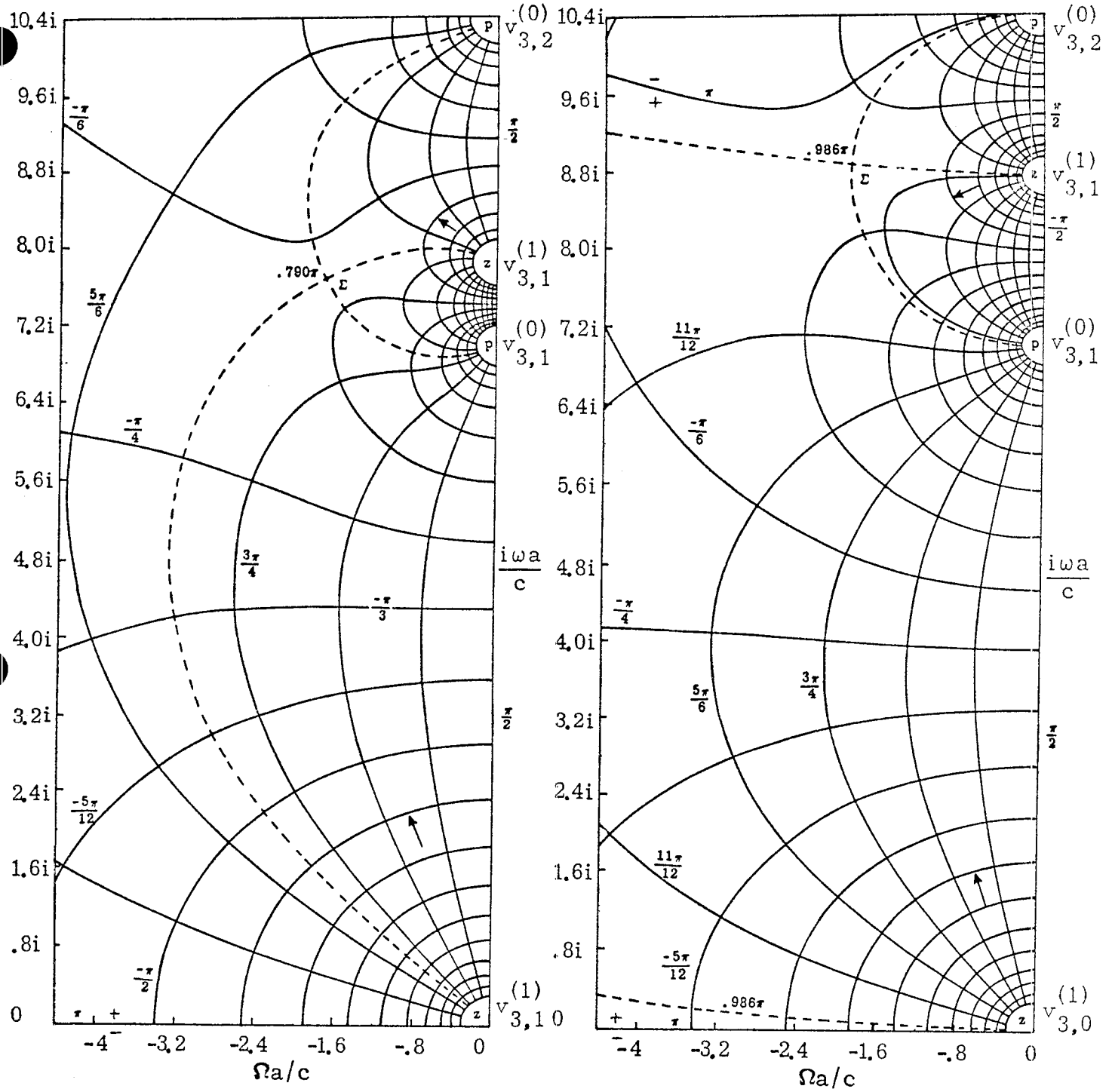

Figure 7.10. Constant Log Magnitude ($\ell n|f_n^H(S)|$) and Phase ($\arg[f_n^H(S)]$) Contours of the Negative Complex H-Mode Impedance Function, n = 3. Saddle Argument Contours are Represented as Dotted Lines. Arrows (←) Indicate Direction of Increasing Magnitude, $\Delta_{phase} = \Delta_{mag} = \pi/12$.

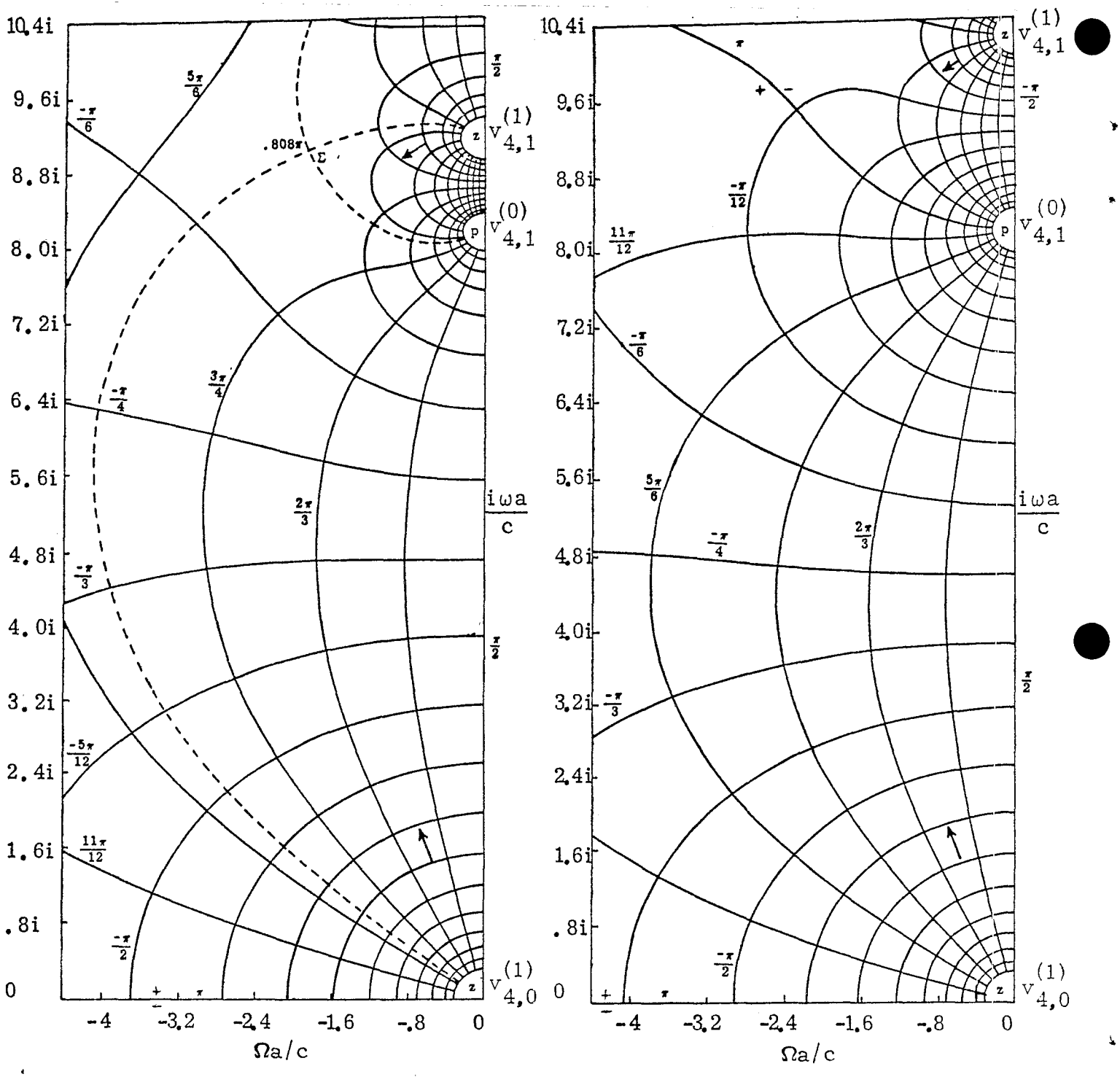

A. d/a = .1

B. d/a = .2

Figure 7.11. Constant Log Magnitude ($\ell n|f_n^H(S)|$) and Phase ($\arg[f_n^H(S)]$) Contours of the Negative Complex H-Mode Impedance Function, n = 4. Saddle Argument Contours are Represented as Dotted Lines. Arrows (⟵) Indicate Direction of Increasing Magnitude, $\Delta_{phase} = \Delta_{mag} = \pi/12$.

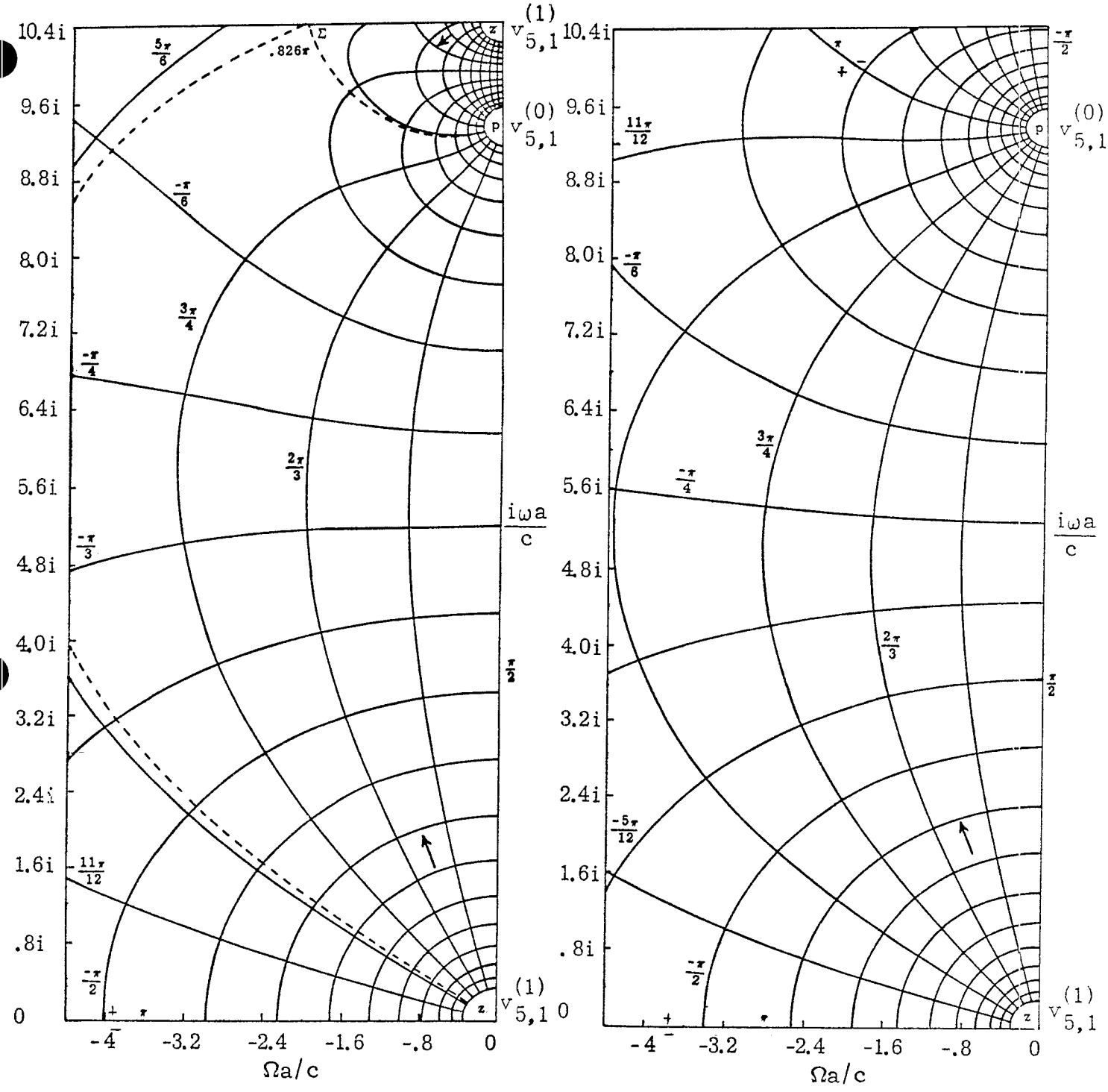

A. d/a = .1

B. d/a = .2

Figure 7.12. Constant Log Magnitude ($\ell n|f_n^H(S)|$) and Phase ($\arg[f_n^H(S)]$) Contours of the Negative Complex H-Mode Impedance Function, n = 5. Saddle Argument Contours are Represented as Dotted Lines. Arrows (←) Indicate Direction of Increasing Magnitude, $\Delta_{phase} = \Delta_{mag} = \pi/12$.

VIII. CONCLUSION

This report has presented an extensive parameter study of the spherically shaped damping structure within a perfectly conducting spherical chamber. The major effort here has been identifying, indexing, tracking, and describing the behavior of the resonant frequencies in this spherical chamber. Ample information is given to gain insight into these resonant frequencies, where they originate, and how and by what degree they can be damped. It is hoped that this report in the future will also shed light on pole/zero behavior in more complex structured models.

The concentration in this report has been on examining pole position in the normalized complex frequency plane for various parameters to determine the resulting damping. In the future, however, an idea that seems to hold promise is reversing the process in that some desired response is selected and then a determination in a least square sense of the complex impedance that will produce this response.

If multiple activity pole and/or zero charting is to be pursued as a viable approach to understanding theoretical EMP problems for a wide variety of parameters, a more dynamic approach also seems to be warranted. The approach of motion pictures with changing parameters in time or some interactively produced plots (points, contours, 3-D projections, etc.) on a terminal CRT would certainly enhance comprehension.

IX. REFERENCES

1. C. E. Baum, Sensor and Simulation Note 156, A Technique for Simulating the System Generated Electromagnetic Pulse Resulting from an Exoatmospheric Nuclear Weapon Radiation Environment, September 1972.

2. Abromowitz and Stegun, ed., Handbook of Mathematical Functions, AMS 55, National Bureau of Standards, 1964.

3. J. P. Martinez, Mathematics Note 4, SBF A Subroutine for the Generation of Spherical Bessel Functions with Real Arguments and Integer Orders.

4. Ibid., Appendix II.

5. C. E. Baum, Interaction Note 88, On the Singularity Expansion Method for the Solution of Electromagnetic Interaction Problems, December 1971.

6. F. M. Tesche, Interaction Note 102, On the Singularity Expansion Method as Applied to Electromagnetic Scattering from Thin-Wires, April 1972.

7. T. L. Brown, Mathematics Note 26, BRUT A System of Subroutines for the Generation of Contours, July 1972.

8. C. E. Baum, Mathematics Note 35, On the Use of Contour Integration for Finding Poles, Zeros, Saddles, and Other Function Values in the Singularity Expansion Method, February 1974.